

1969

Electrostatic Precipitation In Electrified Media And Positive Corona Ozone Generation In The Design Of High Efficiency Air Cleaners

George Samuel Castle

Follow this and additional works at: <https://ir.lib.uwo.ca/digitizedtheses>

Recommended Citation

Castle, George Samuel, "Electrostatic Precipitation In Electrified Media And Positive Corona Ozone Generation In The Design Of High Efficiency Air Cleaners" (1969). *Digitized Theses*. 321.
<https://ir.lib.uwo.ca/digitizedtheses/321>

This Dissertation is brought to you for free and open access by the Digitized Special Collections at Scholarship@Western. It has been accepted for inclusion in Digitized Theses by an authorized administrator of Scholarship@Western. For more information, please contact tadam@uwo.ca, wlsadmin@uwo.ca.

The author of this thesis has granted The University of Western Ontario a non-exclusive license to reproduce and distribute copies of this thesis to users of Western Libraries. Copyright remains with the author.

Electronic theses and dissertations available in The University of Western Ontario's institutional repository (Scholarship@Western) are solely for the purpose of private study and research. They may not be copied or reproduced, except as permitted by copyright laws, without written authority of the copyright owner. Any commercial use or publication is strictly prohibited.

The original copyright license attesting to these terms and signed by the author of this thesis may be found in the original print version of the thesis, held by Western Libraries.

The thesis approval page signed by the examining committee may also be found in the original print version of the thesis held in Western Libraries.

Please contact Western Libraries for further information:

E-mail: libadmin@uwo.ca

Telephone: (519) 661-2111 Ext. 84796

Web site: <http://www.lib.uwo.ca/>

ELECTROSTATIC PRECIPITATION IN ELECTRIFIED MEDIA
AND POSITIVE CORONA OZONE GENERATION IN THE
DESIGN OF HIGH EFFICIENCY AIR CLEANERS

by

George Samuel Peter Castle

Faculty of Engineering Science

Submitted in partial fulfillment
of the requirements for the degree of
Doctor of Philosophy

Faculty of Graduate Studies
The University of Western Ontario

London, Canada

March 1969

ABSTRACT

Two stage electrostatic precipitators are widely used for high efficiency collection of submicron particulates in air cleaning applications. A different approach to the design of such precipitators has been proposed, based upon a concentric cylindrical geometry combined with dielectric media in the collection region. This has two main advantages over existing designs in that it; a) allows high collection efficiency and reliability due to the large collection area afforded by the dielectric media and the utilization of collection forces other than just the coulomb force, b) results in a compact self contained cartridge suitable for easy replacement.

An expression was derived for the collection efficiency where instead of the usual migration velocity, a dimensionless collection parameter was introduced as the figure of merit for the collection. This, coupled with a dimensionless geometrical parameter called the specific collection area, completely specifies the collection efficiency. While this is shown to be equivalent to the traditional expression for collection efficiency, it has the advantage of being readily extended to include all electrical

and mechanical collection forces. The experimental studies which were carried out on the concentric geometry precipitator showed general agreement with the predicted values over a broad range of conditions and collector geometries.

Since ozone generation is of prime concern in an air cleaning precipitator, a portion of the study was devoted to the investigation of the mechanisms affecting its generation. As a result, a quantitative expression was found relating the ozone concentration to the corona current, the air flow and a "corona potential function". In addition, the effect of wire geometry and wire aging was shown to have a considerable influence on the ozone generation.

Based upon the results of the study, two prototype precipitators were designed, built and tested in practical air cleaning situations.

ACKNOWLEDGEMENTS

I would like to acknowledge my deep indebtedness and express my appreciation to Professor I.I. Inculet, my chief adviser, who suggested this project and contributed so much to it through his enthusiasm, constant interest, and invaluable advice. Also I wish to thank my advisory committee, Dr. K.A. Shelstad and Dr. B.J. Vickery of the Faculty of Engineering Science and Dr. R.C. Murty of the Department of Physics, for their efforts on my behalf. To Mr. G.R. Yaworski, C.E.T., I owe a special debt of gratitude for his unique contributions in the areas of the design and construction of the test apparatus and the performance of the majority of the experiments reported here.

The project was made possible through the generous financial support of the Ontario Department of Health (Environmental Health Branch) through their continuing research grant APR. 1, 64.

Several field tests were carried out and the co-operation of Mr. A.P. Ruffo, Research Manager, Industrial Air Filters Limited*, Montreal and Mr. M.W. Hollands, General Manager, General Smelting Company, Burlington, Ontario is sincerely acknowledged. Johnson & Johnson provided

*Subsidiary of Johnson and Johnson Ltd.

special filter material and performed many tests on a test precipitator in their laboratory. General Smelting allowed the use of their facilities to test the precipitator in a practical situation. Also a special contribution has been made by Dr. N. Lefcoe of Victoria Hospital, London, who has assigned financial support for a prototype filter to be used in the air cleaning system of a trial clean room.

I am extremely grateful to the National Research Council of Canada for the support received through a P.I.E.R. Fellowship for the period September 1966 to August 1967, and to the Faculty of Engineering Science who provided Demonstratorships and a Lectureship during the course of the project.

In conclusion, I wish to extend my sincere thanks to the many individuals in the Faculty of Engineering Science who have helped me in so many ways; through shop, library and secretarial work as well as numerous informative discussions.

G.S.P.C.

TABLE OF CONTENTS

	Page
ABSTRACT	iii
ACKNOWLEDGEMENTS	v
TABLE OF CONTENTS	vii
LIST OF TABLES	xi
LIST OF FIGURES	xii
NOMENCLATURE	xvi
CHAPTER 1 Introduction	1
1.1 Electrostatic Precipitation .	1
1.2 Air Cleaning	3
1.3 Note on Units	6
CHAPTER 2 Objectives	7
2.1 Scope of Investigation	7
2.1.1 Concentric Geometry Electrostatic Precipitator	8
2.1.2 Dielectric Media in the Collection Region	12
2.1.3 Ozone Generation	13
2.1.4 Importance of the Particle Size Range of the Order of One Micron	14
CHAPTER 3 Previous Contributions	16
3.1 Summary of Previous Work	16
3.1.1 General	16
3.1.2 Collection Mechanisms	17
3.1.3 Filters with Electrified Media	19

	Page
3.1.4 Two-Stage Electrostatic Precipitation with Electrified Collection Media	21
3.2 Introduction to Background Theory	22
3.3 Aerodynamic Drag Force - Stokes' Law.	24
3.4 Mechanical Forces.	28
3.4.1 Inertial Impaction.	29
3.4.2 Interception.	30
3.4.3 Combined Effects.	32
3.4.4 Diffusion	34
3.5 Electrostatic Forces	35
3.5.1 Coulomb Force	37
3.5.2 Image Force	39
3.5.3 Dielectrophoretic Force	40
3.6 Efficiency of Collection	42
3.7 The Positive Corona Discharge in Air.	45
3.7.1 Particle Charging	50
3.7.2 Ozone Generation	54
CHAPTER 4 Test Procedures.	59
4.1 Experimental Apparatus.	59
4.1.1 Air Supply.	59
4.1.2 Aerosol Generator	61
4.1.3 Particle Counter	64
4.1.4 Other Instrumentation and Equipment	68
4.1.5 Probable Measurement Errors.	70
4.1.6 Test Units.	75
4.1.7 Measurement of Collection Efficiency.	79
CHAPTER 5 Collection Efficiency	82
5.1 Theory	82
5.1.1 Migration Velocity and the Collection Parameters.	82
5.1.2 Collection Efficiency Equation for a One Stage Cylindrical Precipitator with a Perforated Wall.	86

	Page	
5.1.3	Collection Efficiency Equation for the Second Stage of the Concentric Geometry Precipitator.	95
5.1.4	Collection Efficiency Equation for the Second Stage of the Concentric Geometry Precipitator with Electrified Media Present	100
5.2	Test Results and Their Interpretation.	110
5.2.1	Air Flow Through the Concentric Geometry Precipitator	110
5.2.2	Collection Characteristics of the First Stage.	116
5.2.3	Collection Characteristics of the Second Stage	128
5.2.4	Collection Characteristics of the Second Stage with Electrified Media Present.	137
CHAPTER 6	Ozone Generation	166
6.1	Introduction.	166
6.2	Ozone Formula	167
6.3	Effect of Wire Geometry	178
6.4	Effect of Wire Aging.	185
CHAPTER 7	Practical Filter	189
7.1	Introduction.	189
7.2	Mark I Design	191
7.2.1	Description.	191
7.2.2	Test Results	194
7.2.3	Discussion of Test Results	202
7.3	Mark II Design.	207
7.3.1	Description.	207
7.3.2	Test Results	210
7.3.3	Discussion of Test Results	214

	Page
CHAPTER 8	
Conclusions	215
8.1 Summary	215
8.2 Recommendations for Future Work.	219
APPENDIX A	
Collection Parameters for Cylindrical Collectors.	224
APPENDIX B	
Graphical Aids to Calculations... .	230
APPENDIX C	
Summary of Further Experimental Results.	235
REFERENCES	240
VITA	xxiii

LIST OF TABLES

<u>Table</u>		<u>Page</u>
4.1	Range of Count Variation From Aerosol Generator.	65
5.1	Axial Air Velocities	115
5.2	Radial Air Velocities.	115
5.3	Collector Geometries	139
6.1	Ozone Generation	173
6.2	Effect of Wire Geometry on Ozone Generation	181
7.1	Pressure Drop Through Mark I Prototype.	197
C.1	Test Results	236

LIST OF FIGURES

<u>Figure</u>		<u>Page</u>
2.1	Two Common Precipitator Designs	9
2.2	The Concentric Cylindrical Geometry Precipitator.	11
3.1	The Cunningham Correction Factor.	27
3.2	Single Fiber Efficiency of Impaction For Spheres on a Cylindrical Collector.	31
3.3	Single Fiber Efficiency of Interception For Spheres on a Cylindrical Collector.	33
3.4	Cylindrical Positive Corona Discharge	46
4.1	Flow Diagram of Test Set Up	60
4.2	Aerosol Generator	63
4.3	Prime Calibration of Royco Particle Counter	66
4.4	Test Units	77
4.5	Overall View of Test Set Up	80
5.1	Forces Acting on a Small Particle Held at Rest Adjacent to a Collecting Surface	85
5.2	First Stage of the Concentric Cylindrical Geometry Precipitator	88
5.3	Derating Factor For the Collection Parameter Due to Finite Charging Time	93
5.4	Possible Orientations of Rod and Flat Plate Collector Relative to the Electric Field Direction and Mean Flow	102
5.5	Second Stage of the Concentric Cylindrical Geometry Precipitator With Dielectric Collection Media.	104

<u>Figure</u>	<u>Page</u>
5.6 Axial Velocity in Corona Section	112
5.7 Particle Leakage From First Stage as a Function of Particle Diameter and Air Flow Rate.	117
5.8 Particle Leakage From First Stage as a Function of Corona Current Density	123
5.9 Effect of Aperture Size on Particle Leakage From First Stage	127
5.10 Particle Leakage From Second Stage as a Function of Repeller Voltage, Polarity and Air Flow Rate.	129
5.11 Particle Leakage From Second Stage as a Function of Particle Size and Repeller Voltage	134
5.12 Particle Leakage as a Function of Corona Current Density For Fixed Repeller Voltage .	136
5.13 Particle Leakage as a Function of Particle Size For Mechanical and Image Collection Mechanisms	142
5.14 Particle Leakage Due to First and Second Stages as a Function of Particle Size.	143
5.15 Particle Leakage For Different Collector Geometries Compared to Theoretical Value of Exponent.	146
5.16 Particle Leakage From Second Stage of Precipitator With "Viskonaire", as a Function of Repeller Voltage and Particle Size.	148
5.17 Particle Leakage From Second Stage With "Viskonaire" Present as a Function of Repeller Voltage	150
5.18 Particle Leakage From Second Stage of Precipitator With "Viskonaire" Present (Mechanical Forces).	153

<u>Figure</u>	<u>Page</u>
5.19 Particle Leakage From Second Stage of Precipitator With "Viskonaire" Present (Dielectrophoretic Force)	156
5.20 Particle Leakage From Second Stage of Precipitator With "Viskonaire" Present (Coulomb and Image Forces)	157
5.21 Correlation Between Experimental Particle Leakage and Predicted Value of Exponent For Different Geometries	159
6.1 Ozone Concentration Versus Corona Current as a Function of Air Flow.	168
6.2 Ozone Concentration Versus Corona Current as a Function of Wire Size	169
6.3 Ozone Concentration Versus Wire Radius as a Function of Corona Current.	170
6.4 Ozone Concentration Versus ϕ as a Function of Corona Current	171
6.5 Normalized Ozone Concentration [O ₃]/I Versus Wire Radius	175
6.6 Corona and Ozone Characteristics For Twisted Copper Wires	180
6.7 Corona and Ozone Characteristics For Fixed Wire Diameter With Different Surface Conditions	184
6.8 Variation in Ozone Generation as a Function of Time	186
7.1 Mark I Prototype	192
7.2 Cartridge Element for Mark I Prototype	193
7.3 Ozone Generation from Mark I Prototype	196
7.4 Cartridge Element for Mark II Prototype.	208
7.5 Complete Mark II Filter.	211

<u>Figure</u>	<u>Page</u>
A.1	Field Distribution Around An Infinitely Long Dielectric Cylinder in a Uniform Field E_0 225
B.1	Radial Electric Field Strength in Corona Section as a Function of Corona Current Density 231
B.2	Correction Factor α as a Function of Particle Size and Relative Permittivity. . . 232
B.3	Particle Saturation Charge as a Function of Particle Size and Charging Field Strength 233
B.4	Relation Describing the Variations of the Coulomb Collection Parameter as a Function of Particle Size and Relative Permittivity 234

NOMENCLATURE

a	particle radius or corona wire radius (meter)
Δa	thickness of ionized sheath in corona discharge (meter)
A	geometric ratio for ozone generation (dimensionless)
A_f'	surface area of a single cylindrical fiber collector (meter ²)
A_c	collection surface area (meter ²)
A_x	cross sectional area of duct or precipitator (meter ²)
b	derating factor due to finite charging time (dimensionless)
B(a)	proportionality factor in ozonizer (dimensionless)
\bar{c}	average molecular velocity of air ions $\frac{(\text{meter})}{(\text{second})}$ $\doteq 5 \times 10^2 \frac{\text{m}}{\text{s}}$ at room temperature
C	Cunningham correction factor (dimensionless)
C_i	circumference of i^{th} increment in collection medium (meter)
d	particle diameter (meter)
	position in 1st stage of precipitator at which air diffusion into 2nd stage begins (meter)
D	depth of collection media (meter)
D_c	collector diameter (meter)

- e electronic charge (coulomb)
 $= 1.6 \times 10^{-19} \text{ C}$
- \vec{E} electric field strength $\frac{\text{(volt)}}{\text{(meter)}}$
- E_{av} average electric field strength in the ionized sheath of a corona discharge $\frac{\text{(volt)}}{\text{(meter)}}$
- E_c critical field strength for onset of corona discharge $\frac{\text{(volt)}}{\text{(meter)}}$
- E_o uniform electric field strength in space $\frac{\text{(volt)}}{\text{(meter)}}$
- E_r radial electric field strength $\frac{\text{(volt)}}{\text{(meter)}}$
- E_p collection field at surface of collector $\frac{\text{(volt)}}{\text{(meter)}}$
- $f(a)$ parameter defining the functional variation of the coulomb collection parameter with particle size and material (meter)
- \vec{F} force (newton)
- \vec{F}_c coulomb force (newton)
- \vec{F}_I image force (newton)
- \vec{F}_d dielectrophoretic force (newton)
- \vec{F}_s Stokes resistance force (newton)
 $= \frac{6\pi\mu a \vec{v}_o}{C}$
- \vec{F}_x average drag force exerted on a particle by an air stream moving in the x direction (newton)
- \vec{F}_y force tending to collect particle in the 1st stage of a precipitator (newton)
- $\vec{F}'_x, \vec{F}'_y \text{ \& } \vec{F}'_z$ drag force fluctuations due to turbulence (newtons)

- G reaction constant (dimensionless)
- H particle leakage through precipitator (dimensionless)
 $= 1 - \eta$
- I corona current (ampere)
- J linear corona current density $\frac{(\text{ampere})}{(\text{meter})}$
- k Boltzmann constant = $1.38 \times 10^{-23} \frac{\text{J}}{\text{°K}}$
- K mobility of air ions $\frac{(\text{meter}^2)}{(\text{volt} \cdot \text{second})}$
 $\doteq 1.8 \times 10^{-4} \frac{\text{m}^2}{\text{V} \cdot \text{s}}$ for positive air ions
- K_C coulomb collection parameter (dimensionless)
 $= \frac{F_C}{F_S}$
- K_d dielectrophoretic collection parameter (dimensionless)
 $= \frac{F_d}{F_S}$
- K_I image collection parameter (dimensionless)
 $= \frac{F_I}{F_S}$
- K_m mechanical collection parameter (dimensionless)
 $= \frac{\eta}{\pi}$
- K' collection parameter for the coulomb force assuming
the maximum charge on the particle and a particle
axial velocity of $1 \frac{\text{m}}{\text{s}}$ • (dimensionless)
- L length of precipitator (meter)
- L' total length of fiber in filter/unit filter face
area $\frac{(1)}{(\text{meter})}$
- m number of collecting fibers at a given cross section
(dimensionless)

- N number of particles (dimensionless)
- ion density in gas $\frac{\text{(coulomb)}}{\text{(meter}^3\text{)}}$
- $[O_3]$ ozone concentration (parts per hundred million by volume, P.P.H.M.)
 $= \frac{\text{ozone generated per unit time (m}^3\text{/s)} \times 10^8}{\text{air flow per unit time (m}^3\text{/s)}}$
- $[O_3]'$ $[O_3] \cdot Q = \text{ozone generated per unit time } \frac{\text{(meter}^3\text{)}}{\text{(second)}} \times 10^8$
- P_i } probability of particle capture in the i^{th}
 $P(x_i)$ } increment (dimensionless)
- \vec{P} induced dipole moment (coulomb-meter)
- q particle charge (coulomb)
- q_s particle saturation charge (coulomb)
- Q air flow $\frac{\text{(meter}^3\text{)}}{\text{(second)}}$
- r radial distance from corona discharge wire or distance of particle from surface (meter)
- \hat{r} unit vector measured from surface towards a particle (dimensionless)
- r_c outer radius of ionized sheath in a corona discharge (meter)
- R radius of collector (meter)
- R' Interception parameter (dimensionless)
- R_1 radius of inner electrode on precipitator (meter)
- R_2 radius of outer electrode on precipitator (meter)
- Re_p Reynolds number referred to particle (dimensionless)

Re_c Reynolds number referred to collector (dimensionless)
 S circumference of first stage of precipitator (meter)
 Δt time increment (second)
 t time or residence time (second)
 T temperature ($^{\circ}K$)
 \hat{u}_r & \hat{u}_θ unit vectors (dimensionless)
 \hat{u}_o mean velocity of air stream $\frac{(\text{meter})}{(\text{second})}$
 u_x axial velocity of air stream at position x in precipitator $\frac{(\text{meter})}{(\text{second})}$
 v_o mean velocity of particle $\frac{(\text{meter})}{(\text{second})}$
 v_x axial velocity of particles at position x in precipitator $\frac{(\text{meter})}{(\text{second})}$
 V_o voltage applied to corona wire in a corona discharge (volt)
 V_c voltage applied to the corona in the 1st stage of the precipitator (volt)
 V_r voltage applied to repeller electrode in 2nd stage of the precipitator (volt)
 v voltage drop across ionized sheath in corona (volt)
 w migration velocity $\frac{(\text{meter})}{(\text{second})}$
 w^2 metallic area reduction factor for perforated metal or solidity factor (dimensionless)
 x_o distance particle travels in charging section during τ sec (meter)
 x distance into 1st stage of the precipitator (meter)

Δx incremental distance along length of precipitator
(meter)

Δy incremental distance (measured from collector)
from which all particles are removed in the time
increment Δt (meter)

y_0 limits of aerosol stream from which particles are
removed by a single collector (meter)

z $\frac{3\kappa_p'}{\kappa_p' + 2}$ (dimensionless)

α charging correction factor (dimensionless)

$$= \left(1 + \frac{\lambda}{a}\right)^2 + \frac{2}{1 + \frac{\lambda}{a}} \frac{(\kappa_p' - 1)}{(\kappa_p' + 2)}$$

β $\frac{\kappa_c' - 1}{\kappa_c' + 1}$ (dimensionless)

ϵ_0 permittivity of free space $\frac{(\text{farad})}{(\text{meter})}$

$$\frac{1}{36\pi} \times 10^{-9} \frac{\text{F}}{\text{m}}$$

γ $4\pi\epsilon_0 \frac{(\kappa_p' - 1)}{(\kappa_p' + 2)} a^3$ (farad) (meter²)

κ_p' relative permittivity of particles (dimensionless)

κ_c' relative permittivity of collector (dimensionless)

ϕ corona potential function (volt)

$$= E_{av} \cdot a$$

ρ air density $\frac{(\text{kilogram})}{(\text{meter}^3)}$

$$= 1.29 \frac{\text{kg}}{\text{m}^3} \text{ at S.T.P.}$$

- ρ_p particle density $\frac{\text{(kilogram)}}{\text{(meter}^3\text{)}}$
- μ viscosity of air $\frac{\text{(Newton} \cdot \text{second)}}{\text{meter}^2}$
 $= 1.8 \times 10^{-5} \frac{\text{N} \cdot \text{s}}{\text{m}^2}$ (in air at 20°C)
- τ field charging time constant (second)
 $= \frac{4\epsilon_0}{NK}$
- λ mean free path of air ions (meter)
 9.4×10^{-8} m at S.T.P.
- η' single fiber collection efficiency (dimensionless)
- η'_e single fiber collection efficiency due to inertia (dimensionless)
- η'_I single fiber collection efficiency due to interception (dimensionless)
- η collection efficiency of filter (dimensionless)
- ψ Inertial impaction parameter (dimensionless)

CHAPTER I

INTRODUCTION

1.1 Electrostatic Precipitation

The term electrostatic precipitation is used to describe the filtration process whereby particles obtain a charge in a gaseous corona discharge and are then collected on a surface by means of electrical attractive forces. Although the principles involved in the operation have been known for several hundred years, their practical application first occurred about 60 years ago. At present, electrostatic precipitators are widely used as a preferred control method in applications requiring very high collection efficiencies of solid or liquid particles in the size range below approximately 10 μm diameter. The use of precipitators fall into two general, but quite different, categories.

The first, and largest, is the primary collection of particulates at a source of emission to prevent air pollution and in some cases to collect valuable by-products. Generally, the particulate loadings are very high, the gas volumes treated are large, and great extremes of gas temperature, particle resistivity etc. are encountered. In this type of application, one stage precipitators are used

almost universally. Here the charging and collection of the particles takes place in a single chamber with the same field that gives rise to the corona discharge also used as the collecting field. Because of the widespread industrial use of this type of unit both the art and science of the subject are fairly well understood.

The second category is high efficiency air cleaning in a local environment such as a clean room, hospital operating room, or a home. Here it is desired to produce very clean air and hence ultra high efficiencies are required. Generally, the ambient conditions encountered are much less stringent than the previous case ie: the dust loadings are relatively light, the volume of gas cleaned is moderate and gas temperatures etc. are usually stable. However, an important limitation to the use of precipitators concerns the ozone produced by the corona discharge. One stage precipitators produce dangerous quantities of this noxious gas which precludes their use in applications where the air is directly used or contained in an enclosed space. Therefore, in this situation the so-called two stage type of precipitator is used. Here the charging of the particles is accomplished in a short corona section and the collection takes place in a static field that does not produce ozone. Comparitively speaking, much more work has been done on the one-stage units than the two stage and for this reason it is this latter

category which is of interest here. Therefore, no further discussion will be made of either large scale industrial primary cleaning or of the single stage precipitator.

1.2 Air Cleaning

The recent increase in the general level of air pollution, coupled with a greater need for air purity for health or manufacturing reasons, has greatly stimulated the construction and use of clean rooms. Moreover, the trend in the design of air systems for modern buildings etc. has been to better cleaning of the air, in addition to controlling the heat and humidity. The growing problem of allergies has forced many people to consider the possibility of installing more efficient filters in their furnace systems.

This increased interest in air cleaning raises the question of whether or not existing filters can be made more efficient. It is important to differentiate here between particle collection efficiency and filter efficiency. The former is a measure of the ability of a filter to collect particles, whereas the latter is a measure of the overall quality of a filter. For instance in determining the efficiency some factors which must be considered are:

- (1) Collection efficiency
- (2) Pressure drop

- (3) Air flow handled per unit filter volume.
- (4) Capital and maintenance costs.
- (5) Reliability.

In the air cleaning application there are two main types of filters that are used ie: high efficiency mechanical filters, consisting of fibrous or granular collectors, and two-stage electrostatic precipitators.

These two types of filters are characterized by the following main properties when constructed for maximum collection efficiency.

Mechanical

- (1) Relatively high pressure drops per unit volume of air treated.
- (2) Efficiency and pressure drop rises with clogging.
- (3) Little maintenance required (filters are replaced when pressure drop rises too high.)
- (4) High reliability.
- (5) Relatively high capital and replacement cost.
- (6) Relatively rapid clogging.

Two-Stage Electrostatic Precipitators

- (1) Very low pressure drops per unit volume of air treated.
- (2) Drop in efficiency with dust build-up.

- (3) Automatic or manual cleaning of filter required.
- (4) Prone to unreliability due to power failures or corona wire breakage.
- (5) High capital and maintenance costs.
- (6) Ozone generation limits the efficiencies obtainable.

It can be seen from these points that the two types of filter have more or less complementary properties and as a result a common configuration used in practice incorporates an electrostatic precipitator as a high efficiency prefilter in series with an absolute type mechanical filter. This greatly extends the life of the mechanical filter while ensuring highest reliability for the system by having a follow-up to the electrostatic precipitator. This being the case, the question arises as to the feasibility of combining the two principles into one filter to obtain the best properties of each. To achieve this it would seem obvious that certain of the less desirable characteristics of each would set restraints on such a filter. In particular it could be predicted that the ozone generation from the particle charging process would set an absolute limit on the device.

1.3 Note on Units

More so than in most other fields, contributions to the literature in the field of electrostatic precipitation have been made by scientists and engineers from many specialties. As a result, the units used have tended to be inconsistent from one author to the next. Moreover, because the forces involve electrical as well as aerodynamic terms, the mixing of such systems of units as the e.s.u. and the English has been quite common. Obviously, there are some arguments in favour of this since common usage tends to utilize the special advantages of any particular system. However, there can be little argument against the overall advantages of standardizing units and it has been suggested that serious effort should be made towards the general adoption of the International System of Units as recommended by many scientific bodies. Therefore, the S.I. is used throughout this thesis for all formulae. For convenience, experimental results are often expressed in the appropriate sub multiples (eg.) micrometer, liter, milliamperes etc. and where common usage suggests clarification, the alternate units are given in brackets.

CHAPTER 2

OBJECTIVES

2.1 Scope of Investigation

Considering the points raised in the introduction, a research project was undertaken the results of which are presented in this thesis. The primary objectives of the study were to investigate the following:

- (1) A new type of concentric geometry two-stage electrostatic precipitator.
- (2) The effect of using dielectric media in the collection region of the precipitator.
- (3) The generation of ozone; to ensure maximum collection efficiency per unit of ozone generated.
- (4) The collection efficiency of the precipitator in the important size range extending from 0.15 + 6 μm diameter.

Based upon the results of these studies a prototype filter was designed to have the following characteristics:

- (1) Collection efficiency $\geq 99.9\%$ for 0.3 μm diameter particles and larger, combined with moderate pressure drops.

- (2) Combined electrostatic and mechanical effects to increase reliability.
- (3) Easily replaceable cartridge type elements (these elements could be disposed of or cleaned and reused.)
- (4) Relatively simple construction.
- (5) Low ozone generation (< 5 P.P.H.M.)
- (6) Readily adapted to in-line installations.

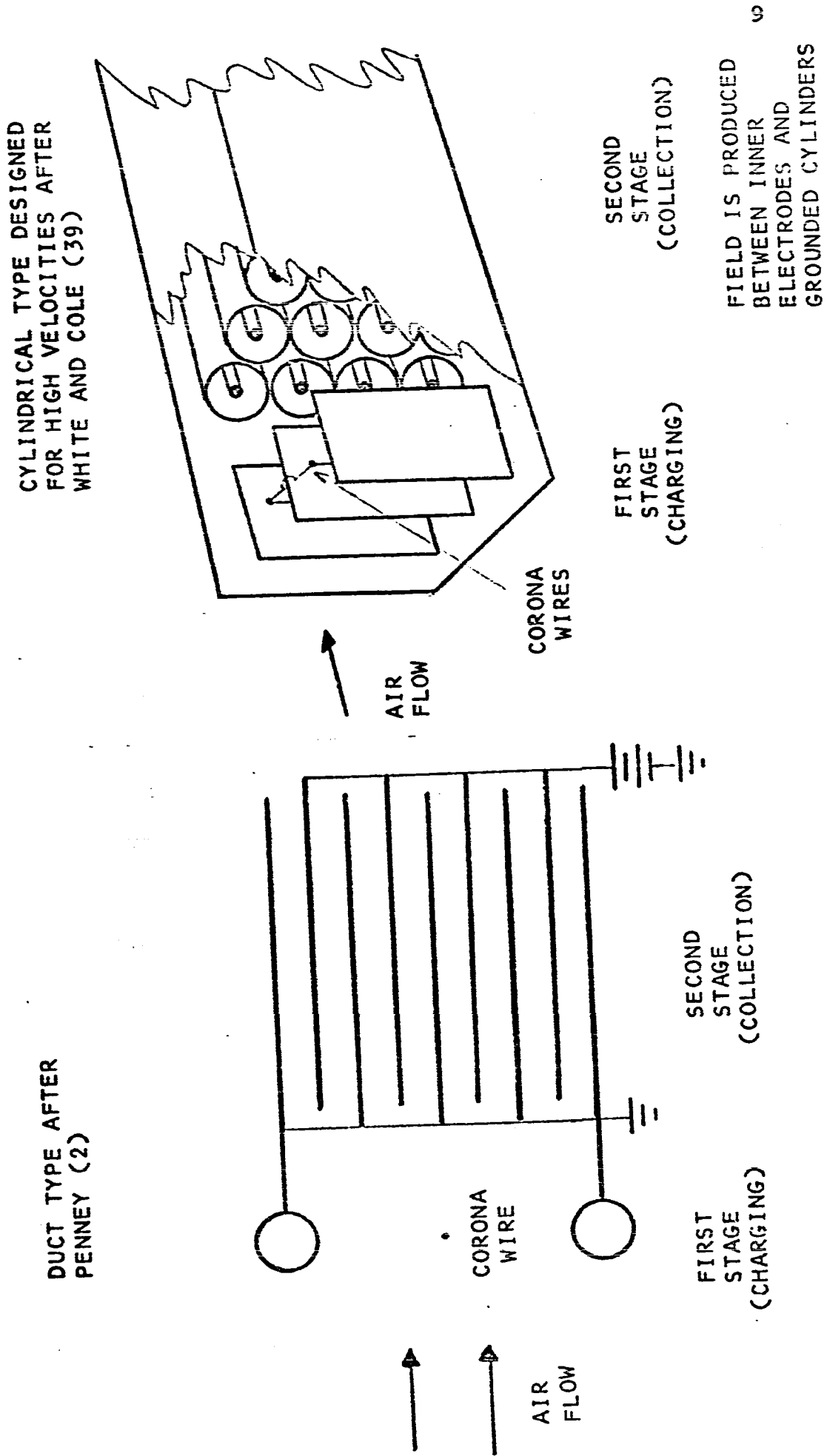
It is proposed that the resulting design produces a unit which has unique advantages for certain classes of air cleaning applications.

2.1.1 Concentric Geometry Two-Stage Electrostatic Precipitator

Existing two-stage electrostatic precipitators are generally modelled on either the duct or cylindrical one-stage units and two common designs are shown in FIG. 2.1 The first stage, where the corona discharge occurs, is the charging section. The second stage, which has a static field, is the collecting section. For best operation it is important to ensure that as much of the aerosol as possible is collected in the second stage ie: if the dust builds up too rapidly in the charger it is possible to run into the problem of back corona which hinders the charging process. In addition, it has been found that the ozone generation is

FIGURE 2.1

TWO COMMON PRECIPITATOR DESIGNS

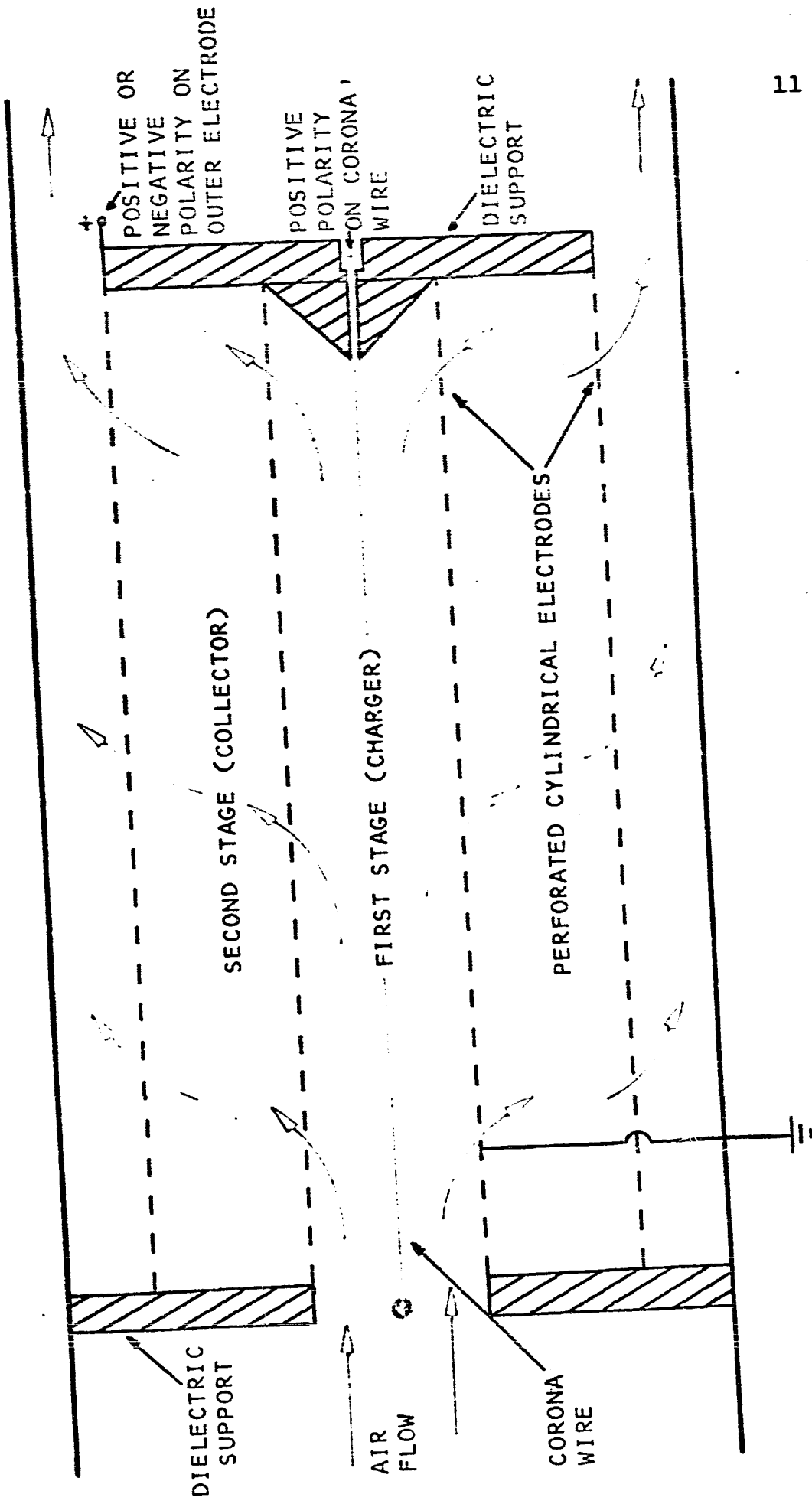


adversely affected by excessive dust collecting on the discharge wire. To reduce the amount deposited in this first stage it is necessary to increase the gas velocity as much as possible while maintaining adequate charging of the aerosol. On the other hand, for good collection in the second stage, it is necessary to have both a large collection area available and maximum residence time of the gas in this collection area. With the straight through designs as shown in FIG. 2.1, it can be seen that the velocity of the gas in the charging section is approximately the same as in the collector and hence for given flow, plate spacing etc. the residence time of the gas in the collector is a direct function of the length of the unit.

A concentric geometry has been suggested which is new to electrostatic precipitators and which has some interesting features.* The basic design is shown in FIG. 2.2. Here the collection and the charging regions are bounded by concentric perforated cylinders which are conductors but are insulated from each other. The charging region consists of a fine wire mounted axially within, but insulated from, the inner grounded cylinder. A high voltage positive polarity source is connected to the wire and the resulting divergent field gives rise to a corona discharge.

*The original idea for this application of the concentric geometry is due to Professor I.I. Inculet and is the subject of Canadian Patent #989457 filed May 2, 1967.

FIGURE 2.2
THE CONCENTRIC CYLINDRICAL GEOMETRY PRECIPITATOR



12

This fills most of the cylinder with a supply of +ve ions, hence acting as the charging mechanism for the particles. By placing a positive or negative polarity potential on the outer cylinder, a collection field exists in the second stage.

An advantage of this geometry is that the air enters the charging section with a relatively high velocity as the particles become charged, and it then expands outwards and passes radially through the collection region at a much lower velocity. With the polarities as shown in the diagram, the electric field tends to repel the particles against the direction of the average air flow and gives rise to collection on the solid portion of the inner cylinder. Another advantage of this geometry is that the functional components are self contained in a compact unit which suggests a cartridge type element which could be replaced as necessary.

2.1.2 Dielectric Media in the Collection Region

It has already been mentioned that the efficiency of collection in an electrostatic precipitator is a function of the collection area that is available. Therefore, it should be possible to increase the specific surface in the collection region by means of an electrified dielectric medium such as a fibrous filter material used for coarser air filtration. This can have large surface to volume ratio and yet because of the electrical collection forces it need

not be packed as densely as is required when used as a high efficiency mechanical filter. Hence the pressure drops should be relatively small.

The use of dielectric collection media in conjunction with a concentric geometry precipitator as described above is a new approach and the investigation and application of this is a primary concern of the present study.*

2.1.3 Ozone Generation

Ozone, which is one of the most powerful oxidants known, is very toxic to humans and animals, causes serious damage to plant life, and produces deterioration in many materials. It has been recognized for many years that an important limitation to achieving peak collection efficiencies in electrostatic precipitators occurs because of the necessity to limit the ozone which forms as a result of the corona discharge. The allowable ozone concentration limits the amount of corona current and hence the charge which can be imparted to the particles.** Therefore, in any electrostatic precipitator which is designed for use in an application where the presence of ozone may be deleterious, the ozone generation must be regarded as an important design

*This development is the subject of a joint patent by Professor I.I. Inculet and G.S.P. Castle: Canadian Patent #991258 filed May 24, 1967.

**American and British industrial standards (1) specify a maximum exposure for humans of 10 P.P.H.M. by volume for an eight hour day. For continuous exposure, such as could occur if a filter was used in a home, this level would have to be reduced by a considerable factor.

factor. For this reason, coupled with the lack of quantitative information on the ozone formation in precipitators, a portion of this work was spent investigating this phenomenon.

2.1.4 Importance of the Particle Size Range of the Order of One Micrometer

In discussing any air filtration problem it is very important to define the range of particle sizes which are of importance since the forces which predominate in any particular size range vary considerably. The region of interest here extends from $0.15 \mu\text{m}$ to $6.0 \mu\text{m}$ diameter and is of particular interest from many points of view.

The first is that this range includes a transition region where the mechanical collection forces which can act on the particles shifts in importance from a Brownian diffusional mechanism to that of interception and impaction.

Secondly, this size range includes particles whose size is of the same order as the mean free path of air molecules at S.T.P. Hence special attention must be paid to particle slippage between molecules in calculating the effect of any external forces. In addition, this factor is important in the mechanisms affecting the charging of the particles in a corona discharge.

Thirdly, the particles found in this range are extremely important from the point of view of human health

since it includes the sizes which have maximum penetration and retention in the lungs. Moreover, the majority of bacteria are found to have diameters falling in this range and in many instances their collection can be of great importance. (Viruses on the other hand are much smaller but are often found in conjunction with particulate matter in this size range.)

Finally, because these small particles have very high specific surfaces, they give rise to a major part of the severe discoloration and staining caused by aerosol deposition on walls, ceilings, etc.

CHAPTER 3

PREVIOUS CONTRIBUTIONS

3.1 Summary of Previous Work

3.1.1 General

Penny (2) in 1937 was the first worker to demonstrate the practicability and to show the advantages of using separate charging and collecting regions for electrostatic precipitators. As mentioned in section 1.1 this enabled the ozone generation to be kept to tolerable limits and hence allowed precipitators to be used in air conditioning applications for the first time. Penny pointed out that the ionization process by its nature requires a non-uniform electric field whereas he felt that most efficient collection demanded a uniformly high field in the collection region. The collecting surfaces consisted of smooth plates and were placed as close together as possible to maximize the collection area available. Since Penny's original work, although some improvements have been made in the technology of precipitators, very little basic change in his original concept has occurred.

More or less in parallel with Penny's work, Hansen (3) in 1930 and later Walton (4) in 1942 demonstrated that the collection efficiency of fibrous wool filters could be

greatly improved by impregnating the fibers with charged resin. This increase in efficiency was ascribed to the superimposed electrostatic attraction forces which acted on the particles in addition to the normal mechanical forces. Since these early demonstrations improvements have been made in the charged materials to lengthen their charge retention and, in certain cases, externally applied fields have been used to provide the electrification.

In spite of the common feature of the two types of filter ie: they both utilize electrostatic forces, there had been no reported investigation of the combining of the two devices into one unit where the particles are charged as in the electrostatic precipitator and collected on an electrified filter medium as in the resin wool filter. However, since the present investigation was started in 1966 two independent references have appeared describing this concept.

In addition to the technological development of air filters many workers have made detailed studies of the basic collection mechanisms affecting particle motion and collection.

3.1.2 Collection Mechanisms

Ranz and Wong (1952)

Ranz and Wong (5) undertook extensive investigation of the mechanisms of collection of particles impinging on

elementary collectors. They introduced dimensionless force ratios which allowed them to develop an approximation method for determining the order of magnitude of the efficiency of impaction, even in the most complicated situations. They discussed the importance of considering electrostatic effects in any impaction problem but did not solve the problem with electrostatic forces included.

Kraemer and Johnstone (1955)

Kraemer and Johnstone (6) have studied the fundamental processes by which electrostatic forces promote the deposition of particles on collecting surfaces. In particular they solved the problem for deposition of particles on isolated spherical collectors subject to the limitation that the air flow moves in fixed trajectories. Knowing the equations governing the air flow and the electrostatic forces, they obtained computer solutions for viscous and potential flow conditions and found very good correlation with experimental results. In addition, they briefly mentioned the problem for cylindrical collectors. They suggested, but did not pursue, the possibility of using a type of electrified bed consisting of pairs of fine insulated wire twisted and distributed randomly. Here relatively small voltages could be applied to these wires and high dipole fields produced.

Dawkins (1958)

Dawkins (7) continued the work of Kraemer and Johnstone and solved the problem for the deposition on isolated cylindrical collectors. He also carried out some preliminary experiments on tangled dipole mats and glass fiber filters. Good agreement was found between the experimental results on the single cylinders and the theoretical predictions. However no attempt was made to extend it to the case of the multiple collectors.

3.1.3 Filters with Electrified Media

Gillespie (1955)

Gillespie (8) developed a theory encompassing the mechanical and electrical collection parameters in a fibrous filter. He approached the problem from the mechanical viewpoint and provided additional electrical terms to account for the increase in efficiency.

Silverman et al (1956)

These authors (9) studied the feasibility of mechanically charging fabric filters and reported a doubling of collection efficiency at no increase in air resistance. Although this work provided some useful approaches, their results show that the use of mechanical charging in practical units appears to be inferior to externally applied electric fields.

Thomas and Woodfin (1959)

They describe (10) an "electrified fibrous air filter" which consisted of fibreglass filter media packed between electrified plates. No attempt was made to pre-charge the aerosol but experiments carried out with cigarette smoke showed considerable improvement in the collection efficiency when a field was applied across the media. They did not discuss the mechanisms causing the improvement but did suggest that the effect is synergistic with the overall efficiency being greater than that expected from each effect considered separately.

Havliček (1961)

Havliček (11) considered the effect of a super-imposed electric field on the efficiency of fibrous filters. He pointed out the advantage of having the air flow and field direction parallel. However, he did not consider the fact that residual charge may exist on particles or that they could be precharged. He has given a detailed analysis of the field distribution within a bed of cylindrical fibres.

Rivers (1962)

Rivers (12) described a commercially available non-ionizing type of electrostatic air filter. The collector consisted of a pleated glass fibre filter medium

with a printed conductive grid serving as electrodes. The importance of the high electrical resistivity and low moisture absorption of the medium was emphasized as a necessity for maintaining high efficiencies. He pointed out that since no adequate theory existed for random fibre filters without electrostatic fields, the problem with electrostatic fields present is even more complicated. He attempted an analysis based upon the migration velocity approach as used in electrostatic precipitation but the results showed very large discrepancies with the experimental results.

Lundgren and Whitby (1965)

Lundgren and Whitby (13) have studied the effect of particle charge on the collection efficiency of fibrous filters and have shown that the image force alone can be very important in certain conditions. They derived an equivalent single fiber collection efficiency and showed that a functional relationship exists between it and a dimensionless image force-drag force parameter.

3.1.4 Two Stage Electrostatic Precipitation with Electrified Collection Media

Mazumder and Thomas (1967)

Mazumder and Thomas (14) in a recent study have measured improvements due to superimposed electrical forces

in the collection efficiencies of filter beds composed of granular collectors in both the packed and fluidized state. They used spherical collectors and discussed the various mechanical and electrical forces which affect collection when charges exist on the particles and/or the collectors. The authors pointed out that the difficulties experienced in any analytical prediction of collection efficiency became prohibitive due to interference and inertial effects. They have suggested an exponential relation in terms of a total target efficiency but do not express it quantitatively.

Carrier "Electronic Air Cleaner" (1966)

A commercially available unit (15) is described which consists of a charging section followed by an acrylic collecting mesh sandwiched between screen electrodes. Reference is descriptive only with no quantitative discussion of performance or operating principles.

3.2 Introduction to Background Theory

Existing theories of electrostatic precipitation are primarily modelled on single-stage duct or tubular geometries having continuous charging. These analyses can be readily extended to two-stage units provided the shape of the collecting section is similar to the model and account is taken for the difference between charging and collecting field strengths. However, in the case considered here, the geometry of the

collecting section differs considerably from the standard duct or tubular precipitator as can be seen from the description in section 2.1.1. Therefore one of the main theoretical problems of interest in this thesis concerns the prediction of the collection efficiency of the concentric geometry filter, both with and without dielectric media in the collection region. More specifically, this prediction is desired for particle sizes in the range $0.15 \rightarrow 6.0 \mu\text{m}$ diameter.

In considering the collection efficiency, attention must first be paid to all the forces which can affect the collection process. These forces are documented in the literature and their main characteristics are fairly well understood. Therefore, it is possible at the outset to ignore certain of these in the present study because their magnitudes are very small compared to others. For example gravitational and centrifugal effects, which are important for particles of larger diameters, are completely negligible for the sizes considered here. Also for the normal conditions encountered in practice, thermal and magnetic forces have no measureable effect. The following sections deal with the more important force components under three headings; the aerodynamic drag force, mechanical forces, and electrostatic forces. The magnitudes of these forces are expressed in terms of dimensionless "collection parameters" as first

suggested by Ranz and Wong (5). The parameters are used in a later chapter in the derivation of an efficiency equation which proves to be equivalent to the generally accepted form of the Deutsch equation yet can be readily extended to the case where dielectric collection media is used in conjunction with the precipitator.

3.3 Aerodynamic Drag Force - Stokes' Law

The force tending to resist the motion of a spherical particle in a still gas for the size range considered here is expressed by Stokes' Law as modified by Cunningham ie:

$$\hat{F} = - \frac{6\pi \mu \hat{v}_o a}{c} \quad (3 - 1)$$

$$\mu \equiv \text{gas viscosity} \quad \frac{(\text{N}\cdot\text{s})}{(\text{m}^2)}$$

$$a \equiv \text{particle radius} \quad (\text{m})$$

$$v_o \equiv \text{particle velocity} \quad \frac{(\text{m})}{(\text{s})}$$

$$c \equiv \text{Cunningham correction factor (dimensionless)}$$

This law applies provided the Reynolds number for the particle is less than 0.1 ie:

$$\text{Re}_p = \frac{2v_o a \rho}{\mu} \leq 0.1 \quad (3 - 2)$$

$$\rho = \text{gas density} \quad \frac{(\text{kg})}{(\text{m}^3)}$$

In addition to the restriction on the Reynolds number the following assumptions are normally made to ensure the validity of the law:

- a) Particle motion follows the motion of the gas i.e. acceleration time is negligible.
- b) Wall and boundary effects can be ignored.
- c) There is no interaction among particles.
- d) The particles are spherical.

The relative magnitudes of these factors have been considered elsewhere (16) and the results have shown that assumption a) can be safely accepted for particles below 10 μm diameter. The wall effects are very complex and even though they may have some minor importance for the case using dielectric collection media, when compared to other factors there appeared to be no real justification for considering them. The interaction among particles was completely negligible for the concentrations considered here. Corrections for particles which are not spherical have been given by various workers (17). However, since there are so many problems in applying these corrections to real dusts, the simpler assumption of pure sphericity appeared justified provided the limitations implied by the assumption were considered.

Finally, one other assumption was made in applying Stokes' Law by assuming that the resistance that the particle

experienced in moving through a still fluid could be extended to the case where the fluid was moving. Here the force could be thought of as a drag that the moving gas exerted on the particle.

Thus equation (3-1) can be written as:

$$\vec{F} = - \frac{6\pi\mu a (\vec{v}_0 - \vec{u}_0)}{C} \quad (3 - 3)$$

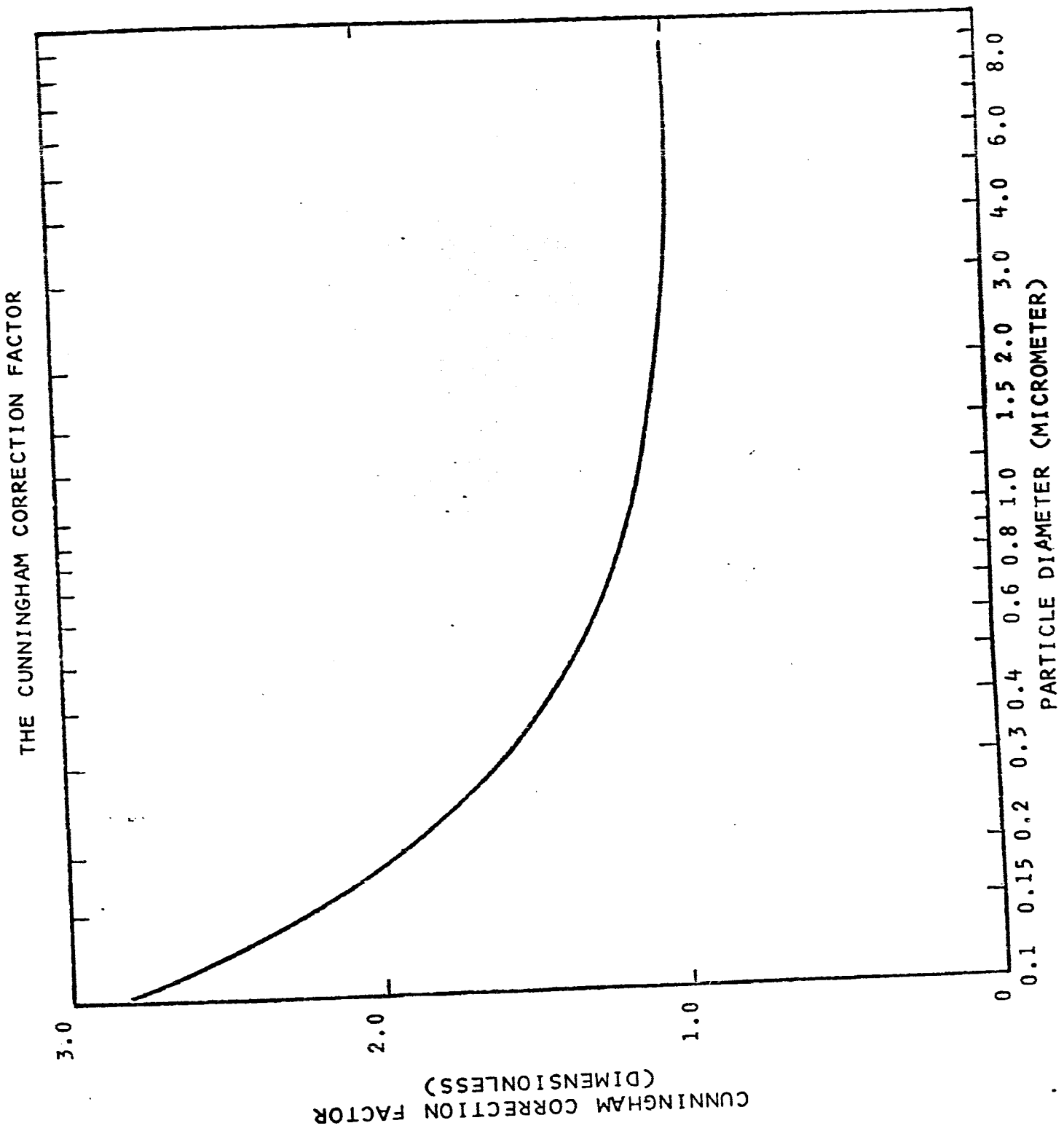
$$u_0 = \text{velocity of air stream } \begin{matrix} (\text{m}) \\ (\text{s}) \end{matrix}$$

For negligible acceleration times, $u_0 = v_0$ and the particle is entrained by the moving gas.

The Cunningham correction factor accounts for the slip which occurs due to the discontinuous nature of the gas when the particle size is of the same order as the mean free path of the gas molecules. Davies (18) has shown that for air at standard temperature and pressure.

$$C = \left[1 + \frac{8.3 \times 10^{-8}}{a} + \frac{2.6 \times 10^{-8}}{a} e^{-(1.66 \times 10^7 a)} \right] \quad (3 - 4)$$

Equation (3-4) is plotted in FIG. 3.1 and it is of interest to note that the Cunningham factor is extremely important for the particle size range which is considered here.



3.4 Mechanical Forces

The mechanisms governing the collection of particles in fibrous or granular type mechanical filters have been considered by many authors and although the theory of operation is by no means complete, a great deal of information is available in the literature. Normally in analysing an electrostatic precipitator the mechanical forces can be completely ignored since their magnitudes are small compared to the electrical force. (If the geometrical dimensions of the collector are much greater than the particle dimensions, the mechanical effects are usually negligible.) However, in certain of the cases considered here, ie: when dielectric media is used in the collection region, mechanical forces could play a part in the collection process and it is important to recognize the relative effects of the electrical and mechanical terms. It is interesting to note that since an electrical force acts only on the particle and not on the air stream as a whole, the resulting pressure drops in precipitators can be made very low. However, for the mechanical forces to operate it is necessary to move the whole air stream and the energy required to do this manifests itself as relatively high pressure drops. Therefore, it could be expected that in a unit combining both collection mechanisms, the pressure drop could be made intermediate between that of a precipitator and a fibrous filter.

The three phenomena generally regarded as being mechanical in nature are collection due to inertial impaction, interception and diffusion.

3.4.1 Inertial Impaction

When a particle is entrained in an air stream the force vector acts in the direction of the streamlines. However, if there is a sudden change in the direction of a streamline, the particle's inertia tends to resist the change in direction and as a result it can move across the streamline. If this occurs adjacent to a collection surface, it is possible for the particle to impact on the surface and be collected.

Ranz and Wong (5) have defined an inertial impaction parameter.

$$\Psi = \frac{C_p v_o d^2}{18\mu D_c} \quad (3 - 5)$$

This parameter expresses the ratio of the force necessary to stop a particle initially travelling at the velocity v_o , in the distance $D_c/2$ to the fluid resistance exerted on a particle travelling at a relative particle velocity v_o .

Since this is an inertial term it can be seen that the momentum of the particle is a main criterion for collection, coupled with the inverse of the collector diameter.

For a single fiber, a collection efficiency has been defined as:

$$\eta'_e = \frac{y_0}{D_c} \quad (3 - 6)$$

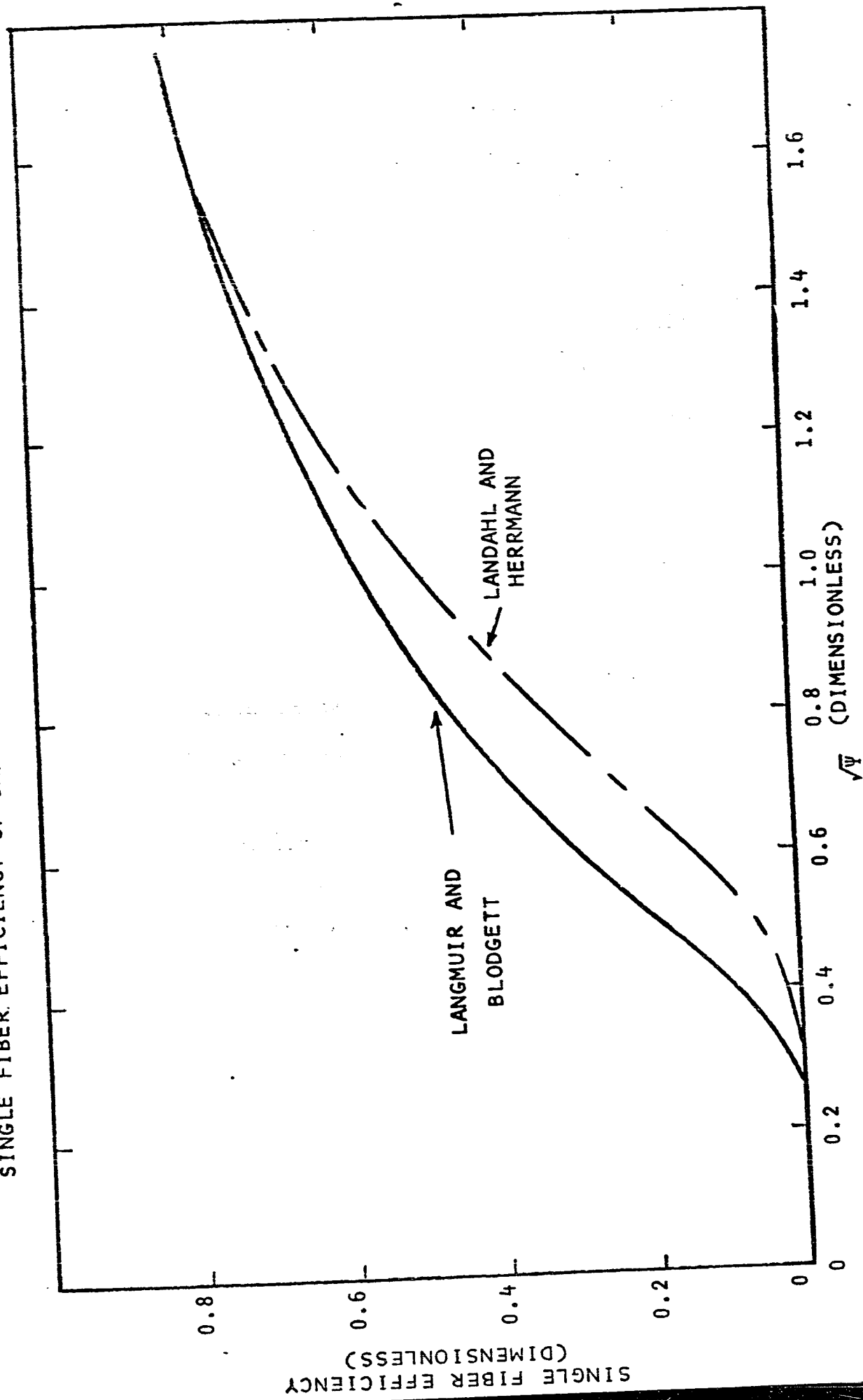
Where y_0 defines the limits of the original aerosol stream from which all particles of a given size are removed, and D_c is the diameter of the collecting cylinder.

Several relationships have been proposed to give the single fiber collection efficiency as a function of the impaction parameter. Strauss (19) shows the results of many investigators and points out that experimental results using cylindrical collectors suggest that the best estimate can be obtained by using values intermediate between the curve due to Landahl and Hermann based upon $Re_c = 10$ and that due to Langmuir and Blodgett who assumed potential flow. (See FIG. 3.2)

3.4.2 Interception

Particles are collected by interception when a particle in following a streamline around a collector touches the surface of the body. This occurs when the centre of a particle follows a streamline which lies closer to the cylinder than the radius of the particle. A dimensionless

FIGURE 3.2
SINGLE FIBER EFFICIENCY OF IMPACTION FOR SPHERES ON A CYLINDRICAL COLLECTOR



parameter characterizing this effect was also given by Ranz and Wong as:

$$R' = \frac{d}{D_c} \quad (3 - 7)$$

It can be seen that whereas the mass of the particle was of prime concern in the inertial term, here it is the size of the particle that is important. Under the assumption of ideal flow they showed that for a single cylindrical collector

$$\eta_I' = (1 + R') - \frac{1}{(1 + R')} \quad (3 - 8)$$

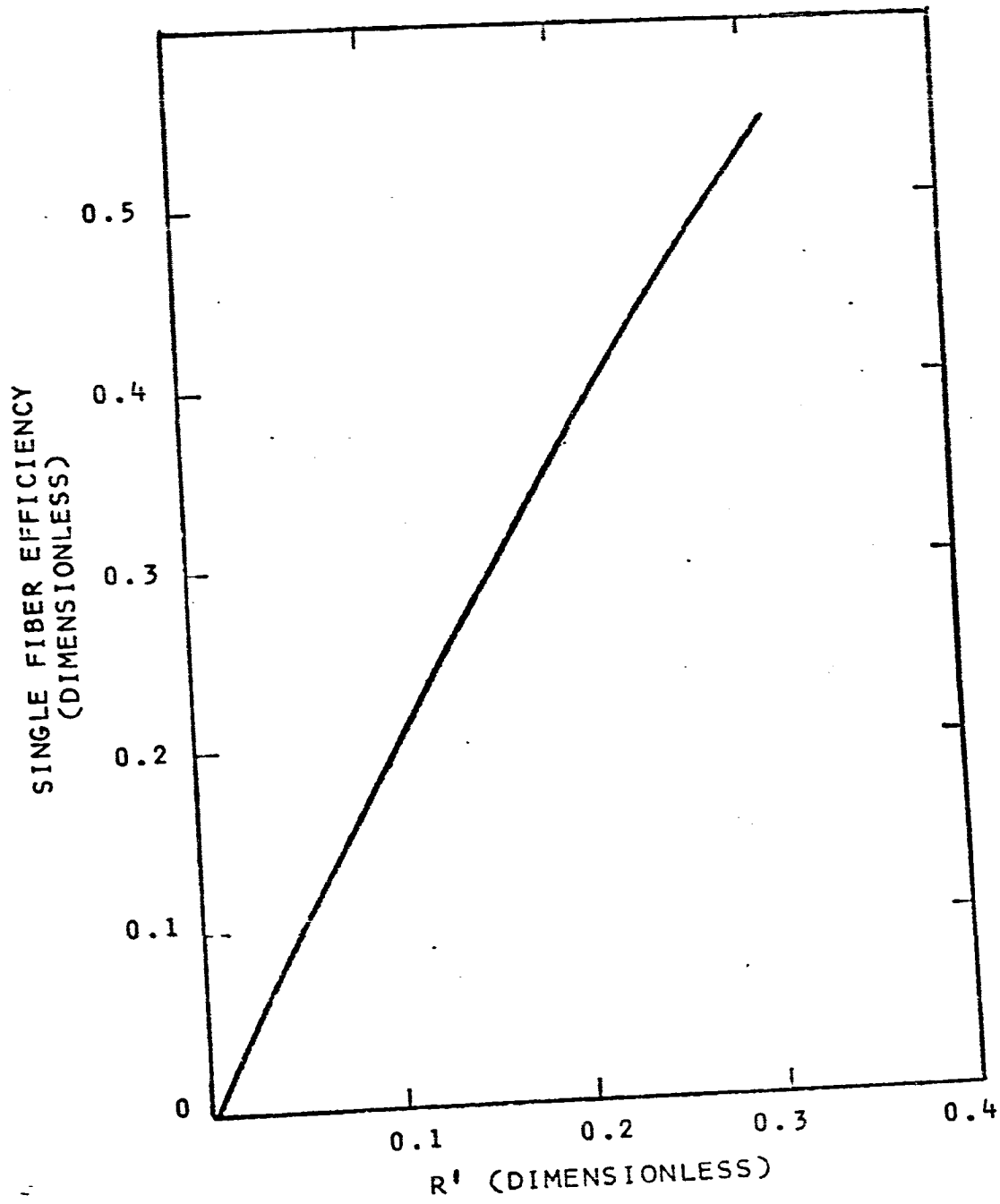
This relation is shown in Fig. 3.3 and it can be seen that for small values of R' , $\eta_I' \doteq 2R'$.

3.4.3 Combined Effects

Because of the complex nature of the above phenomena, various approaches have been made in determining the actual total collection efficiency of a fiber. For instance, it is recognized that the inertial and interference effects are interrelated and that if a particle is caught by one mechanism it cannot be caught again by a second. Moreover, the relative effects are a function of the Reynolds number calculated with respect to the collecting cylinder. However, for cases where the magnitude of each efficiency term is ≤ 0.1 , a good approximation is to add the individual

FIGURE 3.3

SINGLE FIBER EFFICIENCY OF
INTERCEPTION FOR SPHERES ON
A CYLINDRICAL COLLECTOR



efficiencies found in the previous sections to form a total single fiber efficiency (19):

$$\eta' = \eta_e' + \eta_I' \quad (3 - 9)$$

to be consistent with the results developed in later sections it was found convenient to define this collection in terms of a mechanical collection parameter, K_m , such that;

$$K_m = \frac{\eta'}{\pi} \quad (3 - 10)$$

3.4.4 Diffusion

The importance of particle collection due to Brownian diffusion has been the subject of much study and there is conflicting evidence on its importance in fiber filters, (24), (25). However, the available results would indicate that this mechanism was completely negligible for the cases of particle size, air flow, and collector diameters considered here.

The effect of eddy diffusion due to the turbulent nature of the air stream is a subject of considerable interest in recent publications dealing with single stage precipitators. Robinson (26) has reviewed the main contributions and shows the different approaches which have been taken to treat the effect of diffusivity. The emphasis in these studies has been on the form of the concentration

profile of the dust under the simultaneous influence of the coulomb force and turbulent re-mixing, with additional complications due to the electric wind and re-entrainment. However, these factors appeared to be unimportant in a two-stage precipitator such as the one considered here since the conditions affecting the problem were on a much smaller scale than in the larger one-stage units. For this reason, the traditional argument regarding turbulent mixing due to White (27) was assumed. (ie: the effect of the turbulent eddies was to continuously remix the particles in the air stream to produce a constant concentration profile.)

3.5 Electrostatic Forces

Kraemer and Johnstone (6) have solved the general problem of the electrostatic forces which can exist between a charged particle and a charged collector. This was further discussed by Dawkins (7) in his analysis of the electrostatic forces as they affect the deposition on cylindrical shapes in potential flow. These studies have shown that there are at least five different force components, of electrostatic origin, which can influence the particle trajectories ie:

a) Coulomb Force

When a charged particle is under the influence of an external electric field, the coulomb force tends to move the particle in a direction such that a positive charge moves in the direction of the field lines. (By

convention, field lines are assumed to be directed from positive to negative).

b) Image Force

When a charged particle approaches any metallic or dielectric surface it induces an opposite charge which tends to attract the particle to the surface.

c) Dielectrophoretic Force

When an uncharged dielectric or metallic particle is subject to a non-homogeneous electric field, a dipole is induced in the particle by the field and a net force acts on the particle in the direction of the increase of field density.

d) Space Charge Force

When a charged particle is one of a cloud of like charged particles, the cloud as a whole gives rise to a field which tends to repel the particle away from the cloud.

e) Induced Space Charge Force

When a cloud of charged particles occupies a volume near a dielectric or metallic surface, the cloud can induce a net charge on the surface which can act to attract individual particles towards the collector.

The coulomb force is well known and is considered in

traditional precipitator analyses as it is by far the most important in conventional cases. The image and dielectrophoretic forces are often ignored as most precipitators are not designed to utilize these components. However, as will be seen in what follows, by appropriate design of the collectors these forces can have an effect on the collection process. The two forces which depend upon space charge can be ignored in the work considered here as the charge densities which are used are far below that required to produce measurable effects. However, it is of interest to note that by proper design, precipitators can be built utilizing only the space charge as the collection field and several recent developments have demonstrated this (20), (21).

The three most important forces for the present work will now be discussed in a quantitative way.

3.5.1 Coulomb Force

When the particle which is charged is small and has its charge distributed over its surface, it can be considered to be a point charge having the total charge concentrated at its center. The force acting on a point charge in an electric field is a basic electrostatic definition as given by Coulomb's Law:

$$\vec{F}_c = q \vec{E}$$

$$\begin{aligned}
 F_C &\equiv \text{coulomb force (N)} \\
 q &\equiv \text{charge on particle (C)} \\
 E &\equiv \text{electric field strength } \frac{(V)}{(m)}
 \end{aligned}$$

It is readily seen that the magnitude of this force depends both upon the charge placed on the particle and the field to which it is subjected. In order for precipitation to occur, the force must be of sufficient magnitude to ensure capture and the direction of the force vector must be towards the collection surface. The relative effect of the coulomb force compared to the aerodynamic force acting on the particle is given by the dimensionless collection parameter K_C

where:

$$\begin{aligned}
 K_C &\equiv \text{coulomb collection parameter} \\
 &= \frac{\text{coulomb force}}{\text{Stokes-Cunningham drag force}} \\
 K_C &= \frac{q E C}{6\pi\mu a v_o} \qquad (3 - 12)
 \end{aligned}$$

For all conditions considered in this thesis,

$$\begin{aligned}
 \mu &= 1.8 \times 10^{-5} \frac{(N \cdot s)}{m^2} \\
 K_C &= 2.94 \times 10^3 \frac{q E_p C}{a v_o} \qquad (3 - 13) \\
 E_p &= \text{collection field at surface } \frac{(V)}{(m)}
 \end{aligned}$$

3.5.2 Image Force

The attractive force caused by a charged particle inducing an opposite charge in a metallic or dielectric plane of infinite extent is well known and is given by:

$$\vec{F}_I = - \frac{(\kappa'_C - 1)}{(\kappa'_C + 1)} \frac{q^2}{4\pi\epsilon_0 (2r)^2} \hat{r} \quad (3 - 14)$$

r \equiv distance of particle from surface (m)

\hat{r} \equiv unit vector measured from the surface towards the particle (dimensionless)

Note the force varies inversely as the square of the distance from the surface. For this reason, this force is very short range and its main effect is often considered to be an aid to the final capture rather than a capture mechanism of any importance in itself.

For the case of a point charge and cylindrical collector, image theory cannot be used because of the non-symmetrical configuration and a series solution is required. However, with the assumption that the collector diameter is much larger than the particle diameter Kraemer and Johnstone (6) have shown that the image theory can be applied and that at the surface of the collector the attractive force is approximately given by:

$$\vec{F}_I = - \frac{(\kappa'_C - 1) q^2 \hat{r}}{\pi \epsilon_0 D_C^2 (\kappa'_C + 1)} \quad (3 - 15)$$

Which gives an image collection parameter;

$$K_I = \frac{\beta q^2 C}{6\pi^2 \epsilon_0 \mu a v_0 D_C^2} \quad (3 - 16)$$

Where

$$\beta = \frac{\kappa'_C - 1}{\kappa'_C + 1}$$

For all cases considered here

$$\mu = 1.8 \times 10^{-5} \frac{(N \cdot s)}{(m^2)}$$

$$K_I = 1.06 \times 10^{14} \frac{\beta q^2 C}{a v_0 D_C^2} \quad (3 - 17)$$

3.5.3 Dielectrophoretic Force

The force exerted by an electric field on a dipole is well known and is given by (55);

$$\vec{F} = \nabla (\vec{P} \cdot \vec{E})$$

For the particular case of an uncharged particle under the influence of an external electric field, the magnitude of the induced dipole is given by (56);

$$\vec{p} = 4\pi\epsilon_0 \left(\frac{\kappa_p' - 1}{\kappa_p' + 2} \right) a^3 \vec{E} \quad (3 - 18)$$

Therefore, the expression for the dielectrophoretic force can be written as;

$$\vec{F}_d = 4\pi\epsilon_0 \left(\frac{\kappa_p' - 1}{\kappa_p' + 2} \right) a^3 \nabla(\vec{E} \cdot \vec{E}) \quad (3 - 19)$$

Here it can be seen that the magnitude of the force depends upon the dielectric constant of the particle, the volume of the particle and, most important, both the field strength and the field gradient. Note that net particle charge is not considered in this force component. The case of the cylindrical collector is of most interest in practice and the analysis for this is given in Appendix A. For the ideal case of a single collector in an initially uniform field the average collection parameter is given by equation A - 10

$$\bar{K}_d = 2.61 \times 10^{-6} \frac{(\kappa_p' - 1)}{(\kappa_p' + 2)} \frac{\beta^2 a^2 E_o^2 C}{\bar{v}_o D_c} \quad (3 - 20)$$

3.6 Efficiency of Collection

The prediction of the collection efficiency is one of the problems of basic interest in any filter analysis. In studying a unit where both mechanical and electrostatic forces may be important, care must be used in the approach used in the analysis. For instance, in the past both electrostatic precipitators and fibrous filters have been extensively studied and general equations for their efficiency have been derived. However, because of the obvious differences between the filters, the approaches used in each case has tended to be different.

Electrostatic precipitator analyses have used as a figure of merit, the so-called "migration velocity" of a particle. This is defined as the velocity with which a particle moves towards a collecting surface under the influence of the electric coulomb force. Having defined this parameter, the efficiency equation for the standard precipitator then becomes a function of the particle residence time in the precipitator, the area available for collection, etc. Deutsch (28) in 1922 showed these factors were related by an exponential relation which can be expressed as:

$$\eta = 1 - e^{-\frac{wA_c}{Q}} \quad (3 - 21)$$

- w \equiv migration vel (m/s)
 A_c \equiv collection area (m²)
 Q \equiv total air flow (m³/s)

Modern theories for precipitators have recently been reviewed by Robinson (26) and in general they agree with the form of the Deutsch equation. The main differences that do exist among the theories concern the relative importance of such factors as the effect of eddy diffusivity, re-entrainment, the electric wind, the form of the cross sectional dust concentration profiles and most important, the effect of these factors on the validity of the concept of migration velocity. However even though experimental results often require an empirical modification for the value of the migration velocity, in general they have all confirmed the exponential form of the equation. Hence the basic problem reduces to finding the functional form of the exponent.

The analysis of fibrous filters, on the other hand, has evolved around the determination of the mechanical "single fiber efficiency", generally expressed in terms of the collection parameters mentioned previously. Knowing the collection for one fiber, the efficiency equation becomes a function of the total number of fibers per cross sectional area, the air velocity, thickness of filter etc. Ignoring complications such as the interference effect, unequal particle mixing, and fiber orientation, it can be easily

shown (13) that the efficiency equation is again exponential having the general form:

$$\eta = 1 - e^{-\eta' D_c L'} \quad (3 - 22)$$

η' \equiv single fiber efficiency (dimensionless)
 D_c \equiv diameter of collecting fiber (m)
 L' \equiv total length of fiber in filter/unit
 filter face area. (1/m)

The only difference between equations 3 - 21 and 3 - 22 is the form of the exponent. Several attempts have been made (see for example Gillespie (8)) to modify the fibrous filter equation to account for the electrostatic forces acting in conjunction with mechanical forces. However, because of the importance of the interference effects etc. as mentioned above, the problem is very complex and agreement between theory and experiment has not been as good as with conventional electrostatic precipitators.

Since the filter considered here is primarily an electrostatic precipitator and the dielectric media acts mainly to increase the area available for collection, it was felt that the best approach in determining the total collection efficiency was by appropriate modification of the existing theories for precipitators.

This is the approach used in section 5.1.

3.7 The Positive Corona Discharge in Air

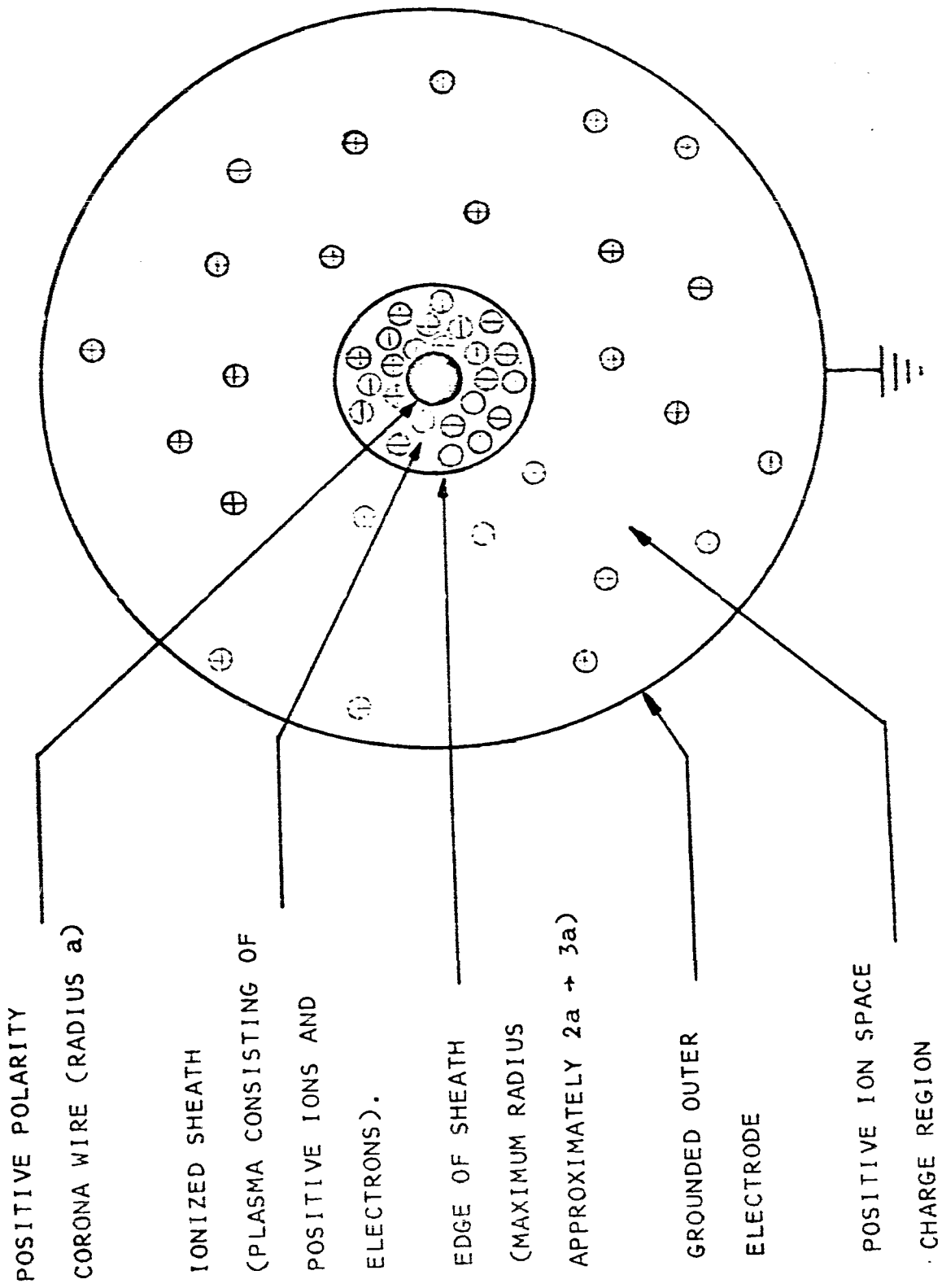
The mechanisms governing the positive corona discharge in co-axial cylindrical geometry were first studied by Townsend (29) and more recently have been further discussed by Loeb (30). The practical application of the corona discharge to the charging of particles in electrostatic precipitation is covered in detail by White (31). However, White's main emphasis is on the negative corona in one stage industrial precipitators where the ozone production is not considered a problem.

The positive corona discharge consists of two distinct regions, as illustrated in Fig. 3.4.

The ionized sheath is a region very close * to the wire where the divergent field strength exceeds that required to cause breakdown of the air. Hence, the gas becomes highly ionized and contains positive ions and electrons. Since the wire is positively charged, all the electrons are accelerated towards it and the positive ions are repelled radially outwards to the outer cylinder. The motion of the charged ions gives rise to the corona current. In addition to producing the current, the ions have a space charge associated with them which acts to limit the current flow and stabilize the

* At atmospheric pressure the thickness of this sheath is a function of the current density and wire diameter and could reach a value equal to the wire diameter.

FIGURE 3.4
CYLINDRICAL POSITIVE CORONA DISCHARGE



discharge. Hence the name "positive ion space charge region". Loeb (32) points out that after the start of the corona discharge, the voltage drop across the ionized sheath remains constant. As the applied voltage increases, the ion concentration increases and the excess potential is absorbed by the resulting increased space charge. Townsend has calculated the value of the critical field strength required to produce corona and has shown that it is a function of the radius of curvature of the wire (see for example Cobine (33)). For smooth round wires at standard temperature and pressure this is given by the expression *:

$$E_c = \left(300 + \frac{9}{\sqrt{a}} \right) \times 10^4 \text{ V/m} \quad (3 - 23)$$

This is the field strength which exists at the surface of the wire at corona onset. However, the field strength of the outer extreme of the ionized sheath must be approximately equal to 3×10^6 V/m which is the value of field at which cumulative ionization ceases. Since the thickness of the sheath is very small, it can be assumed that the average field strength in the ionized region will be approximately

* Cobine also mentions the expression derived semi-empirically by Peek which gives

$$E_c = \left(310 + \frac{9.55}{\sqrt{a}} \right) \times 10^4 \text{ V/m}$$

Note that this has the same form as equation 3-23 differing only slightly in the constants used. The results derived here are unaffected if this is used instead, the only change being a slightly different value for the constant G which appears in a later section.

given by:

$$E_{av} = \frac{E_c + 3 \times 10^6}{2} = \left(300 + \frac{4.5}{\sqrt{a}}\right) \times 10^4 \text{ V/m} \quad (3 - 24)$$

Therefore the voltage drop across the sheath can be written as

$$V = E_{av} \cdot \Delta a \quad (3 - 25)$$

Before the onset of the corona discharge the radial field distribution is given by the electrostatic formula for concentric cylinder electrodes i.e.

$$E_r = \frac{V_0}{r \ln \frac{R_1}{a}} \quad \frac{V}{m} \quad (3 - 26)$$

However, once the discharge begins, the radial field strength is modified due to the space charge effect of the ions (34) and the field is described by:

$$E_r = \sqrt{\frac{J}{2\pi\epsilon_0 K} + \left(E_c \frac{r_c}{r}\right)^2} \quad \frac{V}{m} \quad (3 - 27)$$

For the normal case of moderate corona currents and $r_c \doteq 2a$ to $3a$ it can be seen that over a large portion of the cross section the radial field is approximately constant and is given by:

$$E_r \doteq \sqrt{\frac{J}{2\pi\epsilon_0 K}} \quad \frac{V}{m} \quad (3 - 28)$$

For positive air ions at atmospheric pressure the mobility
K is approximately $1.8 \times 10^{-4} \frac{\text{m}^2}{\text{s.V}}$

Therefore

$$E_r = \sqrt{J} \times 10^7 \frac{\text{V}}{\text{m}} \quad (3 - 29)$$

Since the corona current is the normal parameter
that is measured and yet E_r is needed to calculate the
charging of particles, equation 3 - 29 is shown in graphical
form as Fig. B.1 in Appendix B.

3.7.1 Particle Charging

Two separate phenomena can cause the charging of particles in a corona discharge and are known as "field charging" and "diffusion charging" respectively.

Field charging occurs as a result of field lines converging on a dielectric or conducting particle. This causes ions to bombard the surface until the resulting charge is strong enough to cancel the effect of the external field and hence the charge reaches a saturation value. This mechanism predominates for particle sizes larger than approximately $1.0 \mu\text{m}$ diameter. Diffusion charging, on the other hand, occurs because of the random collisions which can take place between the particle and the ions. This is the main effect for particles below about $0.2 \mu\text{m}$ diameter. However, between these two size limits both field and diffusion charging must be considered. It happens that this is a very critical size range; at atmospheric pressure the change in the charging mechanisms, plus molecular slippage, results in a predicted minimum in the electrical mobility for particles approximately $0.2 \mu\text{m}$ diameter (35).

Various approaches have been taken to the problem of charge prediction, ranging from simple addition of the two charge components due to each effect (6) to numerical solution of the differential equations governing the charging rates (36). Also several authors have shown that, even for

particles previously thought to be influenced only by diffusion effects, the strength of the electric field in the charging region can play a very important role. (35) (37).

Cochet (38), has derived an expression which is a modification of the classical field charging equation as originally derived by Pauthenier and accounts for the diffusion effect by means of a correction factor. The validity of the formula was checked by Cochet over the size range 0.04 μm diameter to 1.0 μm diameter with positive polarity corona charging at field strengths normally encountered in practice. Above 1 μm diameter the formula reduces to the classical equation. Therefore, this expression which is given as equation 3 - 30 is used to estimate the charge magnitudes for all cases considered in this thesis.

Cochet's Formula

$$q_s = 4\pi\epsilon_0 \alpha E a^2 \quad (C) \quad (3 - 30)$$

Where:

$$\alpha \equiv \text{correction factor}$$

$$= \left(1 + \frac{\lambda}{a}\right)^2 + \frac{\left(\frac{2}{1 + \frac{\lambda}{a}}\right) \frac{(\kappa'_p - 1)}{p}}{(\kappa'_p + 2)} \quad (3 - 31)$$

$$\lambda \equiv \text{mean free path of air ions}$$

Equation 3 - 30 gives the saturation charge for the particle. To account for the finite charging time, a time constant has been introduced such that the actual charge is given by:

$$q = q_s \left(\frac{t}{t + \tau} \right) \quad (3 - 32)$$

where $\tau \equiv$ time constant $= \frac{4\epsilon_0}{N K}$

For the co-axial geometry as found here in the corona discharge, the current density;

$$J = 2\pi r N K E_r \quad \frac{A}{m} \quad (3 - 33)$$

and it can be easily shown that:

$$\tau = \frac{4r}{E_r K} \quad (3 - 34)$$

Alternatively, for particles moving with an average axial velocity v_0 in the x direction into the charger, a distance X_0 can be defined such that $v_0 \tau = X_0$ and equation 3 - 32 can be expressed as:

$$q = q_s \left(\frac{x}{x + X_0} \right) \quad (3 - 35)$$

The correction factor α is seen to be a function of both the particle radius and the relative permittivity of the material. This relation is shown in Fig. B.2, Appendix B with $\lambda = 9.4 \times 10^{-8}$ m as given by Cochet. With this expression and $\kappa'_p = 11$ the relation between particle saturation charge, particle size and charging field strength is given

in Fig. B.3 Appendix B.

Coulomb Collection Parameter

For the case of a cylindrical geometry corona discharge, $E = E_r$ in equation 3 - 30. Therefore, assuming a particle charged to saturation, the coulomb collection parameter given as equation 3 - 13 can be written as:

$$K_C = 3.27 \times 10^{-7} f(a) \frac{E_r E_p}{v_o} \quad (3 - 36)$$

where

$$f(a) = a \alpha C \quad (3 - 37)$$

$$= a \left[\left(1 + \frac{\lambda}{a}\right)^2 + \frac{\left(\frac{2}{1 + \frac{\lambda}{a}}\right) \left(\frac{\kappa'_p - 1}{\kappa'_p + 2}\right)}{1} \right]$$

$$\left[1 + \frac{8.3 \times 10^{-8}}{a} + \frac{2.6 \times 10^{-8} e^{-1.66 \times 10^7 a}}{a} \right]$$

This expression $f(a)$ describes the form of variation of the collection parameter as a function of a and κ'_p and is shown in graphical form in Fig. B.4 Appendix B. Note that a minimum appears in the curve at approximately $0.3 \mu\text{m}$ diameter.

3.7.2 Ozone Generation

Penney (2), White and Cole (39), and Lagarias (40) among others, have discussed ozone generation in electrostatic precipitators. Some design criteria which have been established to minimize the formation of ozone, include the following:

- a) Use of positive polarity corona rather than negative.
- b) Use of a two-stage design where the charging and collection functions are separated.
- c) Use of smooth, round, corona wire of the smallest possible diameter compatible with mechanical strength.
- d) Use of the lowest possible corona current compatible with satisfactory collection efficiency.
- e) Use of the maximum air flow rate compatible with satisfactory collection efficiency.
- f) Elimination of any stray discharges such as may occur due to end effects, sharp points or edges etc.

In addition, it is known that the ozone concentration in air is influenced by the presence of other molecular species such as hydrocarbons and water vapour.

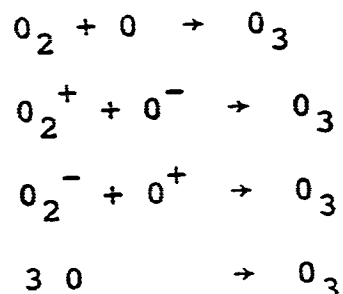
Considering the importance of the problem, very little

has been published of a quantitative nature concerning the ozone generation in positive corona electrostatic precipitators. (On the other hand, commercial ozonizers have been subject to much more attention in the literature (41). The object there, of course, is to maximize the ozone production).

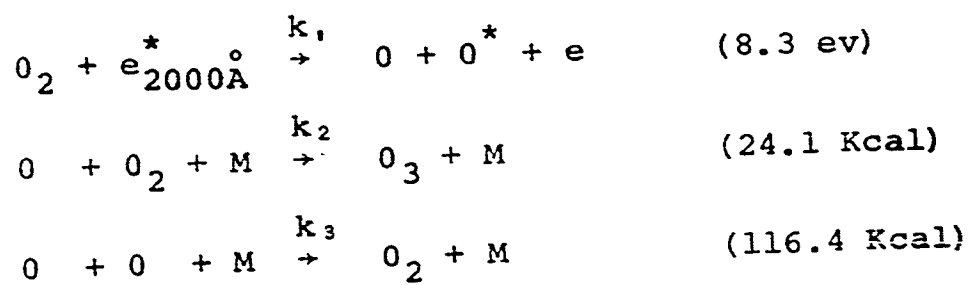
The formation of ozone in an electrical discharge is not completely understood as there are many possible reactions which could create the O_3 molecule (42). However, some general principles can be discussed concerning the electrochemistry of a gaseous reaction.

The electrical discharge, which occurs in the ionized sheath immediately surrounding the corona wire, initially generates ions. (At corona onset some free electrons are accelerated in the high field and collide with neutral air molecules. If the electrons have enough energy they generate electron-positive ion pairs by impact ionization.) However, in addition it is known that various short-lived species of particles are generated by a series of secondary reactions. These may be gaseous ions with positive and negative charges, free atoms, or radicals, and may be in the fundamental or electronically excited state. These particles are very reactive, and include all possible species of oxygen required for the formation of ozone. The resulting reactions are known to be influenced by the catalytic action of foreign substances such as neutral gas molecules, container walls

etc. Also, further complications occur because of local temperature effects and ultraviolet radiation emitted as a result of the ionization. Theoretically, ozone could be formed from any one of the following reactions.



The most probable reaction is thought to consist of the following (43).



Where k_1 , k_2 and k_3 are reaction constants and M represents a neutral energy absorbing molecule.

Thus although the dominant form of the reaction occurring in the discharge cannot be predicted with complete accuracy, on the basis of the above considerations the following assumptions have been made regarding the ozone formation;

a) since the ionized sheath represents the most chemically active region in the discharge, it is assumed that

the ozone production takes place entirely within the ionized sheath.

b) because of the existence of the most energetic electrons immediately adjacent to the wire surface and the probable function of this surface as a catalytic reaction site, it is further assumed that most of the ozone is formed very close to, or even at, the surface of the wire.

Experimental evidence supporting both these assumptions has been found. Burgess (45) took measurements of ozone concentration as a function of radial position from the wire. Under laminar flow conditions they showed maximum concentration near the wire with a very rapid drop off as the probe was withdrawn. The importance of the wire surface will be discussed in section 6.4 where measurements have shown that the ozone generation for a given wire increases as surface oxide forms on the wire.

The major constituents of air are oxygen and nitrogen. However, because it requires less energy to ionize an oxygen molecule than a nitrogen molecule, the majority of the ionized species in air will be due to the breakdown of oxygen. This explains one reason why the ozone production from a corona discharge is a serious problem, whereas the generation of oxides of nitrogen, which are also noxious, is so minute that it can usually be ignored.

Experience with ozonizers has shown (44) that the

amount of ozone produced per unit time is a direct function of the amount of electrical power which is dissipated in the discharge. It is reasonable to expect that a similar relationship should exist in a corona discharge: i.e., for a given wire size, relative humidity, temperature, and pressure we could expect:

$$[O_3] \cdot Q = [O_3]' = B(a) \cdot (\text{Power dissipated in ionized sheath}) \quad (3 - 38)$$

which can be written using equation 3 - 25.

$$[O_3]' = B(a) \cdot V I = B(a) \cdot (E_{av} \cdot \Delta a) I \quad (3 - 39)$$

Note that $B(a)$ the proportionality factor is dimensionless because a given volume of ozone can be represented by the energy required to form it.

CHAPTER 4

TEST PROCEDURES

4.1 Experimental Apparatus

4.1.1 Air Supply

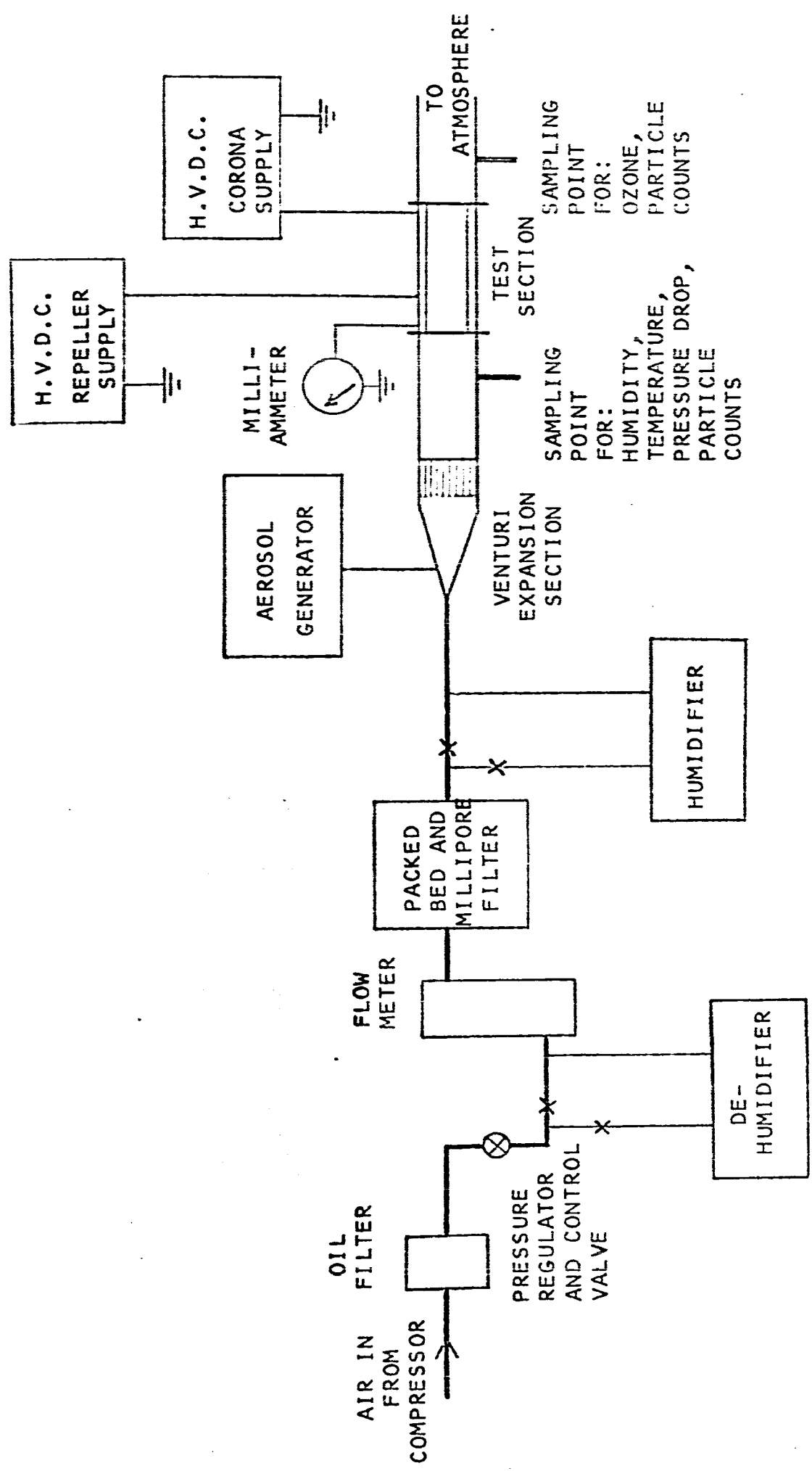
The air system used in all the experimental work is shown in outline form in Fig. 4.1.

Air was supplied by the buildings' central compressor system which used outside air as its source. To eliminate pressure fluctuations caused by compressor cycling, the air was passed through a pressure regulating valve at the inlet to the system. This maintained the pressure at 60 ± 0.5 psig.

Oil from the compressor and water droplets from the air line were removed by means of a commercial oil filter. The air temperature was that of the ambient and ranged from $20^\circ \rightarrow 26^\circ\text{C}$ throughout all of the tests. The humidity could be varied by means of an in-line dryer and evaporative type humidifier over a range from 2% \rightarrow 85% R.H. Air flow was monitored with a rotameter and could be accurately varied over the range 1.9 \rightarrow 9.5 l/s (4 \rightarrow 20 S.C.F.M.). The air was cleaned of particulate matter by two stages of filtration. The first was a deep filter bed consisting of a drum

FIGURE 4.1

FLOW DIAGRAM OF TEST SET UP



packed tightly with "Viskonaire"* filter media. This was followed by a specially built unit providing 0.12 m^2 of millipore filter area having a pore size $0.1 \mu\text{m}$. The air quality achieved met the Class 100 standard as specified by the American Federal Standard #209 (49). This clean air was then passed through a venturi expansion section, where the aerosol was added from the aerosol generator, and through a flow straightener to the main test duct. The test duct consisted of a 4" diameter acrylic tube, flanged to receive removable test sections. Appropriate sampling points for particulates, ozone, pressure, humidity and temperature were provided in this section. Following the test section, a short length of duct provided similar monitoring points and led to a flexible tube which exhausted the air to the atmosphere.

4.1.2. Aerosol Generator

Two types of aerosol generation were used in the present studies. The first consisted of a commercial D.O.P. atomizer** which produced a dense smoke consisting of Dioctyl Phthalate droplets. These droplets were polydisperse with a median diameter of approximately $0.3 \mu\text{m}$.

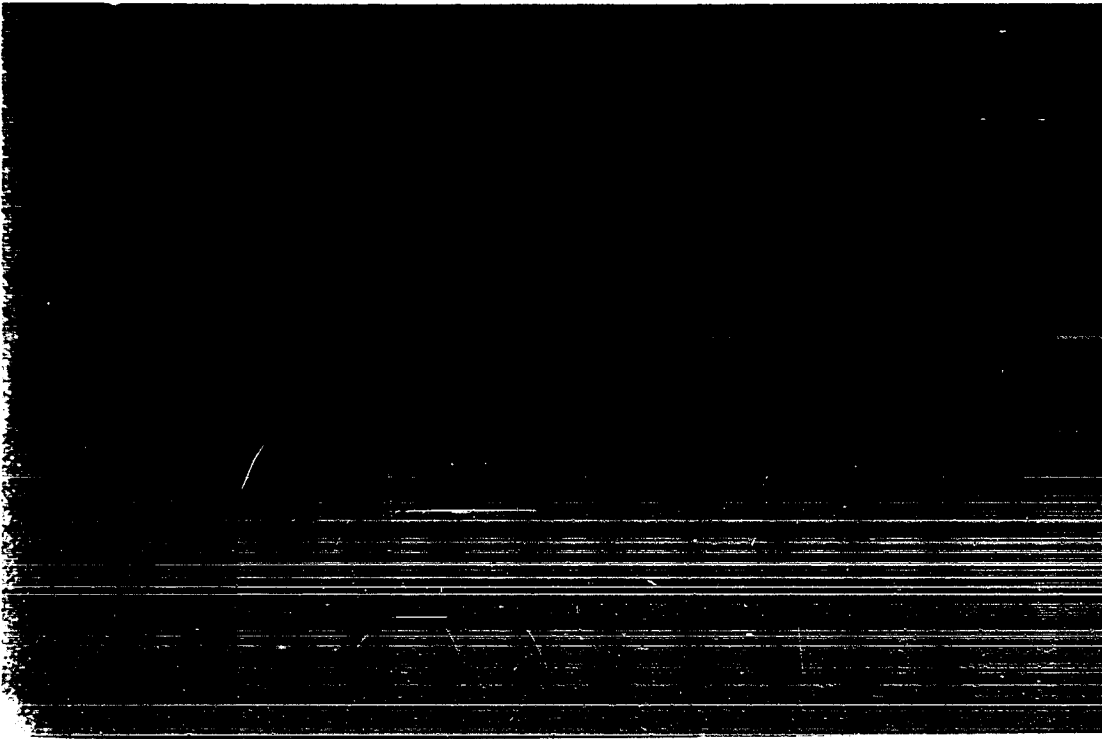
The second generator was an adaptation of another commercial unit and was based upon a Vaponefrin type nebulizer.

* Registered trademark, Johnson & Johnson Limited.

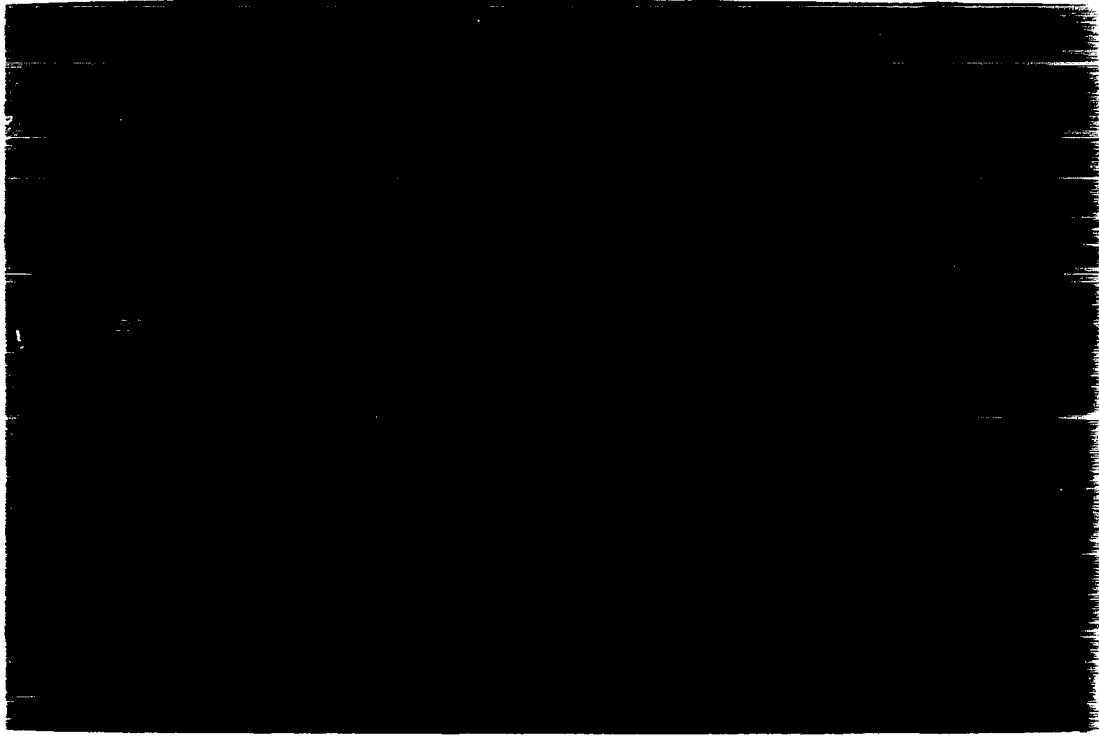
** Royco Model WA Smoke Generator.

Here particulates, preselected as to size and material, were placed in suspension in distilled water. The mixture was then atomized in the nebulizer and the water evaporated by mixing with dry air. The concentration of the aerosol could be controlled by adjusting the percentage of particulates in the water mixture and also by the air flow used. This unit offered more flexibility than the D.O.P. unit and hence was used for the majority of the tests.

To ensure the particles stayed in suspension while in the nebulizer, an agitating tube was added to the system which allowed clean air to bubble through the liquid and prevent settling (see FIG. 4.2). The drier tube provided intimate mixing of a relatively larger volume of dry air with the atomized particles. From here the drying process continued in the mixing sphere and ensured that all the moisture was in the vapour state. In addition, this large volume acted as a buffer between the nebulizer and entry port to the system. This helped to counteract any short term variation in the atomization which could change the aerosol concentration, (eg.) refilling the nebulizer. It is known that any atomization process can give rise to charge separation and hence the possibility that the particles may have finite positive or negative charges. To eliminate any variation due to this cause, the aerosol was passed through a region subjected to low energy alpha radiation to ensure the particles were discharged prior to entry into the test



NEBULIZER



MIXING SPHERE

FIGURE 4.2
AEROSOL GENERATOR



duct. The nebulizer had approximately a 90 minute capacity before refilling was necessary. As a result of the precautions taken to ensure stability the aerosol concentrations could be maintained over long test periods. As an example, Table 4-1 shows the results of particle counts taken at two hour intervals throughout an eight hour period where each figure represents an average of three counts.

4.1.3 Particle Counter

All the collection efficiency measurements taken in this study were based upon particle analysis using a light scattering particle counter* which could count the number of particles in a sampled volume in incremental size ranges extending from 0.15 \rightarrow 6.0 μm diameter. The principle of operation and details of this instrument can be found in the operating manual (50).

Primary calibration of the counter was carried out periodically using monodisperse spherical latex particles. A sample calibration run is shown in FIG. 4.3. The particles** used here had a mean diameter of 0.796 μm with a standard deviation of 0.0083 μm .

It can be seen from the graph that a distinct maximum was produced with over 50% of the counts recorded

* Royco Model 202 Particle Counter, Royco Instruments Inc. Menlo Park, California.

** Obtained from Dow Chemical Company.

AIR FLOW 4.72 L/S
 PARTICLES KAOLIN
 SAMPLING TIME 0.3 MIN.
 SAMPLING RATE 300 CC/MIN.

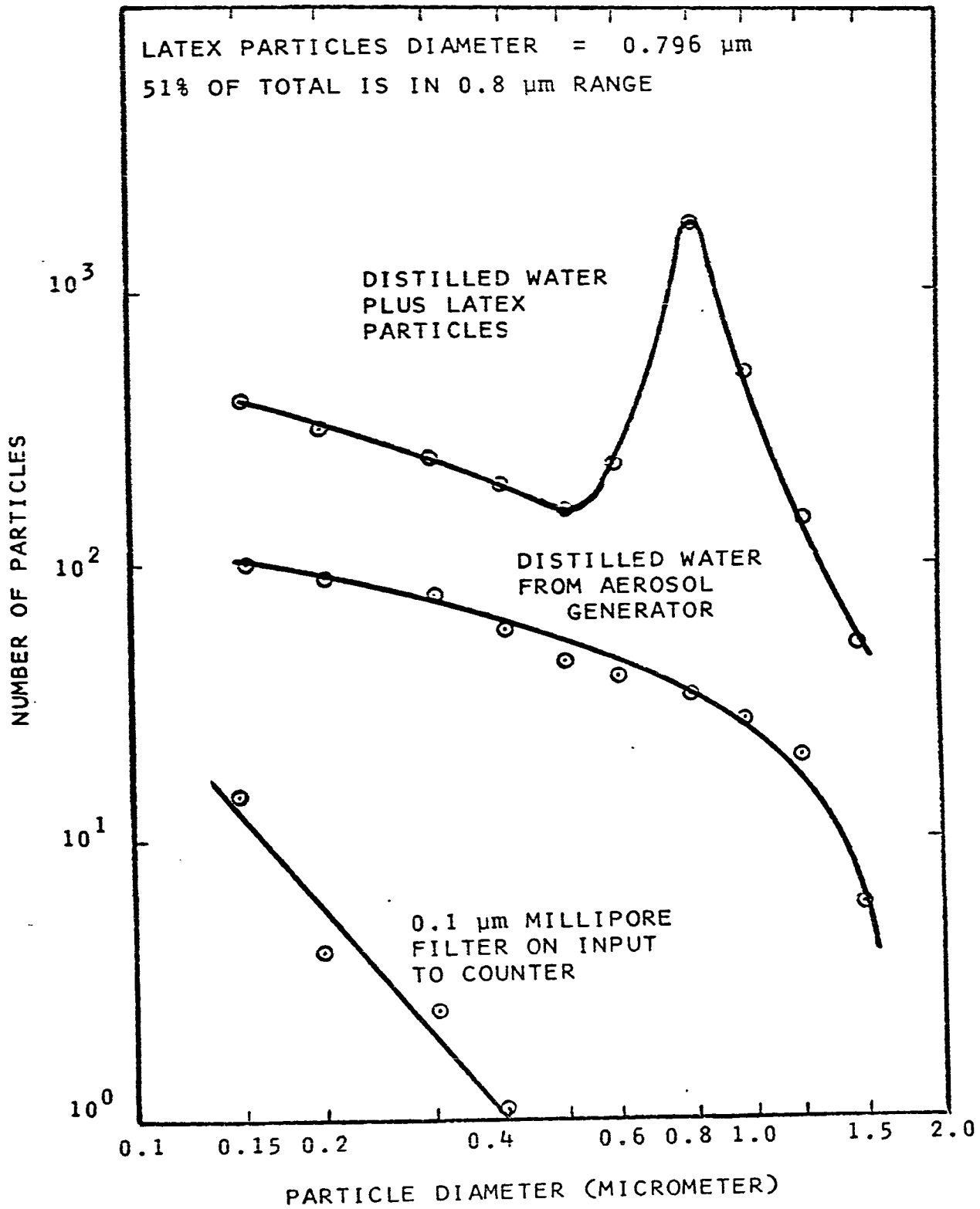
TABLE 4.1

RANGE OF COUNT VARIATION
 FROM AEROSOL GENERATOR

DATE: NOVEMBER 4, 1966

PARTICLE SIZE (μm)	PARTICLE COUNTS								AVERAGE	STANDARD DEVIATION	STANDARD DEVIATION AVERAGE
	0 HOURS	2 HOURS	4 HOURS	6 HOURS	8 HOURS	8 HOURS	8 HOURS	8 HOURS			
.15	1058	1001	1051	1012	1084				1040	31	3 %
.2	1034	1025	979	978	958				995	28	2.8%
.3	964	1000	1034	960	1008				990	28	2.8%
.4	933	987	926	887	948				937	33	3.5%
.5	822	862	788	863	842				835	28	3.4%
.6	576	632	585	629	589				602	23.4	3.9%
.8	429	435	444	451	477				447	16.7	3.7%
1.0	290	295	312	278	326				298	14.1	4.7%
1.2	210	188	198	217	200				203	10	4.9%
1.5	118	136	111	110	124				120	9.4	7.8%
2.0	57	64	61	63	70				63	4.25	6.8%
3.0	28	28	24	22	25				25.4	2.3	9 %
4.0	13	7.3	11	14	17				12.4	2.68	20.6%
5.0	6	4.3	4	2.7	3				4	1.35	34 %
6.0	1	.33	2	2	1				1.27	.64	51%

FIGURE 4.3
PRIME CALIBRATION OF ROYCO PARTICLE COUNTER SEPT. 19/67



as 0.8 μm . The background counts were due to normal impurities in the distilled water and aerosol system which were very difficult to eliminate. However, the tests indicated that any error due to the skew distribution of the background count was completely negligible. Other sizes used in the calibration included 0.357 and 1.30 μm . In addition to this periodic primary calibration, the recommended field calibration of the instrument was carried out before, during and after every test.

An important limitation of a light scattering type counter is the "coincidence loss" which occurs if the concentration of the aerosol is too great and light scatters from more than one particle simultaneously. This results in individual pulses merging into one larger pulse, giving rise to abnormal counts. To minimize the possibility of errors due to this, most tests were carried out with dilute aerosols having total particle concentrations of approximately 7×10^4 particles/liter (2×10^6 particles/ft³) or less. The counter was equipped with a dilution system of up to 10/1 which allowed the measurement of concentrations up to 7×10^5 particles/liter (2×10^7 particles/ft³) for specific tests. Also, when total counts were taken for all particles ≥ 0.15 μm diameter (known as total mode counts) it was possible to use concentrations up to 4.2×10^6 particles/liter (1.2×10^8 particles/ft³) by using an empirical correction factor supplied by the manufacturer. (50)

4.1.4 Other Instrumentation and Equipment

Ozone Meter

A significant portion of this study was devoted to quantitative measurements of ozone generation. In addition, as a safety precaution, the ozone was always monitored for all tests performed. The ozone concentration was measured with a commercial instrument using a microcoulomb sensor.*

(51) This detected the current flow which resulted when the ozone contained in a sampled volume of air reacted with a buffered KI solution. The range of the instrument was 0 + 100 P.P.H.M. by volume of ozone. No primary calibration was attempted as the $KI + O_3$ reaction is regarded as being the standard reaction. For sampling purposes a short length of teflon tubing was used and was located approximately 1 meter downstream from the test section.

Hot Wire Anemometer

All velocity measurements were made with a hot wire anemometer. This instrument** was equipped with a long slim sampling probe which enabled measurements to be made within the test unit. The air velocities which were measured were always mean values, for although the flow was generally turbulent the scale of the turbulent intensities were too small to be detected accurately with this equipment.

* Mast Model 724-2 Ozone Meter, Mast Instrument Company.

** Model HWB3 Hot Wire Anemometer, Flow Corporation.

High Voltage Supplies

Two high voltage power supplies were used in most experiments to allow independent variation of the charging and collecting fields. The supply used for charging* had a full wave, voltage doubler rectified, positive polarity output, variable from 0 → 60 kV R.M.S. at 0 → 5 mA. The collector supply** had a full wave, voltage doubler rectified output with either positive or negative polarity and a range of from 0 → 150 kV R.M.S. at 0 → 5 mA. Stability of the high voltages was assured by connecting a constant voltage transformer between it and the line voltage. Two voltmeters were used to monitor the corona and collector voltages. One was an electrostatic meter reading from 0 → 30 kV in three ranges. The other was an A.V.O. Model 8 multimeter equipped with high voltage dropping resistors to extend the range to 25 kV. The current monitor for the corona supply was a milli-ammeter connected between the outer corona cylinder and the ground.

Miscellaneous

Humidity and temperature measurements were made with a Honeywell Model W611A relative humidity indicator. Pressure drops across the test section were taken with a differential liquid manometer.

* Del Model #60TC5-1 Power Supply, Del Electronics Corp.

** N.J.E. Model #HO-150-5C N.J.E. Corp.

4.1.5 Probable Measurement Errors

In any discussion of errors it is important to differentiate between the accuracy and precision of a measurement. The accuracy of any measured value refers to the degree to which it conforms with an accepted standard. The precision refers to the quality of sharpness of definition and is related to the total measurement process, not just the instrument. The term precision will be used to refer to the reproducibility of a particular measurement.

Air Flow

The rotameter had a quoted accuracy of $\pm 1\%$ of the full scale reading. (The meter was calibrated from 4-40 S.C.F.M. (1.89 - 18.9 l/s). When the aerosol generator was used in the tests, the air flow was corrected to account for the air added by the drier and atomizing sources.

Particle Counter

The inevitable problems and errors involved in particle analysis using light scattering can be conveniently treated under three headings; sampling, counting, and size discrimination.

a) Sampling

The aerosol was sampled from the duct by short lengths of copper tubing bent to face into the air stream. (Some measurements using Tygon tubing showed certain discrepancies

which were ascribed to electrostatic deposition in the sampler. The copper apparently eliminated these effects.) Some concern was felt initially regarding the necessity for isokinetic sampling techniques. However, because the size range of most concern was less than 5 μm diameter no sampling error due to non-isokinetic sampling could be detected. In fact, no measurable difference was found for a sampling tube facing into the air stream or one drawing its sample from right angles to the air flow. In addition to these factors, since the important relationship was the reading after the precipitator relative to the reading before, the same type of sampling geometry was always used in the two positions. Hence any sampling error which was present in the absolute sense should not affect the precision of the collection efficiency calculations.

b) Counting

To ensure stable operation of the instrument it was found desirable to leave it on continuously during periods when tests were being run. In determining particle concentration the sampled volume was required. This was calculated using the rate of air flow measured by a flow meter incorporated in the sampler and the sampling time as set by a cam driven stepping switch. Errors were due to the combination of these two measurements and the accuracy was $\pm 4\%$. However, again because of the fact that ratios of readings were taken

the precision was estimated as $\pm 2\%$ based upon the stability of the flow meter. The dilution system introduced much larger errors however, with both the accuracy and precision leaving much to be desired. As a result, the use of the dilution system was avoided where possible and, when required, the flow meter setting was carefully controlled. An estimate of the error in percent, due to the dilution system, was given by the manufacturer as $\pm 6 \cdot (\text{dilution ratio})$. The statistical error due to sampling from a large population is proportional to $\frac{1}{\sqrt{N}}$ where N is the number counted. In practice this meant that the counts in the smaller size ranges were the most reproducible since the numbers counted were larger here. (eg: see the ratio of the standard deviation to the average count for the different sizes as shown in Table 4.1). In taking measurements after the precipitator when the efficiency was high, the sampling time was increased from the normal 1 minute to 10 minutes or longer to ensure a larger count. This was possible due to the stability of the aerosol generator which ensured little variation of the initial concentration during the life of the test. Also in all cases where the different sizes were sampled, the counter was stepped through the ranges three times and the average count was taken. Counts were always taken both before and after the precipitator for each test. However, the after counts were taken first since the purging time required when moving the sampler from a low concentration to high concentration was

much less than vice versa. Errors due to coincidence loss always increased as the aerosol concentration increased. However, these errors were minimized by using the correction factor referred to previously and operating with "total mode" counts where possible.

c) Size Discrimination

Sizing was obtained within the instrument by circuitry which sensed the magnitude of the light pulse scattered by a particle. The calibration was based upon spherical particles and the normal accuracy for size resolution as determined by the manufacturer was $\pm 22\%$. For aerosols made up of other than spherical particles, the recorded size was an "effective area diameter" where the size was given as the diameter of a sphere which would scatter the same amount of light as the non-spherical particle. However, the effective cross-sectional area of such a particle depends upon its aspect relative to both the light beam and the photomultiplier detector. This meant that the error in sizing was much larger than the $\pm 22\%$ and in fact was estimated at several hundred percent for cases of particles having a large dissymmetry. Error in size discrimination was also very dependent on coincidence loss. It was not possible to correct for this, other than by dilution of the aerosol, since the correction factor could only be applied for total mode counts. For this reason, it was found that many collection efficiency measurements were

more usefully measured using the total mode range. This had the following advantages:

- a) Error in particle sizing due to non-spherical particles was not a factor.
- b) The correction factor could be applied in cases of overloading.
- c) Less measurement time was required and hence there was less chance of error due to instabilities.
- d) Most essential information regarding collection efficiency was specified by such a measurement since standard filter specifications usually specify efficiency on a total mode basis.

Ozone Meter

The ozone meter was found to have two main sources of error. The first was caused by the formation of air bubbles in the reagent solution which caused non-uniform flow over the sensor. This error could be readily recognized by the erratic nature of the readings. The biggest source of probable error in the measurements was due to variation in the air sampling pump. This was checked periodically as drifts of $\pm 10\%$ in the calibration were found in some extreme cases. However, because of the averaging of results and frequent calibration the accuracy was estimated as $\pm 5\%$. The precision of all readings was approximately ± 1 P.P.H.M.

Air Velocity

The sensing head of the hot wire anemometer was calibrated in a special wind tunnel at a fixed velocity. For this one point calibration the manufacturer claimed $\pm 5\%$ precision in the range of velocities measured. The measurement of positioning the probe was also a source of error associated with the velocity measurement and was approximately $\pm 2\%$.

Current and Voltage Metering

All current metering was accurate to $\pm 1.5\%$. High voltage metering was calibrated referred to the electrostatic voltmeter. Accuracy was estimated at $\pm 5\%$ with a precision for each meter of $\pm 2\%$.

4.1.6 Test Units

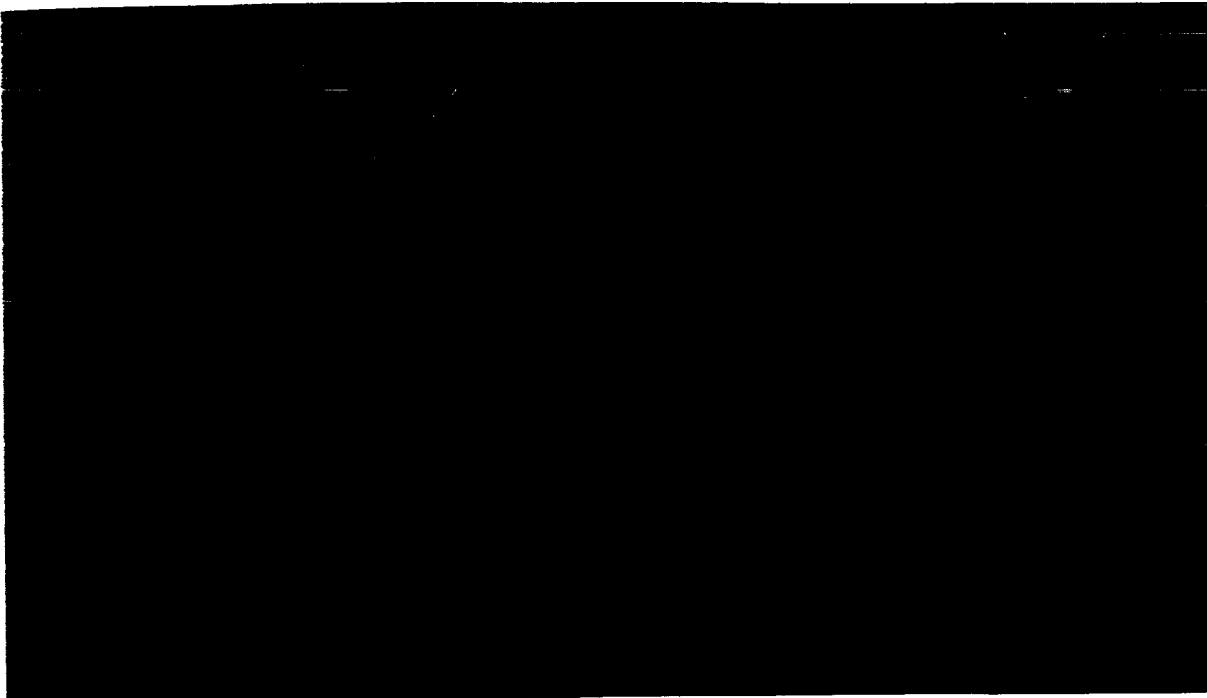
The geometry of the concentric geometry test units was as shown diagrammatically in Fig. 2.2. Unless otherwise noted, the dimensions used were; diameter of inner cylinder 3.8 cm (1.5"), diameter of outer cylinder 7.6 cm (3.0"), length 30.5 cm (12"). The assembled unit was mounted in an acrylic tube having an inside diameter of 10.1 cm (4"). The electrodes were constructed of perforated brass sheet with the insulating support structures made of acrylic plastic. Sealing at the inlet end was achieved with an O ring contact between the support ring and mounting tube. Unless noted otherwise, all the collection efficiency experiments employed a corona wire running the full length of the unit having a

diameter of 1.27×10^{-2} cm (0.005"). The corona wire was supported in the center of the inner cylinder under slight tension by a nylon support at the inlet end of the precipitator and at the other end by a special high voltage connector which also supplied the corona voltage to the wire. Each end of the corona wire was soldered to small brass spheres to eliminate end effects. The inner cylinder was grounded through a contact at the inlet end and voltage was applied to the repeller by a contact point drilled through the outer acrylic tube.

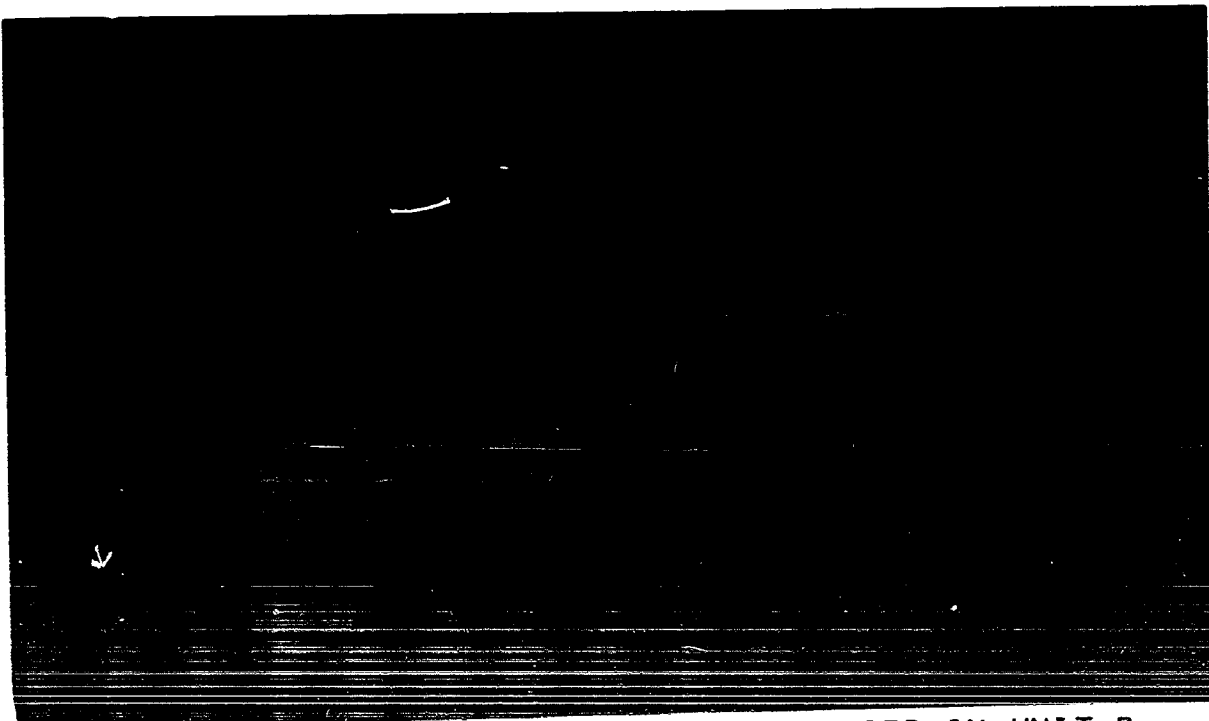
Two test units were constructed. Unit A (shown in exploded view in Fig. 4.4.a) was made of perforated brass plate; thickness 1.27 mm (0.05"), hole size 1.52 mm (0.06"), $W^2 = .72$. The inner cylinder consisted of two close fitting concentric cylinders which could be moved relative to one another so that the effective hole size could be varied and hence the solidity ratio could be changed over the range 0.72 to 0.9. Access holes were provided through the ends of the acrylic supports so that velocity measurements could be made inside the unit by means of a hot wire anemometer probe.

Unit B was dimensionally identical to Unit A but was constructed so that the main elements could be easily interchanged. The inner electrode could be removed and replaced with cylinders having several different mesh sizes and

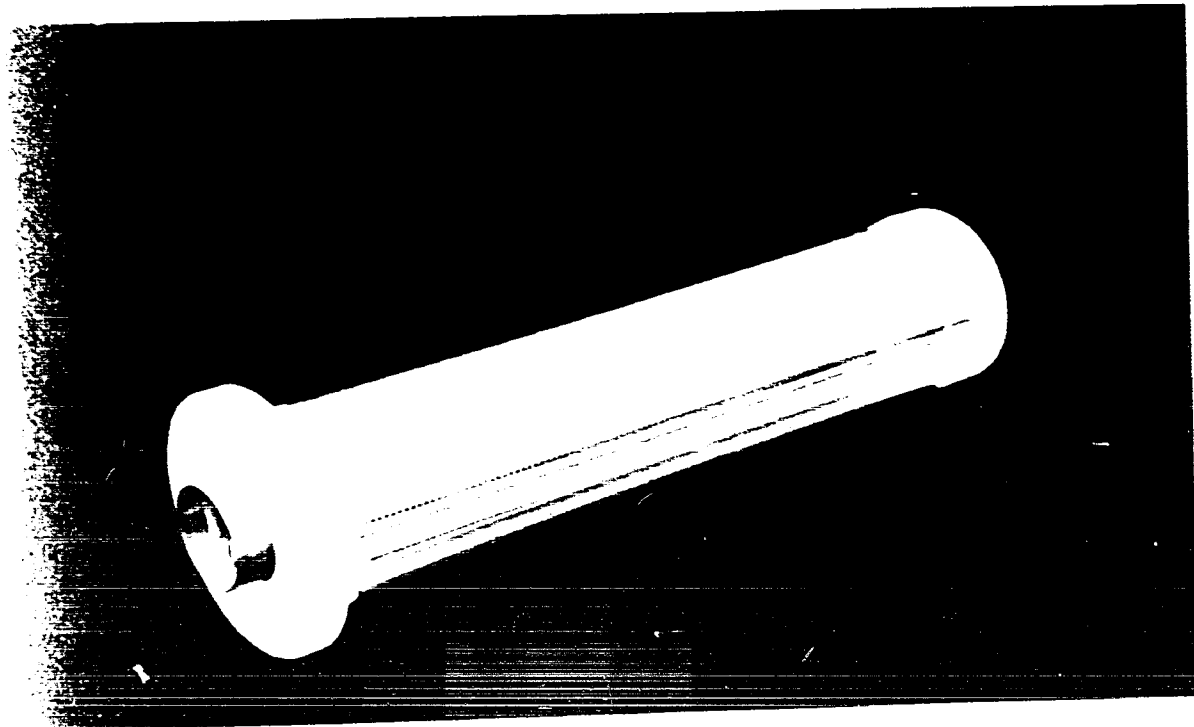
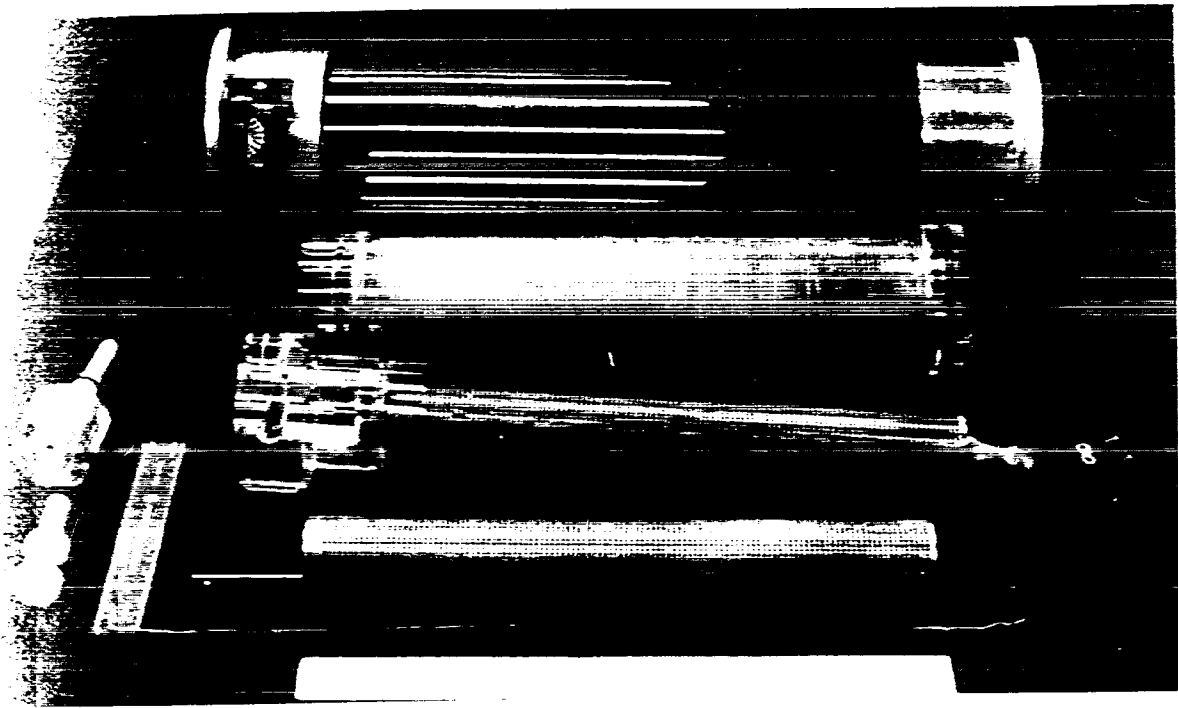
FIGURE 4.4
TEST UNITS



A) EXPLODED VIEW OF TEST UNIT A



B) ONE OF THE COLLECTOR ARRAYS USED IN UNIT B



solidity ratios. Also, an acrylic plug blocking the axial air flow at the exit end could be removed and replaced with a thin corona wire support so that air could pass straight through the unit as in a standard single stage precipitator. (The ozone measurements reported in Chapter 6 were made with this plug removed and the inner cylinder replaced with a solid brass electrode, the ends of which were carefully smoothed to reduce end effects and the possibility of back corona.) Different collector arrangements could be introduced into the second stage of this unit and Fig. 4.4.b) shows an example of an array of acrylic rods ready for mounting in the precipitator. The different collector geometries and their characteristics are described in Chapter 5.

Finally, a third unit was constructed for a series of tests to check the effect of the electrified media in a parallel plate geometry. In this case two perforated brass electrodes 23 cm. (9") square were insulated from each other with a spacing of 1.9 cm (0.75"). They were mounted normal to the mean air flow in an acrylic housing. This arrangement provided the same electrode spacing and average cross sectional area to the flow as the concentric geometry collectors. For this unit the particles were precharged in Unit B operated with the solid inner electrode and the end plug removed.

An overall view of the test facilities with Unit A in place is shown in Fig. 4.5.

4.1.7 Measurement of Collection Efficiency

All collection efficiencies reported in the following sections were based upon number counts. For fixed flows and sampling times the collection efficiency was defined as:

Collection efficiency (η)

$$\begin{aligned}
 &= \frac{\text{number of particles collected in the precipitator}}{\text{number of particles at the inlet to the precipitator}} \\
 &= 1 - \frac{\text{number of particles at the outlet of the precipitator}}{\text{number of particles at the inlet to the precipitator}} \\
 &= 1 - H
 \end{aligned}$$

where H is the particle "leakage" through the precipitator.

It is important to realize that this is equivalent to other efficiency measurements based upon weight, surface area, etc. only for the case where a single particle size is considered. When a range of particle sizes is measured such as 0.15 μm and larger, then considerable differences would result between measurements made by number and weight. Since the number of particles is largest for the small sizes, a collection efficiency based upon number of particles would be very close to that of the smallest particle (eg: for the size distributions used here, an efficiency measured



FIGURE 4.5
OVERALL VIEW OF TEST FACILITIES

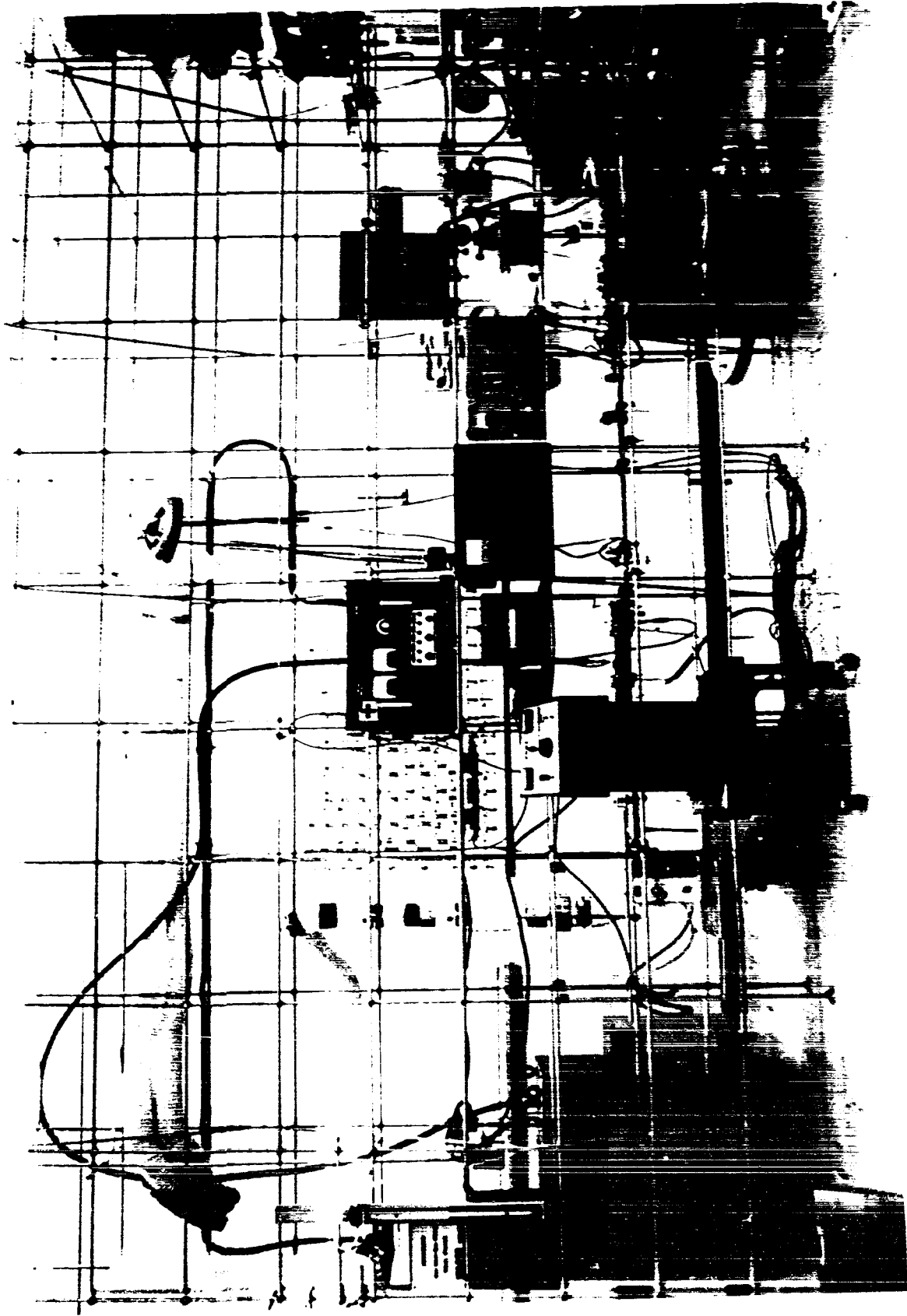


FIGURE 4.1
CONTROL VIEW OF THE ASSEMBLY

for 0.15 μm and larger proved to be very close to the efficiency measured for 0.3 μm alone). However, since the bulk of the weight is concentrated in the larger particle sizes, a collection efficiency based upon weight would misrepresent the efficiency for the smaller size range.

The over-all leakage of a two-stage precipitator is equal to the product of the leakages in each stage.

ie:
$$H = H_1 H_2$$

$$= \frac{\text{number of particles at outlet of 1st stage}}{\text{number of particles at inlet to the precipitator}} \times$$

$$\frac{\text{number of particles at outlet of the precipitator}}{\text{number of particles at inlet of 2nd stage}}$$

CHAPTER 5

COLLECTION EFFICIENCY

5.1 Theory

5.1.1 Migration Velocity and the Collection Parameters

Historically the concept of migration velocity has grown out of consideration of a particle in a still gas, ie: in a still gas a charged particle under the influence of an electric field will migrate, under steady state conditions, at a velocity such that the electric coulomb force is balanced with the aerodynamic drag force. From here the notion extended to laminar flow where particles moved in fixed trajectories and again, under the influence of an electric field, could migrate across the streamlines towards a collection surface. However, in the case of turbulent flow, a condition met in almost all practical units, the particle motion is more complex. Here particles below about 10 μm diameter move in a random fashion following the turbulent gas fluctuations. This tends to continuously remix the particles. Hence, even though the particles are influenced by the electric field, it would seem unrealistic to talk about them steadily migrating towards the collection surface. Various authors have avoided this

difficulty by referring to the parameter as an "effective migration velocity" (52) or even a "mass transfer coefficient" (53). It is true that even in turbulent air flow a laminar sublayer can exist where a steady migration can occur. However, since this laminar layer is very close to the collector surface and final capture must occur right at the surface, any consideration of the collection efficiency should emphasize the surface properties which actually control the collection process such as the electric field strength at the surface, and the area available for collection. To this end, it is suggested here, that rather than using migration velocity as a measure of the collection, an equivalent but more appropriate factor can be found in the dimensionless "collection parameters" as defined in the previous sections. This allows the efficiency to be specified in terms of the collection process at the collector surface and hence can be readily extended to the case of force components other than just the coulomb force. Also, by concentrating on the collection process at the surface, account can be taken of any effects due to collector geometry.

It can be readily appreciated that in turbulent air flow the capture of any particular particle is basically statistical in nature. Moreover, to be captured, a particle must experience simultaneously two necessary but not

sufficient conditions. These are:

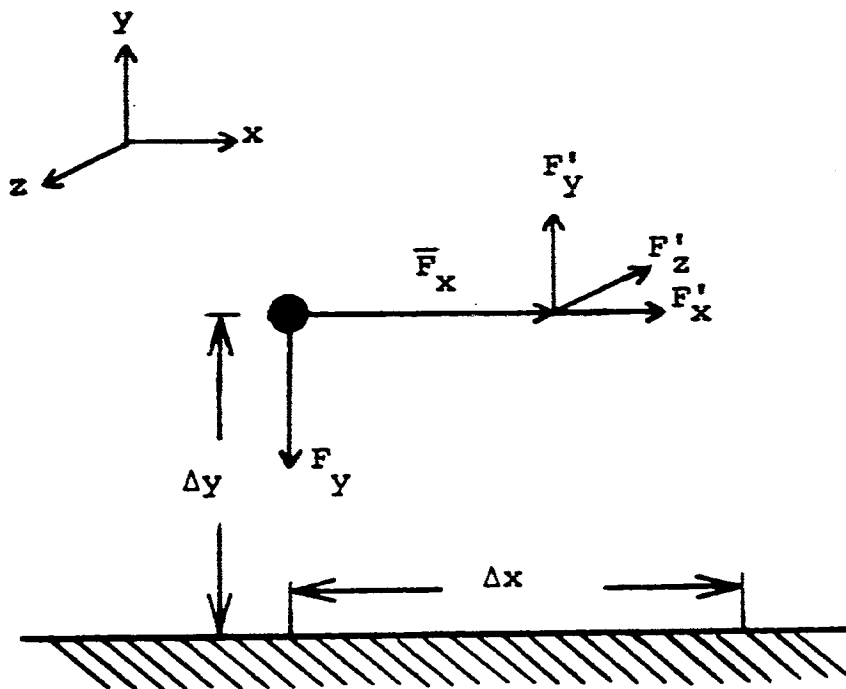
- a) the particle must be immediately adjacent to a collection surface.
- b) the force field at this surface must be of the right sign and magnitude to ensure capture.

Consider the situation as shown in Fig. 5.1, where a particle is held at rest adjacent to a collection surface. The force vectors as shown in the diagram describe the forces which tend to move the particle. \bar{F}_x is the average drag force exerted by the moving air stream on the particle at rest, F'_x , F'_y , F'_z , are the instantaneous fluctuations due to any turbulence in the air stream. It will be assumed that $F'_x = F'_y = F'_z$, ie: isotropic turbulence, and that $|F'_x| \ll \bar{F}_x$. The vector component F'_y describes the net attractive force tending to move the particle to the surface.

If the particle is free to move and acceleration times can be assumed negligible (47), the particle will be instantaneously accelerated to the velocity of the gas u_x in the x direction. This can be expressed by Stokes' Law as $u_x = v_x = \frac{\bar{F}_x C}{6\pi\mu a}$. In the y direction, the particle will instantaneously reach a velocity $v_y = \frac{F'_y C}{6\pi\mu a}$. (After release, the particle motion in the y direction is opposed by a Stokes' viscous force equal to F'_y .)

From this it follows that in a time interval Δt , the particle will move an incremental distance Δx due to the

FIGURE 5.1
FORCES ACTING ON A SMALL PARTICLE HELD
AT REST ADJACENT TO A COLLECTING SURFACE



aerodynamic drag and on average will also move a distance Δy towards the collector given by:

$$\frac{\Delta y}{\Delta x} = \frac{F_y}{\bar{F}_x} \quad (5 - 1)$$

(In general, as the particle approaches the collector, the velocity v_x will decrease due to the velocity reduction in the boundary layer. However, by considering v_x as constant a capture probability of 100% is assured.) But from section 3.5

$$\frac{F_y}{\bar{F}_x} = K \equiv \text{"collection parameter"}^*$$

therefore $\Delta y = K \Delta x \quad (5 - 2)$

In words, the distance Δy represents the limit of a sector from which on average a particle would be captured and this distance is characterized by the dimensionless parameter K . With this coefficient defining the probability of particle capture it is possible to derive an expression for the collection efficiency of the concentric geometry precipitator.

5.1.2 Collection Efficiency Equation for a One-Stage Cylindrical Precipitator with a Perforated Wall

Consider the first stage of the concentric geometry

* Note that since F_y has been defined as the net attractive force, the collection parameter will be the sum of the individual collection parameters contributing to the capture.

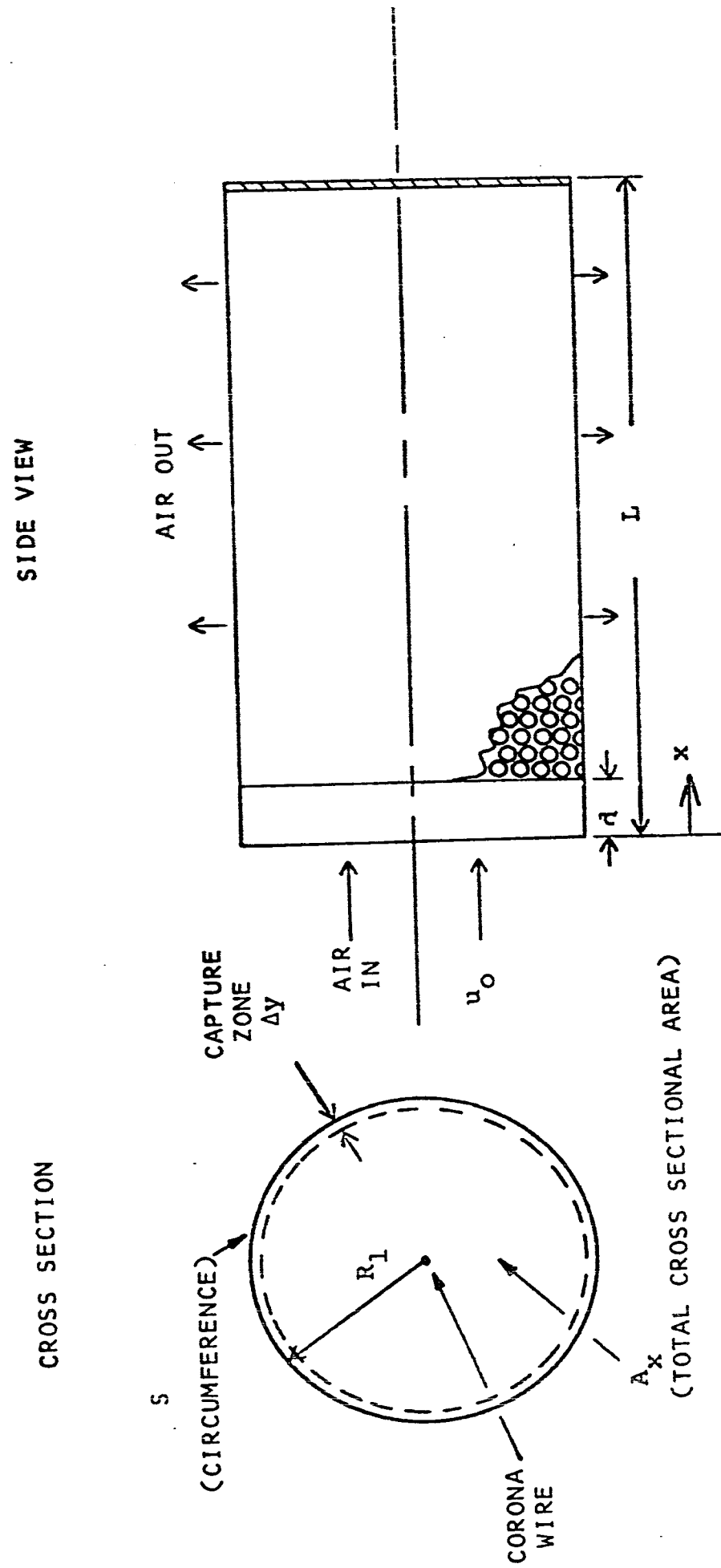
precipitator as shown in Fig. 5.2 The efficiency for this section can be calculated quite readily by extending existing theory to allow for the gas passing through the walls of the collecting surface. The procedure is analagous to that due to White to treat the effect of time variation in the voltage waveform (48).

Here the problem takes on four aspects. First, because of the finite charging time required for the particles to achieve maximum charge, the K parameter for a particle will increase to a saturation value as the particle passes down the charger. Secondly, because of the air lost through the walls, the K parameter will also increase with distance into the unit because of the corresponding reduction in axial velocity. Thirdly, from the point of view of the efficiency of the first stage, once the gas passes through the walls, the gas remaining in the collection section is only a fraction of the total and hence the collection efficiency referred to the total flow must be correspondingly less. Finally, because of the perforations in the metal, the area available for collecting the particles is less than the total area of the cylindrical surface of the grounded collector.

To treat the problem, the following simplifying assumptions have been made:

- a) The air flow is turbulent (average forward movement plus small scale random turbulence).

FIGURE 5.2
 FIRST STAGE OF THE CONCENTRIC CYLINDRICAL GEOMETRY PRECIPITATOR



- b) At any cross-section there is uniform particle concentration (ie: complete remixing of particles due to turbulent fluctuations).
- c) There is no re-entrainment of particles once precipitation has occurred.
- d) There is no interaction among the particles.
- e) No air is lost between $x = 0$ and d . Thereafter, the air passes through the wall of the collector at a constant rate over the whole length so that the axial velocity is described by:

$$u_x = u_0 \quad 0 < x < d$$

$$u_x = \left[\frac{u_0(d-x)}{L-d} + u_0 \right] \quad d < x < L$$

where u_0 = average velocity across the inlet of the precipitator ($\frac{m}{s}$).

- f) The velocity of the air parallel to the perforated surface of any distance x is approximately equal to the average axial velocity at that point.
- g) The thickness of the cylinder is small enough so that precipitation inside the perforations may be neglected.

$$\text{Metallic area of cylinder} = S \cdot L \cdot W^2$$

where W^2 is a dimensionless solidity factor defined

$$\text{as } W^2 = \frac{\text{Metallic area of cylinder}}{\text{Total area of cylindrical surface}} .$$

h) At any position x , the average particle velocity

$$v_x = u_x \cdot$$

Consider the cross section of the precipitator as shown in Fig. 5.2. Using White's argument, consider the length L to be divided into n length increments Δx . For evenly distributed dust, the probability that capture of any one particle will occur in the i^{th} increment in travelling an incremental distance Δx is given by:

$$P(x_i) = \frac{\Delta y \cdot S \cdot W^2}{A_x} \left(\frac{\text{air flowing through cross section at } x_i}{\text{total air flow through precipitator}} \right) \quad (5 - 3)$$

For constant cross sectional area and from equation 5 - 2 noting that K is a function at x

$$P(x_i) = \frac{K(x_i) \cdot S \cdot W^2 \cdot \Delta x}{A_x} \left| \frac{\text{axial velocity at } x_i}{\text{axial velocity at inlet}} \right|$$

For convenience in the derivation we can write:

$$K(x_i) = K' \frac{\frac{x_i}{x_i + X_0}}{\left| \text{axial velocity at } x_i \right|} \quad (5 - 4)$$

K' \equiv the value of the collection parameter calculated for the maximum charge possible on the particle and for an axial air velocity of 1 meter/sec.* (dimensionless)

$\frac{x_i}{x_i + X_0}$ \equiv reduction factor to account for the charging time lag. (dimensionless) (see section 3.7.1)

* Note that by setting the axial velocity equal to 1 meter/sec the magnitude of K' is identical to the "measure" of the migration velocity as normally defined.

|axial velocity at x| \equiv "measure" of the axial velocity
(dimensionless).

Therefore,

$$P(x_i) = K' \frac{x_i}{x_i + X_0} \frac{S \cdot W^2 \cdot \Delta x}{A_x |v_0|} \quad (5 - 5)$$

The probability of a particle passing through the precipitator without being captured will be termed the "leakage" and is given by:

$$H = (1 - P(x_1))(1 - P(x_2)) \dots (1 - P(x_n))$$

therefore

$$\ln H = \ln(1 - P(x_1)) + \ln(1 - P(x_2)) + \dots + \ln(1 - P(x_n))$$

Now since $P(x_i) \ll 1$

$$\begin{aligned} \ln(1 - P(x_i)) &= - (P(x_i)) + \frac{P(x_i)^2}{2} + \frac{P(x_i)^3}{3} + \dots \\ &\approx - P(x_i) \end{aligned}$$

Therefore

$$\ln H \approx - \sum_{i=1}^n P(x_i)$$

Let $n \rightarrow \infty$ & $\Delta x \rightarrow 0$ such that $n \cdot \Delta x = L$

Therefore

$$\begin{aligned} \lim_{n \rightarrow \infty} \ln H &= \lim_{n \rightarrow \infty} \sum_{i=1}^n - P(x_i) \\ &= \lim_{n \rightarrow \infty} \sum_{i=1}^n - K' \left(\frac{x_i}{x_i + X_0} \right) \frac{S \cdot W^2 \cdot \Delta x}{|v_0| A_x} \\ &= - \frac{S \cdot W^2 \cdot K'}{|v_0| A_x} \int_0^L \left(\frac{x}{x + X_0} \right) dx \end{aligned}$$

which can be written

$$H = e^{-\frac{S \cdot W^2 K'}{A_x |v_0|} \int_0^L \frac{x}{x + X_0} dx} \quad (5 - 6)$$

or

$$\eta = 1 - H \quad (5 - 7)$$

Now $\frac{K'}{|v_0|} = K \equiv \text{constant}$

In this case the coulomb force is by far the most important collection force therefore $K = K_c$

Also note that:

$$\begin{aligned} \int_0^L \frac{x dx}{x + X_0} &= L \left[1 - \frac{X_0}{L} \ln \left(1 + \frac{L}{X_0} \right) \right] \\ &= Lb \end{aligned} \quad (5 - 8)$$

where $b =$ derating factor due to finite charging time
(dimensionless).

The derating factor b is plotted on Fig. 5.3 as a function of $\frac{X_0}{L}$.

Equation 5 - 6 becomes:

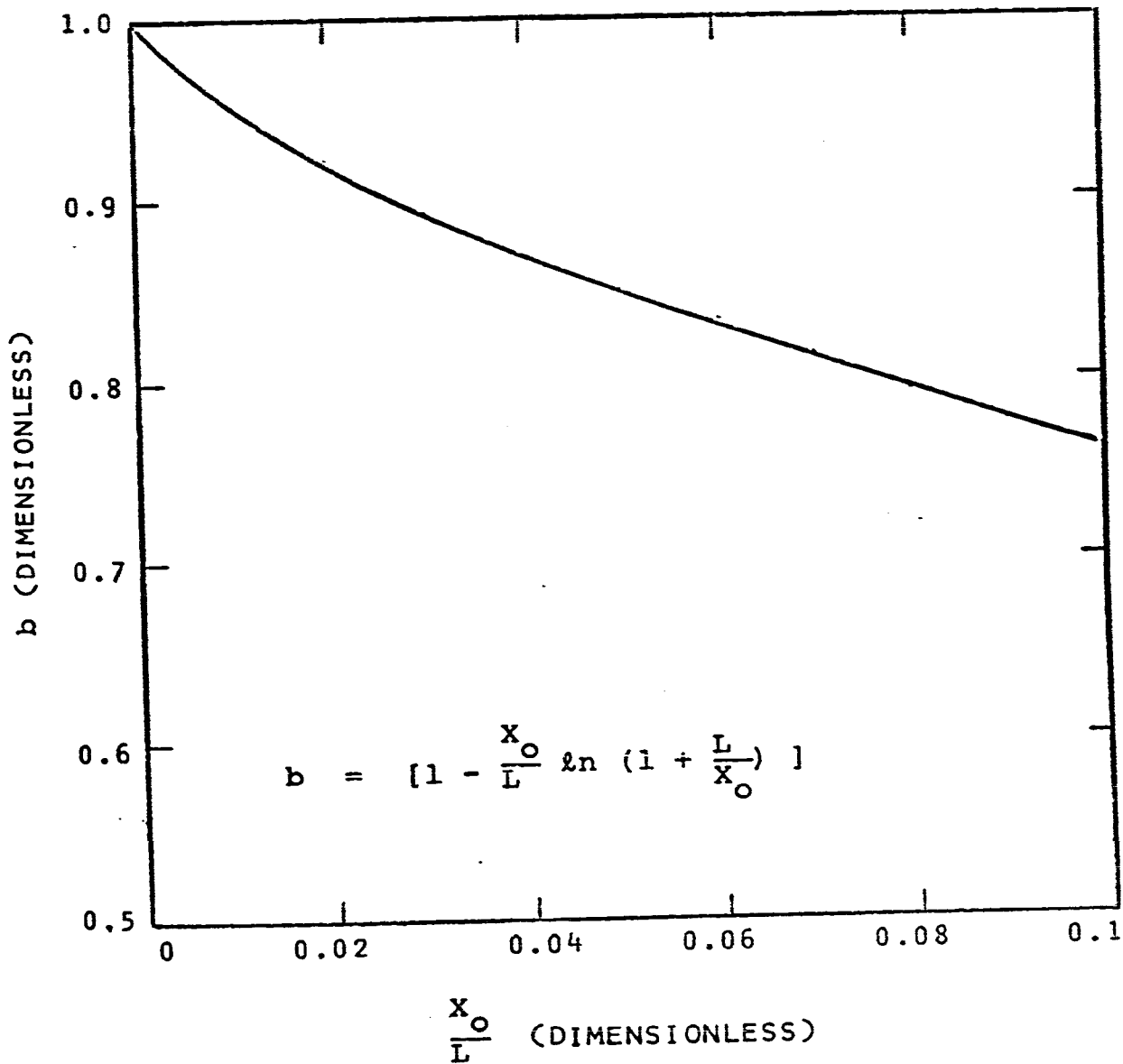
$$H = e^{-\frac{S \cdot W^2 \cdot L \cdot b}{A_x} K_c}$$

But $S \cdot W^2 \cdot L \equiv$ metallic collection area A_c

$$\therefore H = e^{-\frac{A_c}{A_x} \cdot b \cdot K_c} \quad (5 - 9)$$

FIGURE 5.3

DERATING FACTOR FOR THE COLLECTION
PARAMETER DUE TO FINITE CHARGING TIME



Note that for $L \gg X_0$, $b \doteq 1$ and the collection efficiency is given by:

$$\eta = 1 - e^{-\frac{A_C}{A_X} K_C} \quad (5 - 10)$$

This equation describes the efficiency of collection for the precipitator in terms of an exponential whose exponent is the product of two dimensionless groups; the collection parameter K_C and the ratio of the collection area to the cross sectional area (this will be termed the "specific collection area").

Moreover, it is readily seen that for only the coulomb force acting, this is the equivalent of the Deutsch equation (53) since

$$K_C = \frac{w}{v_0}$$

and hence the exponent

$$\frac{A_C}{A_X} \cdot \frac{w}{v_0} = \frac{A_C w}{Q}$$

It is interesting to note that the predicted efficiency of this first stage is the same as if the aerosol had traversed the full length of the pipe and that the pattern with which the aerosol escapes through the wall along the length does not affect the predicted efficiency. Note also that for normal values of $\frac{X_0}{L}$ used in the later experiments, (which ranged from 0.01 to 0.06), the effect of the charging time could not always be ignored.

5.1.3 Collection Efficiency Equation for the Second Stage of the Concentric Geometry Precipitator

After being charged in the first stage of the precipitator, the particles which have escaped collection pass through the perforated grounded cylinder and enter the second stage.

Here a collecting field may be applied in two ways;

- a) A high voltage of the same polarity as the particle charge may be placed on the outer cylinder creating a repelling field tending to drive the charged particles back towards the grounded cylinder.
- b) A high voltage of the opposite polarity to the particle charge may be placed on the outer cylinder creating an attracting field tending to drive the charged particles towards the inside surface of the outer cylinder.

The air flow in the second stage is influenced by several factors. The first is that the distribution of air through the perforated plate in the axial direction depends upon the pressure drop across the plate. Whereas the predicted results from the first stage were unaffected by the flow pattern, it is obvious that for optimum collection efficiency in the second stage, the air distribution should be uniform along the length of the cylinder. The second factor is that the flow through the plate creates high velocity jets

with large shearing effects giving rise to turbulent eddies. The scale of these jets and eddies will be related to the relative size and spacing of the perforations. Finally, because of the concentric geometry, an expansion in the flow area results which causes a decrease in the mean velocity as the flow moves radially outwards.

Aside from this relatively complicated flow pattern, there are two major differences from the situation in the first stage:

- a) The collection field is directed parallel to the direction of mean flow.
- b) The collection surface exists in one plane perpendicular to the direction of mean flow.

These factors would appear to preclude any analysis similar to that used before. However, it is proposed that these points can be resolved to justify a similar approach.

For the field direction parallel to the air flow, the view of the force balance as cited in section 5.1.1 would not seem applicable. However, it must be recalled that the actual collection process only occurs at the collector surface and here the air flow must be parallel to the collector. The velocity of the air at this point will be a complicated function of the plate geometry but its magnitude will be related to the mean forward velocity of the air stream. Therefore, for the localized region where the collection

actually occurs, the previous model proposed is valid and the collection probability can be characterized by a collection parameter K .

In applying the probability analysis to the collection process in the first section it was necessary to hypothesize a series of incremental areas down the length of the precipitator where the probability of capture was specified. It will be recalled that this led to the exponential form of the equation. In this case, the existence of the collector in one plane would appear to indicate that the collection could be specified by a single probability of capture at that plane. However, this would only be true if there was no mechanism to return a particle to the collector if it escaped capture during its initial passage near the collector. For instance, if it was possible for a given particle to be returned to the vicinity of the collector a number of times during its residence time in the collecting region, then an analysis analagous to that in section 5.1.2 would be possible.* It is proposed that this situation does in fact occur with the turbulent re-mixing providing the major mechanism. In addition, in the case of the repelling field the net result of the velocity decrease and the repelling field would be to increase even more the probability of a particle being

* In this case, rather than defining the probability of capture in terms of incremental lengths down the collector, the analysis would proceed in terms of time increments during the residence time of the particle in the collector region.

returned in an eddy to the vicinity of the collector.

On the basis of these considerations it is proposed that the collection efficiency equation for the second stage is of the same form as equation 5 - 10 for the first stage except for the following assumptions and modifications:

- a) Since charging normally occurs in the first few inches of the first stage, it is assumed that a particle has achieved its saturation charge
ie: $b = 1$.
- b) The dielectrophoretic force may have a small effect in collection on the inner surface but is negligible compared to the coulomb force term.
- c) The effective velocity of the particle near the surface is related to the mean flow but the prediction of the magnitude appears impractical.
- d) The specific collection area in this case will be defined in terms of the metallic collection area divided by the open area at the plane of collection
ie: $\frac{W^2}{1-W^2}$.

Having established this model for the collection there are a few predictions which are possible. The precipitator as it stands is not a particularly useful form since the second stage really adds very little additional collection area. (In the case of the inner cylinder as collector the additional area is the same as that in the first stage.)

Therefore, although the electric field could be made stronger in the static field, than in the corona discharge, thus increasing the collection efficiency, dust build-up resulting in clogging and re-entrainment would soon occur.

The difference in collection on the inner and outer cylinders is also interesting. Since the field established between these cylinders is due to a constant electric flux, the product $E \cdot A_c$ will be the same for both the inner and outer cylinders and hence the collection efficiency should be similar for the case of attracting and repelling fields. However, considering the air flow and practical considerations the following differences exist:

Repelling Field (Collection on Inner Electrode)

- a) mean flow is away from collector,
- b) high velocity jets point away from collector,
- c) high mean velocity near collector,
- d) field directed to increase residence time of particle in the second stage,
- e) possible to use same power supply for first and second stage,
- f) dust is collected on grounded electrode.

Attracting Field (Collection on Outer Electrode)

- a) mean flow in direction of collector,
- b) jets point towards collector but have much decreased intensity,

- c) low mean velocity near collector (due to radial expansion of air),
- d) field directed to decrease residence time of particle in second stage,
- e) separate power supply required for first and second stage,
- f) dust collected on high voltage electrode.

Of these points, a), b), and c) would favour collecting on the outer electrode whereas d), e) and f) would act in favour of the inner. However, it could be expected that the mean velocity adjacent to the collector would have the most influence and hence point c) would favour collection on the outer electrode.

5.1.4 Collection Efficiency Equation for the Second Stage of the Concentric Geometry Precipitator with Electrified Media Present

As pointed out in the last section, the concentric geometry precipitator could be made to have good collection efficiency but is limited due to the minimal increase in collection area afforded by the second stage. To overcome this drawback, additional collection surfaces could be provided in the collection region. The considerations in the previous sections have pointed out that to maximize collection efficiency it is necessary to maximize both the collection

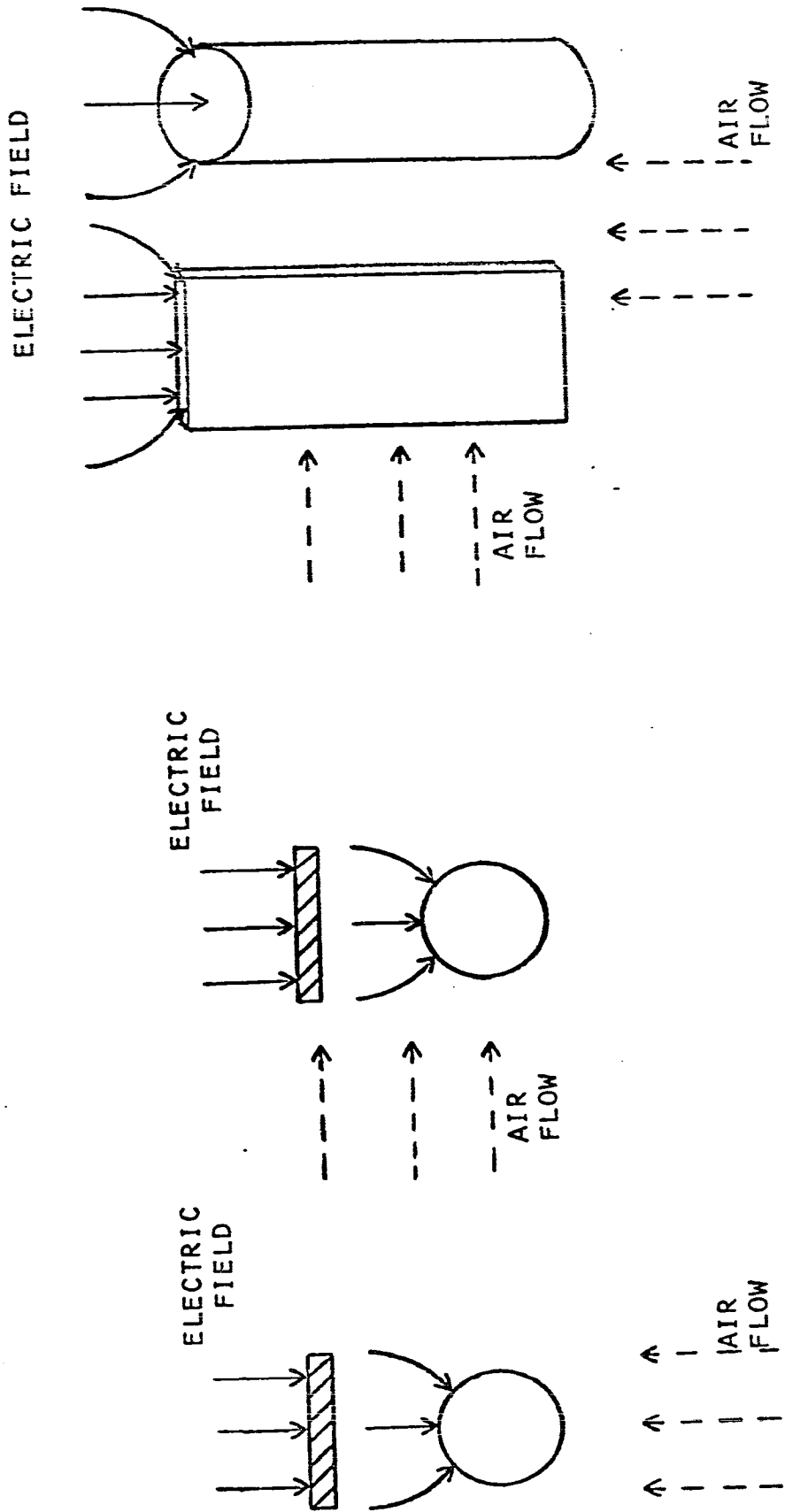
field strength and the collection area. It is obvious that to maintain an electric field in the collection region it is necessary to ensure that the collection media is insulated with respect to the electrodes. This could be achieved either through the use of dielectric collectors or alternatively, conductors mounted in insulating supports. By increasing the collection area it should be possible to increase both the total collection efficiency and reliability by ensuring that the geometry of the collection media produces the maximum beneficial effects for both the mechanical and electrical forces. Of the many possible collector geometries two main ones will be considered here; the cylindrical rod or fiber and the flat plate. Aside from the geometry of the collector, two other important considerations are the orientation relative to the mean flow and to the electric field. Consider the three different cases as shown in Fig. 5.4 for both rod and plate collectors.

In case a) the field direction is such as to cause coulomb collection on the upper surface of each collector. Note that in this case the maximum field strength and minimum air velocities occur at the same region. This is a condition conducive to maximum collection efficiency.

In case b) the field is the same but now the maximum air velocity occurs adjacent to the region of maximum field strength and the collection efficiency would be less than in a).

FIGURE 5.4

POSSIBLE ORIENTATIONS OF ROD AND FLAT PLATE COLLECTOR RELATIVE TO THE ELECTRIC FIELD DIRECTION AND MEAN FLOW



CASE C)

CASE B)

CASE A)

In case c) the electric field lines are essentially confined within the dielectric collectors with the remaining field parallel to the surface and hence no coulomb collection could occur.

In order to maximize the collection area available it would be desirable to introduce a collector with a high specific surface such as some form of fibrous media. Consider such a medium to consist of an idealized array of cylindrical dielectric fibers oriented as shown in Fig. 5.5. The collection occurring in this situation can be treated by extending the previous approach of section 5.1.2.

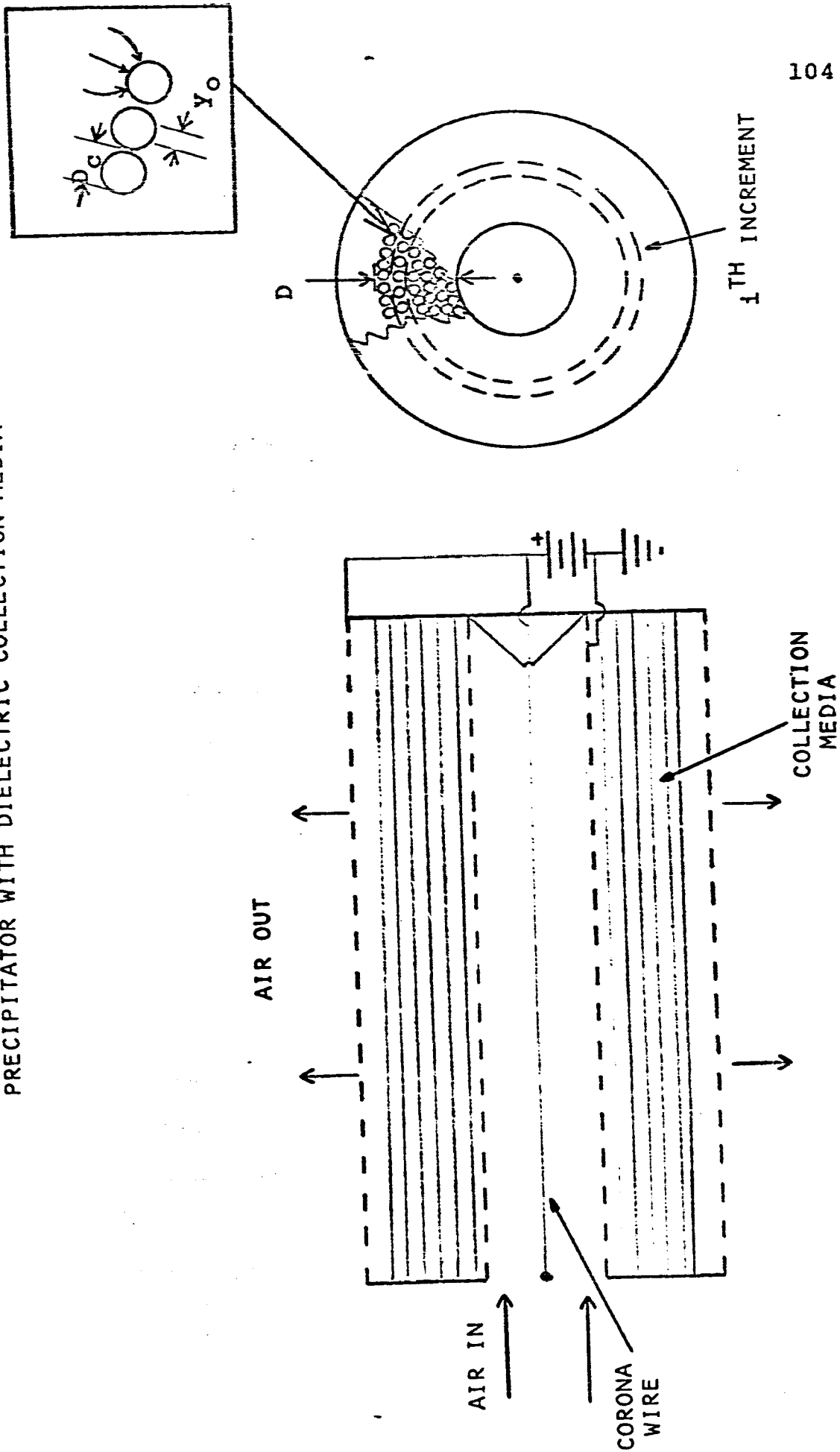
To simplify the analysis the following assumptions will be made:

- a) The fibers are sufficiently far apart so that the presence of one does not affect the collection or field distribution of the other.
- b) The fibers are a regular array having equal diameter D_c .
- c) $D \gg D_c$.
- d) Complete remixing of the particles occurs after each layer of fibers.

Under suitable conditions with this array it is possible that at least four collection mechanisms could have importance.

- a) Coulomb force.
- b) Dielectrophoretic force.

FIGURE 5.5
 SECOND STAGE OF THE CONCENTRIC CYLINDRICAL GEOMETRY
 PRECIPITATOR WITH DIELECTRIC COLLECTION MEDIA



- c) Image force.
- d) Mechanical forces.

Coulomb Attraction

The presence of a dielectric cylinder in an electric field causes the field lines to converge on the cylinder. For small cylinders with no interference the radial field will be approximated by the expression given as equation A-1 in Appendix A. Considering the total area of a cylinder and the field direction as shown in Fig. A-1 it can be seen that the field over the top half of the cylinder will act to aid collection whereas that on the lower half will act to repel the particle and hence have no contribution to the collection.

Consider the probability of collection of a particle on any of the fibers in the i^{th} segment as shown in Fig. 5.5.

$$P_i = \bar{K}_{ci} \frac{A_f' \cdot m_i}{A_{xi}} \quad (5 - 11)$$

where:

\bar{K}_{ci} \equiv an average value of the coulomb collection parameter based on the average collection field strength over the surface of the fiber and an average velocity of the particle in the vicinity of the fiber. (See equation A-6 Appendix A.)

- A_f' \equiv surface area of a fiber (m^2).
 m_i \equiv number of fibers in the i^{th} segment.
 A_{xi} \equiv cross sectional area at the i^{th} segment
 through which the total air flow passes (m^2).

Using the same arguments as in section 5.1.2 it can be seen that the total collection efficiency can be written as:

$$\eta_c = 1 - e^{-\frac{\bar{K}_c A_c}{\bar{A}_x}} \quad (5 - 12)$$

where:

- \bar{K}_c \equiv average coulomb collection parameter based upon equation A-6 with a value for E_o and \bar{v}_o averaged over the thickness of the filter media.
 A_c \equiv total surface area of fibers (m^2).
 \bar{A}_x \equiv average cross sectional area through which the total air flow passes (m^2).

Dielectrophoretic Attraction

Since the field around the fibers is non-uniform, the dielectrophoretic force can be important. The average collection parameter over the surface of a fiber has been derived as equation A-10 in Appendix A and it is interesting to note that this collection force acts on both the upper and lower surfaces of the fiber. Using the same analysis as before the collection efficiency due to this term becomes:

$$\eta_c = 1 - e^{-\frac{\bar{K}_d A_c}{A_x}} \quad (5 - 13)$$

Image Attraction

It was mentioned in section 3.5.2 that the image force is very short range and is normally negligible. However, since its effect occurs only at surfaces it could have added importance in a collection media having a high specific surface area. This would result in the expression

$$\eta_I = 1 - e^{-\frac{\bar{K}_I A_c}{A_x}} \quad (5 - 14)$$

Mechanical Collection

It will be recalled from section 3.4.3 that the combined inertial and interception effects were expressed in terms of the collection parameter $K_m = \frac{\eta'}{\pi}$ (equ. 3.10) where

$$\eta' = \frac{y_o}{D_c}$$

Again considering the i^{th} row of fibers in Fig. 5.5 the probability of capture of a particle due to mechanical forces will be given by:

$$P_i = \frac{y_o^{m_i}}{C_i} \quad (5 - 15)$$

$C_i \equiv$ circumference of i^{th} increment (m).

But

$$P_i = \frac{y_o}{\pi D_c} \cdot m_i \cdot \frac{\pi D_c \cdot L}{C_i \cdot L}$$

$$= K_m \frac{A'_f \cdot m_i}{A_{xi}}$$

Or as before

$$\eta_m = 1 - e^{-\frac{\bar{K}_m A_c}{A_x}} \quad (5 - 16)$$

Note that this has exactly the same form as the previous electrical expressions, the only difference being the definition of K_m which is directly related to the existing single fiber relations referred to in section 3.4.

The previous considerations have assumed that each collection parameter acts independently. It is recognized of course that all would act simultaneously, although the relative importance of each would depend upon the conditions for each case considered. In section 3.4.3 for mechanical forces it was assumed that for small magnitudes of the efficiencies simple addition of the single fiber efficiencies would suffice. However, this did not take into account the fact that if a particle is caught by one mechanism it cannot be recaptured again by a second or third. Therefore, to account for this it is necessary to consider the product of each of the leakages due to each component so that the total collection

efficiency in the media is given by:

$$\eta = 1 - (H_c) (H_d) (H_I) (H_m)$$

$$\text{ie: } \eta = 1 - e^{-\frac{A_c}{A_x} (\bar{K}_c + \bar{K}_d + \bar{K}_I + \bar{K}_m)} \quad (5 - 17)$$

Note that this just accounts for the collection in the media. The additional deposition in the first stage and on the electrode in the second stage would also have to be considered in determining the overall efficiency by including the leakage terms in equation 5 - 17.

This analysis has given rise to an expression giving an estimate of the collection efficiency for combined electrical and mechanical effects. However, in any attempt to apply this prediction in practice, special attention would have to be paid to the simplifying assumptions which were made in the derivation. In particular, the interference effects among the fibers would be expected to cause some difficulties.

5.2 Test Results and Their Interpretation

5.2.1 Air Flow Through the Concentric Geometry Precipitator

Referring to Figures 2.1 and 2.2 it could be expected that a higher pressure drop per unit flow would result from the concentric geometry precipitator than from the standard type of precipitator. In the normal precipitator the pressure drop is due primarily to frictional wall losses. However, in the concentric geometry the pressure drop also depends upon the energy lost through the following:

- a) Constriction of the air at the inlet
- b) Change in the air direction
- c) Constriction and expansion of the air due to the perforated cylinders
- d) Air passage through the dielectric media (if present)
- e) Expansion of the air at the outlet.

These losses involve the transfer of kinetic energy into heat. The relative importance of the above losses depends upon many factors but generally speaking flow expansion contributes more loss than flow contraction. In the case of drag losses the magnitude will vary as the product of the square of the air velocity, the air density and a drag coefficient. (This coefficient is primarily a function of the Reynolds number and the geometry of the body being considered.) Hence the main losses will usually occur

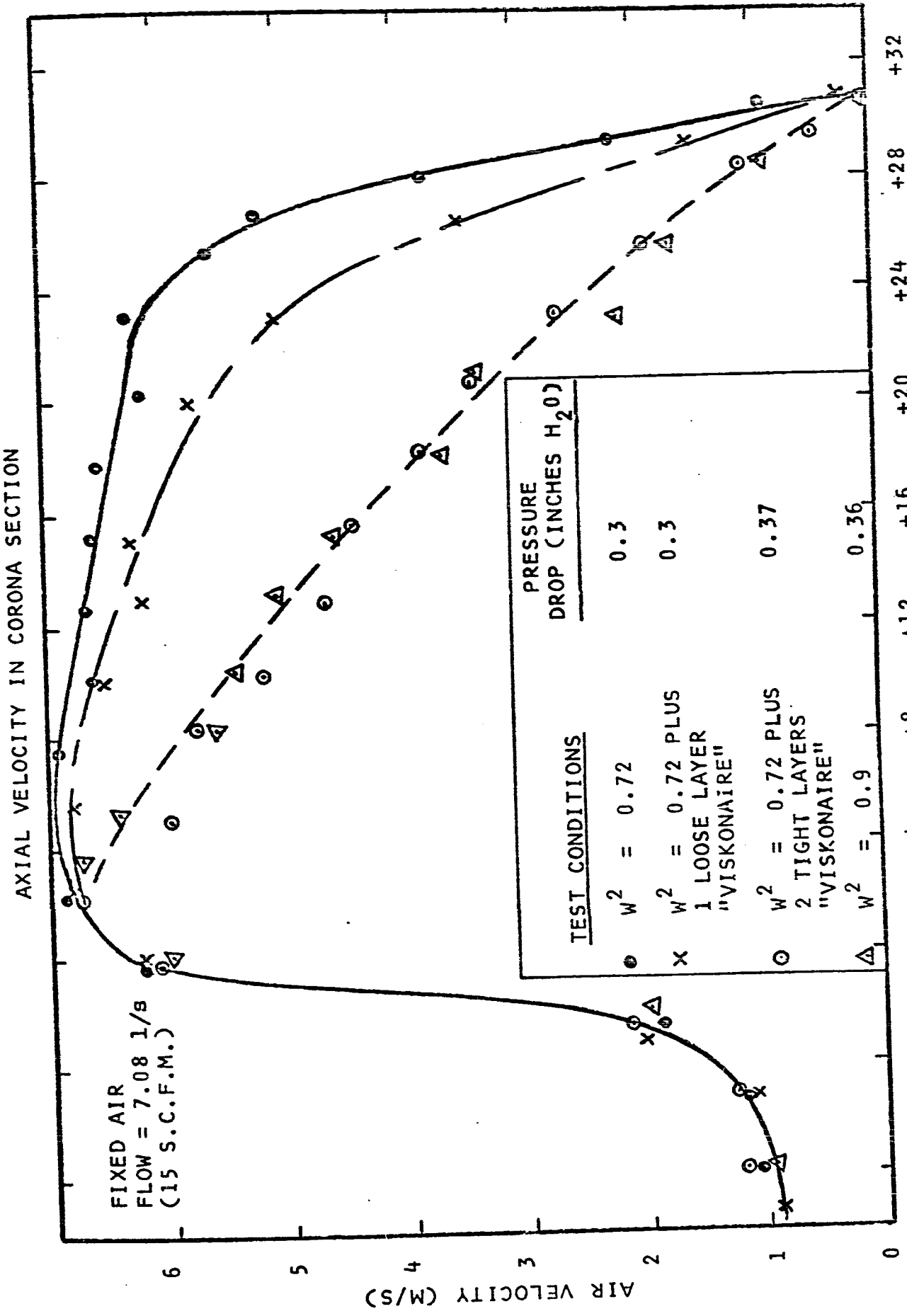
at the areas where the velocity is highest.

From the point of view of the concentric geometry precipitator, the ideal air flow would be a high velocity axial flow in the corona section until the particles were fully charged, then the air would expand radially through the cylinder to provide constant air distribution in the second stage. The air flow in the second stage would ideally be a diffuse turbulent flow with complete air mixing occurring as the mean flow moved radially through the section.

Study of the air flow in this work was limited to a series of experiments to see how closely this flow condition was achieved in practice. Experiments were carried out using test section A which had the variable aperture adjustment on the grounded cylinder. In addition, the effect of wrapping "Viskonaire" on the outside of this cylinder was tested. The axial air velocity was measured in the corona section as a function of position along the length of the section. The measurements were made with the hot wire anemometer probe positioned slightly off center and the sensing wire oriented radially to ensure that only the axial velocity component was detected.

The results for one value of flow are shown on Fig. 5.6. (Similar curves were found for the other flows tested.) Note that for the apertures fully open ie: 28% open area, very little air passed through the perforated cylinder

FIGURE 5.6



until the last few centimeters of the section. This meant that the air distribution in the collection region was concentrated at one end, resulting in a high velocity with only a small portion of the collection area being utilized. However, as the percentage open area was reduced either by changing the actual aperture size or its effective size, by wrapping "Viskonaire" around the cylinder, an improved air flow resulted. The increased pressure drop across the perforated cylinder equalized the distribution as can be seen by the curve showing a near linear change of velocity with length. It is of interest to note that the radical change in flow distribution observed in Fig. 5.6 was achieved through modification of factors c) and d) mentioned earlier. However, this resulted in only a relatively small difference in the total pressure drop. This would indicate that a large portion of the total loss was due to factors a), b) and e). In particular e) was suspected of being the most important since on this unit the ratio of the area at the outlet of the unit to the area of the duct was less than 0.1.

The velocities and flow characteristics in the second stage were not measured directly. The problem of flow through perforated screens has been studied in the literature (54) and from these results it was possible to predict the flow pattern. As mentioned in section 5.1.3 air passing through a perforated plate forms high velocity jets which

give rise to turbulent eddies. The general scale of the turbulence and the rate of velocity reduction in the jets is related to the aperture size and solidity ratio. The desired condition of diffuse turbulent flow can be achieved by using small apertures and low percentage open area. This coincides with the condition required for equalized air distribution.

In the precipitation tests which follow, care was taken to ensure equal velocity distribution in the second stage either through the use of the "Viskonaire" media or using aperture settings of the order of 10% for the cases of the geometries which had inadequate pressure drops associated with them.

The mean velocities in the inlet section and in the second stage were calculated for use later. These calculations were based upon the assumption of equal velocity distributions and ignored any contraction effects due to the constrictions.

First Stage

Velocity at Inlet to Precipitator

The calculations were checked using measurements taken in connection with the axial flow tests and were taken as the maximum value of velocity recorded near the inlet.

TABLE 5.1

FLOW		AXIAL VELOCITY (m/s)	
$\frac{(m^3)}{(s)}$	(S.C.F.M.)	Calculated	Measured
2.36×10^{-3}	5	2.07	2.2
4.72×10^{-3}	10	4.14	4.5
7.08×10^{-3}	15	6.21	6.7
9.44×10^{-3}	20	8.28	8.4

Second Stage

The mean velocity in the second stage decreases as the air moves radially outwards. The velocities shown below are given for the mean velocities in the jets for two solidity ratios. The mean velocities that would exist at the surface of the inner cylinder and half way across the collection region are also given assuming diffuse radial flow conditions.

TABLE 5.2

AIR FLOW S.C.F.M.	MEAN VELOCITY (m/s)			
	IN JETS		IN COLLECTION REGION	
	$W^2 = .72$	$W^2 = .9$	AT INNER SURFACE	HALF-WAY
5	0.23	0.65	0.065	0.043
10	0.46	1.3	0.13	0.086
15	0.69	1.9	0.19	0.13
20	0.92	2.6	0.26	0.17

5.2.2 Collection Characteristics of the First Stage

A) Effect of Particle Size and Air Flow

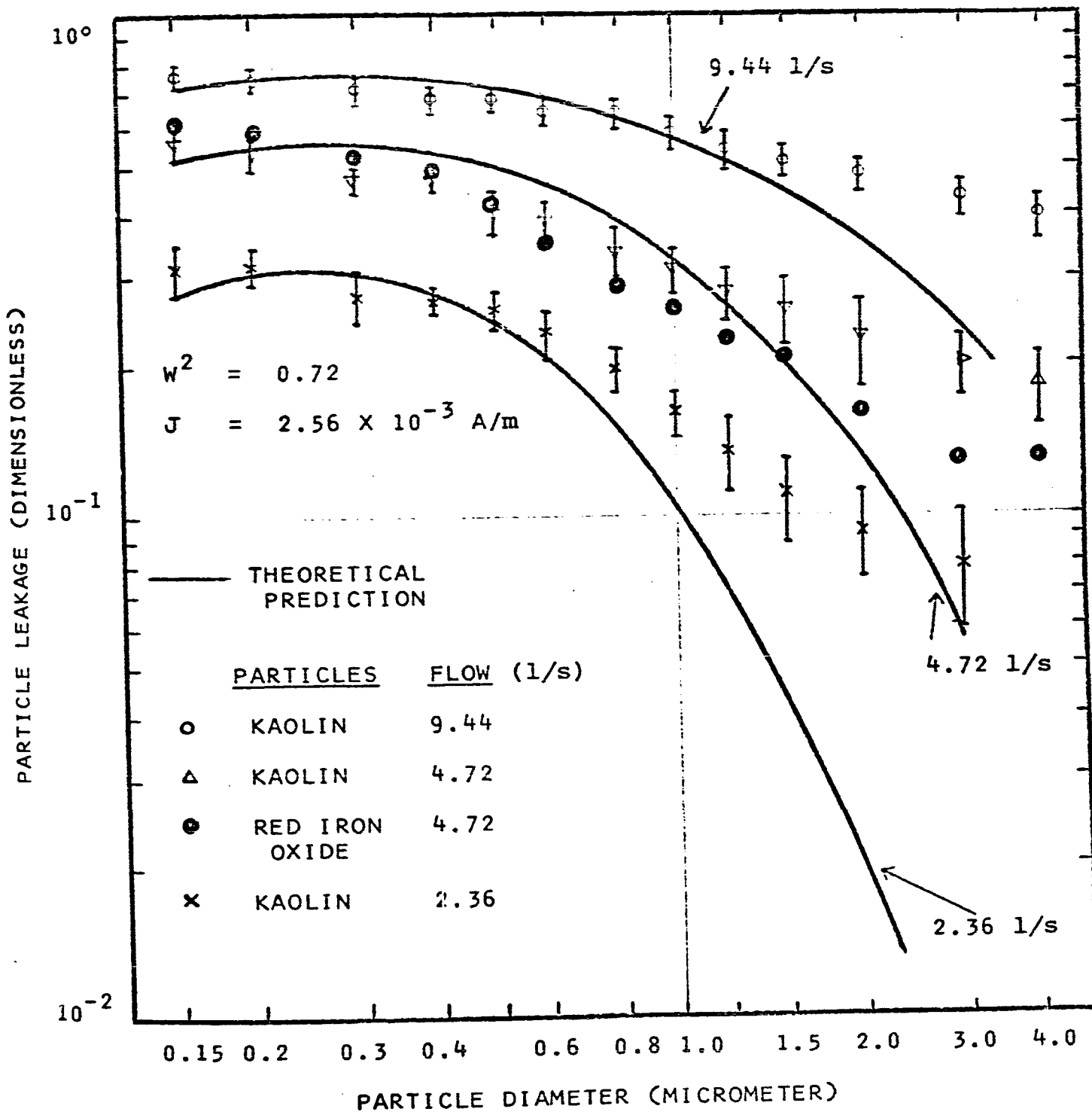
The effect of particle size and air flow rate on the collection efficiency in the first stage of the concentric geometry precipitator was tested by connecting the repeller electrode to ground so that no collecting field existed in the second stage. The results are shown in Fig. 5.7 and the theoretical prediction based upon the analysis of section 5.1.2 is also shown on the graph. The theoretical points were normally arrived at with the aid of the graphs in Appendix B. However, for this case a sample calculation is given to show the steps involved.

Sample Calculation

Experimental Conditions

Air flow (Q)	=	4.72 l/s (10 S.C.F.M.)
Corona current density (J)	=	2.56×10^{-3} A/m
Inlet area of precipitator (A_x)	=	1.14×10^{-3} m ²
Metallic collection area (A_c)	=	2.61×10^{-2} m ²
Percentage open area on collector electrode	=	28%
Solidity ratio (W^2)	=	.72
Radius of collector electrode (R_1)	=	1.9×10^{-2} m
Length of collector (L)	=	3.05×10^{-1} m
Particles used - Kaolin ($\kappa'_p \doteq 11$)		
Particle concentration	\doteq	3.5×10^4 /liter (10^6 /ft ³)

FIGURE 5.7
 PARTICLE LEAKAGE FROM FIRST STAGE AS A FUNCTION
 OF PARTICLE DIAMETER AND AIR FLOW RATE



The predicted leakage is given by equation 5 - 9;

$$H = e \frac{-A_c \cdot b \cdot K_c}{A_x}$$

a) Determination of derating factor b;

From equation 3 - 34

$$\tau = \frac{4 r}{E_r K}$$

Since τ is a function of radial position and since complete turbulent mixing was assumed, the effective value of τ can be approximated by using the value of radius which encloses one half the cross section area.

$$\therefore r = \sqrt{\frac{R_1^2}{2}} = 1.34 \times 10^{-2} \text{ m}$$

$$\text{For } J = 2.56 \times 10^{-3} \frac{\text{A}}{\text{m}}$$

$$E_r = 5.1 \times 10^5 \frac{\text{V}}{\text{m}} \quad (\text{See Fig. B.1})$$

$$\text{Also } K \doteq 1.8 \times 10^{-4} \frac{\text{m}^2}{\text{SV}}$$

Assume maximum axial velocity

$$\therefore v_o = 4.14 \frac{\text{m}}{\text{s}} \quad (\text{From Section 5.2.1})$$

$$\therefore x_o = v_o \tau = 2.5 \times 10^{-3} \text{ m}$$

$$\therefore \frac{x_o}{L} = 8.1 \times 10^{-3}$$

From Fig. 5.3 this gives a derating factor for the coulomb collection parameter = 0.96.

b) Specific collection area

$$\frac{A_c}{A_x} = \frac{2.61 \times 10^{-2}}{1.14 \times 10^{-3}} = 23$$

c) Collection parameter

From Equation 3 - 36

$$K_c = 3.27 \times 10^{-7} f(a) \frac{E_r E_p}{V_o}$$

Consider a particle 0.3 μm diameter with $\kappa'_p \doteq 11$

$$f(a) \doteq 9 \times 10^{-7} \text{ m} \quad (\text{See Fig. B.4})$$

Also from before

$$E_r = 5.1 \times 10^5 \frac{\text{V}}{\text{m}}$$

In calculating the collecting field at the surface of the collector is must be noted that the metallic area is smaller than the enclosed area. Since the field lines must end on metal, there will be a local increase in the field strength which on average will be approximately given by:

$$\frac{E_r}{W^2} = \frac{5.1 \times 10^5}{.72} = 7.1 \times 10^5 \frac{\text{V}}{\text{m}}$$

$$\therefore K_c \cdot b = 2.47 \times 10^{-2}$$

$$\therefore \text{Total exponent} = K_c \cdot b \cdot \frac{A_c}{A_x} = 0.57$$

$$\therefore H = e^{-.57} = .57$$

For flow of 9.4 l/s (20 S.C.F.M.)

$$\frac{X_o}{L} = 1.6 \times 10^{-2} \quad \therefore \text{derating factor} = 0.94$$

$$\therefore \text{Exponent} = 0.28 \quad \text{and} \quad H = 0.76$$

For flow of 2.36 l/s

$$\frac{X_o}{L} = 4 \times 10^{-3} \quad \therefore \text{derating factor} = 0.98$$

$$\therefore \text{Exponent} = 1.16 \quad \text{and} \quad H = 0.31$$

The resulting values for the other sizes are shown plotted on Fig. 5.7.

The experimental results shown in Fig. 5.7 were obtained using kaolin particles at three values of air flow and also for red iron oxide particles at the air flow of 4.72 l/s. The results of these tests show excellent agreement with the theoretical predictions of the effect of air flow rate on the collection efficiency as can be seen by the

close correspondence to the predicted values for the particles in the smaller size ranges. However, it can be seen that the variation of the collection efficiency as a function of particle size shows two discrepancies.

The first is that no real experimental evidence can be seen to support the predicted minimum value of collection efficiency. This could possibly be due to instrumentation limitations since the size range from $0.15 \mu\text{m}$ to $0.3 \mu\text{m}$ is very near the lower limits of resolution for the counter and overlap in size discrimination would be quite probable. The effect of particle shape did not appear to be a factor in this case since the kaolin (flake structure) and red iron oxide (irregular spheres) gave approximately the same results in this size range. Also for these collection efficiencies, it can be seen that the magnitude of the effect was of the same order as the spread of experimental readings.

The second discrepancy concerns the divergence of the test results from the predicted curve for particles above approximately $1.0 \mu\text{m}$. This was felt to be due to the effect of the particle shape on a) the accuracy of size discrimination by the counter and b) the maximum charge placed on the particle. The size discrimination would obviously be less accurate for the kaolin particles because of their flakey structure. Moreover, it could be expected that a flat disk

of given cross sectional area would not hold as much charge as a sphere having the same cross sectional area since the actual surface area of the former would be less. This would result in a particle having less charge than expected for its measured size and hence would result in lower efficiency. This interpretation is supported by the results with red iron oxide for although there was still some discrepancy, the agreement was closer to the theory. The general agreement in the smaller sizes can be explained by the fact that the dissymmetry becomes less important as size is reduced and the particles approach a spherical shape.

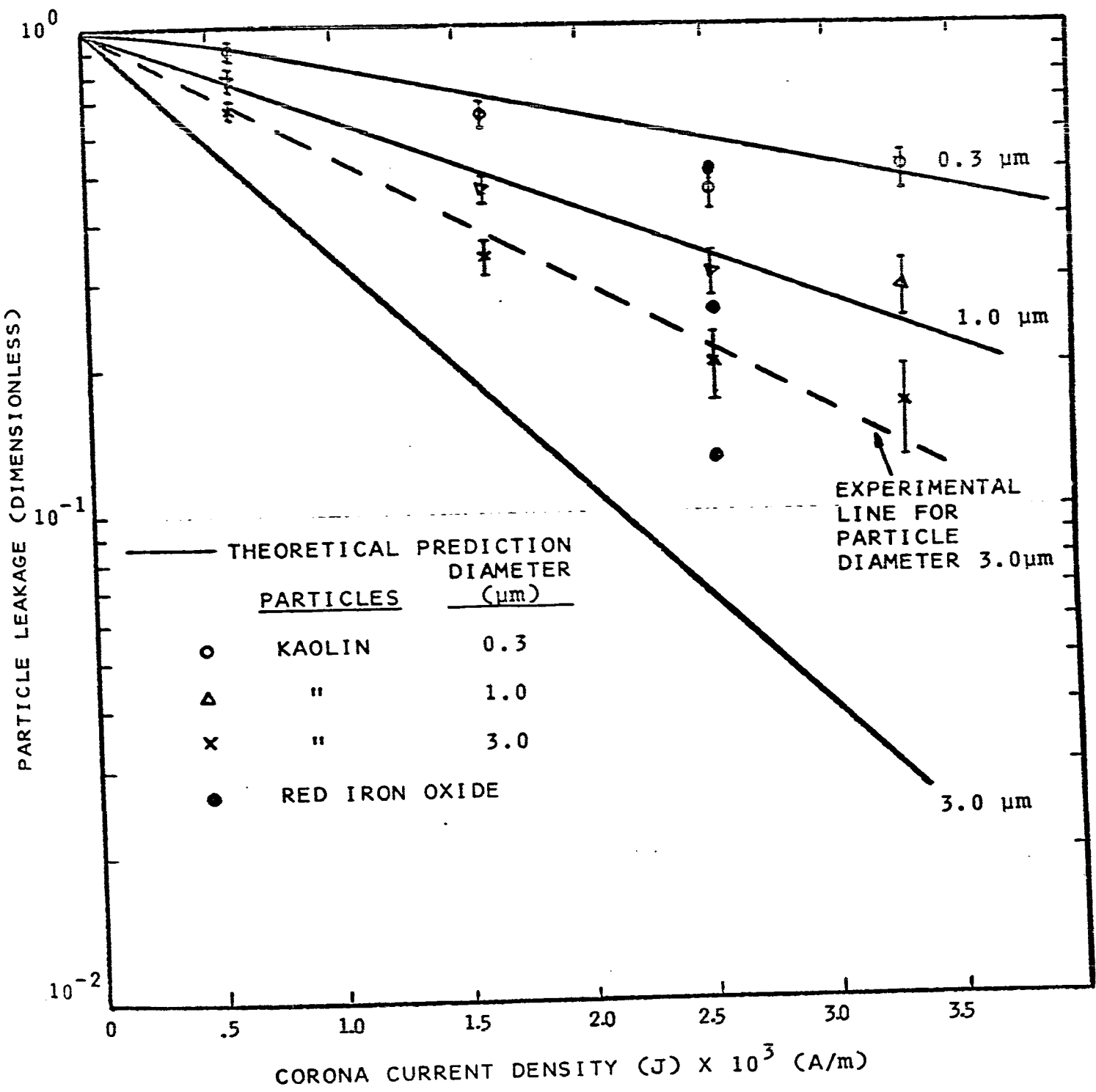
B) Effect of Corona Current Density

A series of tests was carried out to check the effect of the corona current density on the collection efficiency. These tests were taken with the air flow constant at 4.72 l/s (10 S.C.F.M.) and at four values of corona current. The results are shown in Fig. 5.8 with the leakage values plotted on a logarithmic scale and the corona current density on a linear scale.

The theoretical predictions were obtained by plotting the exponent of equation 5 - 9 on the graph (note that on a log-linear graph, the plotted value of leakage varies linearly as the value of the exponent).

Considering a fixed particle size of $0.3 \mu\text{m}$ the

FIGURE 5.8
 PARTICLE LEAKAGE FROM FIRST STAGE AS A
 FUNCTION OF CORONA CURRENT DENSITY



exponent becomes;

$$\frac{A_C \cdot b \cdot K_C}{A_X} = 1.63 \times 10^{-12} E_r E_p b$$

But

$$E_r = \sqrt{J} \times 10^7$$

$$E_p = \frac{E_r}{W^2}$$

$$\therefore \frac{A_C \cdot b \cdot K_C}{A_X} = 2.26 \times 10^2 \cdot (J \cdot b) \quad (5 - 18)$$

Calculations were made for three sizes, 0.3 μm , 1.0 μm and 3 μm diameter, and the resulting predictions are shown as the solid lines on the graph. Note that b is a function of J but since it ranged in value from .93 to .97 for the current densities considered, the resulting curve is very close to a straight line and negligible error results in considering that the exponent varies directly with J . This is a rather interesting case which results from the fact that the particle charging and particle collection are accomplished by the same field.

The experimental results show good agreement with the predicted values, except for the results with the 3 μm size which shown a similar discrepancy to that found in the last test. However, it is significant to note that the experi-

mental values did fall along a straight line showing that although the absolute values were different from those predicted, the form of variation with J was the same. The red iron oxide was only tested for the one value of J but this point again showed better agreement with the theory. The reason for this difference is probably the same as discussed before.

C) Effect of Aperture Size

As pointed out in section 4.1.6, the grounded cylindrical electrode was constructed so that the percentage open area could be varied over the range of approximately 10% + 28%. In addition, an interchangeable fine mesh cylinder having an open area of 44% and a solid cylinder * with an open area of 0% were employed. Tests were carried out at these four values of open area to determine a) the voltage-current characteristic of the corona discharge and b) the first stage collection efficiency.

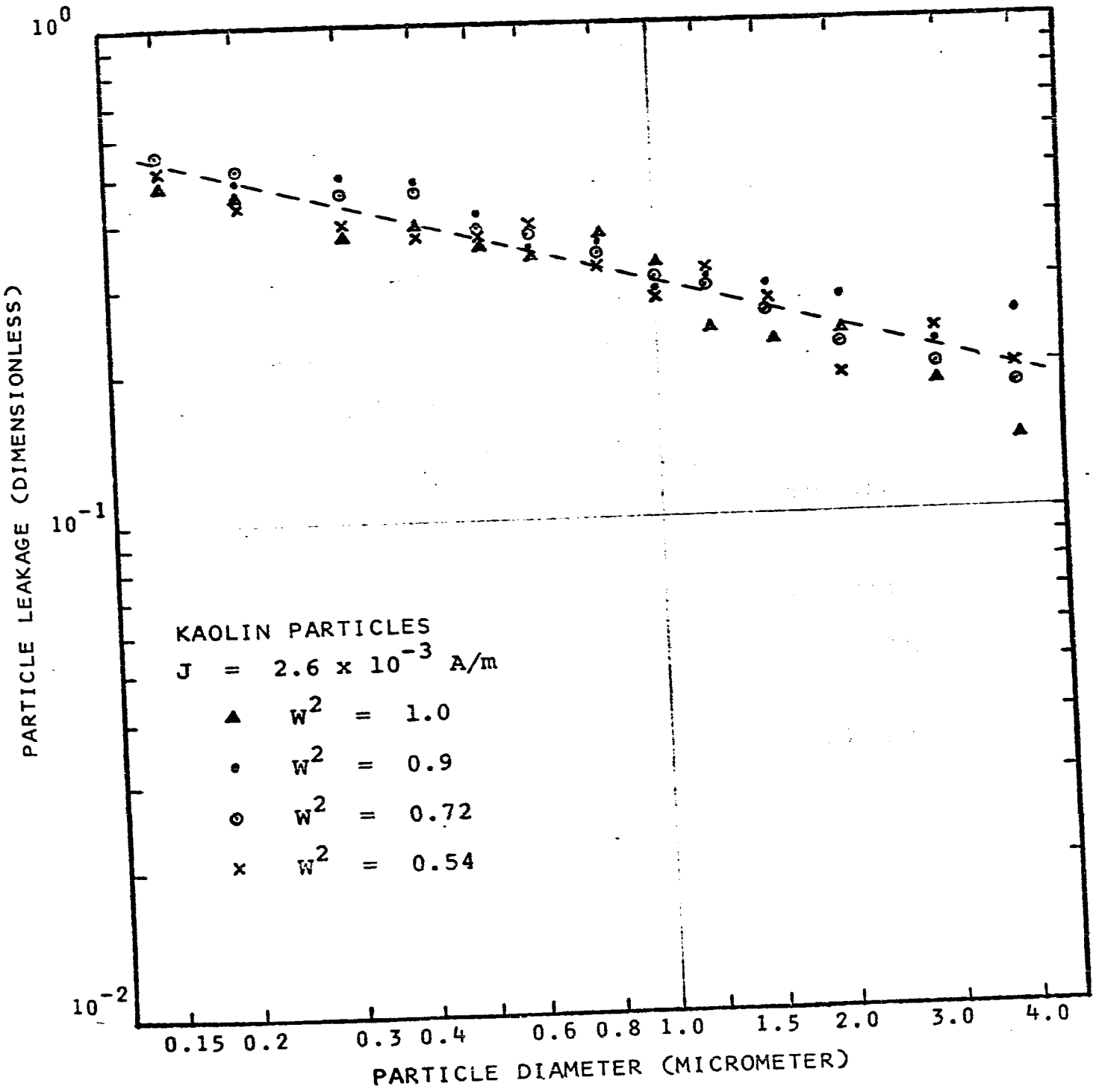
No detectable change was found for the corona characteristic for the four cases (see Fig. 6 - 7. and the curve for wire diameter 1.27×10^{-4} m (0.005") for the voltage-current characteristic). This result was not surprising since it is well known that it is the geometry of the centre conductor rather than the outer which has the main influence on the corona characteristic.

* For this test the flow was straight through the cylinder with no blockage at the far end.

The results for the collection efficiency measurements are shown in Fig. 5 - 9. They are very interesting since once again no significant change could be detected. The results agree with the derivation in section 5.1.2, and justify the assumption that was made regarding the particle velocity v_o . (It was thought that possibly the stated assumption that v_o represented the average velocity adjacent to the collector surface, would not be valid over the broad range of flow conditions ranging from straight axial to considerable radial flow components.) The other factor was that as the actual collection area available was reduced due to the increase in the open area, this was compensated by an increase in the field density at the surface. (The collection area is reduced by the factor W^2 but the average collection field is increased by $\frac{1}{W^2}$ and so the product $A_c \cdot E_p$ remains approximately constant.) This is an important point since it re-emphasizes the necessity of considering the mechanisms affecting the collection right at the surface of the collector rather than in the main volume of the air stream. Moreover, from the point of view of collection in the first stage, for the conditions studied the perforated cylinder is shown to be equivalent to a solid cylinder (long term effects could presumably affect this conclusion since maximum dust loadings and the importance of re-entrainment would probably differ for the various

FIGURE 5.9

EFFECT OF APERTURE SIZE ON PARTICLE
LEAKAGE FROM FIRST STAGE



solidity ratios).

5.2.3 Collection Characteristics of the Second Stage

A series of tests were carried out to test the validity of the assumptions made regarding the collection efficiency equation in section 5.1.3.

A) Effect of Collecting Field

Fig. 5 - 10 gives the results of the particle leakage as a function of the voltage applied to the outer electrode. Tests were taken at two values of air flow with both positive and negative polarity. Results shown on the graph are for particles of 0.3 μm diameter and also for the total mode range 0.15 μm and larger.

The theoretical prediction of the collection efficiency will be given by equation 5 - 9 with the appropriate modifications as discussed in section 5.1.3.

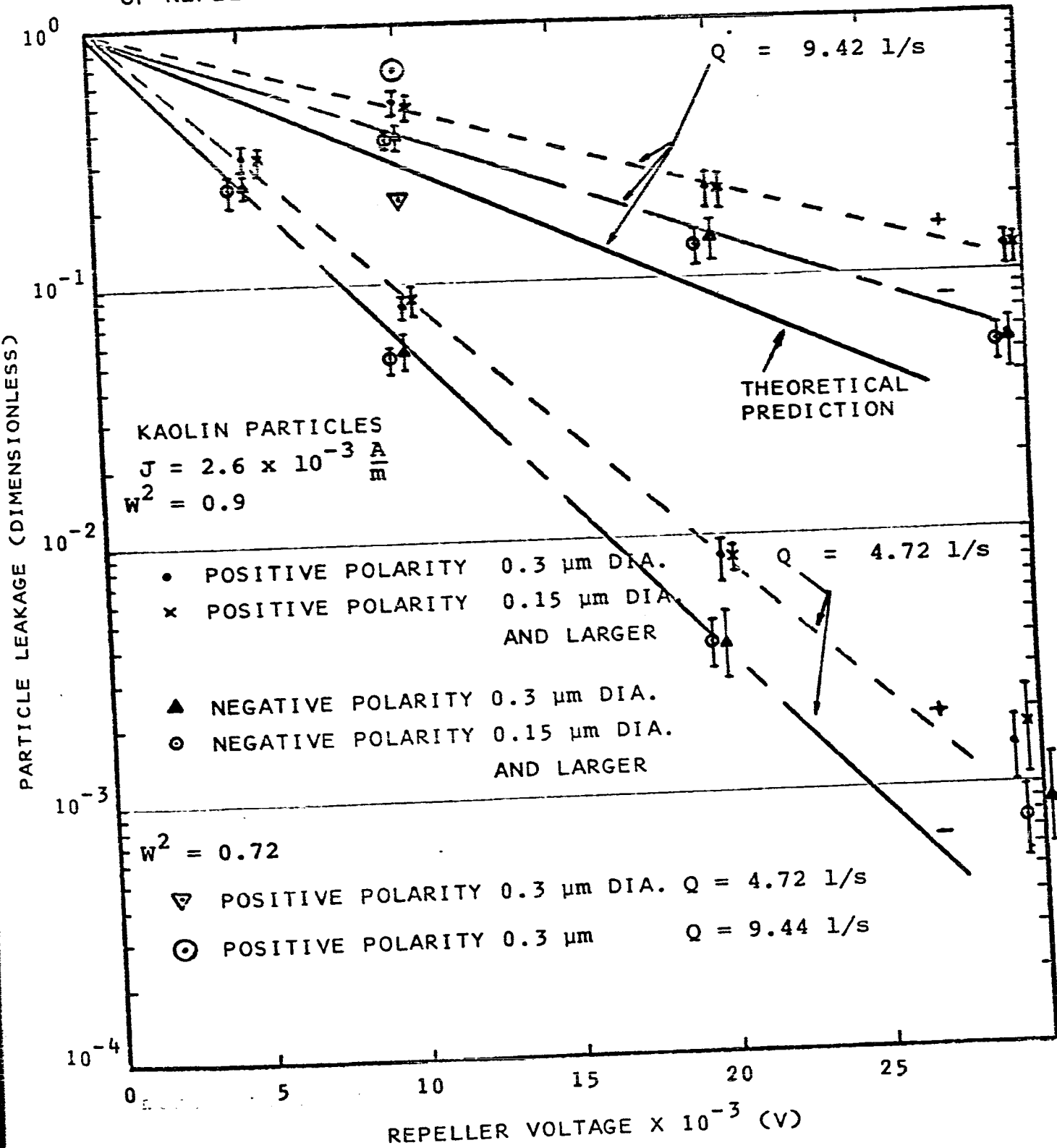
Substituting for K_c from equation 3 - 36 the exponent becomes:

$$\ln H = 3.27 \times 10^{-7} f(a) \frac{E_r E_p}{v_o} \frac{A_c}{A_x} \quad (5 - 19)$$

Consider the case of a kaolin particle of 0.3 μm diameter and collection on the inner electrode. The experimental values were:

FIGURE 5.10

PARTICLE LEAKAGE FROM SECOND STAGE AS A FUNCTION OF REPELLER VOLTAGE, POLARITY, AND AIR FLOW RATE



$$E_r = 5.1 \times 10^5 \left(\frac{V}{m}\right)$$

$$f(a) \doteq 9 \times 10^{-7} \text{ m}$$

$$W^2 = 0.9$$

$$E_p = \frac{V_r}{R_1 \ln \frac{R_2}{R_1}} \cdot \frac{1}{W^2} = 76 \frac{V_r}{W^2} \left(\frac{V}{m}\right) \quad (\text{see footnote})^*$$

$$\frac{A_c}{A_x} = \frac{W^2}{1 - W^2} = 9$$

v_o unknown.

These values give:

$$\ln H = 1.14 \times 10^{-4} \frac{V_r}{v_o} \quad (5 - 20)$$

Referring to Fig. 5-10, the experimental results were significant in several respects:

a) All the experimental points for fixed flows closely follow a straight line on the log-linear plot. (The points at ± 30 kV for the lower flow show a discrepancy which was probably due to a combination of sampling error plus the added importance at these high efficiencies of extraneous effects such as re-entrainment of the dust and possibly small air leaks.) These curves agree with

* This expression for field strength was based upon the assumptions that:
 A) the field strength between the perforated concentric cylinders was approximately the same as for solid cylinders.
 B) end effects were neglected.

equation 5 - 20 which gives the exponent of the leakage as varying directly with the voltage on the repeller, and therefore confirms the exponential form of the relationship.

b) Note that the measured results for 0.3 μm particles were practically indistinguishable from the results for 0.15 μm and larger. This was found to be true in general for the size distribution and concentrations of kaolin particles used in the tests. Hence, this enabled measurements to be made on a total mode basis, whereas the calculations could be based upon a particle size of 0.3 μm diameter.

c) For each case, the negative polarity on the outer electrode gave slightly higher collection efficiencies than the positive polarity. This showed that the collection process was slightly more effective at the outer electrode. Of the various factors which were discussed in section 5.1.3 as possibly affecting this, the main reason for the higher efficiency was probably due to the lower mean velocity in the vicinity of the outer electrode compared to the inner.

d) Two points are shown on the graph for the + 10 kV potential and the solidity ratio of the inner cylinder at 0.72. The relatively lower collection efficiencies were presumably due to the non-uniform air distribution in the

second stage resulting in higher mean velocities during collection.

e) Finally, the expression given by equation 5 - 20 was used to check the effect of the air flow rate. No practical means could be used to characterize the velocity v_o . Therefore, the value of v_o was determined for the flow of 4.72 l/s from the experimental curve. From this value a predicted curve was drawn for the flow of 9.44 l/s based upon the assumption that the effective value of velocity would be doubled at double the flow.

ie: from Fig. 5 - 10, at $V_r = + 10$ kV and

$$Q = 4.72 \text{ l/s}$$

$$H = 0.09$$

$$\therefore \ln H = \frac{1.14}{v_o} = 2.4$$

$$\therefore v_o = 0.48 \frac{\text{m}}{\text{s}}$$

\therefore For $V_r = + 10$ kV and $Q = 9.44$ l/s

Assume $v_o = .95 \frac{\text{m}}{\text{s}}$

$$\therefore \ln H = \frac{1.14}{.95} = 1.2$$

$$\therefore H = 0.3$$

The predicted curve can be seen to give efficiency values higher than the experiment and would indicate that

when the flow was doubled, the actual effective velocity was somewhat more than double the value at half the flow. However, the predicted curve was of the same order as the experimental values and would again justify the approach taken in section 5.1.3. Note that the value of the effective velocity for the 4.72 l/s is a reasonable value when compared to the predicted velocities shown in Table 5.2. Here the velocity in the jet would be 1.3 m/s and the mean velocity at the surface 0.13 m/s whereas the effective velocity was 0.48 m/s which lies between the two extremes.

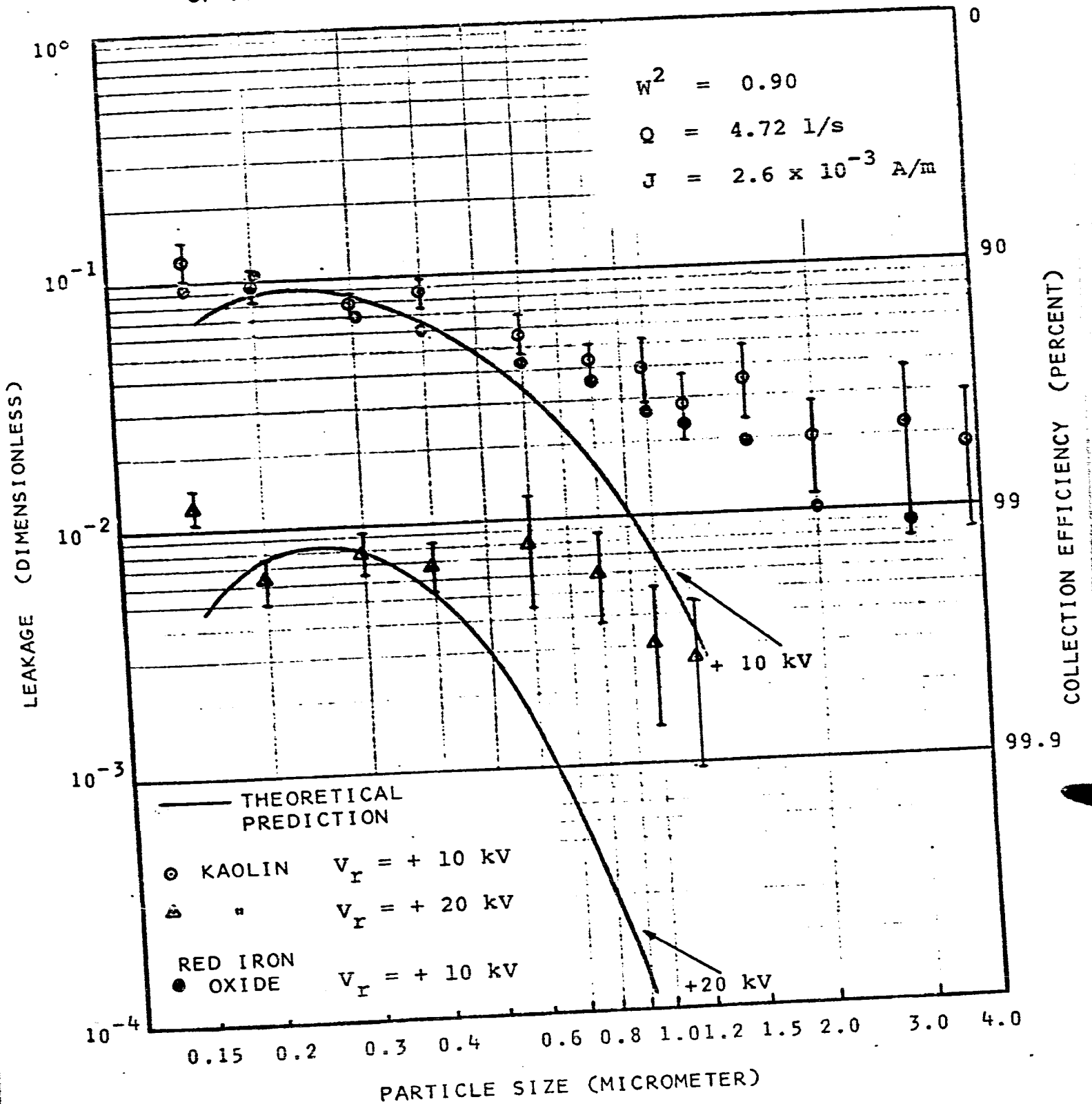
B) Effect of Particle Size

Fig. 5.11 shows the measured collection efficiencies as a function of particle size, for an air flow of 4.72 l/s and two values of repeller voltage for kaolin and at one value of voltage for red iron oxide. The theoretical prediction of the collection efficiency was based upon equation 5-19 using the value of effective velocity as found empirically from Fig. 5.10.

The results of this test show a similar pattern to those found for the first stage. Once again no minimum could be detected and the larger sizes were collected less efficiently than predicted. The explanation for this would be the same as before, as again the red iron oxide had slightly higher efficiency than the kaolin.

FIGURE 5.11

PARTICLE LEAKAGE FROM SECOND STAGE AS A FUNCTION OF PARTICLE SIZE AND REPELLER VOLTAGE



Note in this case the excellent agreement with the 0.3 μm particles was due primarily to the fact that the value of velocity used in the expression for the exponent was based upon the test results for the 0.3 μm size. However, the general pattern for all the sizes showed agreement with the effect of doubling the repeller voltage.

C) Effect of Corona Current Density

Fig. 5.12 shows the results of a series of tests to determine the effect of the corona current density on collection in the second stage.

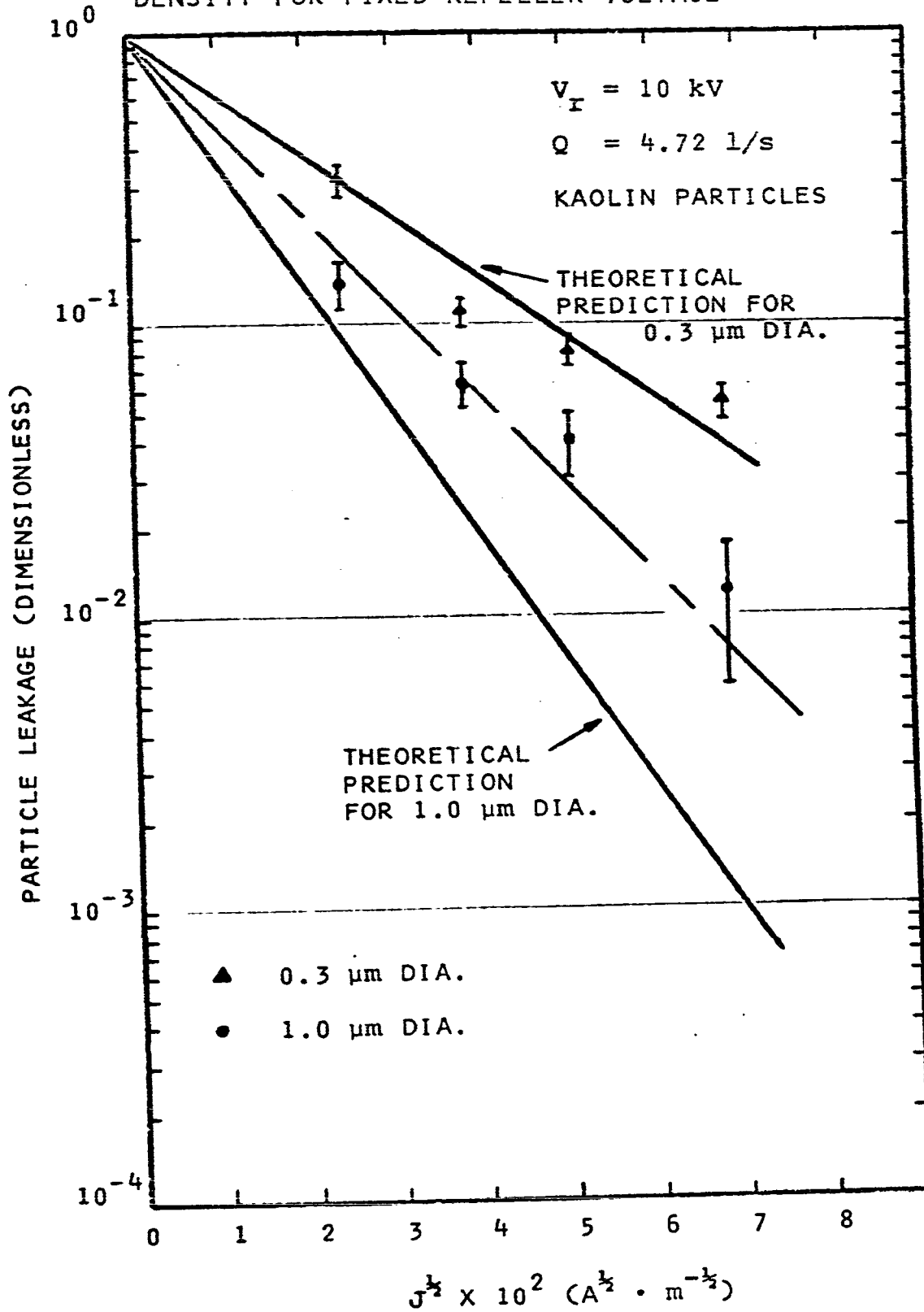
The theoretical predictions were obtained from the curves on Fig. 5.11 for 0.3 μm and 1.0 μm diameter particles for the corona current density $J = 2.56 \times 10^{-3}$ A/m. From equation 5 - 19 and 3 - 29 the form of variation of the exponent is such that for fixed particle size, air flow and repeller volts:

$$\ln H \propto \sqrt{J}$$

This relation would produce a straight line on a log-linear graph if the \sqrt{J} was plotted on the linear axis. This has been done in Fig. 5.12 and the results agree well with the predicted relation. Note as in the first stage, the results for the larger sizes, for example 1.0 μm diameter, differ from the predicted value but follow a straight line relation.

FIGURE 5.12

PARTICLE LEAKAGE AS A FUNCTION OF CORONA CURRENT DENSITY FOR FIXED REPELLER VOLTAGE



The results of this series of experiments has justified the assumptions made regarding the collection efficiency in section 5.1.3. Moreover, it has been shown that reasonable collection efficiencies, ie: 99% are possible with this geometry.

5.2.4 Collection Characteristics of the Second Stage with Electrified Media Present

This section deals with an extensive series of experiments to determine the effect of increasing the available collection area in the second stage by means of dielectric media.

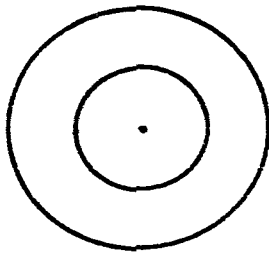
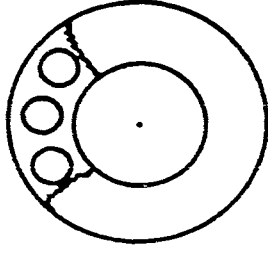
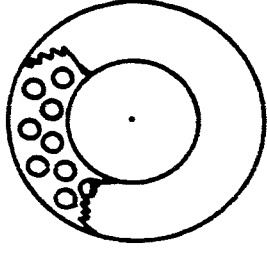
The purpose of the tests was three-fold:

- a) to determine the relative importance of the various collection force components
- b) to justify the theoretical approach used in section 5.1.4
- c) to find the optimum design parameters for a practical air filter.

Because of the large number of tests carried out during the course of this portion of the work, it proved impractical to discuss the significance of each test individually. For this reason, the following approach was adopted. The most important results are presented in graphical form and their particular significance discussed.

TABLE 5.3

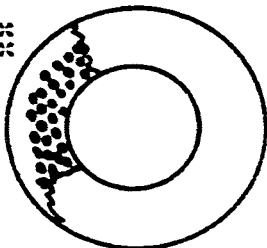
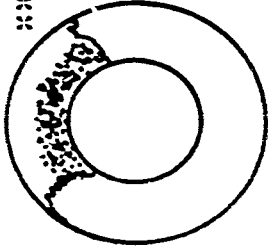
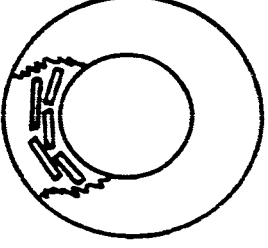
COLLECTOR GEOMETRIES

DESCRIPTION	DESIG-NATION	CROSS SECTION	SPECIFIC COLLECTION AREA ***	RATIO OF OPEN. AREA TO CROSS SECTIONAL AREA	k_c'	COMMENTS
NOTHING IN COLLECTION REGION	A		$\frac{W^2}{1 - W^2}$	$1 - W^2$	$\frac{1}{2}$	
TEN ACRYLIC RODS 12" X .375" DIA.	B		1.6	.47	$\frac{1}{2}$	RODS WERE COATED WITH GRAPHITE
TWENTY-EIGHT ACRYLIC RODS IN TWO CON-CENTRIC ARRAYS 12" X 0.2" DIA.	C		2.5	.61	$\frac{1}{2}$	RODS WERE COATED WITH GRAPHITE

*** CHARACTERIZED IN PLANE OF COLLECTION

TABLE 5.3 (CONT'D)

COLLECTOR GEOMETRIES

DESCRIPTION	DESIG-NATION	CROSS SECTION	SPECIFIC COLLECTION AREA ***	RATIO OF OPEN AREA TO CROSS SECTIONAL AREA	k_c'	COMMENTS
WIRE MAT (MADE OF INSULATED COPPER WIRE AS TWO INSULATED CIRCUITS.) 2000 FT OF WIRE $D = .008"$ MAT = $\frac{1}{2}"$ DEEP	D		5.9 *	.76	$\frac{\infty}{3}$	ELEMENTS OF WIRE MAT WERE ALIGNED AT RIGHT ANGLES TO FIELD
"VISKONAIRE" $D_c = 2.5 \times 10^{-5}m$	E		36/LAYER* OF "VISKONAIRE"	.87	$\frac{3}{3}$	
TWENTY-FOUR FLAT PLATES IN TWO CONCENTRIC ARRAYS 12-12"X.55" 12-12"X.45"	F		3.4	.16	$\frac{3}{3.4}$	

** ESTIMATE BASED UPON VOLUME OF FIBER AND FIBER DIAMETER
 *** ALSO TESTED IN PLANE GEOMETRY TEST SECTION
 **** CHARACTERIZED IN PLANE OF COLLECTION

TEST	Fixed Flow = 7.1 l/s		Possible Collection Parameters
	Particles - Kaolin I (mA)	V_r (kV)	
I	0	0	K_m
II	0.5	0	K_m, K_I
III	0	+20	K_m, K_d
IV	0.5	+20	K_c, K_I, K_d, K_m

The results from tests I and II are shown on Fig. 5.13 and tests III and IV on Fig. 5.14.*

The general results of these tests indicated that:

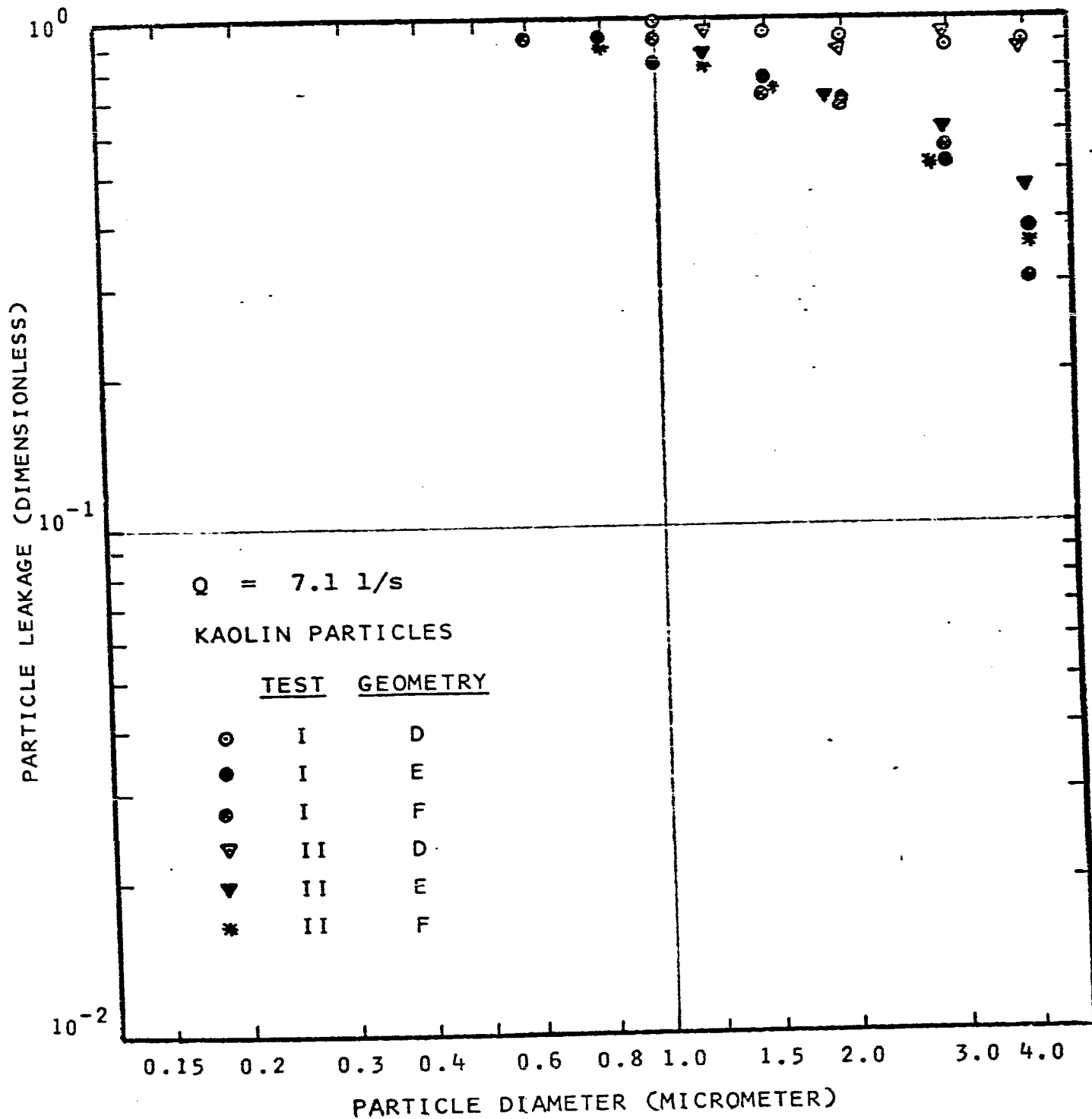
- a) For geometries A, B and C no collection component other than K_c could be detected.
- b) For geometry F, K_m had a significant effect, particularly in the larger size range.
- c) For geometries D and E, both K_m and K_d had significant effects, particularly in the larger size range.
- d) No K_I component could be detected for any case.
- e) For the experimental conditions in these tests K_c was the most important parameter for all cases in which it was present. In particular, for the size range of 0.3 μm diameter, negligible error would result by only considering the K_c term as causing the collection.

On the basis of point d) the effect of the geometry change was determined by assuming only K_c was operative. To establish quantitative estimates for the exponent in

*Note that the results for the dielectrophoretic force on Fig. 5.14 have been shown independent of the mechanical effects, whereas the results for test IV include all the force components as well as the collection of the 1st stage.

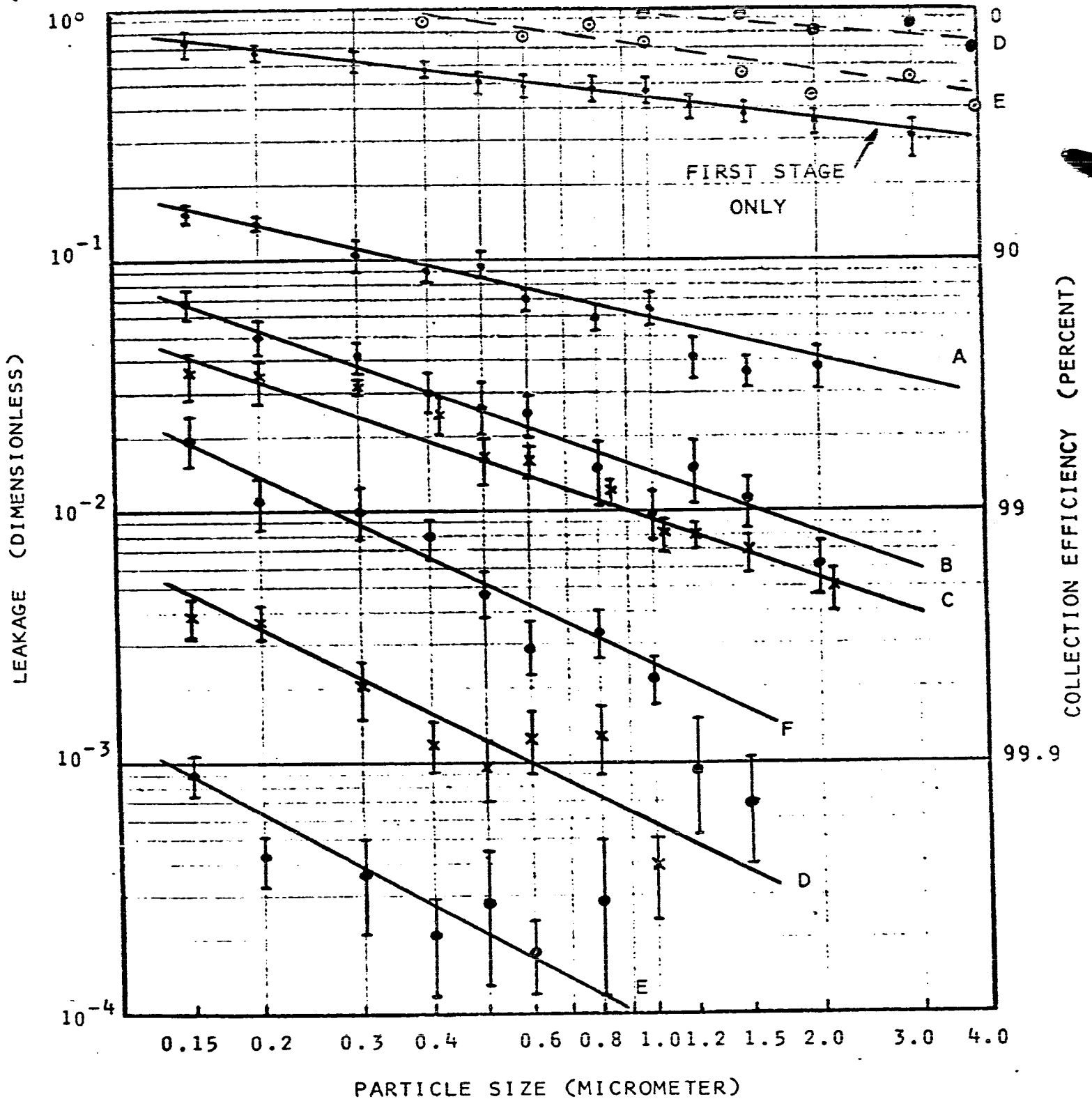
FIGURE 5.13

PARTICLE LEAKAGE AS A FUNCTION OF PARTICLE SIZE FOR MECHANICAL AND IMAGE COLLECTION MECHANISMS



PARTICLE LEAKAGE DUE TO FIRST AND SECOND STAGES AS A
FUNCTION OF PARTICLE SIZE

(DASHED LINES-DIELECTROPHORETIC COMPONENT)(SOLID LINES-ALL COMPONENTS)



NOTE: LETTERS REFER TO GEOMETRY OF COLLECTORS

equation 5 - 17 it was necessary to know for each geometry; the specific collection area, the mean velocity in the vicinity of the collectors, and the average electric field strength at the collector surface. The specific collection area for each geometry as calculated is shown in Table 5.3. The mean air velocity for cases A and F was difficult to estimate due to the presence of the air jets. Therefore, for both these cases the effective mean velocity was taken as a value between the velocity in the jets and the mean flow velocity at that point in the same ratio as was found experimentally for case A in section 5.2.3. (For case F the mean flow velocity used was taken as the velocity midway between the two layers of collectors.) For the cylindrical collectors B and C, the effective mean velocity was taken as the average of the maximum and minimum velocities that would exist for the air passing around the cylinders. For both D and E the mean velocity was defined by equation A - 3a, in Appendix A. The effective field strength at the surface of the collectors was determined as shown in Appendix A, by assuming that there was no interference effects and that the collector was in an initially uniform field whose magnitude was the mean of the field that would exist within the collector if it had a relative permittivity of 1.

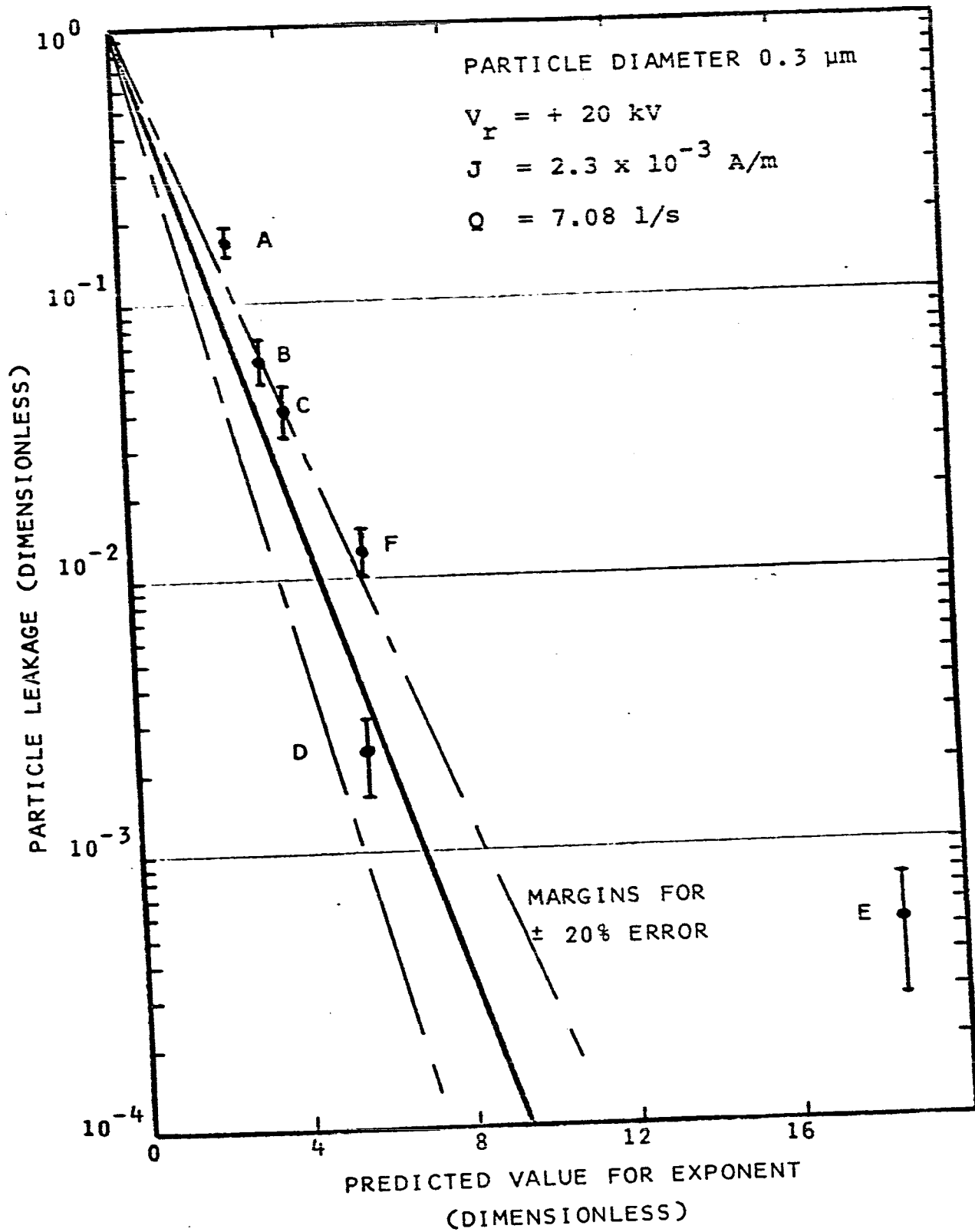
Based upon these several assumptions, a theoretical

value for the exponent defining the particle leakage was calculated for the single particle size $0.3 \mu\text{m}$ diameter. The experimental results were taken from Fig. 5.14 and are shown on Fig. 5.15 with the theoretical value of the exponent plotted on the linear scale. The straight line on this graph signifies exact correspondence between theory and experiment. For comparison the curves are also shown defining $\pm 20\%$ discrepancy. (Note that points lying to the right of the line show experimental efficiencies less than predicted, points to the left give values greater than predicted by theory.

The results of Fig. 5.15, although admittedly of an approximate nature, were significant in that with one exception (Case E), they agreed reasonably well with the predicted results. Moreover, Case E shows a discrepancy which was not unexpected. In the measurement of the specific collection area for the "Viskonaire" media, no attempt was made to account for such things as clumping of fibers, orientation of fibers relative to electric field, interference effects, etc. It would be expected that the effect of these factors would be to considerably reduce the effective specific area that was available for collection. (The close agreement of the wire mat can be explained by the fact that the packing density was much less and the fibers were specially arranged to meet the field lines at right

FIGURE 5.15

PARTICLE LEAKAGE FOR DIFFERENT COLLECTOR GEOMETRIES COMPARED TO THEORETICAL VALUE OF EXPONENT



angles.)

The most important result of these tests must be the fact that in all cases, the collection efficiency increased as the specific collection area increased. Therefore, the addition of dielectric collection media alone increased the usefulness of the electrical collection forces and allowed them to work more efficiently.

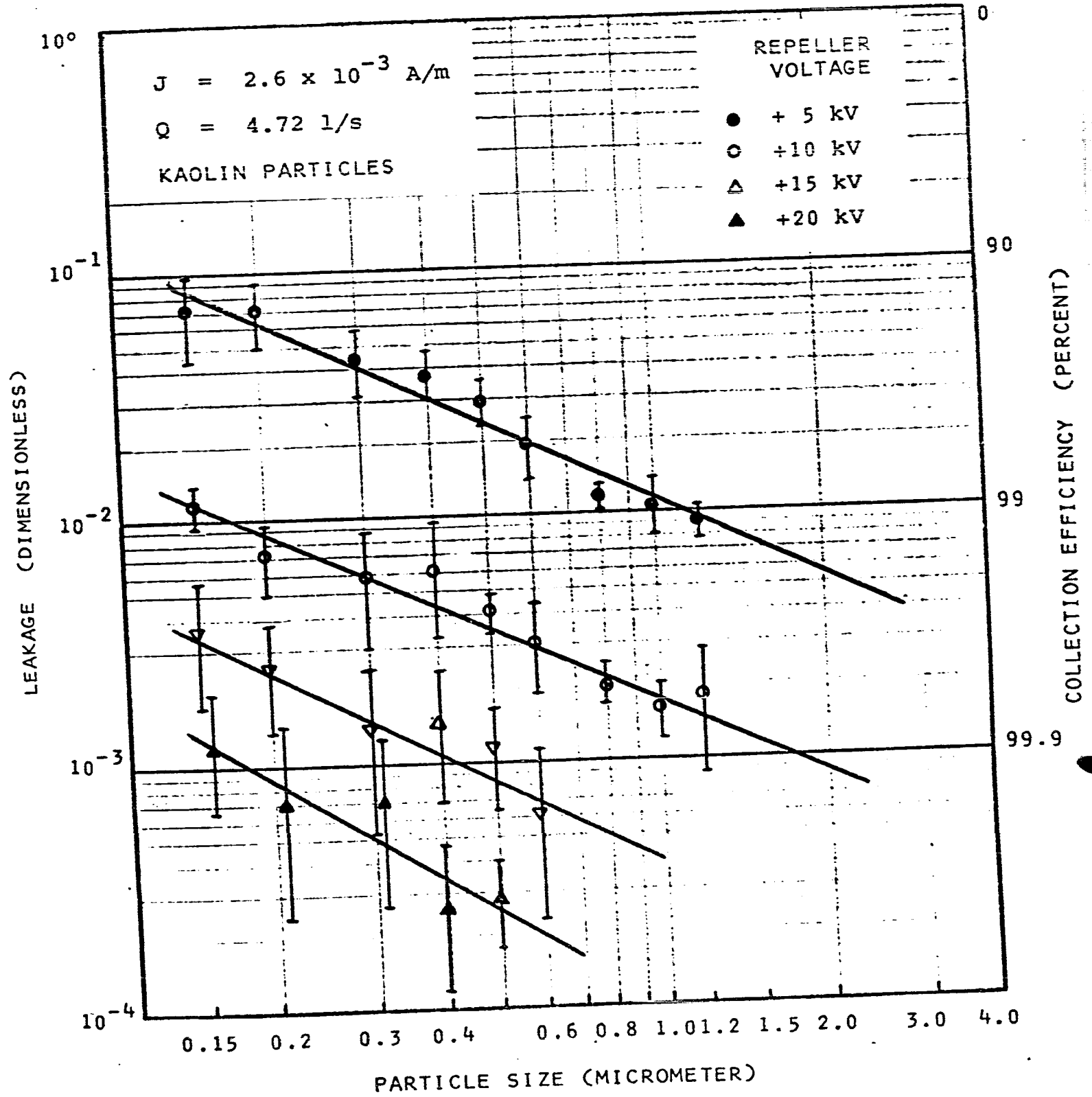
B) Collection Parameters in "Viskonaire"

In spite of the fact that the actual collection efficiency did not increase as much as would be expected from the measured specific surface area of the "Viskonaire", it still represented the maximum collection efficiency obtained with any of the geometries. For this reason, the properties of this collection media were investigated in more depth than any of the others.

Fig. 5.16 shows the results of a series of tests on a filter containing 2 tightly wound layers of "Viskonaire" for various conditions of applied voltage but with fixed air flow. To calculate the relative importance of the different force components it was necessary to know the effective value for $\frac{A_C}{A_X}$ for this configuration. This was determined from the experimental results with the assumptions that:

- a) For large collection efficiencies, K_C is the most important component and the other collection parameters

PARTICLE LEAKAGE FROM SECOND STAGE OF PRECIPITATOR WITH "VISKONAIRE" AS A FUNCTION OF REPELLER VOLTAGE AND PARTICLE SIZE



can be ignored compared to it.

b) Since the collection area available in the media is much greater than for the grounded cylinder and since the media was in direct contact with it, the collection was considered to occur only on the area provided by the media.

c) The effect of fiber interaction, orientation, etc. can be accounted for by the determination of an effective specific surface area.

The collection efficiency in the fibrous media for the particle size $0.3 \mu\text{m}$ is plotted in Fig. 5.17 as a function of repeller volts. For the predicted exponential relation a straight line would result and the best fit straight line is shown on the graph.

The experimental conditions were:

$$Q = 4.72 \text{ l/s (10 S.C.F.M.)}$$

$$J = 2.3 \times 10^{-3} \frac{\text{A}}{\text{m}} \text{ (0.7 mA/ft.)}$$

$$\therefore E_r = 4.8 \times 10^5 \frac{\text{V}}{\text{m}}$$

$$v_o = v_{av} \text{ through bed} = \frac{0.086}{0.87} \doteq 0.1 \frac{\text{m}}{\text{s}}$$

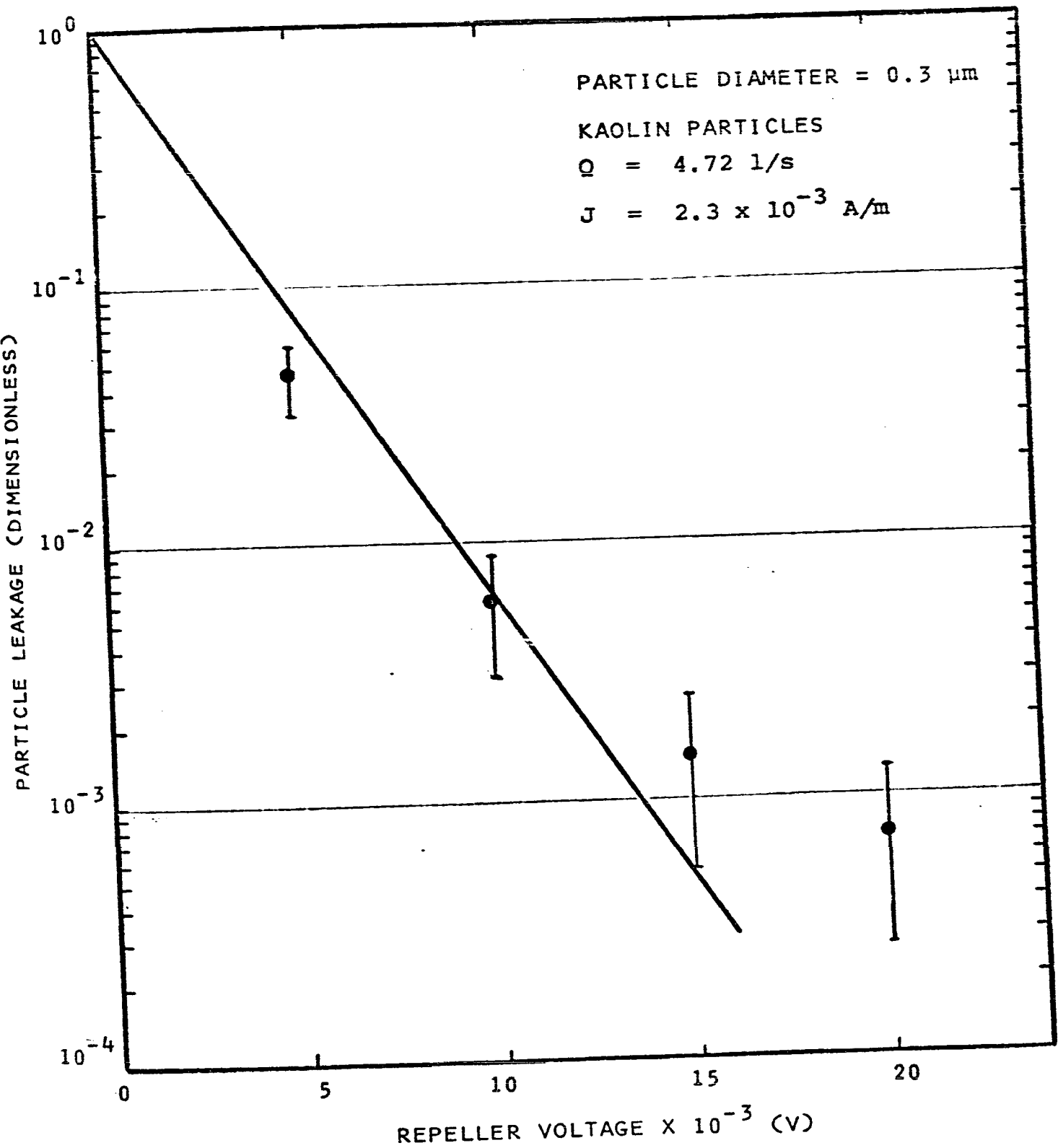
$$\kappa_p' \doteq 11 \text{ (Kaolin)}$$

$$\kappa_c' \doteq 3 \text{ (Terylene)}$$

$$f(a) \doteq 9 \times 10^{-7} \text{ (for } 0.3 \mu\text{m)}$$

FIGURE 5.17

PARTICLE LEAKAGE FROM SECOND STAGE WITH "VISKONAIRE"
PRESENT AS A FUNCTION OF REPELLER VOLTAGE



∴ From equation A - 6

$$\bar{K}_C = 1.55 \times 10^{-7} \frac{f(a) E_r E_o}{\bar{V}_o}$$

For the mid-point of the dielectric bed:

$$E_{oav} \doteq \frac{V_r}{(2.54 \times 10^{-2})(0.69)} \doteq 57V_r$$

From the slope of the curve on Fig. 5.17

$$\bar{K}_C \frac{A_C}{A_X} = 2.3$$

when

$$V_r = 4.4 \text{ kV}$$

$$\therefore \frac{A_C}{A_X} \doteq 13.5$$

Note that this value was approximately 0.2 of that which would be expected for two layers of "Viskonaire" (see Table 5.3). This is not unreasonable considering the packing density effects mentioned earlier.

Using this above value of the specific collection area, it was possible to obtain a quantitative estimate of the importance of the various force components.

I) Mechanical Forces

The theoretical predictions were obtained by considering the effects of Impaction and Interception from

equation 3 - 10 and Figures 3.2 and 3.3. The calculations were based upon a density for kaolin of $\rho_p = 2.6 \times 10^3$ kg/m³ and the particle velocity was taken as the velocity through the holes in the perforated cylinder (ie: for this case $w^2 = 0.72$. \therefore at $Q = 4.72$ l/s, $v_o = 0.46$ m/s).

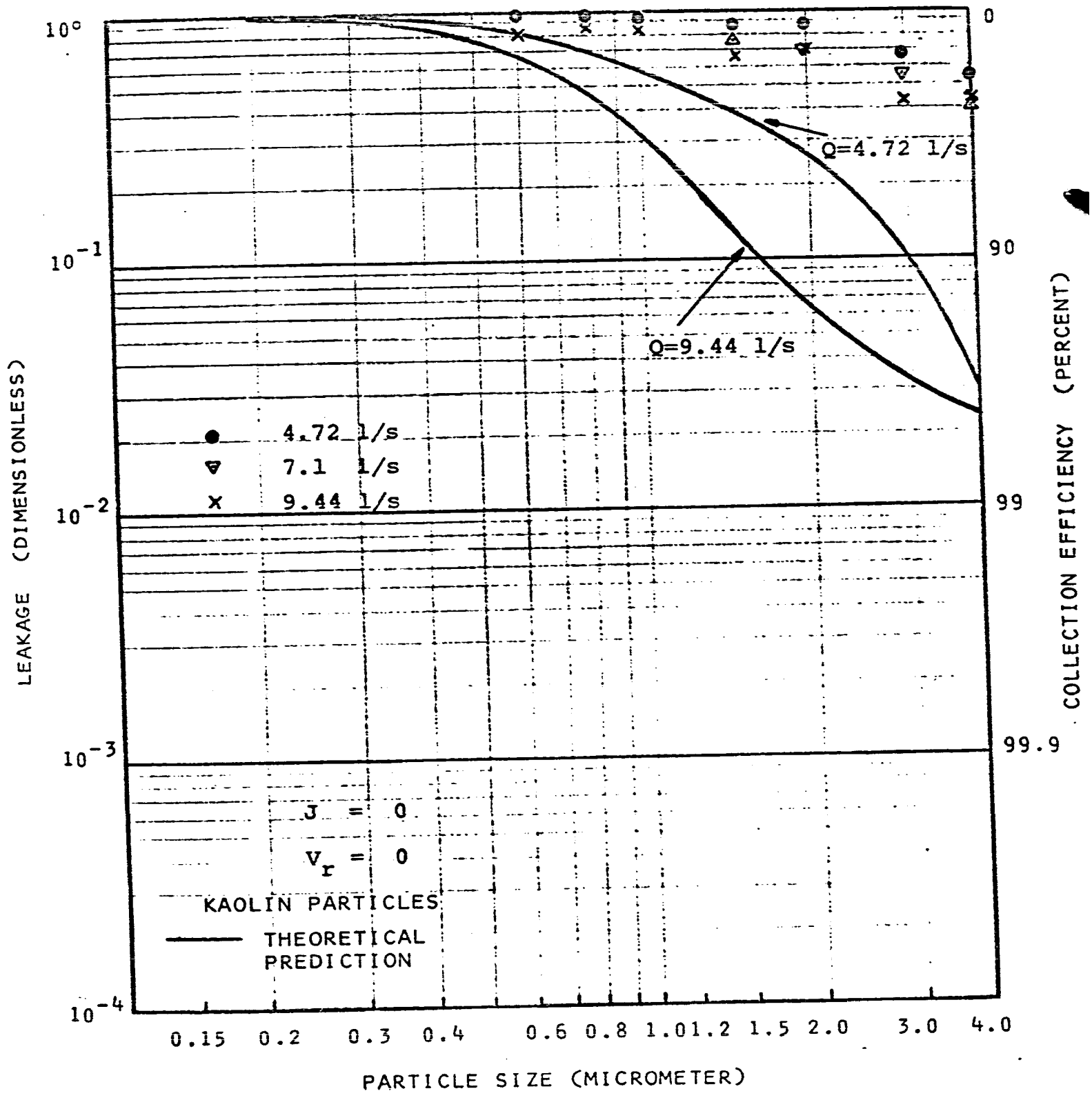
The results of the theoretical predictions for two values of flow are shown in Fig. 5.18. In addition, the experimental results taken at three values of flow are shown. These experiments were carried out with V_r and V_c set to zero. Care was taken to ensure no electrostatic effects by discharging both the particles and fibrous media with alpha radiation.

The results of this experiment show several interesting points:

- a) The experimental efficiencies are considerably below those predicted by theory although the general form is confirmed ie: efficiency increases with size and flow.
- b) The experimental results with this geometry show little or no collection for particles below approximately 1.0 μ m.

At least two factors are probably involved in the discrepancy between theory and experiment. The first concerns the probable uncertainty in particle size discrimination which was mentioned in section 5.2.2. Another is related to the possible change in the effective fiber diameter in the media

PARTICLE LEAKAGE FROM SECOND STAGE OF PRECIPITATOR
WITH "VISKONAIRE" PRESENT
(MECHANICAL FORCES)



due to compaction and clumping of the fibers. This possibility would not be accounted for in the method used for establishing the effective collection area and since the impaction parameter varies inversely with the fiber diameter, an increase in this would adversely affect the collection. In addition it will be recalled that the mechanical collection parameters were based upon single fibers whereas, in a bed such as this, interference effects will no doubt occur. In any case, it can be seen that the mechanical effect is a relatively minor force component for this size range but would have added importance for larger particles.

II) Image Force

The theoretical prediction for the collection due to the image force was obtained from equation 3 - 17 and is given by the curve in the upper right-hand corner of Fig. 5.20. Note that no collection should occur due to this effect for particles below about 1.0 μm diameter for the conditions studied.

Experiments to determine any image effects were carried out using 0.7 mA corona current and the repeller voltage set at zero. After correction for the collection in the 1st stage, the resulting leakages were compared with the results of Fig. 5.18 in an attempt to determine any difference. However, no consistent experimental

evidence was found to indicate any contribution due to image forces. (It was found in some cases that unless the "viskonnaire" was completely discharged before each test, measurable efficiencies could be obtained. However, this was due to the fields within the fibrous bed and was really due to a coulomb effect.)

III) Dielectrophoretic Force

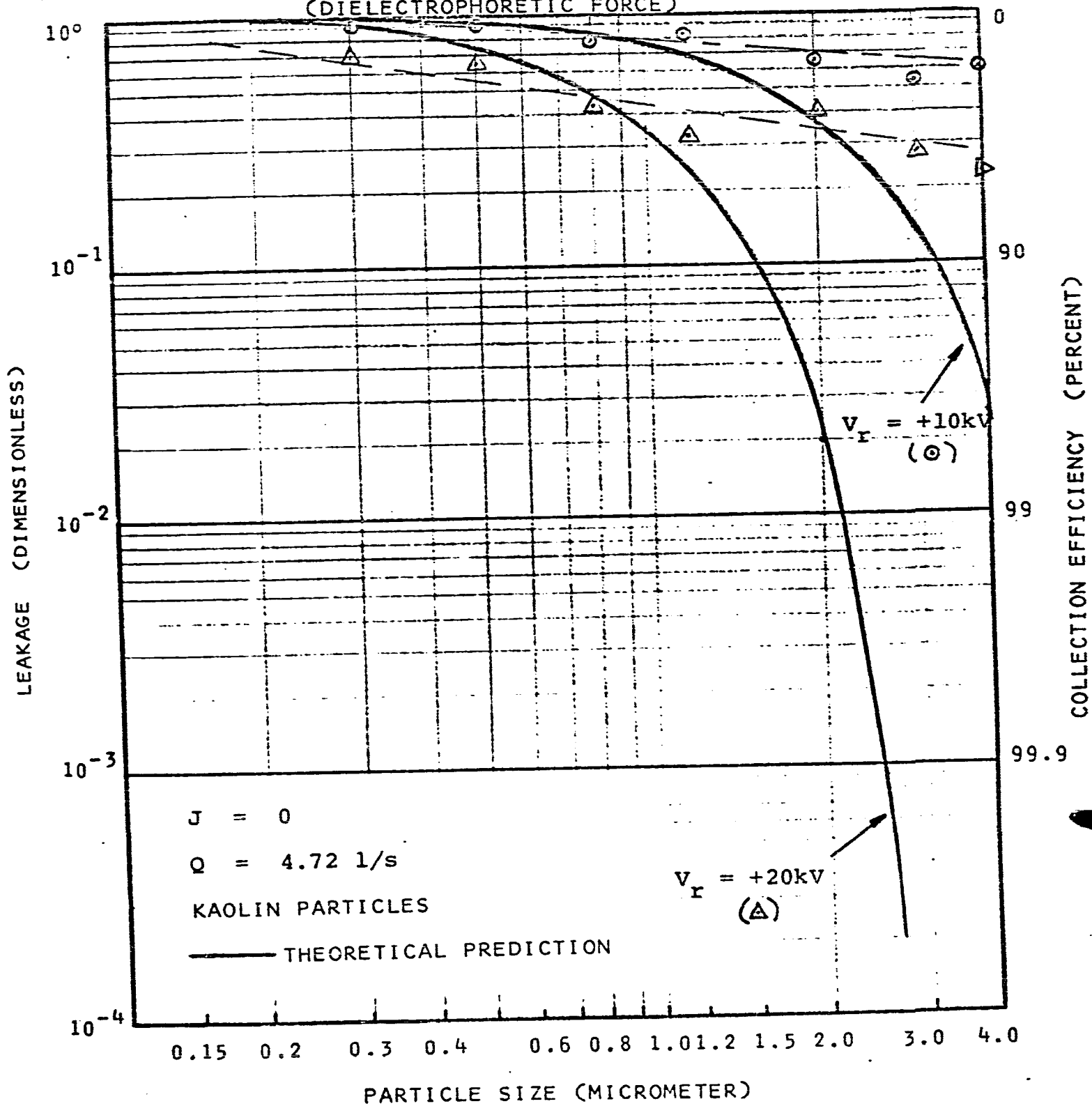
The prediction of the collection efficiency due to this effect is given for two values of field on Fig. 5.19. The experiments were carried out with no corona current and the particles discharged. The results show a discrepancy with respect to size of the same sort as shown before and the same reasons were presumed to cause the difference. Both the theoretical predictions and experimental results showed that next to the coulomb parameter, this term had the most effect on collection with small efficiencies recorded in even the 0.3 μm size range. (It should be noted, that even though the particles were discharged, it is highly probable that some small charges existed on the particles. Thus, the recorded results, particularly for the small sizes which show efficiencies higher than predicted, probably include some coulomb effects as well.)

IV) Coulomb Force

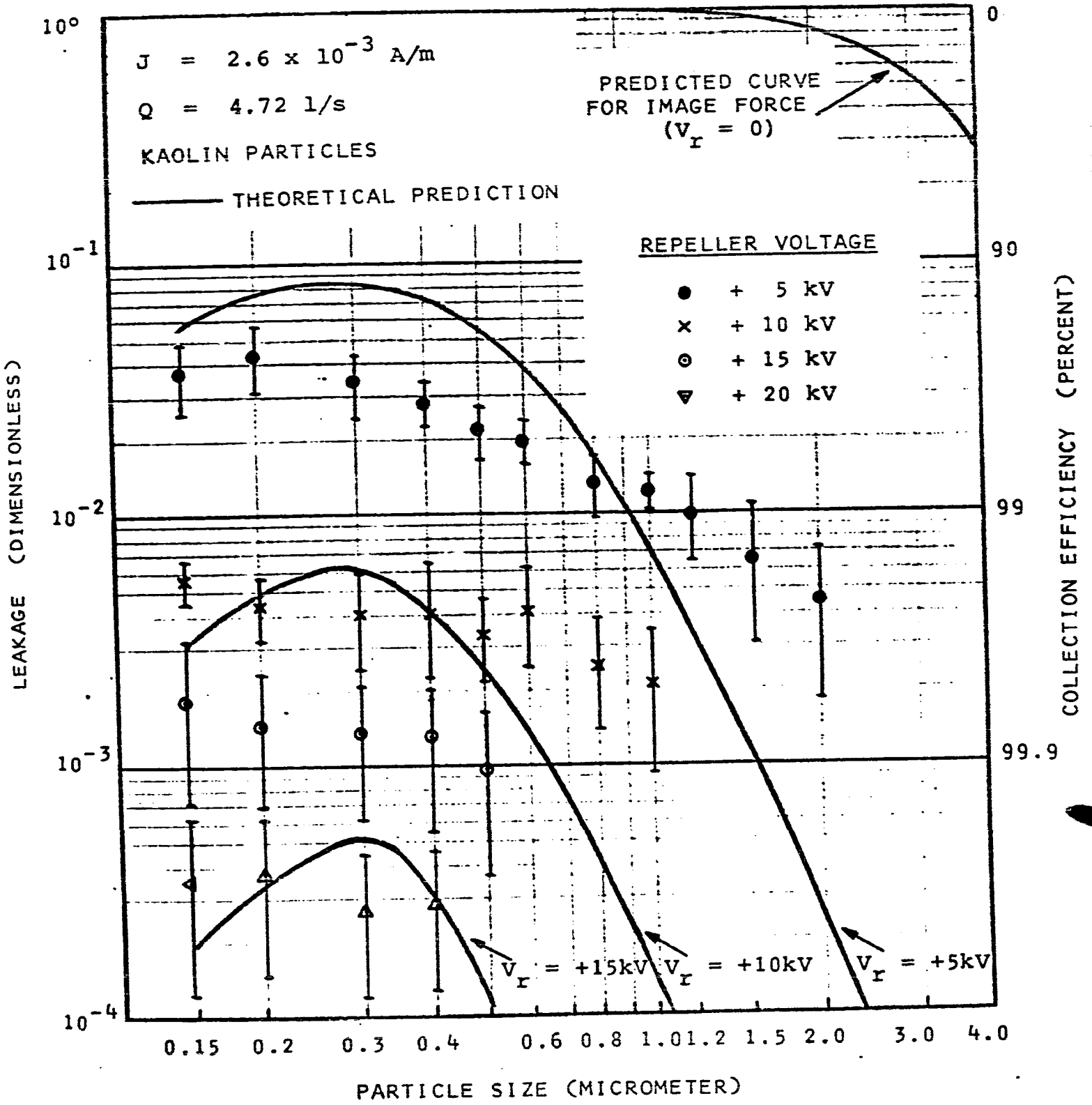
The theoretical prediction for the collection efficiency due to the coulomb force is given on Fig. 5.20.

FIGURE 5.19

PARTICLE LEAKAGE FROM SECOND STAGE
OF PRECIPITATOR WITH "VISKONAIRE" PRESENT
(DIELECTROPHORETIC FORCE)



PARTICLE LEAKAGE FROM SECOND STAGE OF
PRECIPITATOR WITH "VISKONAIRE" PRESENT
(COULOMB AND IMAGE FORCES)



In addition, the experimental results for the collection due to the coulomb component are given for a fixed corona current and four values of repeller voltage. (Because of the small values of the other terms, they are neglected when compared to the coulomb component.)

The results show general agreement with the theoretical values. The over prediction at the high values of efficiency were again presumably due to leakage and re-entrainment effects which placed a practical limit on the maximum efficiency it was possible to obtain. From the point of view of a practical filter the most important result shown by this graph was that for the conditions of flow, corona current etc. used here, very high efficiencies ie: $\approx 99.97\%$ were possible with a repeller voltage of +20 kV.

C) Collection Parameters in Other Geometries

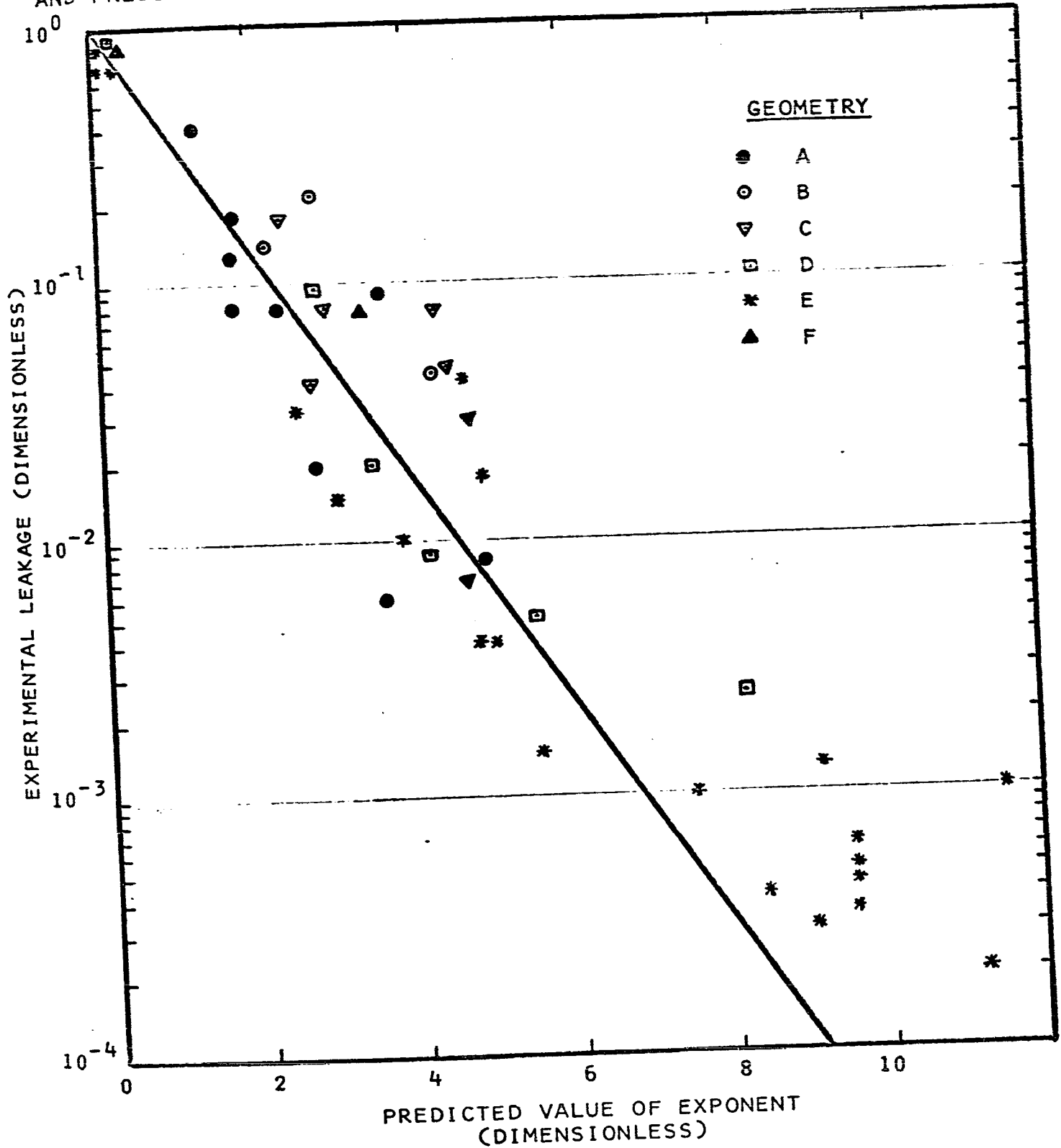
The results of a series of experiments with different geometries and conditions are summarized in Appendix C.* The measured values of leakage and calculated values for the exponent in equation 5 - 17 for the size $0.3 \mu\text{m}$ diameter are shown on Fig. 5.21.** The predicted value of the exponent is plotted on the linear axis and the measured leakage on the log axis with the straight line signifying

*Included in this series are several tests using the parallel plate rather than concentric cylindrical in the collection region.

**Also summarized on this graph are results already discussed.

FIGURE 5.21

CORRELATION BETWEEN EXPERIMENTAL PARTICLE LEAKAGE AND PREDICTED VALUE OF EXPONENT FOR DIFFERENT GEOMETRIES



exact correspondence. The calculations were based upon certain assumptions and in several cases it was necessary to use coefficients obtained experimentally from other tests (in particular the effective particle velocity for cases A and F and the specific collection area for case E). Because of the several approximations which were necessary in arriving at a predicted value, the spread of results is understandably wide. However, because of the large number of tests the overall general correlation shown on Fig. 5.21 is believed to be significant and to justify the theoretical expressions. The general trend to the overprediction at the higher values of efficiency has been previously mentioned and tends to limit the practical upper limit for the efficiencies.

D) Further Tests With "Viskonaire"

Since the "Viskonaire" media produced the highest collection efficiencies some particular experiments were carried out to study the factors involved in optimizing the collection. The following general observations were made.

I) Effect of Number of Layers of "Viskonaire"

Tests were carried out for the case of 1, 2 and 3 layers of "Viskonaire". In each case the thickness of the filter was kept constant to prevent direct contact with the

repeller electrode and care was taken to ensure the pressure drop across the combination of the perforated plate and filter media was adequate to allow equal air distribution. The results showed that there was very little difference in the three results with only a marginal improvement in each case where an additional layer was used. This appeared to be due to the packing effect which removed certain fibers from having any effect on collection. Other experiments using a grounded cylinder with $W^2 = 0.72$ did show considerable difference between the three cases. However, this was due to the fact that the air distribution was affected by the presence of the media with both the two and three layers giving better air distribution than the single layer. Therefore, it was concluded that the main effect that could be ascribed to the number of layers of "Viskonaire", was to equalize the velocity distribution.

II) Effect of Surface Conductivity of "Viskonaire"

It was speculated that if a semi-conducting surface was placed on the "Viskonaire" fibers, the field convergence per fiber should increase and also the collected charges could slowly leak off to ground. To study this effect "Viskonaire" was obtained from Johnson and Johnson Ltd. which had been specially treated with small amounts of carbon added to the surface coating of the fiber providing surface conductivities of from $10^6 \rightarrow 10^{10}$ ohm-cm. At

resistivity of 10^{10} ohm-cm no difference could be detected between the treated surface and the ordinary surface and the maximum efficiencies were obtained. As the resistivity was reduced the efficiency decreased and at 10^6 ohm-cm the measured efficiency was of the same order as measured if no "Viskonaire" was present at all. In addition for two tightly wound layers of material the maximum voltage that could be applied before breakdown occurred in the second stage was only 12 kV. This effect was presumably due to the semi-conducting volume excluding the field from the inside of the material so that only the outer surface was effective for collection. Therefore, it was concluded that for this material no advantage was gained by attempting to increase the field convergence per fiber.

III) Effect of Air Humidity

The short term effects of the humidity of the air was studied over a range from 2 → 80% R.H. and it was found that any changes which occurred in the charging or collection mechanisms as a result of the humidity change was completely negligible. However, on longer term life tests, more serious problems were encountered which resulted in marked decreases in efficiency and in several instances, complete failure of the collecting field. This problem occurred only at relative humidities greater than approximately 50% and can be explained in the following manner. At the high

humidities, some of the water vapour condenses on the available surfaces in the collection region because the air moving through the filter cools the surfaces just enough below the dewpoint for condensation to occur. The presence of a film of water makes the surface conductive and hence destroys the field within the fiber bed, and in the worst case provides a discharge path to ground either through the bed or along the insulating support structure.

This problem pointed out a limitation for this type of precipitator and would tend to preclude its use in relative humidities in excess of 50%. (Fortunately most applications which would require air cleaning, would also be equipped with air conditioning.)

IV) Effect of Voltage Polarity

The results of Fig. 5.10 showed a larger collection efficiency for negative polarity on the outer electrode. However, this was found to be of no advantage since life tests showed efficiency drops after a period of time when using negative polarity. This was felt to be due to the positive charge build-up in the bed causing the collection field to be reduced and hence nullifying any advantage of using negative polarity. On the other hand, with positive polarity on the outer electrode, the particle deposition would only increase the field strength within the bed. This was confirmed with life tests where it was found that the

measured efficiencies were higher than for the same test on the short term. (Another factor possibly affecting this was felt to be the fact that the measurement accuracy was improved on the long term tests since the counter could be purged in a clean environment much longer and also individual sampling times could be increased.)

V) Effect of Charge Retention

The fact that the charges deposited in the bed had a relatively slow leakage time* proved to be very important in practice as they greatly improved the reliability of the unit. For instance the presence of the charge was found to give rise to an electric field which remained in the bed and maintained the coulomb collection force even after the power was turned off. As an example, in one case the filter was operated continuously for 48 hours and had a measured leakage of 0.001 for 0.3 μm diameter particles from room air. It was switched off and when retested after 48 hours, had a measured leakage of 0.15 on room air with no charging or collection field applied and 0.02 with charging field only applied. (This showed that the natural charges on the dust in room air could have considerable effect on collection even with no corona power.) As another example, a life test on a dense aerosol of D.O.P. and only

*Provided the relative humidity was below approximately 50%.

corona power applied, showed very small initial collection efficiencies, ie: leakage \doteq 0.6. This gradually improved with time as the charge build-up occurred until a leakage of 0.004 was achieved. (In comparison, a leakage of 0.0003 was possible with +20 kV applied to the repeller.)

VI) Effect of Corona Current

An interesting saturation effect was noted for the "Viskonaire" filter when operating close to its maximum efficiency ie: \doteq 99.9%. Changing the corona current from 0.7 mA to 0.4 mA had no measureable change on the efficiency and at 0.2 mA only a minor reduction was noted. This again tended to indicate that the maximum efficiency was limited by a combination of chance effects such as re-entrainment, small air leaks, and measurement accuracy rather than the collection process itself.

CHAPTER 6

OZONE GENERATION

6.1 Introduction

Three series of tests were carried out in this portion of the study. The first was directed at establishing a quantitative relationship among the main variables involved in the corona discharge ie: wire size, corona current, and the air flow. In this series, the discharge electrode consisted of a wire mounted axially in the inner cylinder of the corona test section as described in section 4.1.6. The diameter of this wire was varied over a size range from 1.27×10^{-2} + 8.13×10^{-2} cm (0.005" + 0.032"). To eliminate any variation due to the type of material, oxidation and surface finish, all the tests, except as noted otherwise, were made with new copper wires which were degreased before each test.

The second series studied some different wire geometries in an attempt to find a wire which would give low ozone generation combined with maximum mechanical strength.

Finally, a third series concerned the effect of aging of the wire on the ozone generation. It is known that the surface condition of a wire in positive corona is not as important to the voltage-current relationship as in negative

corona since the positive wire is an acceptor rather than emitter of electrons. However, some evidence was shown in these tests that the surface condition of the wire has great importance in that surface oxidation can cause a considerable increase in the rate of ozone formation.

6.2 Ozone Formula*

The most important experimental results in this series are summarized in Figures 6.1, 6.2, 6.3, and 6.4.

Fig. 6.1 shows typical results for a fixed wire size giving the ozone concentration as a function of corona current and air flow. It can be seen that:

- (a) a linear relation exists between the ozone concentration and corona current.
- (b) an inverse relation exists between the ozone concentration and air flow.

As a corollary of these two results one can state that for fixed conditions:

$$[O_3]' \propto I$$

Fig. 6.2 shows the ozone concentration versus corona current as a function of wire size. Fig. 6.3 gives the same information only in terms of ozone concentration versus wire radius as a function of corona current. These two graphs show that:

* The material in this section is the subject of a technical paper entitled "Ozone Generation in Positive Corona Electrostatic Precipitators" by G.S.P. Castle, I.I. Inculet, and K.I. Burgess. This paper has been accepted for publication in the Transactions of the Industry and General Applications Group of the Institute of Electrical and Electronics Engineers as paper number TOD 68-44, EP 68-3.

FIGURE 6.1

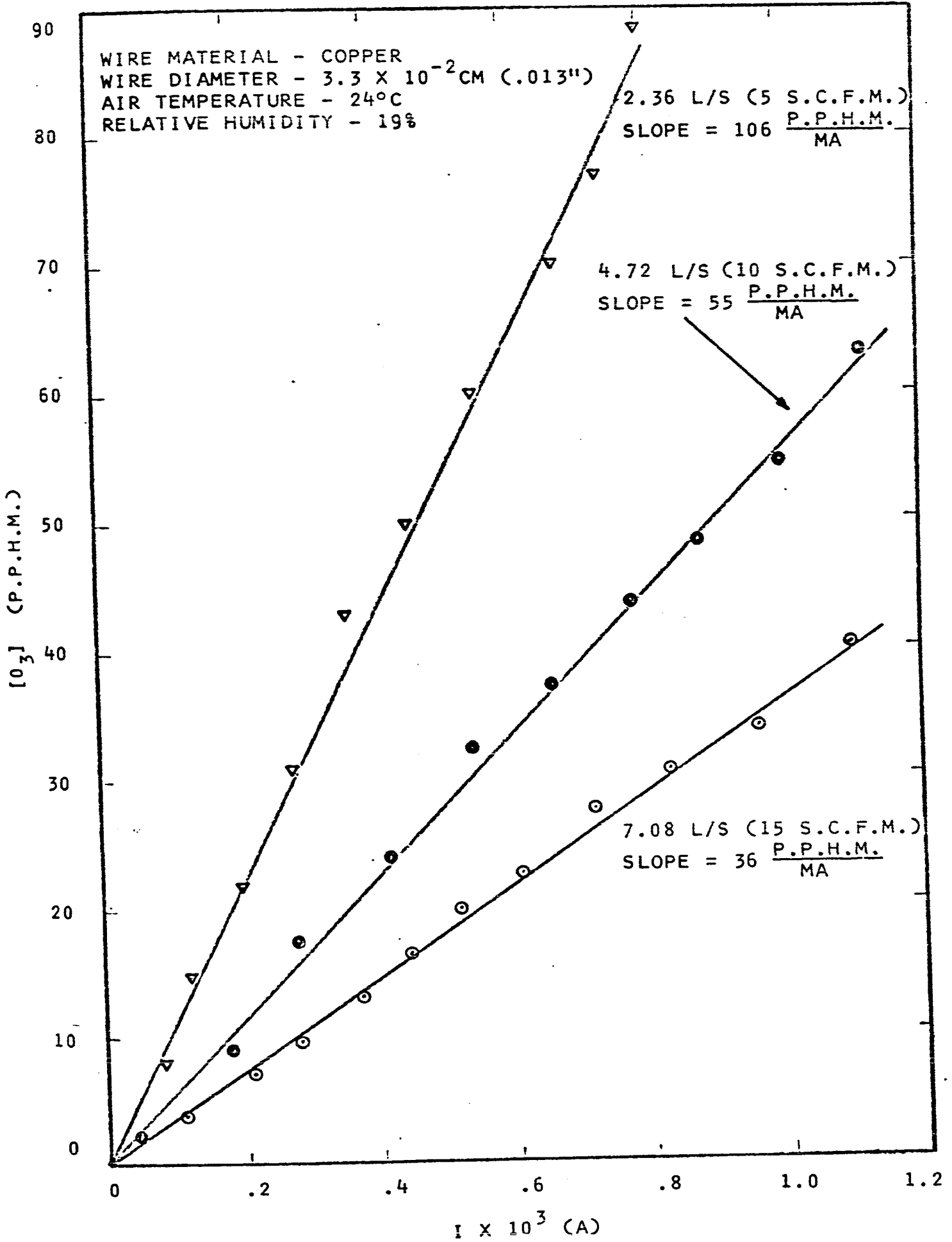


FIGURE 6.2

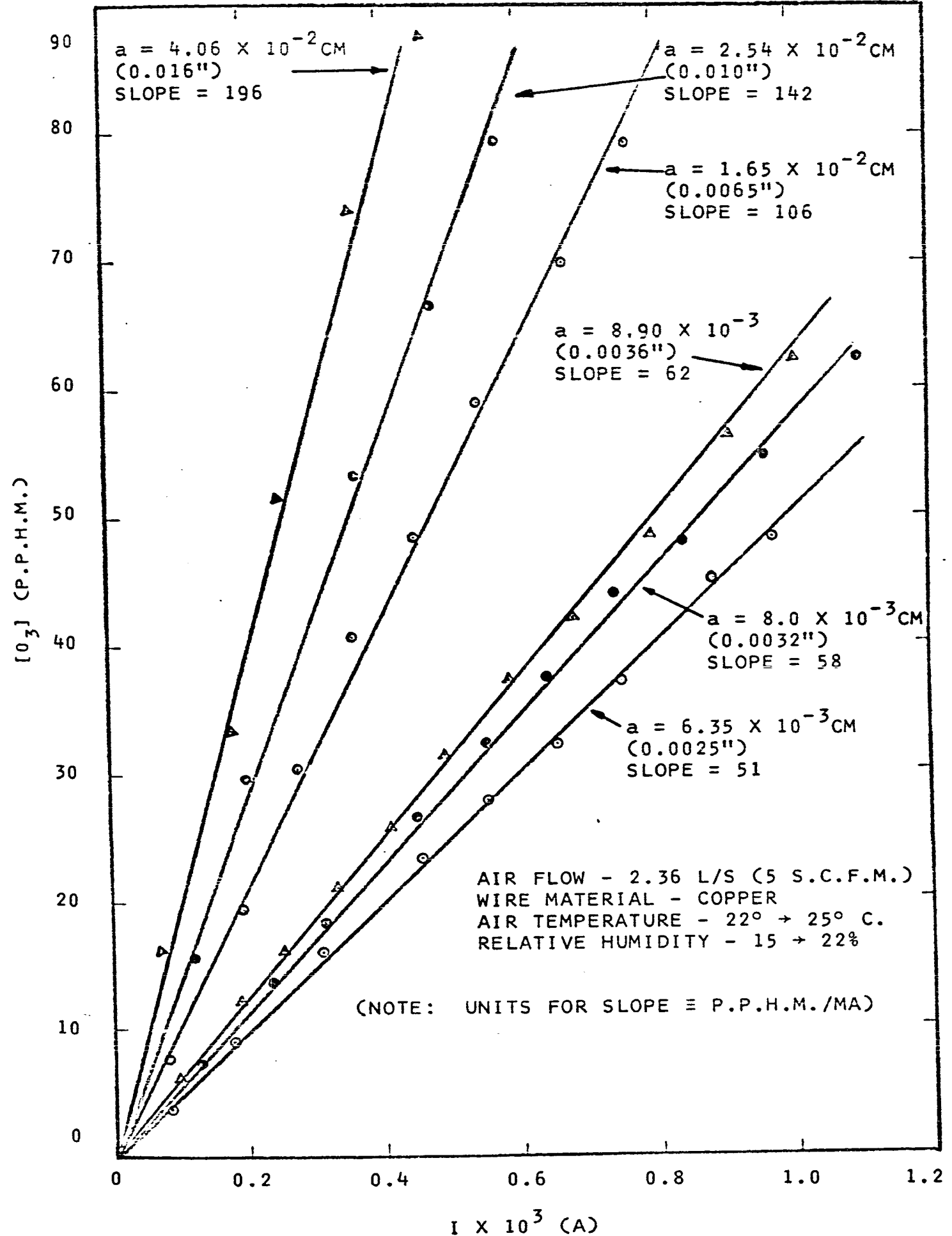


FIGURE 6.3

AIR FLOW - 2.36 L/S (5 S.C.F.M.)
 WIRE MATERIAL - COPPER
 AIR TEMPERATURE - 22° → 25°C.
 RELATIVE HUMIDITY - 15 → 22%

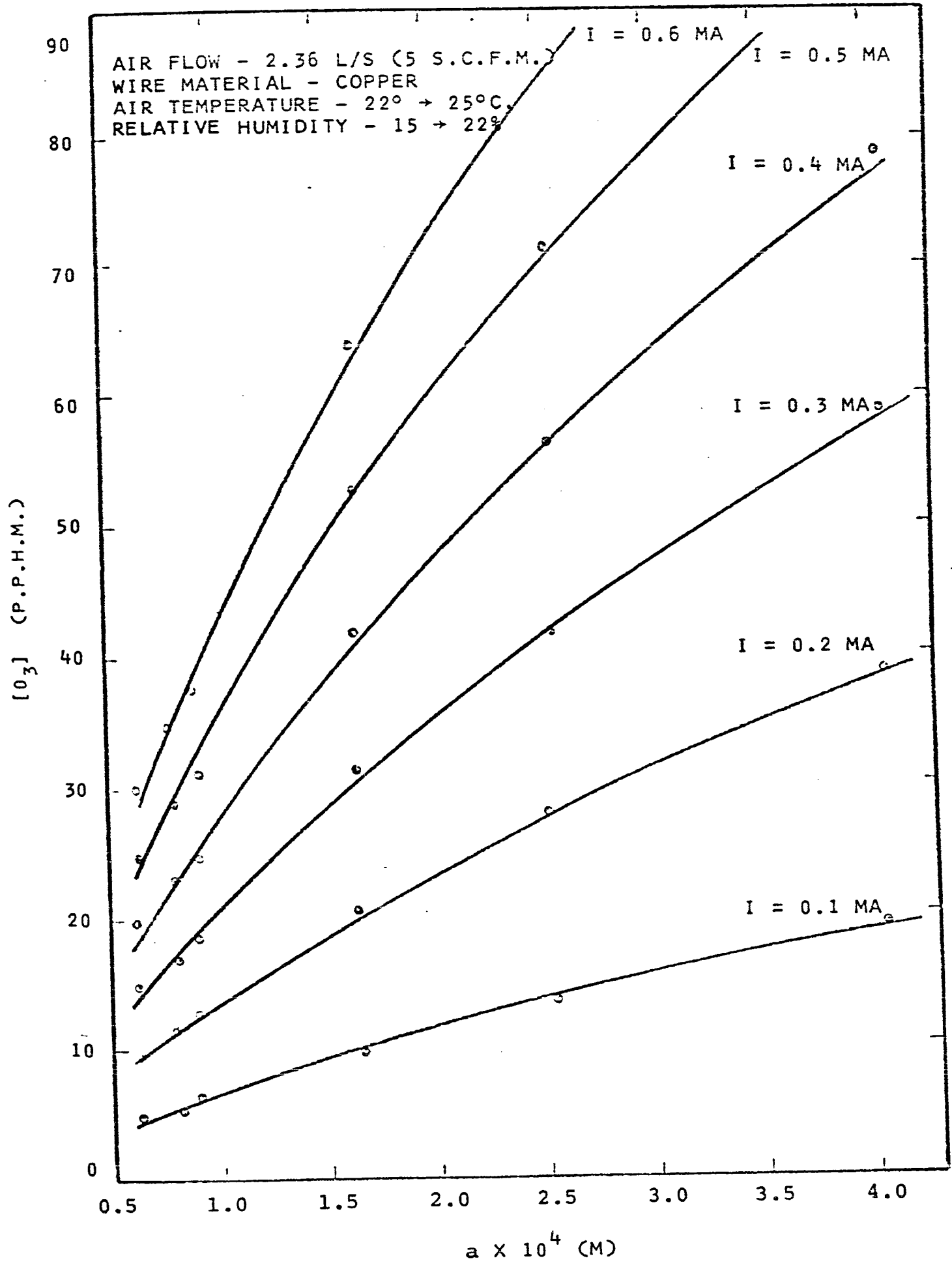
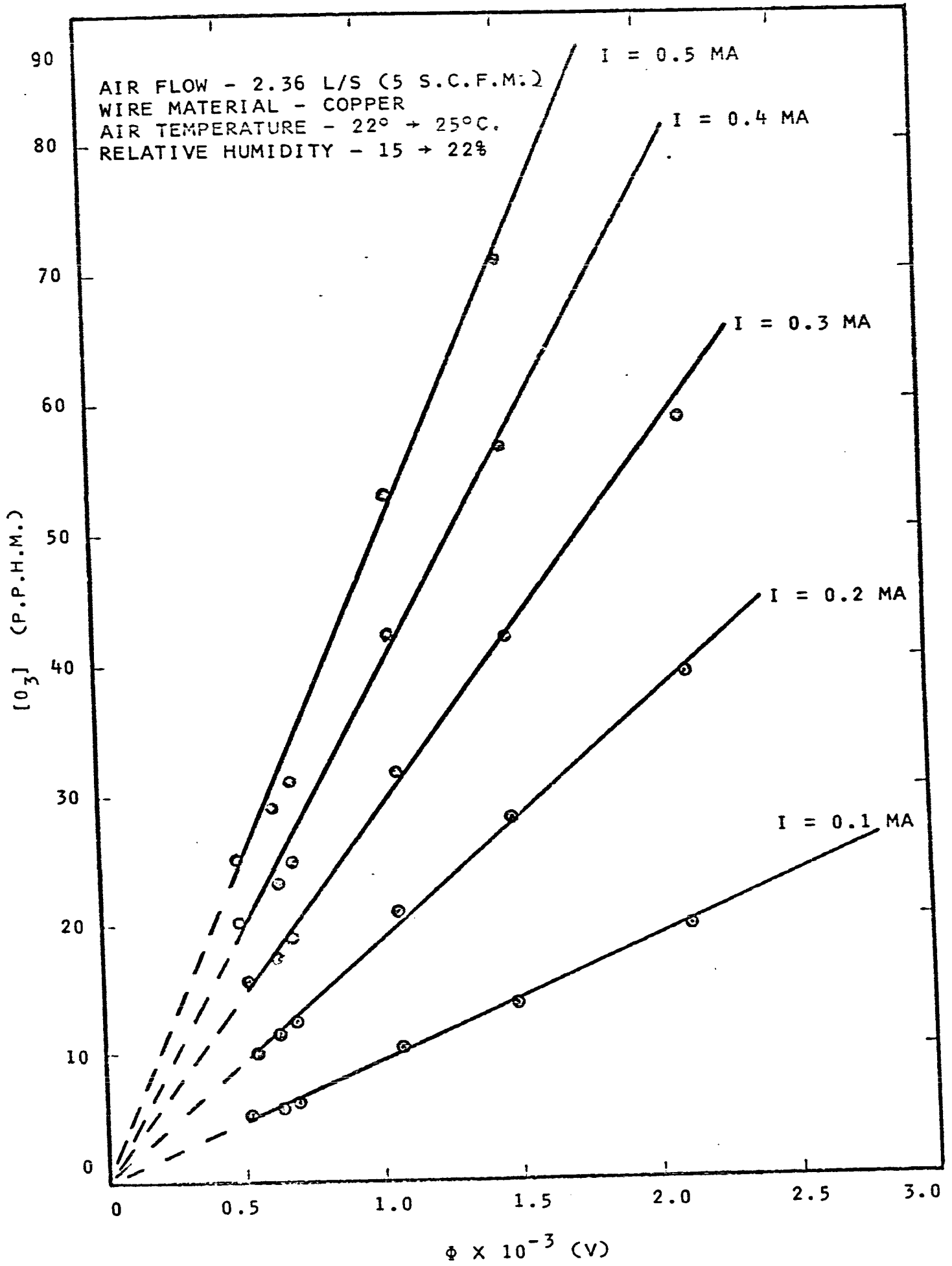


FIGURE 6.4

AIR FLOW - 2.36 L/S (5 S.C.F.M.)
 WIRE MATERIAL - COPPER
 AIR TEMPERATURE - 22° → 25°C.
 RELATIVE HUMIDITY - 15 → 22%



- (a) a linear relationship exists between ozone concentration and corona current for all wire sizes tested.
- (b) for a given current flow, the ozone concentration increases as the wire size increases, but the relationship is not linear.

Finally, Fig. 6.4 gives the ozone concentration versus the product $\phi = [E_{av} \cdot a]$ as a function of current. This product has the dimensions of a voltage and has been called the "Corona Potential Function". In this figure it can be seen that for a given current flow, the ozone concentration bears a linear relationship to ϕ .

The results of Fig. 6.1 have been reported by other investigators (see White & Cole (39)) and are merely confirmed in this work. However, the results shown in the other three Figures are key relationships and together with the results of Fig. 6.1 lead, by obvious deduction, to the following formula for ozone concentration.

$$\begin{aligned}
 [O_3] &= \frac{G \phi I}{Q} \\
 &= \frac{G[E_{av} \cdot a] I}{Q} \qquad (6 - 1)
 \end{aligned}$$

The dimensionless constant G is a fixed reaction constant and can be determined from the experimental results. Table 6.1 summarizes the results for six different wire sizes and shows

TABLE 6.1

$$G = \frac{[O_3]}{I} \frac{Q}{E_{AV} \cdot a}$$

a	$\frac{[O_3]}{I}$	Q	E_{AV}	G
WIRE RADIUS (M)	(P.P.H.M.) A	AIR FLOW $\frac{M^3}{S}$	AVERAGE ELECTRIC FIELD $\frac{V}{M}$	REACTION CONSTANT (DIMENSIONLESS)
MEASURED	MEASURED (SLOPES FROM FIGURES 6.1 AND 6.2)	MEASURED	CALCULATED FROM EQUATION 3-24	CALCULATED FROM DATA AT LEFT

6.35×10^{-5}	5.1×10^4	2.36×10^{-3}	8.65×10^6	2.19×10^{-1}
8 X "	5.8 X "	2.36 X "	8.03 X "	2.13×10^{-1}
8.9 X "	6.2 X "	2.36 X "	7.77 X "	2.12 X "
1.65×10^{-4}	1.06×10^5	2.36 X "	6.51 X "	2.33 X "
1.65 X "	5.5×10^4	4.72 X "	6.51 X "	2.41 X "
1.65 X "	3.6 X "	7.08 X "	6.51 X "	2.37 X "
2.54 X "	1.42×10^5	2.36 X "	5.83 X "	2.26 X "
4.06 X "	1.96 X "	2.36 X "	5.23 X "	2.18 X "

AVERAGE G = 2.2×10^{-1}

that the average value of G was 0.22 for the conditions of temperature, atmospheric pressure and relative humidity recorded during the experiments.

Therefore, equation 6-1 becomes:

$$[O_3] = 2.2 \times 10^{-1} \frac{\phi I}{Q} \quad (\text{P.P.H.M.}) \quad (6 - 2)$$

where

$$\phi = a \left(300 + \frac{4.5}{\sqrt{a}} \right) \times 10^4 \quad [\text{see equation 3-24}]$$

Equation 6-2 is plotted in the normalized form $\frac{[O_3]^t}{I}$ vs. a in Fig. 6.5. The experimental results shown by \odot were made during the present study in late 1966. As additional confirmation on the validity of the formula, the results of Burgess (45) are shown by \bullet on the same graph. His investigation was a continuation of the work reported here, and although the test set up he used was the same, it is significant to note that his corona test section was larger ie: 7.62 cm dia x 38 cm. long (3.0" dia. x 15.0" long). It can be seen from the graph that good agreement is shown between the formula and the experimental points.

It is interesting to compare equation 6-2 which has been derived from the experimental curves found here, to equation 3-39 which is based upon experimental evidence with ozonizers as reported in the literature. Dimensionally the two equations agree as they both describe the ozone generation in terms of electrical power. In addition, equation

AIR TEMPERATURE 20° → 25°C.
 RELATIVE HUMIDITY - 10 → 22%

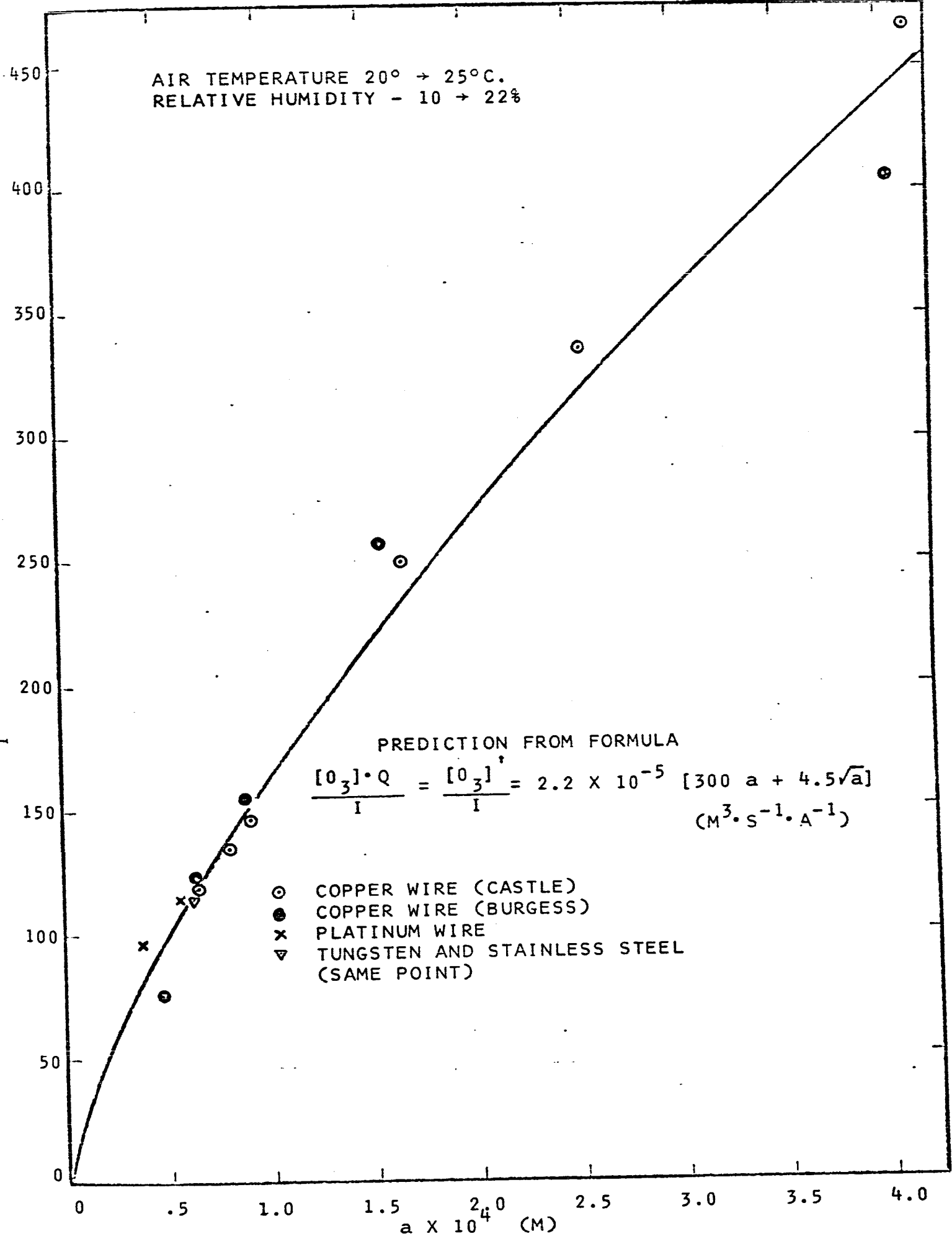
$\frac{10^3}{I} \times 10^8 \text{ (M}^3 \cdot \text{s}^{-1} \cdot \text{A}^{-1}\text{)}$

PREDICTION FROM FORMULA

$$\frac{[O_3] \cdot Q}{I} = \frac{[O_3]^*}{I} = 2.2 \times 10^{-5} [300 a + 4.5\sqrt{a}]$$

(M³ · s⁻¹ · A⁻¹)

- COPPER WIRE (CASTLE)
- COPPER WIRE (BURGESS)
- x PLATINUM WIRE
- ▽ TUNGSTEN AND STAINLESS STEEL (SAME POINT)



3-39 predicts the linear relation with current that is shown in Figures 6.1 and 6.2 since it has been already pointed out that V remains constant* as the current increases. Finally, the form of equation 6-1 allows the functional relation governing B(a) to be defined as

$$B(a) = G \frac{a}{\Delta a} \quad (\text{dimensionless}) \quad (6 - 3)$$

Limitations of Formula

The derivation of the formula has neglected any discontinuities due to end effects, flaws on the surface of the wire, or electric field stress points at the outer cylinder which could give rise to back corona. Since it would be expected that any of these factors would increase the ozone production, special care was taken to reduce them in the corona test section. However, it could be foreseen that in any practical form of precipitator these factors would play a more important role than in the ideal experimental case.

Furthermore, only copper wires have been considered whereas in practice other materials are used. Tests were carried out using new stainless steel, tungsten and platinum wires and the results which are plotted on Fig. 6.5 are also seen to agree with the predictions of the formula.

It is important to note that the formula was based upon test results taken for wire sizes ranging from 1.27×10^{-2} → 8.13×10^{-2} cm (.005" → .032") diameter. The larger

* See section 3.7.

size marks the upper limit for wire that would normally be considered for use in an air cleaning type of precipitator. Therefore, although there is no reason to suspect that the formula would not be valid at larger wire sizes, there was no point in extending the range. Two tests were taken at wire sizes less than 1.27×10^{-2} cm (.005") and as shown in Fig. 6.5 good agreement is shown with the formula.

Although the formula was based upon experimental work carried out with a fine wire in a cylinder, it is expected that it should be equally applicable to a single fine wire mounted between parallel plates. The reason for this is that the corona discharge is essentially controlled by the geometry of the wire rather than that of the outer electrode and, for comparable wire to electrode spacing, very little difference in the corona characteristics is found between the cylindrical and duct geometry (46). In the case of multiple wires mounted in a duct, account would have to be taken of the interference effect between wires which would presumably change the conditions in the ionized sheath as well as the current flow. Since this geometry is quite extensively used in practice, it would be useful to confirm this interpretation through further experiments.

Finally, these results are restricted to new, clean wires to eliminate any variations due to aging.

6.3 Effect of Wire Geometry

The opinion generally held in the literature is that smooth round wires are the most satisfactory geometry to minimize ozone generation in practical electrostatic filters. Other wire geometries, eg: square, starshaped, serrated etc., have been found to increase corona currents in certain cases and they find some use in one stage units using negative corona. However, they usually lead to higher ozone generation per unit of current. Also it has been mentioned in section 3.7.2 that for the lowest ozone generation it is necessary to use the smallest, practical wire diameter. (This lower limit is set by mechanical considerations.)

Since the corona characteristics are essentially set by the outer radius of curvature of the center conductor, some attempts were made to find a method of creating a small outer radius of curvature on a relatively larger core which could provide the mechanical strength. Geometries tested included fine wires spiralled around dielectric and metallic cores, bundles of fine wires twisted together, and a commercially available spiral cut saw blade.

Since the mechanical strength of a given material is dependent upon its cross-sectional area, a useful criterion for indicating the relative performance of a given geometry can be obtained from the following dimensionless ratio:

$$A = \frac{\frac{[O_3]}{I} \cdot Q \text{ for test geometry}}{\frac{[O_3]}{I} \cdot Q \text{ for a round wire having the equivalent cross sectional area.}} \quad (6 - 4)$$

This ratio compares the ozone generating properties of a given geometry to the ozone generating properties of a round wire having the equivalent mechanical strength. For instance, a value of 1.0 would indicate no improvement over a round wire; a value less than 1.0 would show that the test geometry would generate less ozone than a single round wire of the same mechanical strength.

The test results obtained with the twisted* wires are shown in Fig. 6.6 (wire radius = 8.9×10^{-3} cm (0.0035")). For comparison, the theoretical prediction is given for a wire having a radius of 1.78×10^{-2} cm (0.007"). The results are tabulated in Table 6.2. Note the values of A which show that a reduction in the ozone generated per unit cross-section was achieved by twisting the wires together.

The explanation for this phenomenon is believed to be related to the electric field strength at the wire surface. With a single wire, the field is uniformly large around the whole circumference of the wire and hence the ozone formation can proceed at any point. However, when two wires are twisted together, the field distribution is changed quite radically.

* The twists had a pitch of approximately 2 cm (0.75").

CORONA AND OZONE CHARACTERISTICS FOR TWISTED COPPER WIRES

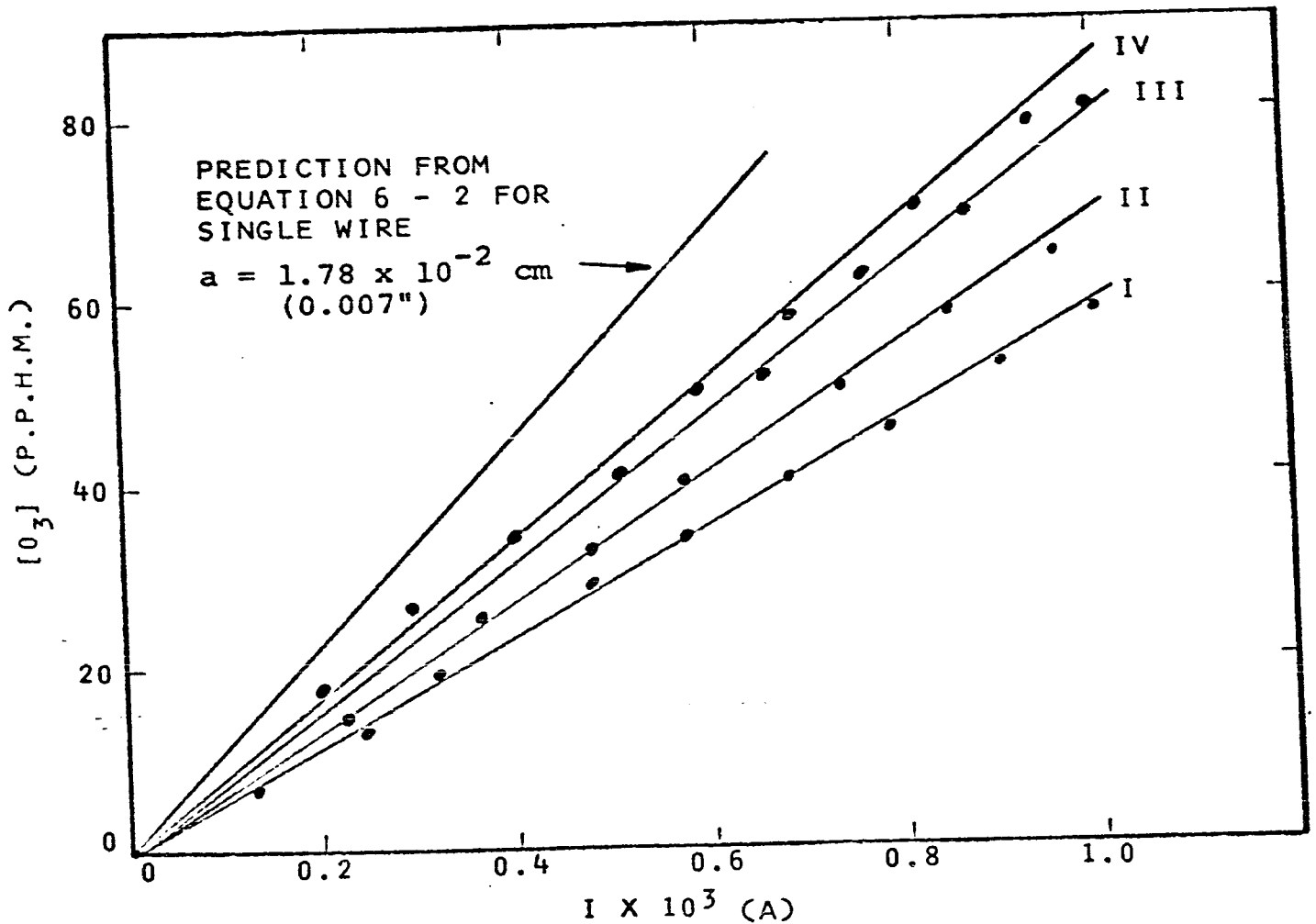
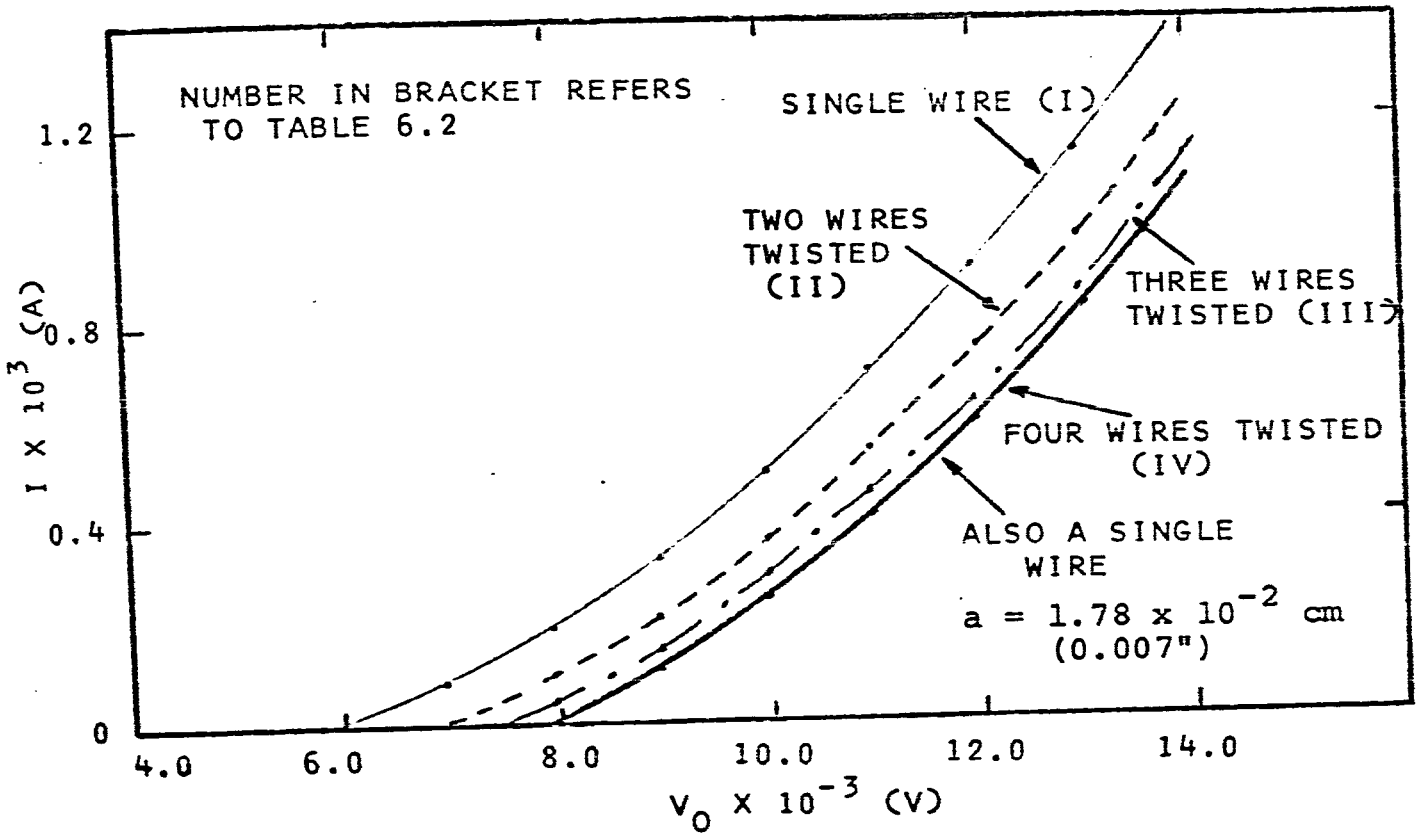


TABLE 6.2

EFFECT OF WIRE GEOMETRY ON OZONE GENERATION

WIRE GEOMETRY CROSS SECTIONAL AREA (m²) RADIUS OF A WIRE HAVING SAME CROSS SECTIONAL AREA (m) A

$\frac{[0.3]}{I}$

(P.P.H.M./mA)

WIRE GEOMETRY	CROSS SECTIONAL AREA (m ²)	RADIUS OF A WIRE HAVING SAME CROSS SECTIONAL AREA (m)	A
I SINGLE WIRE a=8.9 X 10 ⁻⁵ m	2.48 X 10 ⁻⁸	8.9 X 10 ⁻⁵	59
II TWO WIRES TWISTED a=8.9 X 10 ⁻⁵ m	4.96 X 10 ⁻⁸	1.26 X 10 ⁻⁴	69
III THREE WIRES TWISTED a=8.9 X 10 ⁻⁵ m	7.44 X 10 ⁻⁸	1.54 X 10 ⁻⁴	80
IV FOUR WIRES TWISTED a=8.9 X 10 ⁻⁵ m	9.92 X 10 ⁻⁸	1.77 X 10 ⁻⁴	86
V SINGLE WIRE a=1.78 X 10 ⁻⁴ m	1 X 10 ⁻⁷	1.78 X 10 ⁻⁴	110
VI SINGLE WIRE a=4.06 X 10 ⁻⁴ m	5.03 X 10 ⁻⁷	4.06 X 10 ⁻⁴	196
VII SINGLE NICKED WIRE a=4.06 X 10 ⁻⁴ m	"	"	1800
VIII SINGLE WIRE a=4.06 X 10 ⁻⁴ m PLUS SPIRAL WIRE a=6.35 X 10 ⁻⁵ m	"	"	800
IX NYLON CORE a=4.06 X 10 ⁻⁴ m PLUS SPIRAL WIRE a=6.35 X 10 ⁻⁵ m	"	"	55 (DEGRADED RAPIDLY WITH TIME)
SPIRAL CUT SAW BLADE I.D.=8.12 X 10 ⁻⁴ m O.D.=1.1 X 10 ⁻³ m	"	"	76

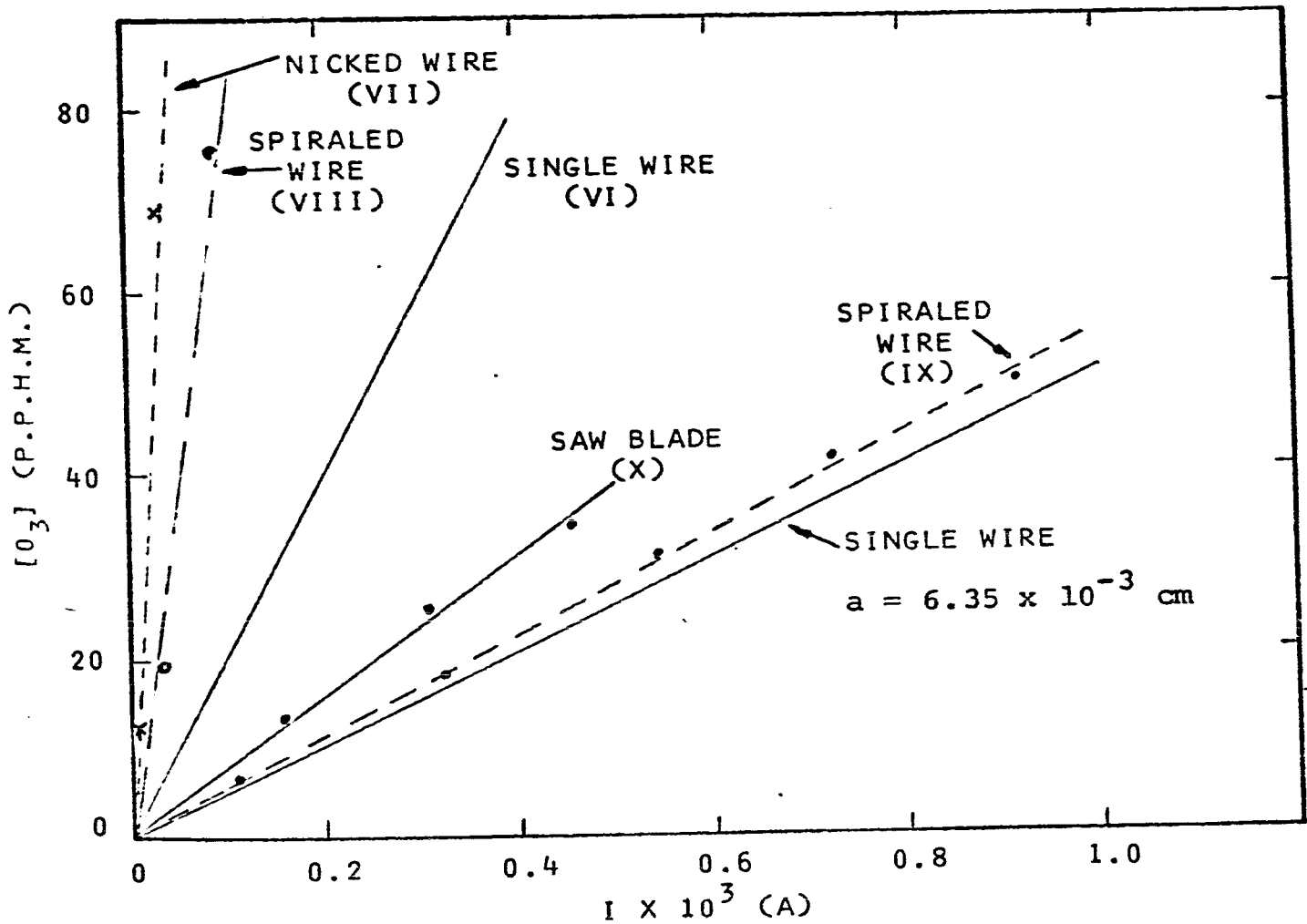
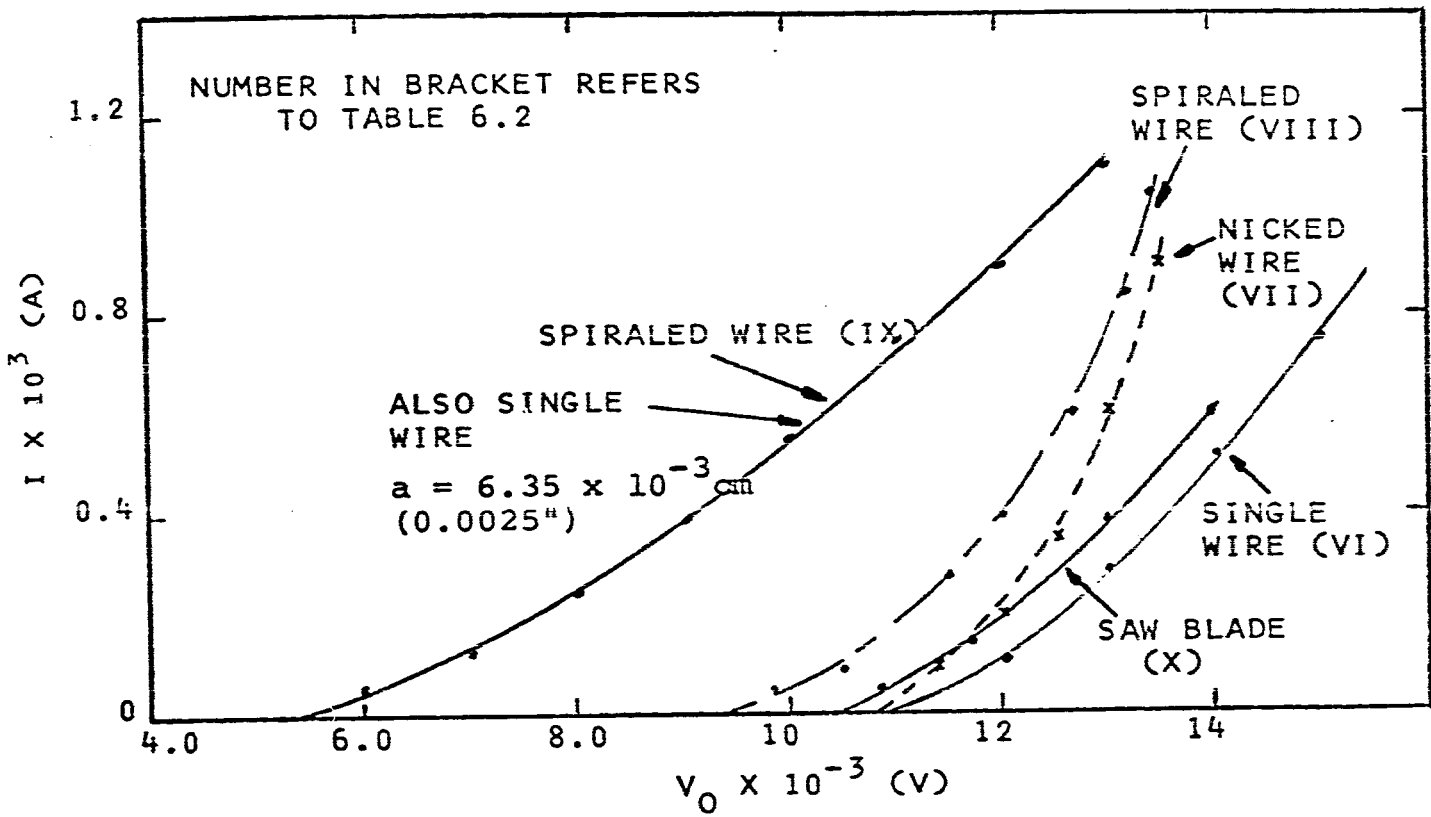
NOTE: ALL WIRES WERE COPPER WITH THE EXCEPTION OF THE NYLON CORE AND THE TOOL STEEL SAW BLADE.

For example, no field can exist at the point of contact between the wires, a reduced field exists at the surface segment adjacent to the contact point and the field on the surface opposite the contact point is relatively unaffected by the presence of the other wire. Therefore, the effective surface area which contributes to the ionization phenomena is considerably less than the total surface area of the wires whereas the portion which does create the ionization field has an effective radius of curvature close to that of the single wire. It is particularly interesting to note the case of the four wires, where the voltage-current characteristic was almost identical to a single wire having a radius of 1.78×10^{-2} cm (.007") but the ozone production was considerably less than that predicted for the single wire. The similar voltage-current characteristic must mean that the number of ionizing collisions less the number of recombinations per unit time was the same for the two cases. (This phenomenon is governed both by the strength of the electric field and the volume of space over which the ionization takes place.) The fact that the ozone generation was less with the twisted wires than the round wire would appear to be due to the smaller active surface at which the reaction could occur. (The ozone formation is governed both by the strength of the electric field and the active area of wire.)

Fig. 6.7 and Table 6.2 show additional results obtained with the other geometries tested. In this set the core radius was 4.06×10^{-2} cm (0.016") and the effect of different surface conditions was studied. The case of the nicked wire and the smaller wire spiralled around the larger both produced ozone much in excess of the smooth round wire. This would indicate that surface discontinuities adversely affect the ozone generation; presumably by creating local regions conducive to ozone formation having above average electric field strengths. However, all the other cases showed an improvement over the single round wire, with the spiral saw blade giving exceptional results. It is interesting to note the case of the fine wire spiralled around the nylon core and the fact that the results are almost the same as with the wire taken by itself. (ie: the core being a non-conductor does not cause the field shielding effect to take place.) However, some problems were encountered with this configuration as the performance degraded with time. This was presumed to be due to charge build-ups on the insulating core which affected both the corona characteristic and the ozone generation.

These results have shown that it is possible to increase the mechanical strength of a corona wire without increasing the ozone generation as much as the test results with round wires would indicate. From the practical point

FIGURE 6.7
CORONA AND OZONE CHARACTERISTICS FOR FIXED
WIRE DIAMETER WITH DIFFERENT SURFACE CONDITIONS



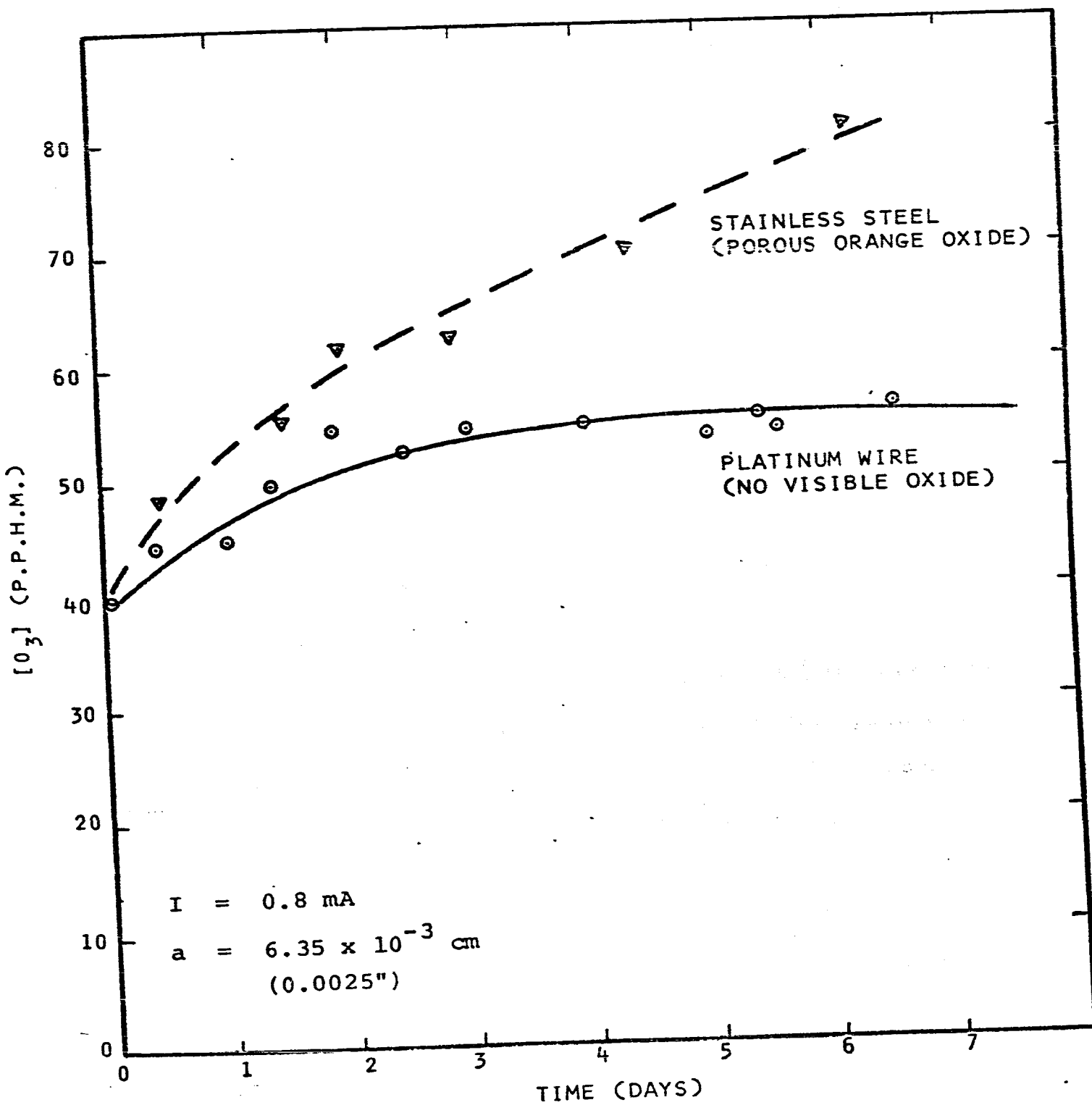
of view, it can be seen that none of the geometries tested produced less ozone than the single wire with radius 6.35×10^{-3} cm (.0025"). Since the mechanical strength of this was adequate for the applications discussed here, no advantage would be gained by using one of these test geometries. However, the results do illustrate the possibility of using other than round wires, where severe stressing of the corona wire could occur. In addition, it is possible that a smaller scale version of the saw blade or even some other geometry such as a razor edge could produce ozone generation characteristics even less than the above wire. This was investigated further by Burgess (45) and he did confirm that it was possible to use a razor edge to obtain even lower ozone generation characteristics.

6.4 Effect of Wire Aging

The observation that the ozone generation was not independent of the length of time the wire had been used, led to some preliminary experiments to check this effect. Measurements of ozone concentration as a function of time were made for two wire materials, stainless steel* and platinum and the results are shown in Fig. 6.8. In addition, the wire was examined under a microscope both before and after the life test.

* Tests using tungsten, copper and "advance" wire showed similar characteristics to the stainless steel but because of the preliminary nature and lack of complete data, the quantitative values are not given for these materials.

FIGURE 6.8
VARIATION IN OZONE GENERATION AS A FUNCTION OF TIME



It was observed that the stainless steel, which gave rise to the greatest increase in ozone generation also developed a noticeable oxide coating (very clean air was used in all these tests, hence dust was not a factor). Whereas with the platinum wire, where the ozone generation initially increased and then appeared to remain constant with time, no noticeable oxidation could be detected under the ordinary microscope. Also, it was noted in both cases, that although the ozone generation changed with time, no appreciable change in the voltage-current characteristic occurred. This meant that the increase in ozone generation could not be explained by the fact that the oxide layer just increased the effective physical diameter of the wire (ie: this would cause a change in the voltage-current characteristic).

From these preliminary measurements it has been concluded that the increase in ozone generation was probably due to the formation of the oxide coating. This agrees with the interpretation given in sections 3.7.2 and 6.3 of the probable importance of the surface of the wire as a catalyst to the reaction, as it would appear that the oxide coating acts primarily to increase the effective surface area of the wire.

Stainless steel and tungsten are usually employed in electrostatic air cleaners because of their strength and the

fact that they are normally regarded as being highly resistant to oxidation. However, these tests have shown that in the presence of ozone and the relatively complicated combination of factors found in the corona, surface oxidation can occur. Moreover, in the corona, the wire undergoes continual mechanical vibration which could cause fracturing of the oxide layer. It would appear to be advantageous to select a wire material which would form a protective rather than a porous oxide. Platinum is such a material and the results appear to confirm this interpretation.

Further study of this phenomenon would seem to be in order and would be of interest from both the practical and theoretical point of view. The practical importance concerns the long term performance of air filters. The theoretical interest hinges on the fact that the oxidation rate is much in excess of what would normally be expected from these materials at room temperature. However, the extreme complexity of the oxidation process under the conditions found in the electrical corona would necessitate a separate study to determine the quantitative effects.

CHAPTER 7

PRACTICAL FILTER

7.1 Introduction

The previous sections have described the theoretical and experimental studies on the concentric geometry precipitator. A prime purpose of the study was to establish design parameters to allow the prediction of the characteristics of a practical air filter. The design aims for such a filter were given in section 2.1. The two main features of the precipitator discussed here as compared to standard units were a) the use of electrified collection media and, b) the cartridge type construction.

The presence of dielectric media acts to increase the collection area per unit volume of filter and helps to ensure high reliability due to the presence of force components other than just the coulomb force. In the case of corona wire breakage, electrical forces could still exist due to the fact that all natural dusts usually have some small charges associated with them. Also, the non-uniform field in the electrified media would still create a dielectrophoretic force component. In the case of complete power failure the electrical forces could still be significant

since it has been shown that the electrified media can maintain localized charged areas for relatively long periods of time. In all cases, the mechanical forces can aid the collection of the larger particles.

The geometry of the precipitator allows ready replacement of the collectors through the use of cartridge type elements. This replacement could be performed very quickly and simply which is an important consideration in servicing a high efficiency filter. Also, although these cartridges could be cleaned and reused, it could be envisaged that with mass production and the use of such materials as metallized paper and plastics, disposal of these elements would be feasible.

On the basis of the results of the previous sections, two prototype units were designed and constructed. For convenience these are designated as Mark I and Mark II respectively. The Mark I version involved the use of replaceable cartridge elements based upon the dimensions of the experimental test unit described in section 4.1.6. Higher flow capabilities were achieved by paralleling these units. Mark II was developed to allow one basic cartridge unit to handle a larger air flow and improve upon deficiencies found in Mark I. Both units were tested in practical air cleaning situations and at the time of writing, the Mark II design is being incorporated in the filtration system

for a test clean room in a hospital.*

7.2 Mark I Design

7.2.1 Description

This unit was designed to handle 95 l/s (200 cfm) of air and consisted of nine replaceable cartridge type elements mounted in parallel. Figure 7.1 gives photographs showing the completed unit and some of the construction details.

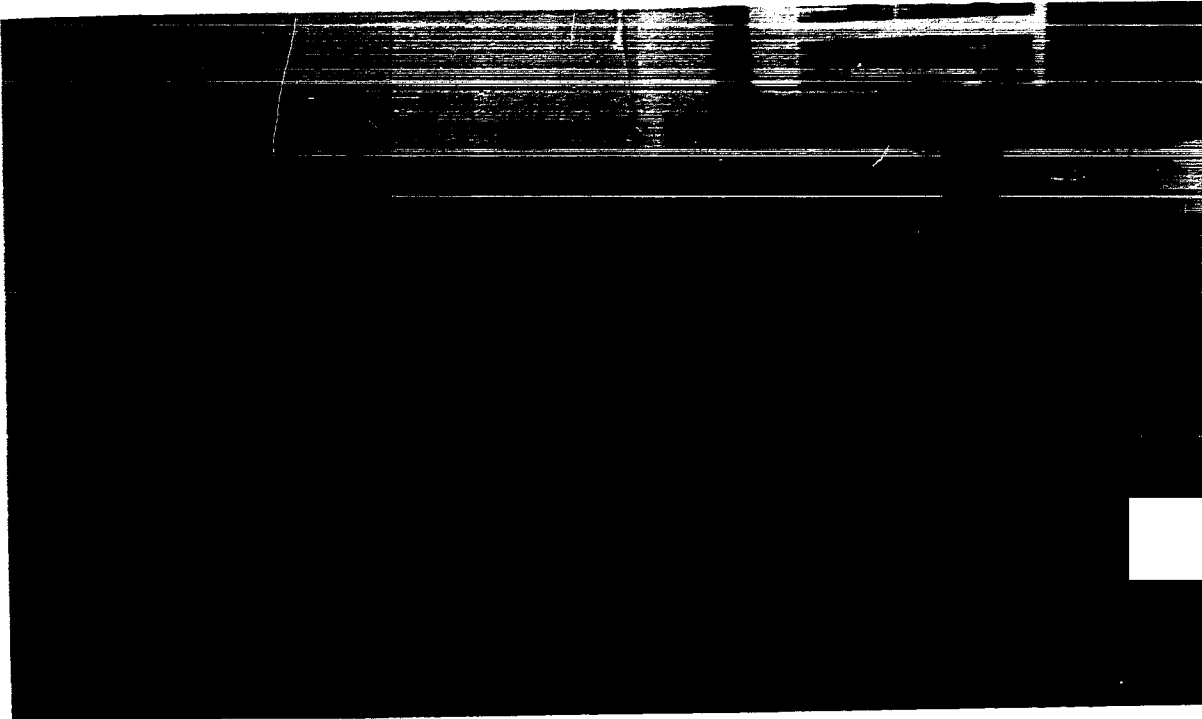
The repeller section consisted of a grounded outer casing which enclosed an insulated assembly, consisting of nine electrified, perforated cylinders which were open at the inlet end and closed at the outlet. The perforated cylinders were connected to a +20 kV D.C. voltage source, and provided the collecting field for the cartridges. Tapered supports in the center of each cylinder were insulated from the repeller and provided the centering for the cartridges. In addition, a common high voltage connection terminated in a spring contact on the end of each support. These points made contact with the contacts on the corona wire of each cartridge thus providing the energization for the corona section. The corona wires were self-supporting, and since they were made from platinum** 1.27×10^{-2} cm (0.005") diameter, were very fragile. Therefore, the wires were mounted

* This room is being constructed on the isolation ward at Victoria Hospital, London, to aid in studies by Dr. N.M. Lefcoe on the effects of air contaminants on patients suffering from acute asthma.

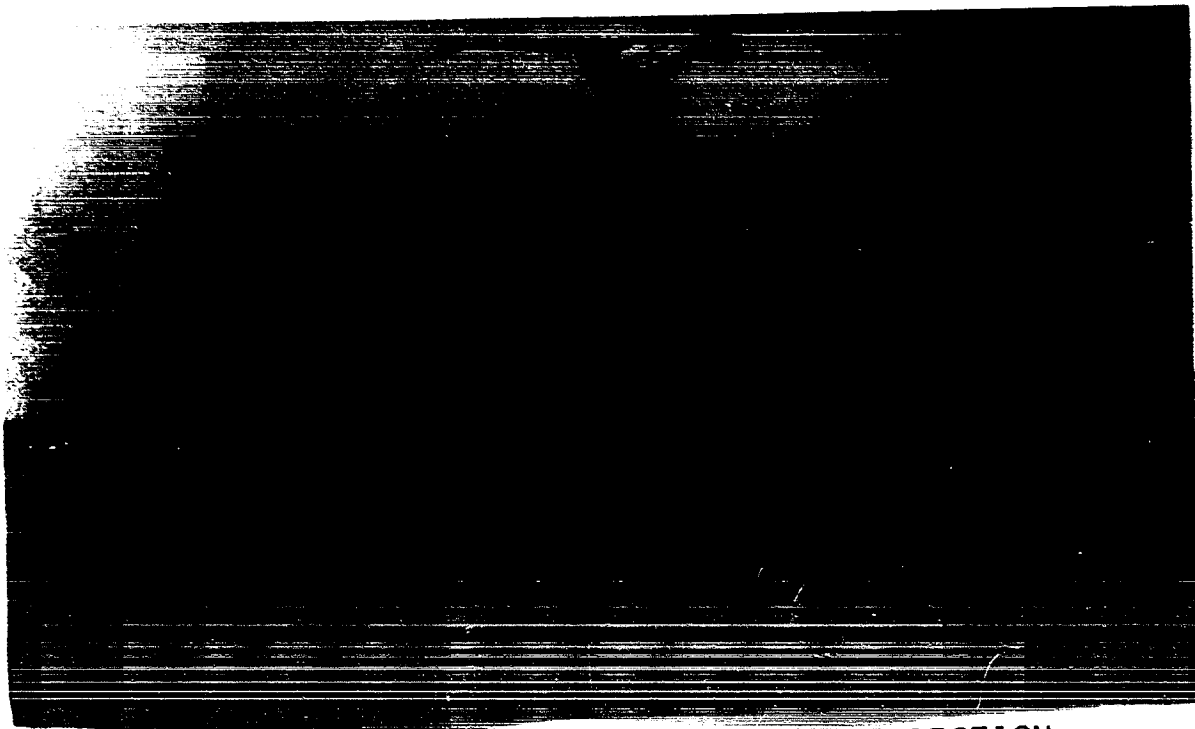
** Platinum wire was used initially on the basis of the results section 6.4 in an effort to eliminate any degradation of the ozone generation with age.

FIGURE 7.1
MARK I PROTOTYPE

192



EXPLODED VIEW OF THE FILTER
(REMOVED FROM OUTER CASING)



FILTER ASSEMBLED EXCEPT FOR INLET SECTION
(NOTE HIGH VOLTAGE CONNECTION POINTS ON SIDE)

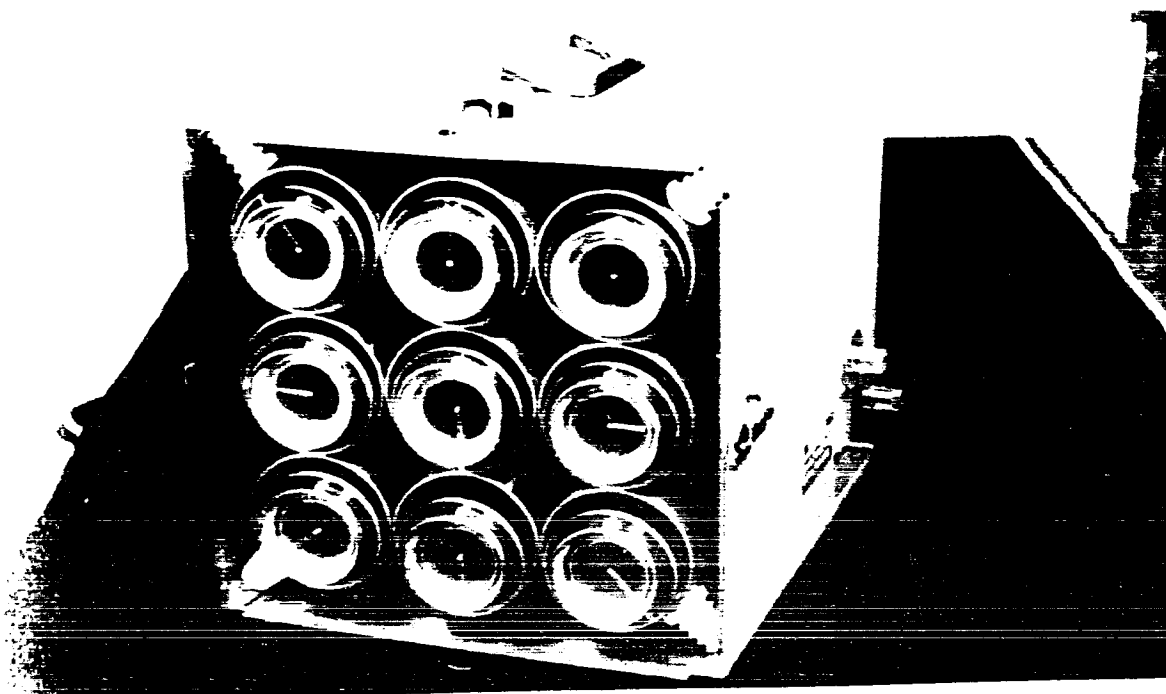
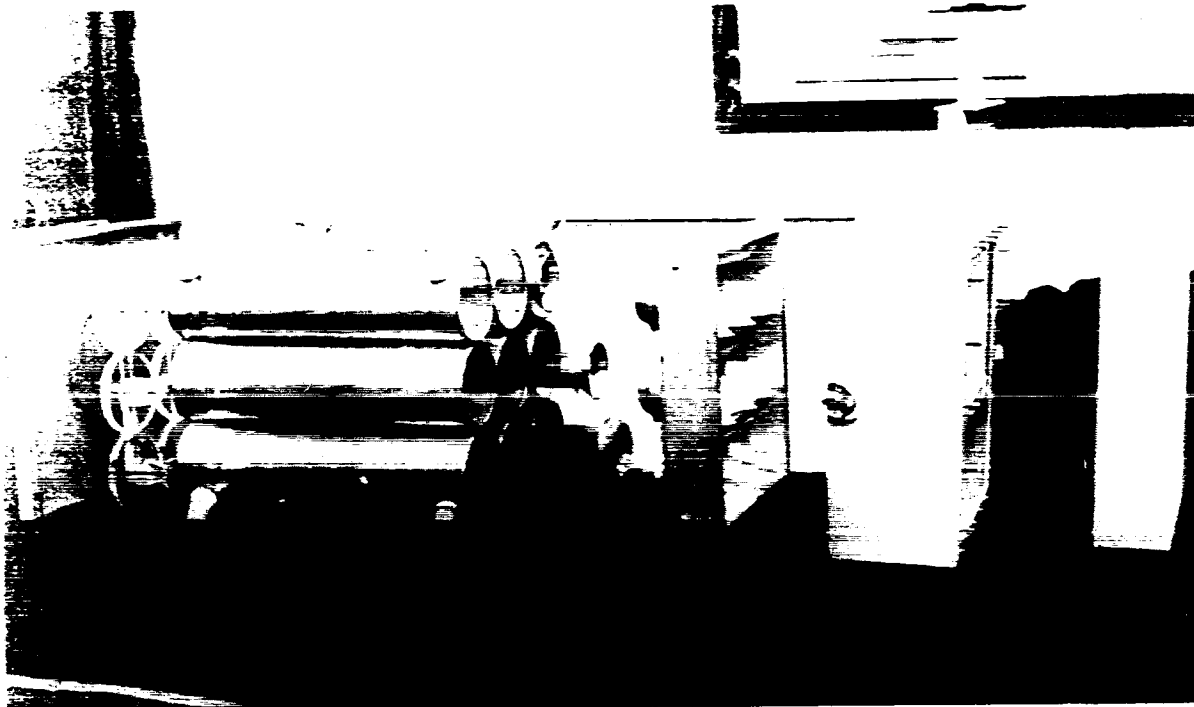
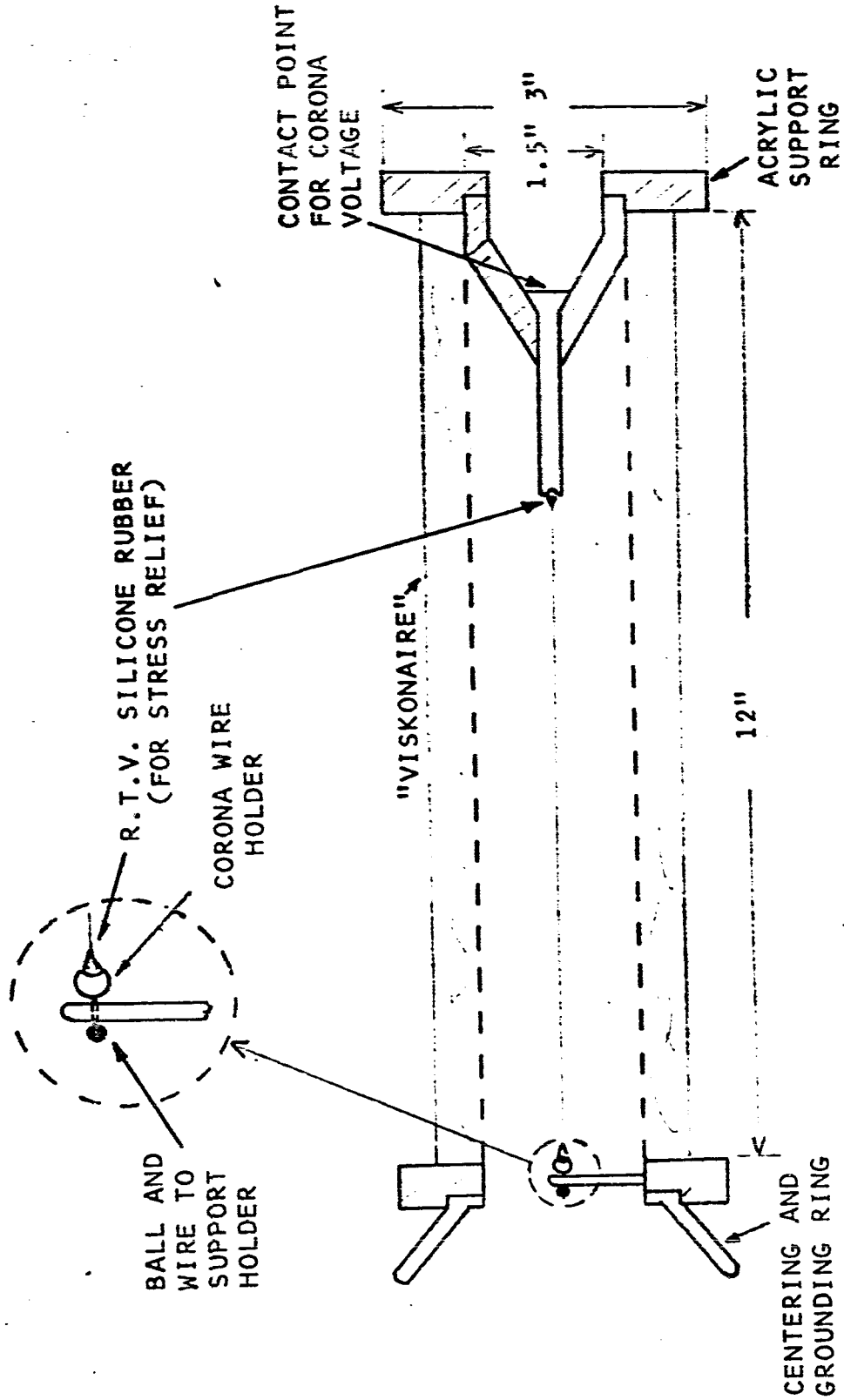


FIGURE 7.2
CARTRIDGE ELEMENT FOR MARK I PROTOTYPE



in special stress relieving supports (see Fig. 7.2) and with this arrangement no wire breakages were experienced throughout the life of the test. The cartridges were self contained elements with the corona wire and "Viskonaire" layer an integral part of the unit.

The inlet section served to center the inlet end of the cartridges and also provided the ground contact for each of the cylinders in the corona section. This grounding was achieved through a pressure contact at a split section of each centering ring. A prefilter element consisting of one thickness of "Viskonaire" was mounted in this inlet section. This prefilter was intended to stop the majority of the particles larger than 10 μm .

The power supply was a self contained unit consisting of two separate commercial power packs.* These units consisted of transformers with encapsulated rectifiers providing positive polarity outputs at +20 kV and +12 kV respectively. Adjustable taps on the input allowed the corona supply to be set to an operating point of approximately 9.5 kV.

The unit was constructed in the shop in the Faculty of Engineering Science at the University of Western Ontario.

7.2.2 Test Results

Initial problems were encountered due to voltage breakdowns in the unit. This breakdown took place between the outer extremes of the repeller section and the grounded

* Universal Voltronics Corp., Models BPE-16-5.5 and BPE-22-1.5.

outer covering. Although this could have been solved simply by increasing the clearance to ground in any new unit, the problem was corrected by liberal use of R.T.V. silicone insulating rubber and acrylic screens between the ground and repeller. The addition of this material added considerably to the weight of the unit, but more importantly, restricted the air flow thus increasing the pressure drop to relatively high values. One other problem was caused by air leakages at several locations in the unit with special grease seals required at the inlet end to prevent some of the air bypassing the cartridges. In addition some leakage occurred through the joints in the outer casing and tape was required at all these points.

Ozone

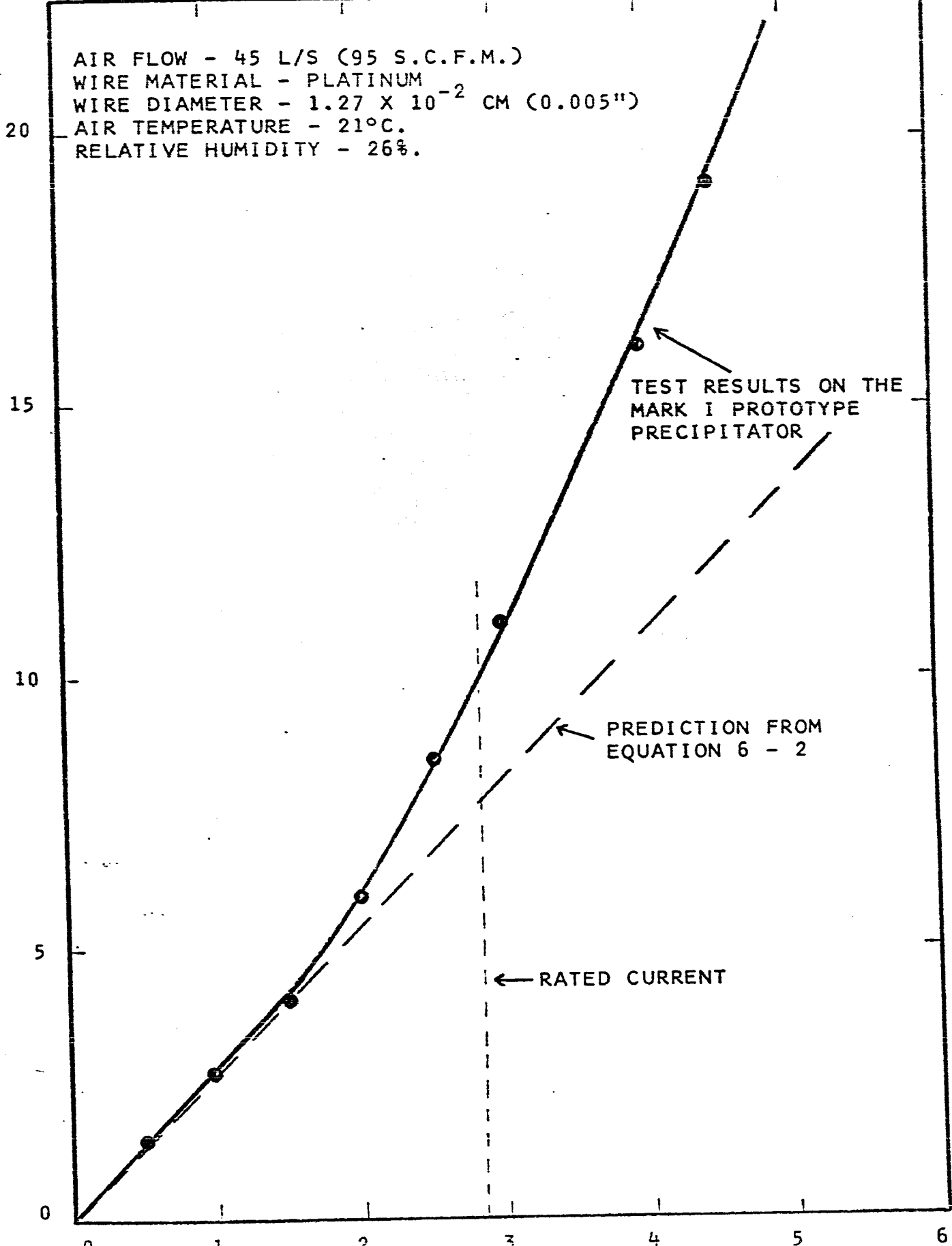
The ozone generation of the prototype was measured for a reduced air flow of 45 l/s (95 S.C.F.M.) as a function of total corona current. The results of this test are given in Fig. 7.3 along with the prediction based upon equation 6-2.

Note that good agreement existed between the formula and experiment up to approximately 2 mA current. Above this the ozone concentration tended to increase at a faster rate than predicted. This was believed to be due to the end effects and possibly to local points of back corona which became important at the higher currents. (The end effects would be

FIGURE 7.3

AIR FLOW - 45 L/S (95 S.C.F.M.)
WIRE MATERIAL - PLATINUM
WIRE DIAMETER - 1.27×10^{-2} CM (0.005")
AIR TEMPERATURE - 21°C.
RELATIVE HUMIDITY - 26%.

[O₃] (P.P.H.M.)



TEST RESULTS ON THE MARK I PROTOTYPE PRECIPITATOR

PREDICTION FROM EQUATION 6 - 2

RATED CURRENT

CURRENT X 10³ (A)

expected to be more pronounced in the prototype than in the test set-up since the wire was mounted differently and there were nine times the number of ends.)

To ensure that the ozone concentration did not exceed the accepted industrial limit of 10 P.P.H.M. a minimum safety factor of two was adopted ie: for a flow of 45 l/s, 10 P.P.H.M. concentration was allowable since at 95 l/s this would correspond to approximately 5 P.P.H.M. From the graph it can be seen that this limited the maximum allowable charging current to something less than 3mA. Therefore, with this restriction on the corona current, the formula gave a reasonably close prediction of the initial ozone generation in the larger unit.

Pressure Drop

The pressure drop measurements were made during the laboratory tests at two values of air flow. The results are given in Table 7.1 below for the unit both before and after modification.*

TABLE 7.1

AIR FLOW (S.C.F.M.)	PRESSURE DROP (INCHES OF WATER)			
	Before Modification		After Modification	
	Filter	Filter + Prefilter	Filter	Filter + Prefilter
180	.45	.65	.55	.85
300	1.0	1.3	1.35	1.8

* The addition of the insulation to prevent breakdown in the region between the repeller and the outer ground.

These values of pressure drop for the filter even before modification were somewhat higher than would be expected from the test results of section 5.2.1 and appeared to be due to the close proximity of the filter holders causing additional constriction of the air at the outlet.

Collection Efficiency

Note that unless otherwise specified, all collection efficiencies were based upon measurements in the size range 0.3 μm and larger. Also, unless specified, all the tests were performed on room air with total counts in the range $10^5 \rightarrow 10^6$ particles/liter ($3 \times 10^6 \rightarrow 3 \times 10^7$ particles/feet³) in the size range 0.3 μm and larger.

I Initial Lab Test (April 4, 1967)

Operating Conditions

$$I_c = 2.4 \text{ mA}$$

$$V_R = 21 \text{ kV}$$

$$Q = 85 \text{ l/s (180 S.C.F.M.)}$$

$$T = 24^\circ\text{C}$$

$$\text{R.H.} = 25\%$$

$$[O_3] = 4 \text{ P.P.H.M.}$$

$$\text{Measured collection efficiency} = 99.65\%$$

$$\text{Predicted collection efficiency from previous test results} = 99.94\%$$

The unit was tested independently at the research center of Johnson & Johnson Limited, Montreal, Quebec. (Manufacturers of "Viskonaire"). Their results were communicated by A. P. Ruffo, Research Manager, Industrial Air Filters Limited on June 23, 1967. The collection efficiency tests were made using a Royco particle counter and also by comparison with a commercial H.E.P.A. filter.

II Lab Test by Johnson & Johnson

A) Operating Conditions

As above except:

Q = 95 l/s (200 S.C.F.M.)

T = Room Temperature

R.H. = Not recorded but believed to be moderate

[O₃] = Not recorded

Measured collection efficiency = 99.54%

Measured collection efficiency

for H.E.P.A. filter = 99.99%

B) A separate test was performed using outside air with a R.H. = 100%. This high humidity caused condensation in the collecting region and resulted in continual arcing. The unit was air dried for six hours and the test continued with room air.

Measured collection efficiency = 91%

III Second Lab Test (June 12, 1967) After receipt from
Johnson & Johnson

Operating Conditions

As before except:

[O₃] = 9 P.P.H.M. as received
= 5 P.P.H.M. after cleaning corona wires.

Measured collection efficiency = 98%

Observation: During the life of the test approximately 10⁸ liter (3.5 x 10⁶ ft³) of air was passed through the filter. It was observed that the collection media was very dirty only on the bottom half of the cartridges indicating very little air was flowing through the upper section.

Following this series of tests some modifications were made to the collecting region. This involved replacing the "Viskonaire" media with an array of flat plate collectors similar to geometry F as described in Table 5.3. On four of the cartridges, a single layer of the media was used in addition to the plates. Also, in an attempt to equalize the air flow, the last 12 cm of the outer electrode was closed to the air flow. After this modification, the filter was tested under the severe field conditions of a zinc foundry (General Smelting Co., Burlington, Ontario). Here the dust loadings were so high, the counter could not be used during the seven day field test. However, collection efficiency measurements were made in the laboratory before and after the test.

IV Initial Lab Test After Modification to Collecting
Region (August 10, 1967)

(Four cartridges with plates plus 1 layer "Viskonaire"
Five cartridges with plates only)

Last 12 cm of outside repeller closed to flow.

Operating Conditions:

I_c = 2.2 mA

V_R = 19.5 kV

Q = 104 l/s (220 S.C.F.M.)

T = 23°C

R.H. = 21%

$[O_3]$ = 6 P.P.H.M.

Pressure drop = 0.6" H_2O

Measured collection efficiency = 99.47%

Field Test Operating Conditions:

Length of test = 7 days

Particles = mainly zinc oxide fume

Particle concentration > 10^8 particles/litre
(3×10^9 particles/feet³)

R.H. = 35 → 60%

T = 19°C - 27°C

V Second Lab Test (October 24, 1967)
(After return from General Smelting)

Operating Conditions:

As above except:

$I_c = 2.0 \text{ mA}$

$Q = 95 \text{ l/s (200 S.C.F.M.)}$

$[O_3] = 8 \text{ P.P.H.M.}$

Pressure drop = $0.95''$ (with existing prefilter)

$0.65''$ (with new prefilter)

Measured collection efficiency = 99.23%

Observations

The dust build-up indicated that the cartridges were being utilized for approximately 3/4 of their length and that the cartridges having both plates and "Viskonaire" had more dust than those having only the plates. The dust collection on the plates showed that both electrical and mechanical impaction forces were operative as pronounced dust build-ups occurred on the inside surface of the plates directly opposite the jets whereas evenly distributed dust was found on the outside surface of the plates.

7.2.3 Discussion of Test Results

The results of the first set of tests have shown several important points:

- a) Initial lab tests at Johnson & Johnson and U.W.O. showed good agreement (99.65% cf. 99.54%).
- b) The initial collection efficiency for the size range $0.3 \mu\text{m}$ and larger is approximately 99.6%, somewhat lower

than the design goal of 99.9%.

- c) The collection efficiency of the filter does not compare too favourably with the H.E.P.A. type filter.
- d) The filter did not operate satisfactorily in high humidity conditions (100% humidity caused failure of the unit and even after drying initial efficiencies could not be regained).
- e) The pressure drop of the unit was considerably higher than desired.
- f) The air distribution within the cartridge did not offer the best possible utilization of filter media.
- g) The ozone generation was found to increase with time due to dust deposition on the wire.
- h) The initial efficiencies of the unit first with "Viskonaire" and then with plate collectors were very similar. This implied that perhaps a small air leak through the filter was limiting the total efficiency since the previous tests indicated that the "Viskonaire" should have been superior to the plates.

The results just discussed and the experience gained in building and operating the Mark I precipitator provided some indication of problems inherent in the design. The most important shortcomings and the proposed corrections for the Mark II design are discussed below.

Cartridge Size

A serious problem concerned the limited air capacity of each cartridge. This resulted in the necessity of using a relatively large number in parallel to handle even a moderate air flow. The resulting housing for these cartridges proved to be very expensive because of tight construction tolerances required to guard against air leakages. Also the close proximity of the cartridges, necessary to make the unit as compact as possible, resulted in unacceptably high pressure drops through the unit. The large number of individual cartridges resulted in a difficult maintenance problem where the probability of a corona wire breakage was high and the replacement of cartridges rather time consuming.

The obvious answer to all these problems was to enlarge the cartridge elements to allow each to handle a larger air flow.

Ozone Generation

Although the ozone generation was maintained below 10 P.P.H.M. the margin of safety was not very satisfactory. For instance, a maximum level of 2 or 3 P.P.H.M. would be more desirable and in some cases would be essential (eg: hospital clean room). Since the ozone generation was found to be proportional to total corona current (equation 6-1), whereas the degree of particle charging was proportional to

the square root of the linear current density (equations 3-28 and 3-30), it would follow that a reduction in the length of the corona wire could lead to lower ozone generation without reducing particle charging. This could again be accomplished by using a larger cartridge since more air could be treated with a given length of corona wire.

(Provided care is taken to ensure that the wire is sufficiently long to provide adequate charging and that the reduced ion density resulting from the larger diameter does not seriously affect the diffusion charging process.) A further point concerned the use of platinum for the corona wire. It was shown that in practice the increase in the ozone generation occurred primarily due to the presence of dust on the wire. Hence no advantage was gained by using platinum and stainless steel or tungsten wire could be used to advantage because of their superior mechanical properties. (This change in ozone generation due to the dust would increase the feasibility of employing disposable cartridges where both the corona section and collection section could be made as a single unit.)

Failures Due to High Humidity Conditions

The arcing under conditions of high humidity was caused by surface conduction paths forming due to condensation on the insulating supports of the outer electrode. (The electrified media had sufficient clearance from the H.V.

electrode so that even in the case of the material becoming semi-conducting due to condensation, the probability of breakdown occurring here was much smaller).

This is a problem characteristic of electrostatic precipitators and the first solution would be to ensure that the filter was not used in high humidities (the lab tests indicated that for below 50% R.H. no condensation effects were noticeable). However, to guard against this problem as much as possible it would be desirable to mount the outer electrode such that the possible discharge paths were lengthened and the contact points between the electrodes and supports protected from the direct air flow. (Surface condensation would be more likely to occur on surfaces where the moving air could give rise to a slight temperature reduction.)

Power Supply

The geometrical ratios which were employed in the Mark I unit were such that it was impossible to use the same power supply for both the corona and repeller supplies and still provide adequate field strength in the collection region. By changing the cartridge size it was possible to design the unit so that the same supply could be used in parallel for both stages thus saving the cost of one transformer - rectifier set.

Non-Uniform Flow

The inefficient utilization of the collection media was felt to be due to added flow constrictions resulting from the filter housing. Thus even though the pressure drop through the "Viskonaire" resulted in equalized flow in the second stage for a single cartridge, the close proximity of the array changed the flow distribution. To eliminate this problem it should be sufficient to allow greater spacing between the cartridges and the housing.

7.3 Mark II Design

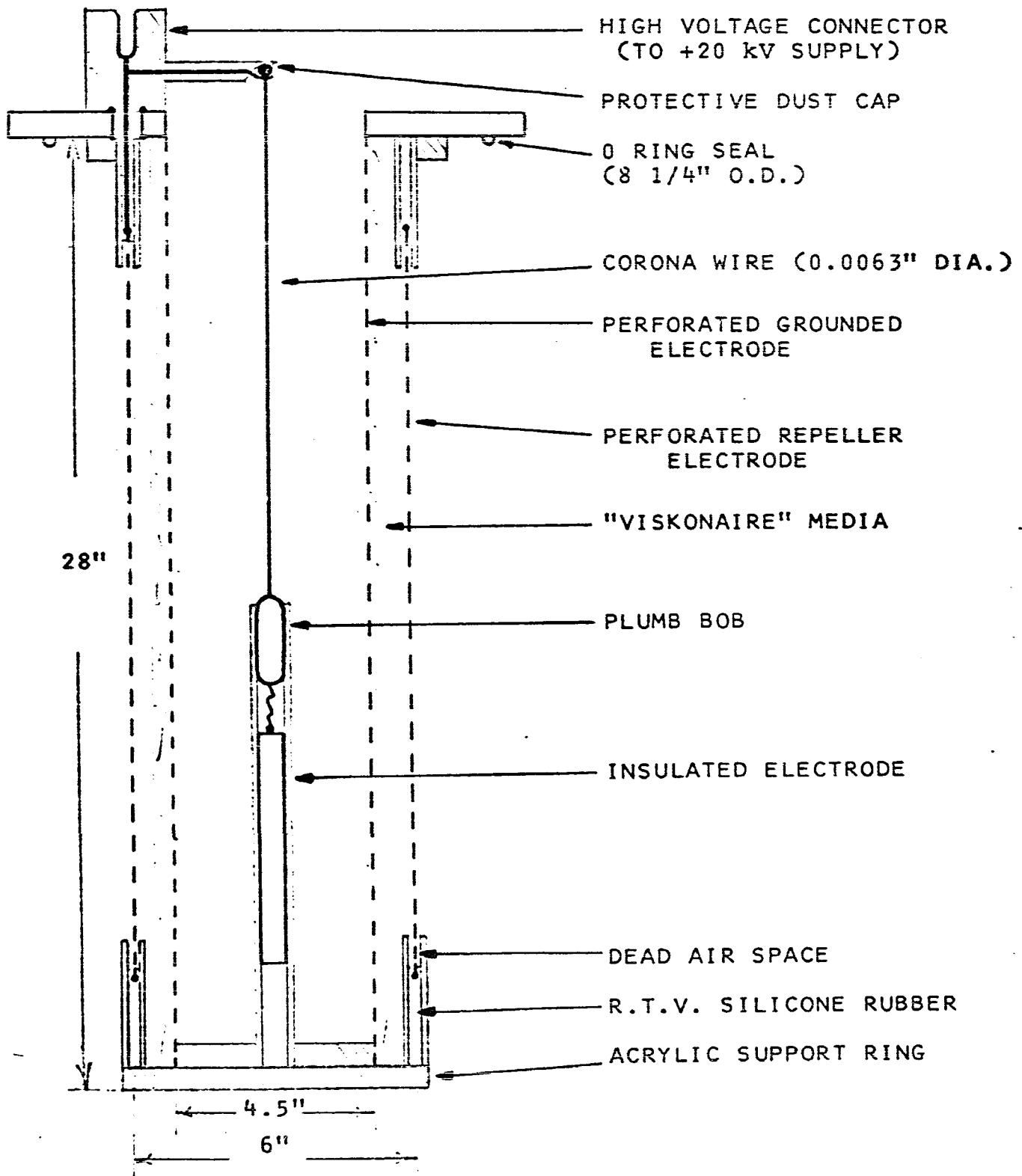
7.3.1 Description

Based upon the points raised in the last section, a new cartridge was designed to handle 110 l/s (235 S.C.F.M.). The dimensions and construction details of the unit are shown in Fig. 7.4.

The inlet dimensions were scaled up from the test unit but the length was set at 0.71 m (28") to ensure ease of handling. The repeller to ground plate spacing was maintained as in Mark I so that +20 kV would provide adequate collection field. The larger cylinder diameter combined with a corona wire diameter of 1.6×10^{-2} cm (0.0063") enabled the same voltage to be used for the corona supply.

The unit was designed to be mounted in a vertical position. This allowed positive sealing at the inlet end

FIGURE 7.4
CARTRIDGE ELEMENT FOR MARK II PROTOTYPE



NOTE: DRAWING NOT TO SCALE. DETAILED SHOP DRAWINGS ARE AVAILABLE ON FILE.

using a commercial O ring held in place by the weight of the cartridge. (As a safety precaution, to guard against possible movement etc., four bolts were used to secure the cartridge in place.) This arrangement removed any lateral stress from the repeller electrodes and allowed a simple suspension of the corona wire. The wire was connected to a metal ball which rested in a yoke connected to the H.V. supply. This connection was protected from the direct air flow by a dielectric cap designed to prevent the accumulation of dust at this point. The corona wire was weighted with a smooth metal plumb bob which made contact with an electrode enclosed in an acrylic sheath. The purpose of the sheath was to prevent vibration of the corona wire while maintaining a "dead air" space around the bob and a long discharge path to ground. The electrode was included in an attempt to utilize the lower portion of the first stage for collection purposes due to the presence of a static electric field. (Since no corona was present in this section, "Viskonaire" could be placed to aid the collection process.)

The outer grounded electrode* acted both to serve as a protective shield for the repeller electrode and to provide some additional collection area as a back-up to the main collection area. The mounting arrangement for the repeller electrode also provided a long discharge path to ground while maintaining a "dead air" space at the contact between the

* Shown on Fig. 7.5 as the perforated grounded screen. This electrode was mounted permanently in the duct.

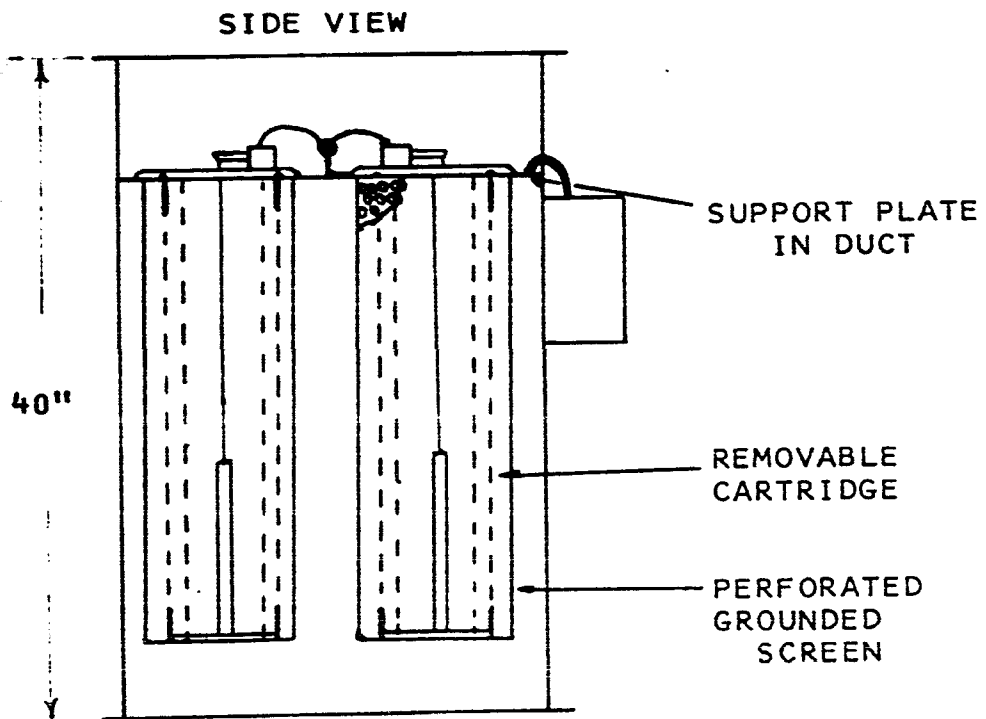
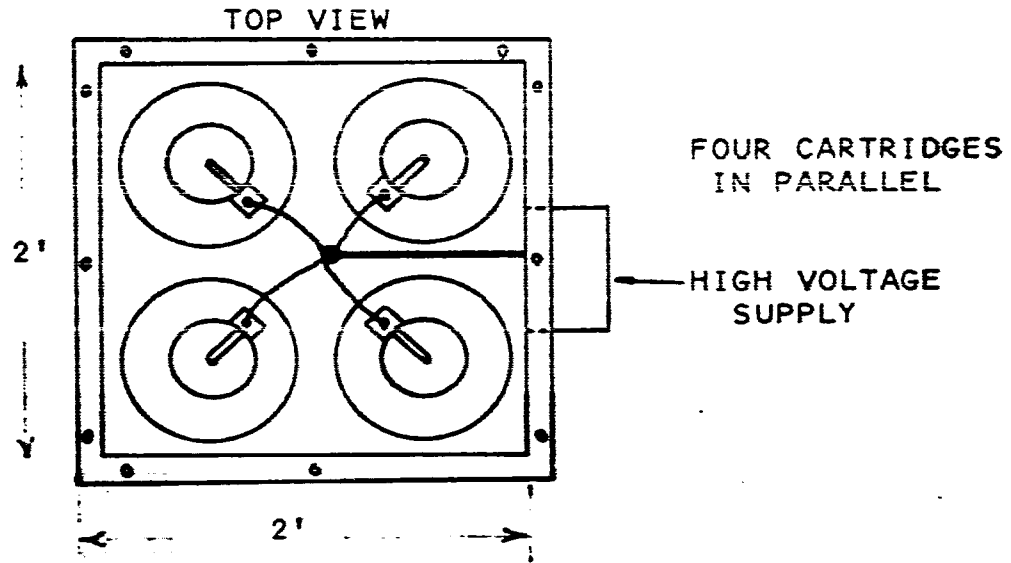
electrode and the dielectric mounting cylinder. This mounting arrangement also ensured that no air could bypass the influence of the electric field.

The complete filter is shown in Fig. 7.5 and is intended to handle 472 l/s (1000 S.C.F.M.). For use in the clean room application it will be used in conjunction with a prefilter, an activated charcoal filter and a H.E.P.A. type absolute filter. Before construction was started on the complete filter, one cartridge was constructed and tested. (Note that this one cartridge had the same capacity as the Mark I filter and therefore the performance of this can be directly compared to the previous results.) At the time of writing the complete filter is undergoing construction in the shop of the Faculty of Engineering Science.

7.3.2 Test Results

The cartridge was tested in a circular air duct using room air forced through by an impeller. It was mounted through a circular flange which was tightly sealed to the wall of the duct. All collection efficiency measurements were based upon total mode counts 0.3 μm and larger. Due to some construction changes the repeller electrode was mounted differently than shown in Fig. 7.4. Due to the temporary nature of the mounting (dielectric spacers) the full design voltage of +20 kV could not be attained without intermittent

FIGURE 7.5
COMPLETE MARK II FILTER



NOTE: DRAWING NOT TO SCALE. DETAILED SHOP
DRAWINGS ARE AVAILABLE ON FILE

breakdowns. Hence all efficiency tests were made at the reduced voltage of +15 kV and should be considered as conservative figures.

Ozone

The ozone concentration was tested under the following conditions with a stainless steel corona wire of diameter 1.6×10^{-2} cm (0.0063").

$$Q = 100 \text{ l/s (210 S.C.F.M.)}$$

$$I = 0.28 \text{ mA}$$

$$V_c = 20 \text{ kV}$$

$$T = 23^\circ\text{C}$$

$$\text{R.H.} = 29\%$$

$$[O_3] = 2 \text{ P.P.H.M.}$$

Based upon these values equation 6-2 gave a predicted concentration of 0.4 P.P.H.M. This is considerably below the measured value. However, it was found that if the corona current was increased to 0.6 mA, the measured value remained at 2 P.P.H.M. This discrepancy was believed to be due to the fact that the reading was just at the threshold of sensitivity of the ozone meter and the normal reading error was ± 1 P.P.H.M. In addition, at these low levels, the normal background concentration of ozone due to ultra-violet radiation from the sun could account for some of the error.

Pressure Drop

With three layers of "Viskonaire" in the collection region the pressure drop at rated flow was 0.15" H₂O increasing to 0.35" at 200% rated flow. This does not include any mutual effects due to mounting cartridges in parallel but does indicate satisfactory performance for the cartridge.

Collection Efficiency

Lab Life Test January 23 + 31, 1969

Operating Conditions:

I_c = 0.29 mA
 V_c = +20 kV
 V_R = +15 kV*
 Q = 100 l/s (210 S.C.F.M.)
 T = 22° - 26° C
 R.H. = 9 - 30%
 [O₃] 2 P.P.H.M.

Measured collection efficiency at start = 99.92%
 Measured collection efficiency at end of 1 week = 99.87%

Observations

Visual inspection of the dust pattern on the media showed that the full length of the collection area was being utilized.

* 5 kV less than design value.

7.3.3 Discussion of Results

Although the final filter has not been tested at the time of writing, it would appear from the test results on the single cartridge that the design specifications and the resulting advantages set out in section 2.1 should be satisfied and were obtained at 75% of the design repeller voltage. The ozone generation was well within the allowable concentration and a considerable safety margin existed in case of degradation due to dust build-up etc. The pressure drop was lower in this large scale cartridge than in the smaller version and even allowing for some increase in the final filter, the total drop should not exceed 0.25" H₂O. The cartridge was not tested at high humidities. However, the clean room has a controlled humidity of approximately 45% R.H. and no difficulties should be experienced due to this.

The construction of the cartridge was very simple and although initially maintenance will be performed by replacing the "Viskonaire" and cleaning the grounded cylinder and corona wire, complete replacement and disposal would be possible on other than a prototype basis. The cartridge elements are self contained (other than for an external power supply) and could readily be placed in existing vertical duct lines simply by adding a mounting flange.

CHAPTER 8

CONCLUSIONS

8.1 Summary

The detailed conclusions and implications of the results have been discussed in the particular section in which they arose. The following describes some of the most significant points.

A different approach was presented for the analysis of the collection efficiency of an electrostatic precipitator in which the concept of migration velocity was replaced with a dimensionless collection parameter. This parameter described the force balance acting on a particle and, when multiplied by another dimensionless parameter called the specific collection area, completely specified the value of the exponent in the collection efficiency relation. This analysis was shown to be equivalent to the standard approach for the case of the coulomb force component. However, it had the added advantage that it could be readily extended to include collection due to the other electrical and mechanical forces which could act when electrified media was added to the second stage. These additional force components were also defined in terms of collection parameters. For a

particular collector geometry the specific collection area was constant and the expression for the collection efficiency was found to have the general form:

$$\eta = 1 - e^{-\frac{A_c}{A_x} \cdot \Sigma K}$$

where ΣK represents the sum of the individual collection force parameters.

The analysis was used to interpret the experimental results in the concentric geometry precipitator. Aside from the divergence found for the particles in the larger size range, the results for the collection efficiency in the first stage showed good agreement with the theoretical predictions. It is interesting that for collection in the first stage, no significant change in collection efficiency could be detected for the range of solidity ratios tested. It was obvious however, that as the collection area was reduced, problems of dust build-up and re-entrainment would become more important as collection proceeded. Collection in the second stage could be made highly efficient but due to the minimal increase in collection area provided by this stage, it did not offer a very practical filter. In spite of the marked change of the geometry in the second stage from the normal type of precipitator, the experimental results confirmed the exponential form of the relation as predicted by

the theory.

As was expected, the introduction of additional collection area into the second stage improved the collection efficiencies as well as producing a more practical arrangement. The theoretical analysis extended to the case of a fibrous media collector was also found to give satisfactory predictions over the broad range of the collectors studied. It was shown that the presence of the dielectric collection media, particularly the "Viskonaire", improved the performance of the filter in ways other than just by increasing the available collection area. For although the coulomb force was shown to be the most important collection force in all the cases where it was present, significant contributions were possible from the dielectrophoretic force and the mechanical forces, particularly in the larger size range. The image force could not be detected in any of the cases studied but it no doubt contributed indirectly by reducing the possibility of particle re-entrainment. An important advantage for the use of electrified media was the increased reliability due to charge build up on the distributed collection surface which allowed both coulomb and dielectrophoretic forces to act for considerable periods after the power was shut off.

The section devoted to the ozone generation showed several significant factors involved in precipitator design.

The ozone formula provides a quantitative relation which predicts the initial amount of ozone generated by a positive corona discharge between a smooth round wire and a coaxial cylinder. This formula uses a dimensionless reaction constant multiplying the following design parameters of an electrostatic precipitator: the total corona current, the product of the average electric field in the corona sheath with the wire radius ("corona potential function") and the inverse of the total air flow. For a clean wire in air at constant pressure, temperature and humidity, the dimensionless constant can be used for all values and combinations of the above design parameters encountered in practice.

The study on the effect of wire geometry showed that it was possible to generate low ozone concentrations with geometries other than smooth round wires. Moreover, these wires could be made mechanically much stronger than an equivalent round wire. In particular, the spiral saw blade geometry showed a remarkable improvement in ozone generated per unit cross sectional area although in practice the improved strength was not required in this application.

The finish and state of oxidation of the surface of the wire was shown to have a marked influence on ozone generation. Oxidation of the wire surface was found to occur under conditions found in the discharge. However, it was found in a practical filter that dust build-up on the corona

wire was a more important source of increased ozone generation.

The results of the study were combined into a practical form of air filter and two prototype units were constructed. Of these two units, the Mark I version proved to have several serious limitations which were eliminated in the Mark II design. The resulting filter is felt to offer a combination of characteristics which have unique advantages for certain classes of air cleaning applications. The filter provides high collection efficiencies (99.9% for 0.3 μm diameter particles and larger) combined with a moderate pressure drop. Particle collection takes place in electrified media which provides a large collection capacity and increases the reliability due to combined electrostatic and mechanical effects. The construction of the filter is very simple and is in the form of self contained cartridge type elements which are easily replaceable and could be either disposed of or cleaned and reused. Ozone generation is well below the recommended industrial standard and the replaceable cartridges have the added advantage that they prevent long term degradation of the ozone generation due to dust build-up on the corona wire.

8.2 Recommendations For Future Work

The use of kaolin particles for the majority of the

collection efficiency tests created some problems in interpretation for the measurements involving size discrimination, due to the uncertain effects of the particle dissymmetry. Therefore, further tests could be carried out to check the effect of particle size on the collection efficiency at the larger sizes using mono-disperse spherical particles.

The present work has concentrated mainly upon "Viskonaire" media which was the best of the collectors tested. However, it was shown with the copper wire bed, that even though the estimated specific collection area was less than for the "Viskonaire", the measured efficiencies were comparable. This was thought to be due to the better utilization of the existing surface since in the construction of the filter care was taken to align the fibers at right angles to the flow and electric field. Therefore, it could be expected that perhaps some other commercially available material could offer superior collection properties more economically. For instance, commercial fiberglass filters are formed with the fibers lying essentially in parallel planes and it would be interesting to test a series of such materials to see if perhaps a better collection media could be found.

Further ozone studies would be of interest from both the practical and theoretical point of view since the mechanisms involved in the formation of ozone are not as yet

completely understood. In particular, a study of the ozone generation and its relationship to surface finish and oxide coating would be valuable both to clarify the role played by the surface as a catalytic reaction site and to help in the selection of the most suitable material for use in practical precipitators. In addition, it would be interesting to investigate the form of the relations for negative corona. Here conditions are perhaps even more complicated since the wire is an active emitter of electrons. The results of the tests using different wire geometries indicated that a smooth round wire is not necessarily the optimum shape when wire strength is a problem. Further investigation of geometries which have the general characteristic of a uniform sharp edge, supported on a core having a much larger radius of curvature would possibly lead to a practical improved alternative to the round wire. (Some preliminary attempts along these lines using band type razor blades have given ozone generating properties equivalent to a wire radius of 4.6×10^{-5} m (0.0018")) (45).

With regard to future work in the field of practical air filters, it is felt that with some further development, the cartridge type unit proposed in section 7.3 could have commercial possibilities in both the industrial and home filtration market. Also, further work could be carried out in introducing dielectric media into the parallel plate type

of precipitator both for the case of air flow through perforated plane electrodes or between solid electrodes. This should result in a reduction in the overall size of a unit for a given air flow.

The concentric geometry precipitator could be applied to other than just the air cleaning situation as discussed in this thesis. For instance, although the one stage precipitator is in almost universal use for industrial process cleaning, there are some particular areas such as collection of high resistivity dusts, or preagglomeration of low resistivity dusts, where two stage precipitators can be used and where this geometry could offer certain advantages. In particular, bag houses are in wide use for the collection of very fine particulates, and have an air flow pattern similar to the precipitator. By using the bag as the electrified media and with suitable precharging of the particulates high efficiencies should be obtainable at lower pressure drops than are presently experienced.

As another example, work is presently underway in the Faculty of Engineering Science at U. W. O. aimed at the development of a practical filter for the solids emission from automobile exhausts. (The lead content of gasoline is of special interest as it is being exhausted to the atmosphere in steadily increasing quantities.) The marked physical similarity between the concentric geometry

precipitator and the standard automobile muffler has led to the incorporation of the two devices into a single unit. Many other examples probably exist and further study along these lines would be in order.

APPENDIX A

Collection Parameters for Cylindrical Collectors

Consider an isolated cylindrical collector located in a uniform field E_0 as shown in Fig. A.1. The radial field in the vicinity of the cylinder is given by : (23)

$$E_r = -E_0 \cos \theta \left(1 + \beta \frac{R^2}{r^2}\right) \quad (\text{A} - 1)$$

where

$$\beta = \frac{\kappa'_c - 1}{\kappa'_c + 1}$$

The field strength in the θ direction is given by:

$$E_\theta = E_0 \sin \theta \left(1 - \beta \frac{R^2}{r^2}\right) \quad (\text{A} - 2)$$

Coulomb Collection Parameter

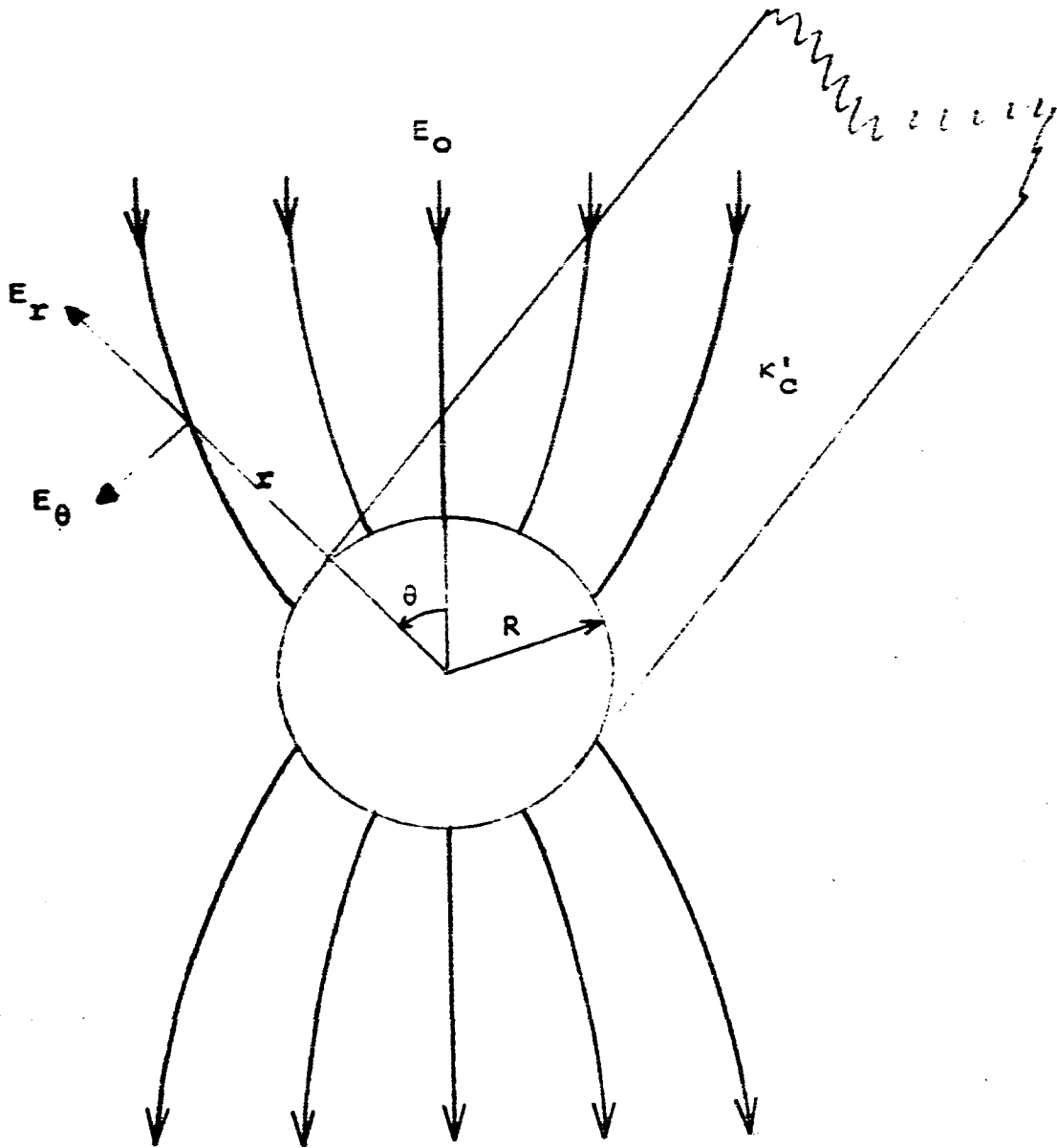
From equation 3 - 13

$$K_c = 2.94 \times 10^3 \frac{q E_p C}{a v_0}$$

To calculate the average collection on a cylindrical collector it is necessary to establish average values for E_p and v_0 .

FIGURE A.1

FIELD DISTRIBUTION AROUND AN INFINITELY LONG DIELECTRIC CYLINDER IN A UNIFORM FIELD E_0



$$E_r = -E_0 \cos \theta \left(1 + \beta \frac{R^2}{r^2} \right)$$

$$E_\theta = E_0 \sin \theta \left(1 - \beta \frac{R^2}{r^2} \right)$$

$$\beta = \frac{\kappa'_C - 1}{\kappa'_C + 1}$$

From A - 1 the electric field strength at the surface of the collecting fiber will be:

$$E_p = -E_o \cos \theta (1 + \beta)$$

Noting that this field will only aid collection over one-half the surface of the fiber (for positively charged particles this will be the upper half.)

$$\begin{aligned} \therefore \bar{E}_p &= \frac{E_o (1 + \beta)}{\pi} \int_{-\frac{\pi}{2}}^{+\frac{\pi}{2}} \cos \theta \, d\theta \\ &= \frac{2 (1 + \beta)}{\pi} E_o \end{aligned} \quad (A - 3)$$

The average velocity of the particle past the fiber must be established for each particular case. As a practical example, when a bed of cylindrical fibers is considered the average velocity can be approximated by:

$$\bar{v}_o = \frac{v_o}{1 - W^2} \quad (A - 3a)$$

where

W^2 = the solidity ratio for the bed

v_o = mean velocity of particle without the presence of the fibers.

Also since A - 3 refers to the average collection field and refers to only one half the total area of the fiber,

it is convenient to refer this average field to the total area of the cylinder ie:

Averaged over whole surface

$$\bar{E}_p = \frac{(1 + \beta)}{\pi} E_o \quad (A - 4)$$

Therefore equation 3 - 13 becomes,

$$\bar{K}_c = 9.35 \times 10^2 \frac{(1 + \beta) q E_o C}{a \bar{v}_o} \quad (A - 5)$$

or from equation 3 - 36

$$\bar{K}_c = 1.04 \times 10^{-7} \frac{f(a) (1 + \beta) E_r E_o}{\bar{v}_o} \quad (A - 6)$$

(Note E_r in this case refers to the radial field strength in the corona discharge.)

Dielectrophoretic Collection Parameter

From equation 3 - 19

$$\vec{F}_d = \gamma \nabla (\vec{E} \cdot \vec{E}) = \gamma \nabla |\vec{E}|^2$$

Where

$$\gamma = 4\pi\epsilon_o \frac{(\kappa_p' - 1)}{(\kappa_p' + 2)} a^3$$

But

$$|\vec{E}|^2 = E_r^2 + E_\theta^2$$

$$\therefore \vec{F}_d = \gamma \left(\hat{u}_r \frac{\partial}{\partial r} + \frac{\hat{u}_\theta}{r} \frac{\partial}{\partial \theta} \right) (E_r^2 + E_\theta^2) \quad (A - 7)$$

This describes the total dielectrophoretic force. However, only the radial component of this force contributes to the collection process. (The θ component would affect the aerodynamic force component but on average, over the whole surface, no net effect would be observed.)

The collection force (ie: the radial component) becomes:

$$F_{dr} = \gamma \left(\frac{\partial E_r^2}{\partial r} + \frac{\partial E_\theta^2}{\partial r} \right)$$

Substituting from equations A - 1 and A - 2 gives

$$F_{dr} = \gamma E_0^2 \left[-\cos^2 \theta \left(\frac{4\beta R^2}{r^3} + \frac{4\beta^2 R^4}{r^5} \right) + \sin^2 \theta \left(\frac{4\beta R^2}{r^3} - \frac{4\beta^2 R^4}{r^5} \right) \right] \quad (A - 8)$$

The closest approach a particle can make to the cylinder is $r = R + a$ and for $R \gg a$, $r \doteq R$

$$\therefore F_{dr} = 4\gamma E_0^2 \left[-\cos^2 \theta \left(\frac{\beta}{R} + \frac{\beta^2}{R^3} \right) + \sin^2 \theta \left(\frac{\beta}{R} - \frac{\beta^2}{R^3} \right) \right]$$

Considering the whole surface of the cylinder, an average value will be given by:

$$\bar{F}_{dr} = \frac{1}{2\pi} \int_0^{2\pi} F_{dr} \, d\theta \quad (A - 9)$$

This gives

$$\bar{F}_{dr} = - \frac{4\gamma E_0^2 \beta^2}{R}$$

which can be expressed in terms of a collection parameter

where

$$\bar{K}_d = \frac{\bar{F}_{dr}}{F_s}$$

Substituting for ϵ_0 and μ

$$\bar{K}_d = 2.61 \times 10^{-6} \frac{(\kappa_p' - 1)}{(\kappa_p' + 2)} \frac{\beta^2 a^2 E_0^2 C}{\bar{v}_0 D_c} \quad (\text{A} - 10)$$

where \bar{v}_0 is an average value of velocity for the particle moving past the collector.

APPENDIX B

Graphical Aids to Calculations

This section contains some of the more frequently used graphical representation of equations used in the calculation of the collection parameters.

FIGURE B.1
RADIAL ELECTRIC FIELD STRENGTH IN CORONA SECTION AS
A FUNCTION OF CORONA CURRENT DENSITY

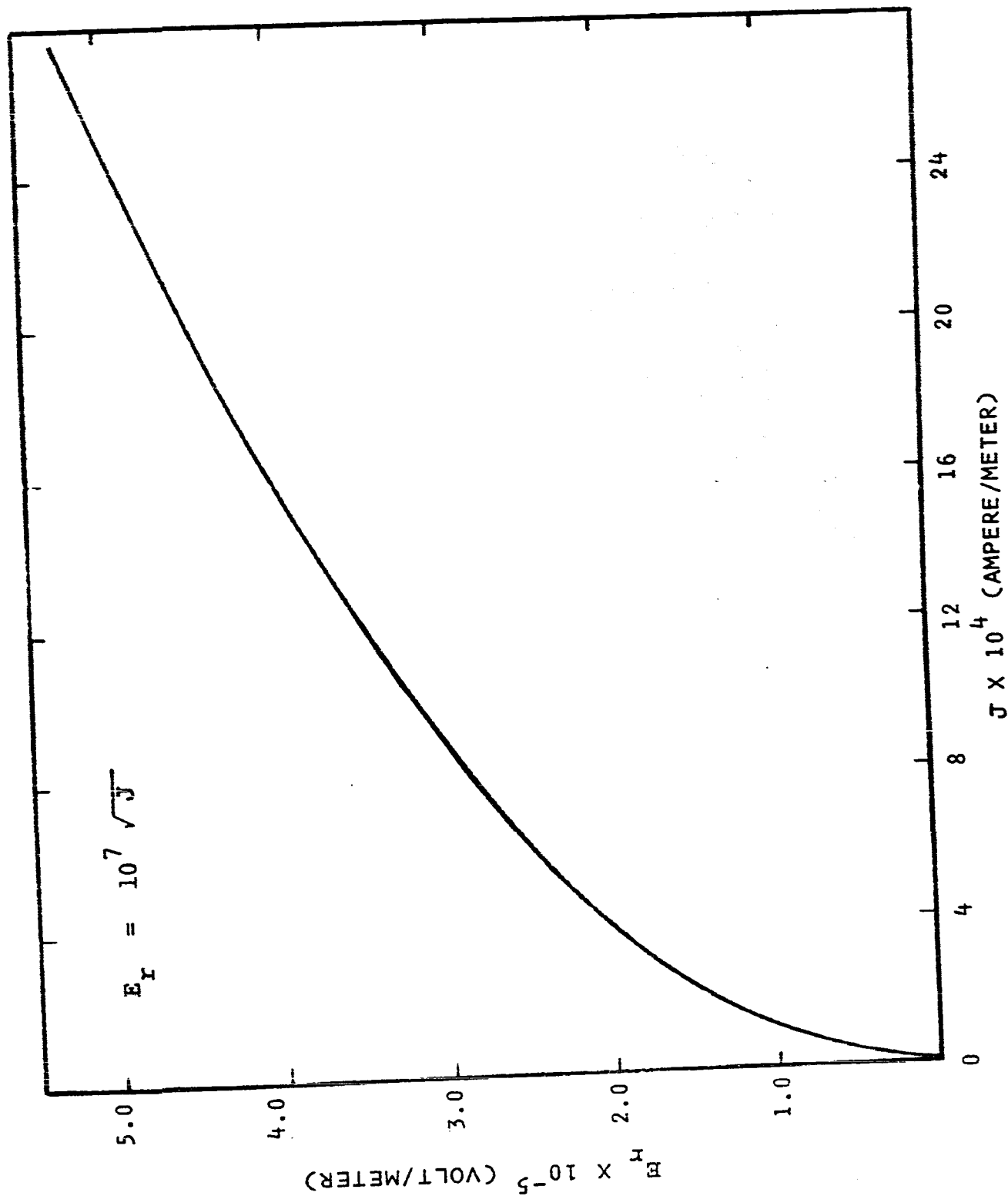
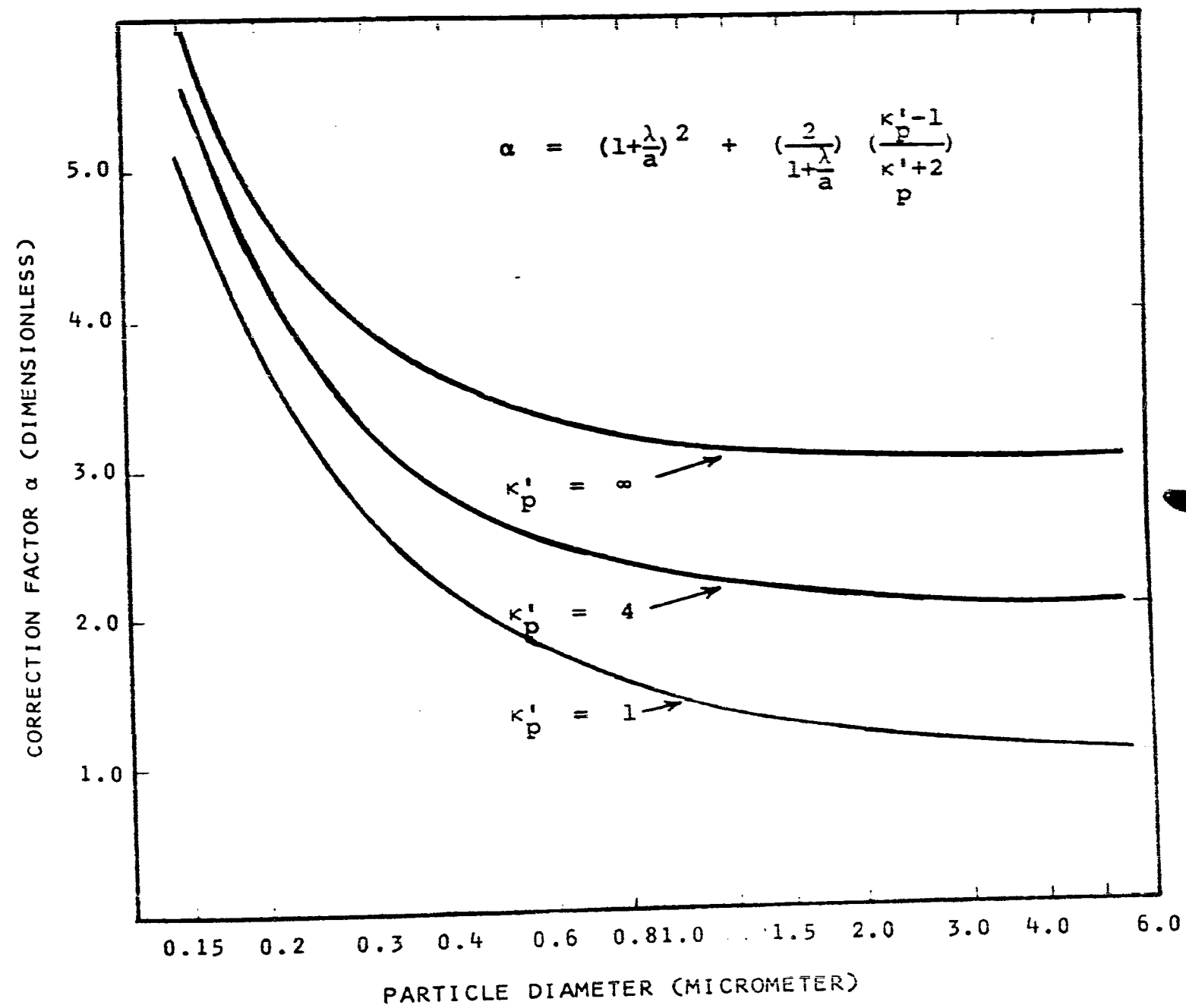


FIGURE B.2
CORRECTION FACTOR α AS A FUNCTION
OF PARTICLE SIZE AND RELATIVE PERMITTIVITY



PARTICLE SATURATION CHARGE AS A FUNCTION OF PARTICLE SIZE AND CHARGING FIELD STRENGTH

$$q_s = \frac{10^{-9}}{9} \alpha E a^2$$

CURVES CALCULATED

FOR $\kappa'_p = 11$

$E = 5 \frac{kV}{CM}$

$E = 3 \frac{kV}{CM}$

$E = 1 \frac{kV}{CM}$

SATURATION CHARGE (COULOMB)

10^{-16}

10^{-17}

10^{-18}

10^{-19}

0.1

0.2

0.4

0.6

1.0

1.5

2.0

3.0

4.0

PARTICLE DIAMETER (MICROMETER)

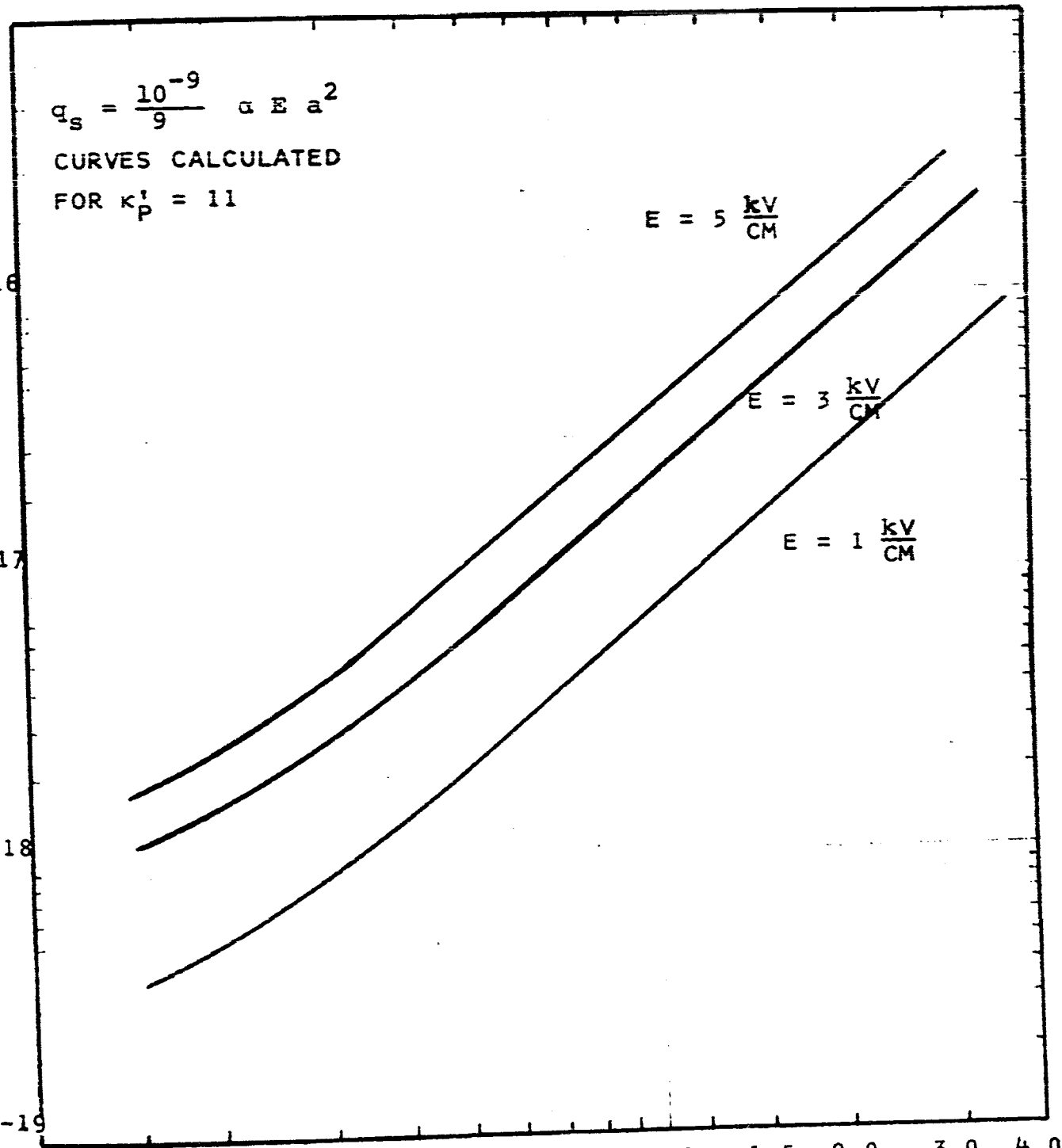
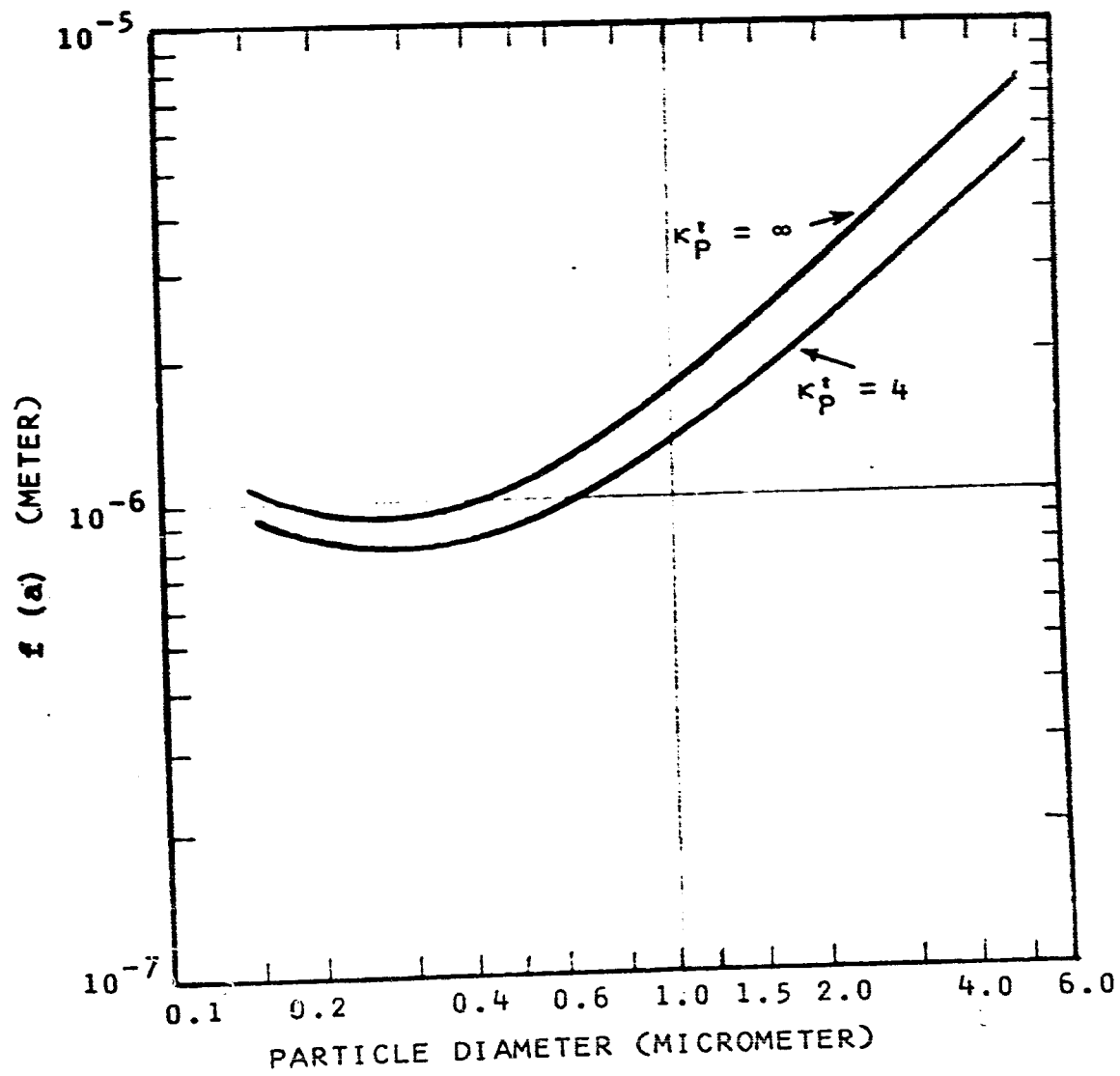


FIGURE B.4

RELATION DESCRIBING THE VARIATION OF THE
COULOMB COLLECTION PARAMETER AS A FUNCTION OF PARTICLE
SIZE AND RELATIVE PERMITTIVITY

(SEE EQUATION 3 - 37)



APPENDIX C

Summary of Further Experimental Results

The experimental results tabulated in this section are from experiments carried out in addition to results already presented in section 5.2.

All the collection efficiencies were measured using total mode counts for particles 0.15 μm diameter and larger. Since the experimental results for this type of sampling always agreed very closely with the measured efficiencies for 0.3 μm diameter, the theoretical predictions were based upon this size. The experimental results were based on the average of two tests. The spread of the results depended upon the magnitude of the leakage but generally was of the same order as those of section 5.2.

In all cases, only the total leakage for the second stage is reported. Unless otherwise specified the following experimental conditions applied to all the tests:

Particles used	-	kaolin
Humidity	-	15% - 25% R.H.
Temperature	-	20° - 25°C.

The tests are grouped together by geometry.

TABLE C.1

TEST RESULTS

AIR FLOW (1/s)	CORONA CURRENT (mA)	REPELLER VOLTS (kV)	COLLECTION PARAMETER	PREDICTED EXPONENT	EXPERIMENTAL LEAKAGE	REMARKS
<u>GEOMETRY A</u> ●						
4.72	0.4	0	$K_I + K_M$	0	1.0	$W^2 = .9$
4.72	0.4	+10	K_C	1.8	.12	$W^2 = .9$
4.72	0.4	+20	K_C	3.6	.006	$W^2 = .9$
4.72	0.2	+20	K_C	2.7	.02	$W^2 = .9$
4.72	0.1	+20	K_C	1.8	.08	$W^2 = .9$
9.44	0.4	+20	K_C	1.8	.18	$W^2 = .9$
9.44	0.2	+20	K_C	1.35	.4	$W^2 = .9$
4.72	0.4	+20	K_C	3.6	.09	$W^2 = .72$
<u>GEOMETRY B</u> ○						
7.1	0.5	0	$K_I + K_M$	0	1.0	
7.1	0.5	+20	K_C	4.2	.045	
7.1	0.5	+10	K_C	2.1	.14	
9.44	0.5	+20	K_C	2.8	.23	

AIR FLOW (l/s)	CORONA CURRENT (mA)	REPELLER VOLTS (kV)	COLLECTION PARAMETER	PREDICTED EXPONENT	EXPERIMENTAL LEAKAGE	REMARKS
<u>GEOMETRY C</u> Δ						
7.1	0	+20	$K_M + K_D$	0	1.0	{ RODS TREATED WITH CARBON ACRYLIC RODS ACRYLIC RODS
7.1	0.5	+20	K_C	4.7	.045	
7.1	0.5	+10	K_C	2.4	1.18	
7.1	0.5	+20	K_C	4.4	.08	
7.1	0.2	+20	K_C	2.8	.04	
<u>GEOMETRY D</u> \square						
7.1	0.5	0	$K_I + K_M$	0	1.0	
7.1	0	+20kV	$K_D + K_M$	0.2	.95	
7.1	0.5	+20kV	K_C	5.5	.005	
7.1	0.5	+10kV	K_C	2.8	.095	
7.1	0.2	+20kV	K_C	3.5	.02	
4.72	0.5	+20	K_C	8.2	.0025	IN PARALLEL PLATE TEST
4.72	0.5	+10	K_C	4.1	.09	IN PARALLEL PLATE TEST

AIR FLOW (L/s)	CORONA CURRENT (mA)	REPELLER VOLTS (KV)	COLLECTION PARAMETER	PREDICTED EXPONENT	EXPERIMENTAL LEAKAGE	REMARKS
4.72	0.5	+20	K _C	9.5	.0005	R.H.=1.5%
4.72	0.5	+20	K _C	9.5	.00035	R.H.=20%
4.72	0.5	+20	K _C	9.5	.00045	R.H.=40%
4.72	0.5	+20	K _C	9.5	.00065	R.H.=60%
4.72	0.2	+20	K _C	4.6	.045	
4.72	0.2	0	K _I + K _M	0	.095	DISCREPANCY DUE TO CHARGE BUILD- UP ON MEDIA
4.72	0.2	0	K _I + K _M	0	1.0	MEDIA DIS- CHARGED
4.72	0	+20	K _D + K _M	.03	0.7	
4.72	0	+10	K _D + K _M	.01	.95	
9.44	0.2	+20	K _C	3.0	.015	
9.44	0.5	+20	K _C	4.8	.004	
4.72	0.5	+10	K _C	4.8	.018	
4.72	0.5	+20	K _C	9.1	.0012	IN PARALLEL PLATE TEST
4.72	0.8	+20	K _C	11.5	.001	IN PARALLEL PLATE TEST
4.72	0.2	+20	K _C	5.5	.0015	IN PARALLEL PLATE TEST
4.72	0.5	+20	K _C	9.0	.0003	LIFE TEST WITH D.O.P. AEROSOL

AIR FLOW (l/s)	CORONA CURRENT (mA)	REPELLER VOLTS (kV)	COLLECTION PARAMETER	PREDICTED EXPONENT	EXPERIMENTAL LEAKAGE	REMARKS
<u>GEOMETRY F</u> ▲						
4.72	0	0	K_M	0.3	0.85	
4.72	0.5	0	$K_M + K_I$	0.3	0.88	
4.72	0	+20	$K_D + K_M$	0.3	0.83	
4.72	0.5	+20	K_C	4.7	0.03	
4.72	0.2	+20	$K_C + K_M$	3.4	0.08	
4.72	0.5	+15	K_C	4.6	.007	SILVER CONDUCTIVE PAINT ON PLATES

REFERENCES

- (1) Strauss, W., "Industrial Gas Cleaning", p. 8, Pergamon Press, (1966)
- (2) Penny, G.W., "A New Electrostatic Precipitator", Elec. Engineering, 56, pp. 159-162, (1937)
- (3) Hansen, N.L., British Patent # 384052, filed, (1931)
- (4) Walton, W.H., "The Electrical Characteristics of Resin-Impregnated Filters", Chemical Defense Experimental Station, Porton, England, Report # 2465, (1942)
- (5) Ranz, W.E. and Wong, J.B., "Impaction of Dust and Smoke Particles on Surface and Body Collectors", Ind. and Eng. Chem. 44, pp. 1371-1381, (1952)
- (6) Kraemer, H.F. and Johnstone, H.F., "Collection of Aerosol Particles in Presence of Electrostatic Fields", pp. 2426-2434, (1955)
- (7) Dawkins, G.S., "Electrostatic Effects in the Deposition of Aerosols on Cylindrical Shapes", Engineering Experiment Station, University of Illinois, Tech. Report # 15, (1958)
- (8) Gillespie, T., "The Role of Electric Forces in the Filtration of Aerosols by Fiber Filters", J. of Colloid Sc., pp. 299-314, (1955)
- (9) Silverman, L., et al, "Electrostatic Mechanisms in Aerosol Filtration by Mechanically Charged Fabric Media and Related Studies", United States Atomic Energy Commission, Report NYO-4610, (1956)
- (10) Thomas, J.W., and Woodfin, E.J., "Electrified Fibrous Air Filters", Trans. A.I.E.E., 78, Part II, pp. 276-278, (1959)

- (11) Havliček, V., "The Improvement of Efficiency of Fibrous Dielectric Filters by Application of an External Electric Field", *Int. J. of Air and Water Poll.*, 4, pp. 225-236, (1961)
- (12) Rivers, R.D., "Operating Principles of Non-Ionizing Electrostatic Air Filters", *A.S.H.R.A.E. Journal*, Reprint # 250, p. 4, (1962)
- (13) Lundgren, D.A., and Whitby, K.T., "Effect of Particle Electrostatic Charge on Filtration by Fibrous Filters", *I. & E.C. Process Design and Development*, 4, pp. 345-349, (1965)
- (14) Mazumder, M.K. and Thomas, K.T., "Improvement of The Efficiency of Particulate Filters by Superimposed Electrostatic Forces", *Filtration and Separation*, 4, # 1, pp. 25-30, (1967)
- (15) Carrier Air Conditioning Company, "The Electronic Air Cleaner", Product 831-006, (1966)
- (16) Strauss, W., op. cit., p. 122-142
- (17) Fuchs, N.A., "The Mechanics of Aerosols", p. 37, Pergamon Press, New York, (1964)
- (18) Davies, C.N., *Proc. Phys. Soc.*, 57, p. 259, (1945)
- (19) Strauss, W., op. cit., p. 219-223
- (20) Collier, E.L., et al, "The Electrogas dynamics and Precipitation", *Ind. and Eng. Chem.*, 58, # 12, pp. 26-29, (1966)
- (21) Faith, L.E., et al, "Particle Precipitation by Space Charge in Tubular Flow", *I. & E.C. Fundamentals*, 6, pp. 519-26, (1967)
- (22) Fuchs, N.A., op. cit., p. 55
- (23) Smythe, W.R., "Static and Dynamic Electricity", p. 68, McGraw Hill, New York, (1950)
- (24) Wilson, L.G., and Cavanagh, P., "The Relative Importance of Brownian Diffusion and Other Factors in Aerosol Filtration", *Atmospheric Environment*, 1, pp. 261-269, (1967)

- (25) Strauss, W., op. cit., p. 225
- (26) Robinson, M., "Turbulent Gas Flow and Electrostatic Precipitation", J. of the Air Pol. Con. Ass'n., 18, pp. 235-239, (1968)
- (27) White, H.J., "Modern Electrical Precipitation", Ind. Eng. Chem., 47, pp. 932-939, (1955)
- (28) Deutsch, W., Ann. der Physik, 68, p. 335, (1922)
- (29) Townsend, J.S., "Electricity in Gases", Oxford University Press, New York, (1914)
- (30) Loeb, L.B., "Electrical Coronas - Their Basic Physical Mechanisms", University of California Press, Berkeley and Los Angeles, (1965)
- (31) White, H.J., "Industrial Electrostatic Precipitation", Addison-Wesley, (1963)
- (32) Loeb, L.B., op. cit., p. 43
- (33) Cobine, J.D., "Gaseous Conductors, Theory and Engineering Applications", pp. 252-258, Dover Publications, New York, (1958)
- (34) White, H.J., "Industrial Electrostatic Precipitation", p. 110, Addison-Wesley, (1963)
- (35) Hewitt, G.W., "The Charging of Small Particles for Electrostatic Precipitation", A.I.E.E. Trans., 76, pp. 300-305, (1957)
- (36) Murphy, A.T., et al, "A Theoretical Analysis of the Effects of an Electric Field on Charging of Fine Particles", A.I.E.E. Trans., 78, Part I, pp. 318-326, (1959)
- (37) Penny, G.W., and Lynch, R.D., "Measurements of Charge Imparted to Fine Particles by a Corona Discharge", A.I.E.E. Trans., 76, pp. 294-299, (1957)
- (38) Cochet, R., "Lois de Charge des Fines Particules (submicronique) Etudes Théoretiques - Controles Récents Spectre de Particules", Colloque International - La Physique des Forces Electrostatiques et Leurs Applications, (published by Centre National de la Recherche Scientifique, Paris, 1961)

- (39) White, H.J., and Cole, W.H., "Design and Performance Characteristics of High-Velocity, High-Efficiency Air Cleaning Precipitators", J. Air Poll. Con. Ass'n, 10, # 3, pp. 239-245, (1960)
- (40) Lagarias, J.S., "Discharge Electrodes and Electrostatic Precipitators", J. Air Poll. Con. Ass'n., 10, # 4, pp. 271-274, (1960)
- (41) American Chemical Society, "Ozone Chemistry and Technology", # 21 Advances in Chemistry Series, 1959 (Section on "Ozone Formation in the Electric Discharge")
- (42) Milazzo, G., "Electrochemistry, Theoretical Principles and Practical Applications", p. 695, Elsevier Publishing Co., (1963)
- (43) American Chemical Society, op. cit., p. 313
- (44) "Kirk-Othmer Encyclopedia of Chemical Technology", 2nd ed., Vol. 14, p. 423, Interscience Publishers, New York, (1964)
- (45) Burgess, K.I., "Ozone Generation in Electrostatic Precipitators", E.S. 400 Project Report, Faculty of Engineering Science, The University of Western Ontario, (1968)
- (46) White, H.J., "Industrial Electrostatic Precipitation", p. 108, Addison-Wesley, (1963)
- (47) Ibid, p. 156
- (48) Ibid, p. 170
- (49) "Clean Room and Works Station Requirements, Controlled Environment", Federal Standard # 209, General Services Administration, Washington, (1963)
- (50) "Operating and Service Manual for Royco Particle Counter, Model 200 and 202", Royco Instruments Inc., Menlo Park, Calif., (1963)
- (51) Mast, G.M., and Saunders, H.E., "Research and Development of the Instrumentation of Ozone Sensing", I.S.A. Trans., 1, # 4, pp. 325-328, (1962)

- (52) Friedlander, S.K., "Principles of Gas-Solid Separation in Dry Systems", Chem. Eng. Progr. Symp. Ser., 55, pp. 135-9, (1959)
- (53) Robinson, M., "A Modified Deutsch Efficiency Equation For Electrostatic Precipitation", Atmospheric Environment, 1, pp. 193-204, (1967)
- (54) Baines, W.D., and Peterson, E.G., "An Investigation of Flow Through Screens", Trans. of the A.S.M.E., pp. 467-480, (1951)
- (55) Harnwell, G.P., "Principles of Electricity and Electromagnetism", 2nd Ed., McGraw Hill, p. 65, (1949)
- (56) ibid, p. 75